Chimeric G protein-coupled receptors mimic distinct signaling pathways and modulate microglia function

by

Rouven Schulz

July, 2022

A thesis submitted to the
Graduate School
of the
Institute of Science and Technology Austria
in partial fulfillment of the requirements
for the degree of
Doctor of Philosophy

Committee in charge:
Edouard Hannezo, Chair
Sandra Siegert
Michael Sixt
Botond Roska

The thesis of Rouven Schulz, titled *Chimeric G protein-coupled receptors mimic distinct signaling pathways and modulate microglia function*, is approved by:

Supervisor: Sandra Siegert, ISTA, Klosterneuburg, Austria

Signature: _____

Committee Member: Michael Sixt, ISTA, Klosterneuburg, Austria

Signature: _____

Committee Member: Botond Roska, IOB, Basel, Switzerland

Signature: _____

Defense Chair: Edouard Hannezo, ISTA, Klosterneuburg, Austria

Signature: _____

Signed page is on file

ISTA Thesis, ISSN: 2663-337X

I hereby declare that this thesis is my own work and that it does not contain other people's work without this being so stated; this thesis does not contain my previous work without this being stated, and the bibliography contains all the literature that I used in writing the dissertation.

I declare that this is a true copy of my thesis, including any final revisions, as approved by my thesis committee, and that this thesis has not been submitted for a higher degree to any other university or institution.

I certify that any republication of materials presented in this thesis has been approved by the relevant publishers and co-authors.

Signature: _____

Rouven Schulz

July, 2022

Signed page is on file

Abstract

G protein-coupled receptors (GPCRs) respond to specific ligands and regulate multiple processes ranging from cell growth and immune responses to neuronal signal transmission. However, ligands for many GPCRs remain unknown, suffer from off-target effects or have poor bioavailability. Additional challenges exist to dissect cell-type specific responses when the same GPCR is expressed on several cell types within the body. Here, we overcome these limitations by engineering DREADD-based GPCR chimeras that selectively bind their agonist clozapine-N-oxide (CNO) and mimic a GPCR-of-interest in a desired cell type.

We validated our approach with β2-adrenergic receptor (β2AR/ADRB2) and show that our chimeric DREADD-β2AR triggers comparable responses on second messenger and kinase activity, post-translational modifications, and protein-protein interactions. Since β2AR is also enriched in microglia, which can drive inflammation in the central nervous system, we expressed chimeric DREADD-β2AR in primary microglia and successfully recapitulate β2AR-mediated filopodia formation through CNO stimulation. To dissect the role of selected GPCRs during microglial inflammation, we additionally generated DREADD-based chimeras for microglia-enriched GPR65 and GPR109A/HCAR2. In a microglia cell line, DREADD-β2AR and DREADD-GPR65 both modulated the inflammatory response with a similar profile as endogenously expressed β2AR, while DREADD-GPR109A showed no impact.

Our DREADD-based approach provides the means to obtain mechanistic and functional insights into GPCR signaling on a cell-type specific level.

Acknowledgements

We thank the scientific service units at ISTA, in particular Flavia Gama Gomes Leite of the Molecular Biology Facility for excellent support with viral vector production, the Imaging and Optics Facility, and the Preclinical Facility. We are grateful to the Novarino group for providing reagents and equipment, Harald Janoviak for sharing his expertise in synthetic biology, and all members of the Siegert group for constant feedback on the project. This research was supported by a DOC Fellowship (24979) awarded to Rouven Schulz by the Austrian Academy of Sciences (OeAW).

About the Author

Rouven Schulz completed a BSc in Biomedical Sciences at the University of Applied Sciences Wiener Neustadt and an MSc in Biomedicine and Biotechnology at the University of Veterinary Medicine Vienna before joining the ISTA in September 2016. His main research interests include neuroimmunology and manipulation of the immune system for therapeutic strategies. During his Master thesis, he investigated epitopes of pathogenic autoantibodies in the neuroinflammatory disease neuromyelitis optica, for which he received an honorary prize for outstanding Master graduates from the Austrian Federal Ministry of Science, Research and Economy. During his PhD thesis, Rouven developed a synthetic biology approach to modulate G protein-coupled receptor signaling in immune cells. His research proposal was awarded with a DOC fellowship from the Austrian Academy of Sciences (OeAW). While working on his project, he also designed and validated several viral vectors in a microglia context. Subsequently, in 2019 he co-authored a review article for *Neuroscience Letters* discussing the current limitations and challenges of employing viruses for microglia transduction.

List of Contributors

Medina Korkut-Demirbaş
Involved in design and execution of validation assays.

Alessandro Venturino
Involved in Ca^{2+} imaging and data analysis.

Gloria Colombo
Performed fluorescence-activated cell sorting to establish stable cell lines.
Involved in primary microglia cultures.

Margaret Maes
Performed optic nerve crush surgery.

Table of Contents

List of Figures

Main Figures

Figures with supplementary information

List of Tables

Main Tables

Tables with supplementary information

List of Abbreviations

AC ..... Adenylyl cyclase
ACTB ..... β-actin
APS ..... Ammonium persulfate
β1AR ..... β1-adrenergic receptor
β2AR ..... β2-adrenergic receptor
BSA ..... Bovine serum albumin
cAMP ..... 3',5'-cyclic adenosine monophosphate
CMV ..... Cytomegalovirus
CNO ..... Clozapine-N-oxide
C-Term ..... C-terminus
CRE ..... 3',5'-cyclic adenosine monophosphate-responsive element
DMSO ..... Dimethyl sulfoxide
DREADD ..... Designer Receptor Exclusively Activated by Designer Drugs
DTT ..... Dithiothreitol
ECL ..... Extracellular loop
ERK1/2 ..... Extracellular signal-regulated kinases 1 and 2
FSK ..... Forskolin
GAPDH ..... Glyceraldehyde-3-phosphate dehydrogenase
GDP ..... Guanosine-5'-diphosphate
GPCR ..... G protein-coupled receptor
GTP ..... Guanosine-5'-triphosphate
HRP ..... Horse radish peroxidase
HSV-TK ..... Herpes simplex virus thymidine kinase
ICL ..... Intracellular loop
IFNγ ..... Interferon γ
IL1β ..... Interleukin 1β
IL6 ..... Interleukin 6
LB ..... Levalbuterol
MAPK ..... Mitogen-activated protein kinase
NECA ..... 5'-N-ethylcarboxamidoadenosine
N-Term ..... N-terminus
OAZ1 ..... ornithine decarboxylase antizyme 1
PFA ..... Paraformaldehyde
PBS ..... Phosphate-buffered saline
RHO ..... Rhodopsine
RPL27 ..... ribosomal protein L27
RT-qPCR ..... Quantitative reverse transcription polymerase chain reaction
SDS ..... Sodium dodecyl sulfate
SDS-PAGE ..... Sodium dodecyl sulfate-polyacrylamide gel electrophoresis
SRE ..... Serum responsive element
TEMED ..... Tetramethylethylenediamine
TM ..... Transmembrane helix
TNF ..... Tumor necrosis factor

List of statistical terms and definitions

Abbreviation	Definition
Chisq	Chi square
Conf.high	Confidence interval high
Conf.low	Confidence interval low
Df	Degree of freedom
t.value	Value of t distribution
z.value	Value of z distribution
F.value	Value of F distribution
Pr>t	P-value for the t-test (proportion of the t distribution which is greater than the absolute value of the t distribution)
Pr>z	P-value for the z-test (proportion of the z distribution which is greater than the absolute value of the z distribution)
Pr>Chisq	P-value for the Chi Square test (proportion of the Chi Square distribution which is greater than the absolute value of the Chi Square distribution)
Pr>F	P-value for the F-test (proportion of the F distribution which is greater than the absolute value of the F distribution)
Std.Error	Standard error
Sum.Sq	Sum of squares
#N/A	Not applicable
Estimate	Mean of group in a t-test
Parameter	Degree of freedom for t-test

Indicators of statistical significance	
*	$p \leq 0.05$
**	$p \leq 0.01$
***	$p \leq 0.001$
n.s.	$p > 0.05$

List of software packages for data visualization and statistical analysis

Information about *R* environment and attached packages

R version 4.0.2 (2020-06-22)
Platform: x86_64-w64-mingw32/x64 (64-bit)
Running under: Windows >= 8 x64 (build 9200)
Matrix products: default

Locale

- LC_COLLATE=English_United Kingdom.1252
- LC_CTYPE=English_United Kingdom.1252
- LC_MONETARY=English_United Kingdom.1252
- LC_NUMERIC=C
- LC_TIME=English_United Kingdom.1252

Attached base packages

- stats
- graphics
- grDevices utils
- datasets
- methods
- base

Other attached packages

- gplots_3.0.3
- RColorBrewer_1.1-2
- gdata_2.18.0
- pheatmap_1.0.12
- ggpmisc_0.3.5
- EnvStats_2.3.1
- readxl_1.3.1
- nlme_3.1-148
- boot_1.3-25
- xlsx_0.6.3
- tximport_1.16.1
- GO.db_3.11.4
- DESeq2_1.28.1
- matrixStats_0.56.0
- logspline_2.1.16
- fitdistrplus_1.1-1
- scales_1.1.1
- multcomp_1.4-13
- TH.data_1.0-10
- MASS_7.3-51.6
- mvtnorm_1.1-1
- influence.ME_0.9-9
- lmerTest_3.1-2
- lme4_1.1-23
- GenomeInfoDb_1.24.2
- BiocGenerics_0.34.0
- topGO_2.40.0
- AnnotationDbi_1.50.3
- AER_1.2-9
- sandwich_2.5-1
- lmtest_0.9-37
- zoo_1.8-8
- car_3.0-8
- carData_3.0-4
- lawstat_3.4
- pastecs_1.3.21
- broom_0.5.6
- dplyr_1.0.0
- Biobase_2.48.0
- IRanges_2.22.2
- SparseM_1.78
- graph_1.66.0
- reshape_0.8.8
- ggrepel_0.8.2
- Hmisc_4.4-0
- Formula_1.2-3
- survival_3.1-12
- lattice_0.20-41
- cowplot_1.0.0
- ggplot2_3.3.2
- Matrix_1.2-18
- S4Vectors_0.26.1
- DelayedArray_0.14.1
- GenomicRanges_1.40.0
- SummarizedExperiment_1.18.2
- ggfortify_0.4.14

Packages loaded via a namespace (and not attached)

- bitops_1.0-6
- numDeriv_2016.8-1.1
- tools_4.0.2
- backports_1.1.7
- R6_2.4.1
- KernSmooth_2.23-17
- rpart_4.1-15
- colorspace_1.4-1
- nnet_7.3-14
- withr_2.2.0
- tidyselect_1.1.0
- gridExtra_2.3
- curl_4.3
- compiler_4.0.2
- htmlTable_2.0.0
- caTools_1.18.0
- checkmate_2.0.0
- stringr_1.4.0
- digest_0.6.25
- foreign_0.8-80
- minqa_1.2.4
- rio_0.5.16
- base64enc_0.1-3
- jpeg_0.1-8.1
- pkgconfig_2.0.3
- htmltools_0.5.0
- bibtex_0.4.2.2
- htmlwidgets_1.5.1
- rlang_0.4.6
- rstudioapi_0.11
- generics_0.0.2
- gtools_3.8.2
- acepack_1.4.1
- zip_2.0.4
- magrittr_1.5
- Rcpp_1.0.4.6
- munsell_0.5.0
- abind_1.4-5
- lifecycle_0.2.0
- stringi_1.4.6
- yaml_2.2.1
- gbRd_0.4-11
- plyr_1.8.6
- grid_4.0.2
- forcats_0.5.0
- crayon_1.3.4
- haven_2.3.1
- splines_4.0.2
- xlsxjars_0.6.1
- hms_0.5.3
- knitr_1.29
- pillar_1.4.4
- codetools_0.2-16
- glue_1.4.1
- latticeExtra_0.6-29
- data.table_1.12.8
- png_0.1-7
- vctrs_0.3.1
- nloptr_1.2.2.1
- Rdpack_1.0.0
- cellranger_1.1.0
- gtable_0.3.0
- purrr_0.3.4
- tidyr_1.1.0
- xfun_0.15
- openxlsx_4.1.5
- Kendall_2.2
- tibble_3.0.1
- rJava_0.9-12
- cluster_2.1.0
- statmod_1.4.34
- ellipsis_0.3.1

1 Introduction

The translation of extracellular signals into an intracellular response is critical for proper tissue function. G protein-coupled receptors (GPCRs) are key mediators in this process with their strategic placement at the cell membrane to bind diverse molecule classes [1,2]. Successful ligand-GPCR interaction triggers intracellular signaling cascades with far-reaching impacts on cell functions like growth, migration, metabolism, and cell-cell communication [3,4]. Approximately 35% of all *food and drug administration* (FDA)-approved drugs target GPCR [5,6], stressing their importance for biomedical research and drug development. However, major challenges exist in investigating GPCR signaling. First, GPCRs often have unidentified ligands, including more than 100 potential drug targets and the majority of olfactory receptors [5,7,8]. Second, GPCR expression and signaling are cell type-specific. For example, β2-adrenergic receptor (β2AR/ADRB2) modulates inflammation in immune cells [9], relaxes smooth muscle in bronchial tubes [10], and impacts pancreatic insulin secretion and hepatic glucose metabolism [11]. Such response diversities hinder dissecting cell type-dependent effects *in-vivo*. Third, GPCR ligands often suffer from poor bioavailability or cause off-target effects. For instance, norepinephrine acts as ligand for β2AR but can also activate other adrenoceptors in the central nervous system [12]. Therefore, novel strategies are required to overcome the limitations of unknown or unsuitable ligands and simultaneously allow selective investigation of GPCR signaling in a cell type-of-interest.

So far, over 800 GPCRs are known, which are structurally conserved with seven transmembrane helices (TM) connected by three extracellular (ECL) and intracellular (ICL) loops [13]. Ligand binding involves N-terminus, ECLs, and TM domains and consequently triggers ICL interaction with heterotrimeric G proteins. These G proteins are composed of α- and βγ-subunits that act as effectors on downstream signaling partners (**Fig.1a**) [13]. Specific subunit recruitment of either $G\alpha_s$, $G\alpha_q$ or $G\alpha_i$ (**Fig.1b**) activates defined canonical pathways [14]. Besides ICLs as critical components for proper GPCR signal transduction [15–17], the C-terminus interacts with β-arrestins, which contribute to receptor desensitization [18–20] and kinase recruitment [21–25] (**Fig.1a**).

Several studies have exploited the concept of ligand binding and signaling domains to control GPCR function [26–31]. Airan *et al.* generated light-inducible GPCR chimeras that mimic the signaling cascades of *e.g*. human α1-adrenergic receptor (hα1AR) by exchanging ICLs and C-terminus of the light-sensitive GPCR rhodopsin with corresponding hα1AR domains [27]. However, caveats exist with this optogenetic approach, as it relies on strong light stimulation which induces phototoxicity [32–35]. Additionally, light exposure *in-vivo* requires invasive procedures that will disrupt tissue integrity and alter the response of resident immune cells [36]. Yet, immune cells are interesting targets for studying GPCR signaling as their function and ability to induce inflammation is tightly controlled by these receptors [3,37,38]. Several immune cells such as circulating leukocytes and lymphocytes are not confined to any light-accessible tissue and therefore cannot be manipulated through light-inducible GPCRs.

Here, we designed chemical-inducible GPCR chimeras based on the DREADD system (Designer Receptor Exclusively Activated by Designer Drugs) [39–41]. DREADDs are modified muscarinic acetylcholine receptors, which are inert to their endogenous ligand acetylcholine and respond to clozapine-N-oxide (CNO), a small injectable compound with minimal off-target effects and suitable bioavailability for *in-vivo* usage [42]. The DREADDs hM3Dq and hM4Di are frequently employed to manipulate neuronal activity [41], whereas rM3Ds has been designed to induce a $G\alpha_s$ response [43]. In our approach, we identified the ligand binding and signaling regions of

hM3Dq and 292 other GPCRs. This enabled us to generate CNO-responsive chimeras that mimic a GPCR-of-interest after exchanging the corresponding signaling domains. We used β2AR as our proof-of-concept candidate due to its well-known ligands and broad physiological importance [10,11], which includes modulating inflammation in various immune cells [9] such as microglia [44]. Our chimeric DREADD-β2AR fully recapitulated the signaling pathways of levalbuterol-stimulated non-chimeric β2AR in HEK cells, and also mimicked the impact on cell motility in primary microglia [45]. Finally, we utilized the microglia-like cell line HMC3 and identified immunomodulatory effects of DREADD-β2AR and two additionally established DREADD chimeras for the microglia-enriched GPR65 and GPR109A/HCAR2. This underlines that our approach can be applied to different GPCRs-of-interest allowing cell type-targeted manipulation of GPCR signaling. In our study, we offer a straightforward design approach for CNO-responsive chimeras to mimic a variety of GPCRs-of-interest. Such a toolbox will be especially useful to study GPCRs with yet unidentified pathways, orphan receptors with unknown ligands, or GPCRs with non-canonical signaling properties which might not be captured by available DREADDs.

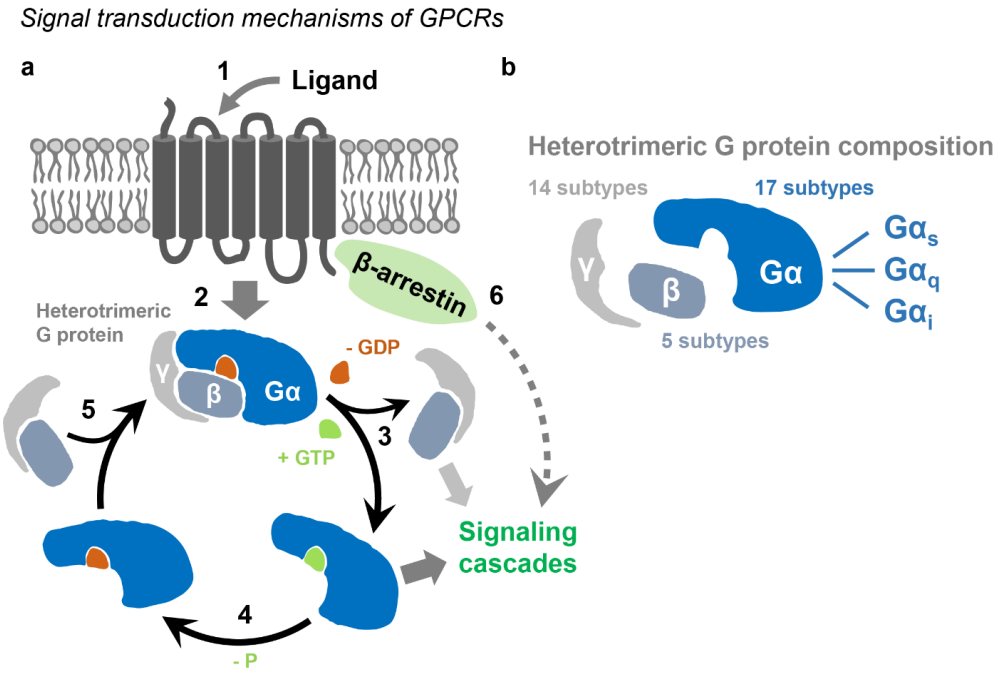

Figure 1: Mechanisms of GPCR signal transduction.
a: Schematic of GPCR signal transduction. Ligand binding (1) induces conformational changes within GPCR domains allowing heterotrimeric G protein recruitment (2). GDP is exchanged by GTP and triggers dissociation of Gα and βγ subunits (3) which activate downstream signaling cascades. The Gα subunit has intrinsic GTPase activity and converts GTP to GDP by removing a phosphate group (4). This allows re-association of all subunits and inactivates the G protein again (5). Additional signaling cascades can be triggered through recruitment of proteins like β-arrestins (6). GTP, Guanosine-5'-triphosphate. GDP, Guanosine-5'-diphosphate. P, Phosphate. **b:** Heterotrimeric G protein composition varies depending on subunit subtypes (numbers refer to known human subtypes) and determines which signaling cascades are initiated. Gα subtypes can be additionally grouped into families with distinct canonical cascades such as $G\alpha_s$, $G\alpha_q$ or $G\alpha_i$. Figure adapted from *Preininger et al.* [18].

2 Methods

2.1 Analysis of retina transcriptome data

A list of GPCRs was manually collected from Class A (rhodopsin-like, excluding olfactory receptors), Class B (secretin receptor family), Class C (metabotropic glutamate), Class D (fungal mating pheromone receptors), Class E (cAMP receptors), and Class F (Frizzled/Smoothened) and contained in total 361 GPCRs. 58 GPCRs were orphans. Analysis was performed as described in Siegert *et al.* 2012 [46].

2.2 Multiple protein sequence alignment

The previously established domains of bovine rhodopsin (RHO) [27] served as reference for the identification of ligand binding and signaling domains. In total, 294 protein sequences were aligned, including RHO, hM3Dq, two sequences (hamβ2AR, hα1AR) from Airan *et al.* [27] as internal control, and GPCRs-of-interest (human and mouse class A GPCRs available at IUPHAR/BPS; www.guidetopharmacology.org). Sequences were combined in a FASTA file, which served as input for the alignment algorithm MUSCLE [47]. To visualize results, the alignment output was imported into the software Jalview 2.9.0b2. Sequences were identified as ligand binding or signaling domains based on their alignment with the RHO reference. Signaling domains were labeled according to their location as intracellular loops (ICL) 1-3 and C-terminus (C-Term).

2.3 Predicting transmembrane GPCR domains

The bioinformatics tool TMHMM (www.cbs.dtu.dk/services/TMHMM) [48] was used to predict transmembrane helices (TMs) for selected GPCRs (RHO, hM3Dq, hamβ2AR, hα1AR, β2AR, GPR65, GPR109A, and GPR183). We highlighted predicted TMs in our alignment output with Jalview 2.9.0b2 (see **Fig.3c** and **Fig.4**).

2.4 Identifying GPCR domains on available crystal structures

We accessed the PDB data base (www.rcsb.org) to download structural representations of bovine RHO, rat CHRM3 as surrogate for hM3Dq, and human β2AR (PDB IDs: 1U19, 4U15 and 2RH1, respectively). Structural data were imported into the software VMD 1.9.2 and oriented with the intracellular domains facing towards the screen. We then highlighted alignment-identified ICL1-3, C-Term, and TMHMM-predicted TMs to see whether they map to their expected locations. In case of partly missing structural data, we used dotted lines as representation.

2.5 Adding N-terminal modifications to GPCRs

The bioinformatics tool SignalP (www.cbs.dtu.dk/services/SignalP) [49] was used to predict whether hM3Dq and β2AR contains a signal peptide. Since such sequence was not found, we added a hemagglutinin-derived signal peptide (KTIIALSYIFCLVFA) at the N-terminus [50,51]. Additionally, we also included a VSV-G epitope (YTDIEMNRLGK) followed by a DSL linker immediately after the signal peptide [52] (see **Fig.6**). In the corresponding DNA sequences, the start codon (ATG) was removed to prevent leaky scanning and to ensure that all proteins contain the VSV-G tag.

2.6 Obtaining DNA sequences for GPCR chimeras via gene synthesis

To generate a chimera for a GPCR-of-interest, we combined ligand-binding hM3Dq domains and GPCR-of-interest signaling domains *in-silico* (see **Fig.34** and **Supplementary Table S1**). We identified the corresponding DNA sequences of these domains through the NCBI Consensus Coding Sequence (CCDS) data base [53] and added our N-terminal modifications. The entire coding sequence was then synthesized (www.eurofinsgenomics.eu) in the pEX-K4 or pEX-A2 vector. During synthesis, recognition sites for restriction enzymes (EcoRI or NotI, BamHI) were added up- and down-stream of the chimera. The same strategy was used to obtain N-terminally modified non-chimeric β2AR, hM3Dq, rM3Ds and hM4Di.

2.7 Cloning

For HEK cell assays, if not otherwise stated, GPCRs were excised from pEX-K4 or pEX-A2 and inserted into the mammalian expression vector pcDNA3.1(-) using EcoRI or NotI, and BamHI.
To study protein-protein interactions, we utilized the NanoBiT system (Promega; N2014). GPCRs were amplified from pEX-K4 with primers carrying restriction sites for NheI and EcoRI. These restriction sites were then used to clone GPCRs into pBiT2.1-C[TK-SmBiT] in order to obtain GPCR-SmBiT fusion constructs. β-arrestin 2 was amplifying from pCDNA3.1(+)-CMV-bArrestin2-TEV (Addgene #107245) with Gibson Assembly primers compatible with the NEBuilder HiFi DNA Assembly Kit (New England BioLabs; E2621). β-arrestin 2 was subsequently assembled into pBiT1.1-C[TK-LgBiT], linearized by NheI and XhoI, in order to obtain β-arrestin 2-LgBiT.
To generate DREADD-β2AR-EGFP, we amplified DREADD-β2AR from pEX-K4, and EGFP from PL-SIN-PGK-EGFP (Addgene #21316) with Gibson Assembly primers. Both fragments were then assembled into pcDNA3.1(-), linearized by NotI and BamHI.
Bicistronic constructs encoding for GPCR-P2A-EGFP were obtained through a cloning step involving an intermediate vector, encoding for mCherry-P2A-EGFP, which was previously generated in the laboratory. First, GPCRs were amplified from pEX-K4 with Gibson Assembly primers and assembled into the intermediate vector, linearized by NheI and BamHI in order to excise mCherry and replace it with GPCRs. Finally, GPCR-P2A-EGFP was amplified from these vector intermediates with Gibson Assembly primers and assembled into pcDNA3.1(-), linearized by NotI and BamHI.
For lentivirus production, we used a modified transfer vector based on PL-SIN-PGK-EGFP. This plasmid was modified through Gibson Assembly by introducing a WPRE sequence downstream of EGFP followed by a microRNA9 sponge (miR9T), which was previously described for optimized microglia transduction [54,55]. WPRE was amplified from pAAV-hSyn-tdTomato (a gift from the Jonas group at ISTA). The miR9T sequence was synthesized (www.eurofinsgenomics.eu) in the pEX-A258 vector and subsequently amplified. Both fragments were then assembled into PCR-linearized PL-SIN-PGK-EGFP, which generated PL-SIN-PGK-EGFP-WPRE-miR9T. Finally, GPCR-P2A-EGFP was amplified with Gibson Assembly primers from the previously established pcDNA3.1(-) vectors and assembled into PL-SIN-PGK-EGFP-WPRE-miR9T, linearized by PstI and BsrGI.

2.8 Cell lines

HEK293T cells were obtained from ATCC (CRL-3216) and cultured in HEK-complete medium, containing DMEM (Thermo Fisher; 31966; with high glucose content, GlutaMAX and pyruvate), 10% (v/v) fetal bovine serum (FBS; Sigma; 12103C; heat-inactivated for 30 minutes

at 56°C), 1% (v/v) non-essential amino acids (Sigma; M7145) and 1% (v/v) penicillin-streptomycin (Thermo Fisher; 15140-122). Medium was sterile filtered (0.22µm; TPP; 99505) and stored at 4°C.
HMC3 cells were obtained from ATCC (CRL-3304) and cultured in EMEM-complete medium, containing EMEM (ATCC, 30-2003), 10% (v/v) FBS and 1% (v/v) penicillin-streptomycin. Medium was sterile filtered (0.22µm) and stored at 4°C.

2.9 Cell maintenance

HEK cells were maintained in T75 flasks with 15ml medium. Culture conditions were 37°C and 5% CO_2. In order to passage cells, old medium was aspirated and cell layer was washed with 10ml DPBS (37°C). PBS was aspirated and 3ml Trypsin-EDTA (Thermo Fisher; 25300-054; 37°C) were added for approximately 1 minute until the cell layer detached. Trypsinization was stopped with 10ml medium (37°C). Cells were pelleted at Trypsin-EDTA (Thermo Fisher; 25300-054; 37°C). Supernatant was aspirated and pelleted cells were resuspended thoroughly in 10ml medium (37°C). Cells were counted and 0.5-0.75 million cells were transferred to a new culture flask within a final volume of 15ml medium (37°C). Cells were passaged every 3-4 days when they reached approximately 80% confluency.
HMC3 cells were maintained in 10cm dishes (Sigma, CLS430167) with 10ml medium. Culture conditions were 37°C and 5% CO_2. For passaging, old medium was aspirated and cell layer was washed with 10ml DPBS (37°C). PBS was aspirated and 3ml Trypsin-EDTA were added for approximately 5-15 minutes until the cell layer detached. Trypsinization was stopped with 10ml medium (37°C). Cells were counted from this suspension and 0.25-0.5 million cells were transferred to a new culture dish within a final volume of 10ml medium (37°C). Cells were passaged every 3-4 days when they reached approximately 80% confluency.

2.10 Coating plates for HEK cell assays and immunostaining

White clear-bottom 96-well plates (Greiner Bio-One; 655098) and 8-well chamber slides (ibidi; 80826; growth area: 1cm^2) were coated with 50µl and 100µl poly-L-ornithine (ready-to-use 0.1% (w/v) solution; Sigma; P4957) respectively. After 1 hour incubation at room temperature, wells were washed three times with 100µl sterile Milli-Q water and left to dry with an open lid for 1 hour under UV irradiation in a sterile laminar flow hood. Culture dished were then wrapped with Parafilm and stored at 4°C.

2.11 HEK cell transfection

Cells were transfected by seeding them into wells of indicated culture vessels containing transfection mix. To avoid toxicity of antibiotics during transfection, cell suspensions were prepared in HEK-complete medium without penicillin-streptomycin. Polyethylenimine (PEI; Polysciences; 24765) was used as transfection reagent. A stock solution (1mg/ml) was prepared by dissolving PEI in Milli-Q water and adjusting the pH to 7. Aliquots were stored at -20°C. To make the transfection mix, plasmids were first diluted in Optimem (Thermo Fisher; 51985034) to a total concentration of 40ng/µl. In parallel, PEI stock was diluted 1:10 in Optimem and incubated for 5 minutes at room temperature. Plasmid and diluted PEI stock were then mixed 1:1 to generate the transfection mix (containing 2.5µl PEI stock per µg DNA). After 20 minutes incubation at room temperature, this transfection mix was pipetted into wells followed by adding the desired number of cells (**Table 1**). Assays were performed 24 hours after transfection.

Table 1: HEK cell transfection scheme.

Culture vessel	Transfection mix per well	Total DNA per well	Cell suspension per well	Total cell number per well
96-well plate	10µl	200ng	90µl	50,000
6-well plate	300µl	6µg	1,700µl	1,500,000
8-well chamber slide	30µl	600ng	170µl	150,000

2.12 Confocal microscopy

Images of immunostainings were acquired on inverted Zeiss LSM800 or Zeiss LSM880 microscopes with either a 63x or 40x oil immersion, or 20x air objective. Live imaging of primary microglia was performed on an inverted Zeiss LSM800 using a 20x air objective.

2.13 Preparation of Antifade mounting medium

Mowiol 4-88 (2.4g; Sigma; 81381) and glycerol (4.8ml; Sigma; G7757) were combined with 6ml Milli-Q water and 12ml Tris buffer (0.2M; pH 8) and stirred overnight at room temperature. After letting the solution rest for 2 hours, it was incubated for 10 minutes at 50°C in a water bath and then centrifuged at 4700 x g for 15 minutes. The supernatant was combined with DABCO (Sigma; D27802) at 2.5% (w/v). Aliquots were stored at -20°C.

2.14 VSV-G immunostaining for confirming cell surface expression of GPCRs

HEK cells were transfected with GPCR (600ng) in coated 8-well chamber slides (ibidi; 80826) as described above. After 24 hours, live cells were immunostained under non-permeabilizing conditions. For this, mouse monoclonal anti-VSV-G antibody conjugated to Cy3 (Sigma; C7706; LOT: 049M4837V) was first subjected to ultrafiltration to reduce the concentration of cytotoxic sodium azide. The required amount of antibody was diluted in PBS (5ml) and applied to a Vivaspin 6 concentrator (Sartorius; VS0601; MWCO: 10kDa; 5ml volume). After centrifugation (4000 x g; 10 minutes; 4°C), the concentrate was diluted in cold cell culture medium to obtain a final 1:250 dilution of antibody. To start the immunostaining, medium was aspirated from the chamber slides and replaced with cold antibody-containing medium. Cells were incubated on ice for 1 hour. Wells were then washed three times with cold medium without antibody for 3 minutes each, followed by fixation with cold 4% (w/v) PFA (Sigma; P6148) in PBS for 15 minutes. After fixing, cells were washed once with PBS for 3 minutes and subjected to nuclear staining with Hoechst (New England BioLabs; 4082S; diluted 1:5000 in PBS) for 5 minutes. Wells were briefly washed with PBS before adding 200µl Antifade mounting medium. Chamber slides were stored at 4°C until imaging. All incubation steps were carried out with 200µl of the respective solution and under protection from light to avoid bleaching of the Cy3 fluorophore.
Confocal images were acquired with a 63x oil immersion objective. Images were processed in Fiji 1.51f by applying a gamma correction of 0.5 for better visualization of faint VSV-G signals, followed by a rolling ball background subtraction and a 2x2x2 median filter.
For VSV-G staining of HMC3 cells, uncoated 8-well chamber slides were used and 3,500 cells were seeded per well together with GPCR-encoding lentivirus at a multiplicity of infection (MOI) of 5. The previously described staining procedure was performed after three to four days when cells reached approximately 80% confluency. Confocal images were acquired with a 20x air objective. Images were processed with 0.5 gamma correction and 2x2x2 median filtering.

2.15 Real-time measurement of cAMP levels

All real-time luciferase assays were performed in CO_2-independent medium (Leibovitz's L15 (Thermo Fisher; 21083027; no phenol red), 10% (v/v) FBS and 1% (v/v) penicillin-streptomycin). The medium was sterile filtered (0.22µm) and stored at 4°C.

To measure $G\alpha_s$-induced increases in cAMP upon ligand stimulation, a cAMP-dependent firefly luciferase (GloSensor) [56] was used (the plasmid was a gift from the Janovjak group formerly at ISTA). As luciferase substrate, a 100mM stock solution of beetle luciferin (Promega; E1602) was prepared in 10mM HEPES and stored at -20°C protected from light. HEK cells were transfected in a 96-well plate with GPCR or empty vector backbone (100ng), and GloSensor (100ng). After 24 hours, medium was replaced with 90µl CO_2-independent medium (37°C) containing 2.22mM beetle luciferin (1:45 dilution of stock). The plate was then incubated for 15 minutes at 37°C in an incubator with atmospheric CO_2 and then transferred to a plate reader (BioTek; Synergy H1) with the lid removed. Total bioluminescence was measured in each well every 1-2.5 minutes (37°C, 1 second integration time; 200 gain) for 30 minutes to establish a baseline. After the last baseline measurement, the plate was ejected and a multichannel pipette was used to quickly apply 10µl levalbuterol or CNO (prepared in CO_2-independent medium; 10 times more concentrated than the desired concentration of either 0.01µM, 0.1µM, 1µM, or 10µM). The measurement was immediately continued for 1 hour. Individual experiments were always carried out in triplicates for each condition. For each well, a fold change in bioluminescence was calculated by normalizing luminescence to the mean of the baseline measurement. For final analysis, baseline-normalized values were pooled from individual experimental repetitions.

To evaluate constitutive GPCR activity and its effect on baseline cAMP levels, we used a different cAMP-dependent firefly luciferase suitable baseline comparisons (GloSensor-22F; Promega; E2301) [57]. As luciferase substrate, a 100X stock solution of cAMP reagent (Promega; E1290) was prepared in 10mM HEPES and stored at -80°C. HEK cells were transfected with GPCR or empty vector (100ng), and GloSensor-22F (100ng). After 24 hours, medium was changed to 100µl CO_2-independent medium (37°C) containing 2% (v/v) cAMP reagent (1:50 dilution of stock). The plate was incubated for 2 hours at room temperature and atmospheric CO_2 before starting a 30 minutes measurement in the plate reader (25°C, 1 second integration time; 200 gain). For each experiment, fold changes were calculated by normalizing GPCR-transfected conditions to the empty vector control. To do this, luminescence values at each time point were divided by the mean of the respective empty vector triplicate. For final analysis, empty vector-normalized values were pooled from different experimental repetitions.

To measure $G\alpha_i$-induced decreases in cAMP, we utilized a cAMP-dependent firefly luciferase suitable for $G\alpha_i$ signaling (GloSensor-22F; Promega; E2301) [57]. As luciferase substrate, a 100X stock solution of cAMP reagent (Promega; E1290) was prepared in 10mM HEPES and stored at -80°C. HEK cells were transfected with GPCR or empty vector (100ng), and GloSensor-22F (100ng). After 24 hours, medium was changed to 80µl CO_2-independent medium (37°C) containing 2% (v/v) cAMP reagent (1:50 dilution of stock). The plate was incubated for 2 hours at room temperature and atmospheric CO_2 before starting the measurement in the plate reader (25°C, 1 second integration time; 200 gain). After a 15 minutes baseline, each well received 10µl CNO (prepared in CO_2-independent medium; 10 times more concentrated than the desired concentration of 10µM), or an equal amount of vehicle (medium only). The measurement was immediately continued for 30 minutes. Then, 10µl forskolin (prepared in CO_2-independent medium; 100µM) was added to each well for a final concentration of 10µM.

The measurement immediately continued for another 30 minutes. Vehicle controls always received the same transfection mix as their corresponding treated condition. Individual experiment were always carried out in triplicates for each condition. For each experiment, fold changes were calculated by normalizing ligand-treated conditions to the respective vehicle controls. To do this, luminescence values at each time point were divided by the mean of the respective vehicle control triplicate. For final analysis, vehicle control-normalized values were pooled from different experimental repetitions.

2.16 Real-time measurement of β-arrestin 2 recruitment

As luciferase substrate, the Nano-Glo Live Cell Substrate (Promega; N2011) was used. HEK cells were transfected in a 96-well plate with GPCR-SmBiT (100ng) and β-arrestin 2-LgBiT (100ng). After 24 hours, medium was replaced with 90µl CO_2-independent medium (37°C) containing 1% (v/v) Nano-Glo Live Cell Substrate (1:100 total dilution; added from a freshly prepared 1:20 pre-dilution in LCS Dilution Buffer supplied with the reagent). The plate was then incubated for 10 minutes at room temperature and subsequently transferred to a plate reader (BioTek; Synergy H1) with the lid removed. Total bioluminescence was measured in each well every 40 seconds (room temperature, 1 second integration time; 200 gain) for 15 minutes to establish a baseline. After the last baseline measurement, the plate was ejected and a multichannel pipette was used to quickly apply 10µl levalbuterol or CNO (prepared in CO_2-independent medium; 10 times more concentrated than the desired concentration of 10µM), or an equal amount of vehicle (medium only). The measurement immediately continued for 45 minutes. Vehicle controls always received the same transfection mix as their corresponding treated condition. Individual experiments were always carried out in triplicate for each condition. For each well, a fold change in bioluminescence was calculated by normalizing luminescence to the mean of the baseline measurement. These values were further used to obtain fold changes by normalizing ligand-treated conditions to the respective vehicle controls. To do this, baseline-normalized values at each time point were divided by the mean of the respective vehicle control triplicate. For final analysis, these values were pooled from different experimental repetitions.

2.17 SRE reporter assay

Transcription-based luciferase reporter assays were performed with the Dual-Glo kit (Promega; E2920). HEK cells were transfected in a 96-well plate with GPCR or empty vector (95ng), SRE-dependent firefly luciferase (95ng; Promega; E1340) [58], and ubiquitously expressed renilla luciferase (9.5ng) to normalize for inter-assay variability (renilla luciferase was inserted into pcDNA3.1(-) and provided as a gift from the Janovjak group formerly at ISTA). After 24 hours, HEK-complete medium was replaced with 90µl fresh HEK-complete medium. Each well was then treated with 10µl levalbuterol or CNO (prepared in HEK-complete medium; 10 times more concentrated than the desired concentration of 10µM), or an equal amount of vehicle (medium only). After 6 hours incubation at 37°C and 5% CO_2, 50µl of medium were removed from each well and replaced by 50µl Dual-Glo luciferase reagent. Following a 10 minute incubation at room temperature, the plate was transferred to a plate reader to measure firefly luminescence (BioTek; Synergy H1; room temperature, 1 second integration time; 200 gain). Then, 50µl Stop&Glo reagent was added to each well, followed by another 10 minute incubation at room temperature, renilla luminescence was measured with the same parameters. For each well, a ratio was obtained by normalizing firefly luminescence to renilla luminescence as a control for transfection efficiency, cell number and

enzyme activity. Vehicle controls always received the same transfection mix as their corresponding treated condition. Individual experiments were always carried out in triplicates for each condition. For each experiment, fold changes between ligand-treated conditions and the respective vehicle controls were obtained by dividing firefly-renilla ratios by the mean of the respective vehicle control triplicate. These values were pooled from different experimental repetitions for final analysis.
To evaluate constitutive GPCR activity and its effect on the SRE reporter, we compared GPCR-transfected conditions with empty vector controls. HEK cells were transfected as described above and after 24 hours HEK-complete medium was replaced with 100µl fresh HEK-complete medium. After 6 hours incubation at 37°C and 5% CO_2, luminescence was measured with the Dual-Glo kit as stated above. For each well, a ratio was obtained by normalizing firefly luminescence to renilla luminescence as a control for transfection efficiency, cell number and enzyme activity. Individual experiments were always carried out in triplicates for each condition. For each experiment, fold changes between GPCR-transfected conditions and empty vector control were obtained by dividing firefly-renilla ratios by the mean of the empty vector triplicate. These values were pooled from different experimental repetitions for final analysis.

2.18 CRE reporter assay

HEK cells were transfected as previously described for the SRE reporter assay with the exception of substituting the SRE reporter with CRE-dependent firefly luciferase [58] (Promega; E8471).
To quantify inhibition of $G\alpha_s$ activity in the competition assay, HEK-complete medium was replaced after 24 hours with 80µl fresh HEK-complete medium. Each well was then treated with 10µl CNO (prepared in HEK-complete medium; 10 times more concentrated than the desired concentration of 10µM), or an equal amount of vehicle (medium only). Immediately afterwards, 10µl 5'-N-ethylcarboxamidoadenosine (NECA; prepared in HEK-complete medium; 50µM) was added to all wells for a final concentration of 5µM. After 6 hours incubation at 37°C and 5% CO_2, luminescence was detected and data were analyzed by normalizing to the respective vehicle controls as previously described for the SRE reporter assay.
To evaluate the effect of ligand-stimulated GPCR in the absence of NECA, medium was replaced 24 hours after transfection with 90µl fresh HEK-complete medium and each well was treated with 10µl CNO or an equal amount of vehicle (medium only).

2.19 Western blot to quantify ERK1/2 phosphorylation

HEK cells were transfected in 6-well plates with GPCR or empty vector (6µg). After 24 hours, cells were serum starved for 4 hours by replacing medium with 1.9ml HEK-complete medium without FBS. Then, cells were treated with 100µl levalbuterol or CNO (prepared in HEK-complete medium without FBS; 20 times more concentrated than the desired concentration of 10µM). Control conditions were left untreated. Treated cells were harvested for protein isolation 2, 5 or 15 minutes after addition of ligand (cells were kept at 37°C and 5% CO_2 during ligand exposure). Untreated cells were harvested immediately. Cells were harvested by placing the plate on ice, aspirating medium and adding 200µl ice cold and freshly prepared lysis buffer (50mM Tris pH 7.4, 300mM NaCl, 1mM EDTA, 1mM Na3VO4, 1mM NaF, 10% (v/v) Glycerol, 1% (v/v) IGEPAL CA-630, 1% (v/v) Protease inhibitor mix set 1 (Calbiochem; 539131); 1 Phosstop tablet (Sigma; 4906845001) per 10ml) to each well. Cells were detached with a

cell scraper, transferred to 1.5ml microcentrifuge tubes and sonicated (15 seconds; room temperature; inside a water bath). Samples were then centrifuged (14,000 x g, 20 minutes, 4°C) and supernatants were transferred to fresh tubes. A small volume of each sample was used to immediately measure protein concentration with the Pierce BCA Protein Assay kit (Thermo Fisher; 23227). The rest was combined with 6x loading dye (375mM Tris pH 6.8, 9% (w/v) SDS, 30% (w/v) glycerol, 0.06% (w/v) Bromophenol blue, 600mM DTT), cooked for 5 minutes at 95°C and stored at -20°C for subsequent Western blot analysis. Three individual experiments were performed with one well per condition in each. SDS-PAGE was performed by loading 10µg protein (approximately 10µl) on 8% acrylamide gels (**Table 2**) with running buffer containing 25mM Tris, 192mM glycine, and 0.1% (w/v) SDS. Electrophoresis was started at 90V constant (two gels per chamber) until samples transitioned from stacking to running gel. Electrophoresis continued at 110V constant until the 25kDa band of the marker left the gel (approximately 2 hours). Proteins were transferred to PVDF membranes (Sigma; IPFL00005) via tank blotting (300mA constant; 2 hours; 4°C; additional cooling insert) with transfer buffer containing 25mM Tris, 192mM glycine, and 20% (v/v) methanol. Successful transfer was briefly checked with Ponceau staining (0.1% (w/v) Ponceau S, 5% (v/v) acetic acid). Membranes were cut to include proteins ranging from 32-80kDa and blocked with 5% (w/v) BSA in TBST (20mM Tris, 150mM NaCl, 0.1% (v/v) Tween 20) for 1 hour at room temperature. Membranes were then incubated overnight at 4°C with rabbit anti-phosphorylated ERK1/2 antibody (Cell Signaling Technology; 9101S; LOT: 30; 1:1,000) in TBST containing 5% (w/v) BSA. Next day, membranes were washed three times with TBST for 10 minutes each and exposed to donkey anti-rabbit secondary antibody conjugated to horse radish peroxidase (GE Healthcare; NA934V; LOT: 16976257; 1:10,000) in TBST containing 5% (w/v) BSA for 2 hours at room temperature. Membranes were again washed three times with TBST followed by signal detection with either SuperSignal West Pico PLUS (Thermo Fisher; 34579) or SuperSignal West Femto (Thermo Fisher; 34094) and imaging (Amersham 600; GE Healthcare). Membranes were then stripped (pH 2.2, 0.2M glycine) for 30 minutes at room temperature, washed three times and blocked again followed by incubation with rabbit anti-GAPDH antibody (Sigma; ABS16; LOT: 3275069; 1:1,000) overnight at 4°C. Membranes were washed three times and subjected to secondary antibody using our standard procedure. The membranes were again washed and GAPDH signal was detected and imaged. Densitometry of bands (pERK1, pERK2, GADPH) was performed with Bio-Rad Image Lab 6.0.1. Densities of pERK1 and pERK2 were then summed to generate a single value (pERK1/2). To normalize for protein loading variability, each pERK1/2 value was divided by the respective GAPDH band on the same membrane after striping.

Table 2: SDS-PAGE gel preparation.

Acrylamide gel composition	5% stacking gel	8% running gel
Total volume	**6ml**	**15ml**
Milli-Q water	4.1ml	7ml
1.0M Tris pH 6.8	0.75ml	-
1.5M Tris pH 8.8	-	3.8ml
30% acrylamide mix (Bio-Rad; 1610154)	1ml	4ml
10% (w/v) SDS	0.06ml	0.15ml
10% (w/v) APS	0.06ml	0.15ml
Polymerization initiator added immediately before gel casting		
TEMED (Bio-Rad; 161-0800)	0.006ml	0.009ml

2.20 GPCR internalization assay

HEK cells were transfected with DREADD-β2AR-EGFP (600ng) in coated 8-well chamber slides (ibidi; 80826) as described above. After 24 hours, live cells were subjected to anti-VSV-G antibody conjugated to Cy3 (diluted 1:250) to label VSV-G-tagged GPCRs expressed on the cell surface. Antibody labeling took place in HEK-complete medium at 37°C and 5% CO_2 for 30 minutes. Wells were then briefly washed with HEK-complete medium (37°C) and 180µl fresh HEK-complete medium was added. Each well received 20µl of CNO (prepared in HEK-complete medium; 10 times more concentrated than the desired concentration of 10µM), or an equal amount of vehicle (medium only). Cells were then incubated for different time periods (0, 15, 30 or 60 minutes) before fixation. The 0 minute time point was only treated with vehicle and immediately fixed. Vehicle controls were included for each time point to control for the potential contribution of antibody labeling to GPCR internalization.
Fixation was carried out with cold 4% (w/v) PFA in PBS for 15 minutes at room temperature. After fixing, cells were washed once with PBS for 3 minutes and subjected to nuclear staining with Hoechst (New England BioLabs; 4082S; diluted 1:5000 in PBS) for 5 minutes. Wells were briefly washed with PBS before adding Antifade mounting medium. Chamber slides were stored at 4°C until imaging. All incubation steps were carried out with 200µl of the respective solution under protection from light to avoid bleaching of Cy3-conjugated antibody and EGFP. Confocal imaging was performed with a 63x oil immersion objective. For each condition, several images each containing one to five cells were taken at random positions within the same well. Approximately 15 cells were acquired per condition with optimal resolution in x, y, and z (71 x 71 x 230nm). Entire images were processed in Fiji 1.51.f by rolling ball background subtraction followed by a 2x2x2 median filter. Regions-of-interest (ROI) were then generated by cropping individual cells and saving them as new images. For further analysis of individual cells, maximum intensity projections of six consecutive z-slices around the center of each cell were obtained. VSV-G and EGFP signals were used to trace the perimeter along the cell surface which separates intra- and extracellular space. A threshold was applied on the VSV-G channel to separate signal from background. The threshold VSV-G area within the cell surface perimeter was then measured (μm^2) to quantify internalized GPCRs. To check if this signal is derived from internalized receptors, we confirmed colocalization of VSV-G and EGFP in both channels.

2.21 Lentiviral vectors

VSV-G enveloped lentiviruses were generated and titered by the Molecular Biology Facility at ISTA. Briefly, HEK293T cells ($5x10^6$) were seeded in 10cm tissue culture dishes and transfected after 24 hours with 6µg packaging plasmid (psPAX2), 2.5µg envelop plasmid (pMD2.G) and 10µg transfer plasmid (PL-SIN-PGK-GPCR-P2A-EGFP-WPRE-miR9T). Culture supernatant containing lentivirus was harvested 24 and 48 hours following transfection. Supernatants from both harvests were pooled, passed through a 0.45µm filter, and stored at -80°C for transduction of HMC3 cells. For primary microglia transduction, supernatants were concentrated through ultracentrifugation (112,000 x g; 1.5h; 4°C) using a 20% sucrose cushion. Pelleted virus was resuspended in PBS and stored at -80°C.
For titration of lentivirus preparations, HEK293T cells were seeded into 6-well plates (10^5 per well) together with a defined volume of virus in various dilutions. After 72 hours, the percentage of EGFP-positive cells was quantified through FACS. Non-transduced cells were

used to set the threshold for the EGFP signal. The titer was calculated as transforming units per milliliter (TU/ml) according to the following formula:

$$\frac{TU}{ml} = \frac{\#Cells\ transduced\ (10^5) * \%\ EGFP\text{-}positive * Virus\ dilution\ factor}{Virus\ volume\ in\ ml * 100}$$

2.22 Generation of HMC3 cell lines stably expressing DREADD-based chimeras

HMC3 cells were seeded into 6-well plates (32,000 per well) together with lentiviral vectors encoding GPCR-P2A-EGFP at a multiplicity of infection (MOI) of 5. Cultures were then expanded for subsequent cell sorting to obtain a pure transduced cell population. For this, cells were trypsinized, pelleted (200 x g; 5min; room temperature) and resuspended in 0.22µm sterile filtered FACS buffer containing 2% (w/v) FBS (Sigma; 12103C; heat-inactivated for 30 minutes at 56°C) and 1mM EDTA in HBSS without Ca^{2+}/Mg^{2+}. EGFP-positive singlets were sorted into EMEM-complete medium using a Sony SH800SFP cell sorter with a 100µm nozzle chip. Non-transduced cells were used as a negative control to set the threshold for the EGFP signal. The sorting mode was set to "purity" to ensure that only EGFP-expressing cells were included. Culturing of these cells was continued under the previously described maintenance conditions.

2.23 Primary microglia cultures

Primary microglia were obtained with adaptations from Bronstein *et al*. [59]. For one preparation, three to four C57BL6/J mouse pups aged P0-P3 were used. Animals were sprayed with 70% (v/v) ethanol for disinfection before decapitation. Heads were placed in a 10cm on ice containing cold HBSS without Ca^{2+}/Mg^{2+}. Brains were removed and placed into a fresh 10cm dish with cold HBSS. Under a dissection microscope, meninges were removed before dissecting the cortices, which were subsequently collected in a tube containing 15ml cold HBSS on ice. HBSS was aspirated and 4ml of Trypsin-EDTA (Thermo Fisher; 25300-054; 37°C) was added. The tissue was then triturated with a 1000µl pipette tip and incubated at 37°C for 15 minutes in a water bath. Digestion was stopped by adding 4ml of HEK-complete medium (37°C). Samples were pelleted (500 x g for 5 minutes at room temperature) and resuspended in 4ml of HEK-complete medium. The previous centrifugation step was repeated and pellets were resuspended in 10-15ml HEK-complete medium. The cell suspension was passed through a 40µm cell strainer (Szabo Scandic; 352340) and then transferred to a T75 flask to establish a mixed glia culture at 37°C and 5% CO_2. After three days, medium was replaced with 10ml of fresh HEK-complete medium. Following a total period of 10-14 days after dissection, microglia were harvested from mixed glia cultures through a combination of lidocaine treatment and shaking. A 150mM lidocaine solution (Sigma; L5647) was prepared in HBSS containing Ca^{2+}/Mg^{2+} and sterile filtered (0.22µm). Lidocaine was added the T75 flask to a final concentration of 15mM before placing them on a shaker inside a cell culture incubator (37°C and 5% CO_2) at 70rpm for 25-30 minutes. After this incubation, the supernatant containing detached microglia was collected in a 50ml tube. The flask was briefly washed with 5ml HBSS containing Ca^{2+}/Mg^{2+} to gather any remaining microglia and the content was pooled with the previously collected supernatant. EDTA was added to a final concentration of 0.05mM before pelleting microglia (1000 x g; 5min; room temperature). Cells were resuspended in 500µl of HEK-complete medium with a wide 1000µl pipette tip to avoid shear stress. Live cells were counted from a dilution in trypan blue (Sigma; T8154). The concentration was adjusted with HEK-complete medium to 0.2-0.25 million cells/ml to seed

approximately 40,000-50,000 cells per well in uncoated 8-well chamber slides (ibidi; 80826; growth area: 1cm^2) within a total volume of 200µl.

2.24 Live imaging of primary microglia

Primary microglia were transduced with lentiviral vectors encoding for DREADD-β2AR-P2A-EGFP approximately 4-24h after seeding. Virus was applied at an MOI of 0.5-3 which resulted in sparsely transduced cells and live imaging was carried out five to seven days after transduction. Three to four days before live imaging, HEK-complete medium was exchanged with freshly prepared TIC medium optimized for primary microglia culture as described in Bohlen *et al*. [60]. TIC medium consisted of DMEM/F12 (Thermo Fisher; 31331093; with GlutaMAX) containing 5µg/ml N-acetyl-L-cysteine (Sigma; A9165), 5µg/ml bovine insulin (Sigma; I6634), 100µg/ml human apo-transferrin (Sigma; T1147), 100ng/ml sodium selenite (Sigma; S5261), 2ng/ml human TGF-β2 (PepoTech; 100-35B), 100ng/ml murine IL34 (R&D Systems; 5195-ML-010/CF), and 1.5µg/ml ovine wool cholesterol (Sigma; 700000P). For live imaging, primary microglia were labeled with tomato lectin conjugated to DyLight 649 (Thermo Fisher; L32472), which was first subjected to ultrafiltration to reduce the concentration of cytotoxic sodium azide The required amount of tomato lectin was diluted in PBS (5ml) and applied to a Vivaspin 6 concentrator (Sartorius; VS0601; MWCO: 10kDa; 5ml volume). After centrifugation (4000 x g; 10-15 minutes; 4°C), the concentrate was diluted in DMEM/F12 (37°C) to obtain a final tomato lectin concentration of 5µg/ml (1:200 dilution of stock). Labeling took place for 20 minutes (37°C and 5% CO_2), after which medium was replaced with 270µl CO_2-independent Leibovitz's L15 (Thermo Fisher; 21083027; no phenol red; room temperature). Samples were then transferred to a confocal microscope and z-stacks were acquired with a 20x air objective every minute for a total period of 55 minutes at room temperature. In all samples, a tomato lectin and EGFP channel was obtained through simultaneous scanning. The tomato lectin channel was used as autofocus reference which was applied before each z-stack to compensate for vertical drifting. After a 10 minutes baseline recording, a pipette was used to carefully apply 30µl of levalbuterol or CNO (prepared in Leibovitz's L15; 10 times more concentrated than the desired concentration of 10µM), or an equal amount of vehicle (Leibovitz's L15 only).
Images were processed in Fiji 1.51 by converting z-stacks to maximum intensity projections, applying a gamma correction of 0.75 for better visualization of faint signals, followed by rolling ball background subtraction and a 1x1 median filter. Regions-of-interest were generated by cropping individual cells. In cases where lateral drifting occurred, image registration was performed with Fiji's *StackReg* plugin using the *Rigid Body* transformation. The tomato lectin signal was used to quantify changes in cell area for non-transduced primary microglia. Microglia transduced with DREADD-β2AR-P2A-EGFP were analyzed through the tomato lectin or EGFP channel, depending on which one provided the best signal. A threshold was applied to separate signal from background. The thresholded area was converted to a binary image and subjected again to a 1x1 median filter to remove unspecific signals. Any remaining signals that did not belong to the respective cell were either removed manually or with Fiji's *Analyze Particle* function. Subsequently, this binarized area was measured in µm^2 at all time points during the 55 minutes recording. For the purpose of data visualization, a fold change was calculated for each cell by normalizing area to the mean of the baseline measurement. For final analysis, values from all cells were pooled at representative time points of 1, 5, 10, 25, 40, and 55 minutes.

2.25 Ca^{2+} imaging of HMC3 cells

HMC3 cells lines were seeded in uncoated 8-well chamber slides (ibidi; 80826; growth area: $1cm^2$) at 3,500 cells per well and within a total volume of 200µl. After three days, cells reached approximately 80% confluency and were labeled with Fluo-4 (Invitrogen; F10471; reconstituted at 1X in supplied buffer; 37°C) for 30 minutes at 37°C and 5% CO_2. Afterwards, cells were further incubated at room temperature (protected from light) and atmospheric CO_2 for another 30 minutes. Labeling solution was then replaced with 270µl CO_2-independent medium (Leibovitz's L15, 10% (v/v) FBS and 1% (v/v) penicillin-streptomycin). Samples were transferred to a confocal microscope and Ca^{2+} imaging was performed at room temperature using a 20x air objective with the pinhole fully opened. Single-plane 16bit images were acquired with a frame rate of 500ms for a total duration of 6 minutes. After a 3 minutes baseline recording, a pipette was used to carefully apply 30µl of ATP, levalbuterol or CNO (prepared in CO_2-independent medium; 10 times more concentrated than the desired concentration), or an equal amount of vehicle (medium only). Final concentrations were 1mM for ATP and 10µM for levalbuterol and CNO.

Images were processed in Fiji 1.51 by applying a Gaussian filter with a sigma of 1.5. ROIs were drawn on the center of individual cells and intensity was measured for each frame. For generation of graphs, the intensity of each cell was normalized to its average intensity throughout the entire 6 minutes recording. For **Figure 24b-h**, normalized intensities were further re-scaled between 0 and 1 within each panel. Ca^{2+} events were automatically detected with the software PeakCaller [61] using the following paramters: required rise = 20% absolute; max. lookback = 700 pts; required fall = 30% absolute; max. lookahead = 700 pts; trend control = exponential moving average (2-sided); trend smoothness = 100; interpolate across closed shutters = true. To remove erroneously detected Ca^{2+} events, the output was additionally filtered in R by including only peaks with a height greater than 0.2 and a FWHM greater than 5.

2.26 Gene expression profiling in HMC3 cells with RT-qPCR

Non-transduced HMC3 cells or HMC3 cells stably expressing DREADD-based GPCR chimeras were seeded in 6-well plates at a density of 32,000 cells per well in a total volume of 2ml. Assays were performed three days after seeding when cells were approximately 80% confluent. Cells were then treated by applying fresh EMEM-complete medium containing the respective compounds. Concentrations of levalbuterol, CNO or forskolin were always 10µM. IFNγ/IL1β was added at 10ng/ml each. Untreated control conditions only received fresh EMEM-complete medium. Every experimental repetition included one well per condition. After 6 hours incubation (37°C and 5% CO_2), wells were briefly washed with DPBS before proceeding with RNA isolation (innuPREP RNA Mini Kit 2.0; Analytik Jena; 845-KS-2040050) according to the manufacturer's instructions. cDNA was synthesized immediately afterwards (Lunascript RT Super Mix; New England BioLabs; E3010L) with 800-1000ng total RNA as input (same amount for each condition within experimental repetitions) and stored at -20°C.

For gene expression analysis, RT-qPCR (Luna Universal qPCR Master Mix; New England BioLabs; M3003L) was performed in 384 well plates (Bio-Rad; HSR4805) on a Roche Lightcycler 480 using the device's "Second Derivative Maximum Method". Total reaction volume was either 5 or 10µl containing 1µl of 1:40 or 1:10 diluted cDNA, respectively. The final concentration for each primer was 0.25µM (**Table 3**). Cycle conditions were 60 seconds at 95°C for initial denaturation, followed by 40 cycles of denaturation (15 seconds; 95°C) and

annealing/extension (30 seconds; 60°C). Each run was completed with a melting curve analysis to confirm amplification of only one amplicon. Each PCR reaction was run in triplicates from which a mean Cq value was calculated and used for further analysis. dCq values were obtained by normalizing mean Cq values to the geometric mean of four reference genes (GAPDH, ACTB, OAZ1, RPL27) measured within the same sample. ddCq values were then calculated by normalizing dCq values to the respective control condition (untreated cells or cells stimulated with IFNγ/IL1β alone) within each experimental repetition. Fold changes were obtained by transforming ddCq values from log2-scale to linear scale.

$$dCq = geometric\ mean_{\text{reference genes}} - Cq$$

$$ddCq = dCq - dCq_{\text{control condition}}$$

$$Fold\ change = 2^{ddCq}$$

For **Figure 26**, fold changes were obtained through normalizing to untreated cells. For final data visualization, the stimulation with IFNγ/IL1β alone was then set to 100% within each experimental repetition. In **Figure 31d-e**, fold changes were directly compared to IFNγ/IL1β alone. Log2-transformed fold changes were then used for principal component analysis in R using the "prcomp" function with the "center" and "scale" argument set to "TRUE". Hierarchical clustering of log2 fold changes was carried out with the pheatmap package (RRID:SCR_016418).

Table 3: List of RT-qPCR primers.

ID	Species	Target transcript	Sequence	Amplicon size	Transcript variants	Targeted exons	Annealing	Efficiency
OAZ1	Human	NM_004152.3	FW: AGGACAGCTTTGCAGTTCTC RV: CGGTTCTTGTGGAAGCAAATG	82bp	1, 2	4, 5	60°C	87%
GAPDH	Human	NM_002046.7	FW: GTCTCCTCTGACTTCAACAGCG RV: ACCACCCTGTTGCTGTAGCCAA	131bp	1, 2, 3, 4, 7	8, 9	60°C	88%
ACTB	Human	NM_001101.5	FW: CACCATTGGCAATGAGCGGTTC RV: AGGTCTTTGCGGATGTCCACGT	135bp	-; also recognizes ACTG1 transcripts	4, 5	60°C	84%
RPL27	Human	NM_000988.5	FW: ATCGCCAAGAGATCAAAGATAA RV: TCTGAAGACATCCTTATTGACG	123bp	1, 2, 3	Variant 1 and 2: 3, 4; Variant 3: 2, 3	60°C	91%
TNF	Human	NM_000594.4	FW: GCACTTTGGAGTGATCGG RV: TTCGAGAAGATGATCTGACTGC	95bp	-	1, 2, 3	60°C	90%
IL1β	Human	NM_000576.3	FW: ATGATGGCTTATTACAGTGGCAA RV: GTCGGAGATTCGTAGCTGGA	132bp	-	2, 3, 4	60°C	90%
IL6	Human	NM_000600.5	FW: GGCACTGGCAGAAAACAACC RV: GCAAGTCTCCTCATTGAATCC	85bp	1, 2, 3	Variant 1 and 3: 3, 4; Variant 2: 2, 3	60°C	91%
β2AR	Human	NM_000024	Commercially available and validated RT-qPCR primer pair (Integrated DNA Technologies; Hs.PT.56a.23196446.g)	NA	-	NA	60°C	NA
GBP2	Human	NM_004120.5	FW: AAGGAAGGGGATACAGGCCAAA RV: TGCATCAGCCACATCCTCCTTG	70bp	NA	NA	60°C	91%
C17orf100	Human	NM_001105520.2	FW: TTTACTGACCGTCCTGCGTCTT RV: AAGGTTTTCTGAGGGCTGTGGA	182bp	NA	NA	60°C	94%
CBWD3	Human	NM_201453.4	FW: GAAACGGTTGCCTCTGCTGTTC RV: AGGGTCTGCTAATCCAGTGGTC	119bp	NA	NA	60°C	99%
FBXO10	Human	NM_012166.3	FW: AGATGGTGTGGTTGTGGGAGAC RV: ACCACAGCCCTTGTTAGCGTA	76bp	NA	NA	60°C	92%
IFI27	Human	NM_001130080.3	FW: CGTCCTCCATAGCAGCCAAGAT RV: ACCCAATGGAGCCCAGGATGAA	147bp	NA	NA	60°C	97%
PAG1	Human	NM_018440.4	FW: TTCAGCCGTTCAGTTACTAGCC RV: TGGACTTCCTCGTAATGCTGC	131bp	NA	NA	60°C	83%
TFAP2A-AS1	Human	NR_033910.1	FW: CCTCGCAGTCCTCGTACTTGAT RV: AGGCTGTTGGTAAAGAGCCAGA	129bp	NA	NA	60°C	95%
EPHA2	Human	NM_004431.5	FW: ACTGCCAGTGTCAGCATCAACC RV: GTGACCTCGTACTTCCACACTC	131bp	NA	NA	60°C	89%
FLT1	Human	NM_001159920	FW: TGCCGGGTTACGTCACCTA RV: GTCCCAGATTATGCGTTTTCCAT	90bp	NA	NA	60°C	97%
H3F3A	Human	NM_002107.7	FW: ACAAAAGCCGCTCGCAAGAGTG RV: TTTCTCGCACCAGACGCTGGAA	157bp	NA	NA	60°C	86%
LIF	Human	NM_001257135.2	FW: AGGTCTTGGCGGCAGTACAC RV: GAGGTGCCAAGGTACACGACTA	161bp	2	NA	60°C	83%

ID	Species	Target transcript	Sequence	Amplicon size	Transcript variants	Targeted exons	Annealing	Efficiency
LINC01003	Human	NR_027387.1	FW: GTAAAGCCGGATCTGTCCAACG RV: AGCATGGAGAAAAGGGATGGGT	99bp	NA	NA	60°C	104%
SCARF1	Human	NR_028075.3	FW: TGACAGTCTCACATCACGACCC RV: CACACAGTAGGCAGGAACCTCA	140bp	NA	NA	60°C	76%
SLC41A2	Human	NM_032148.6	FW: GCCAAACATCCAGCCACAAGAAC RV: GGGTCTGATACAGTTGTGTCCAG	113bp	NA	NA	60°C	93%
SLIT2	Human	NM_001289136	FW: CAGAGCTTCAGCAACATGACCC RV: GAAAGCACCTTCAGGCACAACAG	153bp	NA	NA	60°C	78%
TGIF2-C20orf24	Human	NM_001199535	FW: AACCTGTCAGTGCTGCAAGATG FW: TCCCAAGAACCCTCGTAATGGC	114bp	NA	NA	60°C	92%

Efficiencies were validated from the slope of four to five serial 1:4 dilutions of cDNA template according to the following formula:

$$Efficiency = (2^{(-\frac{1}{Slope})}) - 1$$

2.27 Next generation mRNA sequencing of HMC3 cells

HMC3 cell lines were treated and RNA was isolated as described above. RNA samples were immediately snap frozen on dry ice and then stored at -80°C. Samples were collected in batches (experimental repetitions) to obtain a total of three replicates per experimental condition. Library preparation and sequencing was carried out by the Vienna BioCenter Core Facility. In brief, libraries were generated with the QuantSeq 3' mRNA kit (Lexogen) and sequenced on an Illumina NextSeq550 SR75 High platform. Transcript abundance was quantified with *Salmon* [62] and we used the resulting "quant.sf" files as input for our downstream analysis with the *DESeq2* [63] package in *R*.
The "quant.sf" files were imported with the *tximport* package with the "countsFromAbundance" argument set to "no". This generates count data and omits correction for transcript length which is not necessary for 3'-mRNA sequencing data. Count data were then imported into *DESeq2* with the "DESeqDataSetFromMatrix" command, using "Experimental repetition" and "Experimental condition" as predictor variables for the design formula. For principal component analysis and sample-to-sample distance (Euclidean) calculation, counts were transformed with the "rlog" command and the "blind" argument set to "TRUE", which avoids bias by disregarding experimental group dependencies. Principal component analysis was performed in *DESeq2* with the "plotPCA" command using all genes. Hierarchical clustering of sample-to-sample distances was carried out with the *pheatmap* package. To identify differentially expressed genes, all experimental groups were included in one model. Subsequently, desired comparisons between experimental groups were extracted by specifying contrasts and conducting the Wald test (*DESeq2* default). P-values were adjusted with the "Benjamini-Hochberg" procedure with an alpha threshold of 0.1. Finally, we filtered the output of these comparisons and included only genes with an absolute linear fold change greater than 2. **Supplementary Table S2** provides a list of all genes that passed these criteria for differential expression. For visualization of differentially expressed genes via heatmaps (*pheatmap* package), correlation plots, or bar graphs (**Fig.28b**, **Fig.29f-g**, **Fig.31a**, **Fig.30**), we operated on normalized counts extracted directly from the *DESeq2* model with the "counts" function. Pearson correlation coefficients were calculated with the "cor.test" function of *R* after log2-transforming the mean of respective fold changes. Gene ontology enrichment of biological processes was performed with the *topGO* package [64,65]. GO terms were mapped to the "org.Hs.eg.db" annotation database including only nodes with a minimum of 10 associated genes. Differentially expressed genes were analyzed for enrichment against a background including all genes where *DESeq2* was able to calculate an adjusted p-value, which excludes non-detected and unreliable low-abundance genes with mostly 0 counts. Enrichment was identified through the Fisher test and using the "elim" algorithm, which aims to eliminate broad and unspecific terms of parent nodes in case a more informative child node can be allocated.

2.28 Animals

C57BL/6J (#000664), B6.129P2(C)-Cx3cr1^{tm2}.1(cre/ERT2)Jung/J (#020940; referred to as CX3CR1-creERT2) and B6N.129-Gt(ROSA)26Sor$^{tm1(CAG-CHRM4*,-mCitrine)Ute}$/J (#026219; referred to as LSL-hM4Di) mice were purchased from The Jackson Laboratories. To obtain mice for microglia-specific expression of hM4Di, homozygous Cx3cr1-creERT2$^{+/+}$ and hemizygous LSL-hM4Di$^{+/-}$ were crossed and offspring hemizygous for both markers were selected (CX3CR1-creERT2$^{+/-}$ x LSL-hM4Di$^{+/-}$; see **Fig.32a**). For simplicity, these animals are referred to as hM4Di. Littermates negative for LSL-hM4Di (CX3CR1-creERT2$^{+/-}$ x LSL-hM4Di$^{-/-}$) were kept as wild type controls. All mice were genotyped and housed in the ISTA Preclinical Facility with a 12 hour light-dark cycle, food and water provided *ad libitum*. All animal procedures are approved by the Bundesministerium für Wissenschaft, Forschung und Wirtschaft (bmwfw) Tierversuchsgesetz 2012 (TVG 2012), BGBI. I Nr. 114/2012, idF BGBI. I Nr. 31/2018 under the number GZ 2021-0.262.895.

2.29 Tamoxifen administration before optic nerve crush experiments

At the age of approximately one month, mice of all experimental groups were injected intraperitoneally with 150mg/kg tamoxifen (Sigma; T5648) dissolved in corn oil (Sigma; C8267) for three consecutive days. Mice were subjected to optic nerve crush not earlier than four weeks after tamoxifen administration to ensure that expression of the floxed gene is only present in resident microglia [66].

2.30 Anesthesia and eye surgery preparations

Anesthesia was induced with 5% (v/v) isoflurane (Zoetis) supplemented with oxygen at a flow rate of 0.6l/minute. Anesthetized mice were placed under a dissection microscope within a biosafety cabinet. Anesthesia was maintained throughout the entire procedure with 2.5% (v/v) isoflurane supplemented with oxygen, via a nose cone. One drop of Proparacaine (0.5%; Ursapharm Arzneimittel) was applied to the eye destined for optic nerve crush (left eye) for additional local anaesthesia. The opposite eye was covered with antibiotic ointment (Oleovital; Fresenius Kabi) to prevent drying and infection of the conjunctiva during surgery. For analgesia, mice were subcutaneously injected with 5mg/kg meloxicam (Metacam; Boehringer Ingelheim; diluted to 1.25mg/ml in 0.9% (w/v) NaCl solution from Fresenius Kabi). Prior to the start of surgical steps, adequate anesthesia was confirmed by absence of a foot withdrawal reflex.

2.31 Optic nerve crush

All animals were approximately six months of age at the time of surgery. After surgery preparation, the tissue at the corner of the eye was pinched with a hemostat for 10 seconds to prevent bleeding. Next, a lateral canthotomy was performed which allowed visualization of the posterior pole. A jeweler forceps was used to hold the eye securely at the limbus of the conjunctiva. A micro-dissection scissors was used to cut the conjunctiva at 90°. To expose the optic nerve, a window was created by carefully dissecting the surrounding muscle and fascia. The optic nerve was pinched 1mm from the posterior pole for 4 seconds using a curved N5 self-closing forceps (Dumont). Afterwards, the conjunctiva was repositioned, and antibiotic ointment (Oleovital; Fresenius Kabi) was applied to the surgerized eye to prevent infection.

2.32 Repeated CNO and saline administration in mice

Mice were injected intraperitoneally with 5mg/kg CNO (Abcam; ab141704) dissolved at 1.25mg/ml in 0.9% (w/v) NaCl solution (Fresenius Kabi). Vehicle controls received an equal amount of NaCl solution without CNO. All animals received their first injection 10 minutes before optic nerve crush surgery and for five consecutive days with a 24 hour interval. All animals were sacrificed one hour after the last CNO or saline injection.

2.33 Retina dissection and preparation for histological analysis

Animals were quickly anesthetized with isoflurane (Zoetis) and secured to a perfusion plate. The chest was open to expose the heart. The left ventricle was cannulated and the right atrium was cut. The animals were initially perfused with 5ml PBS containing 100mg/l heparin (Sigma; H0878), followed by 10ml of 4% (w/v) PFA (Sigma; P6148) in PBS using a peristaltic pump (Behr PLP 380; speed: 25rpm). The eyes were enucleated, the retinas explanted and post-fixed with 4% (w/v) PFA in PBS for 30 minutes. Retinas were washed in PBS. For

cryoprotection, the tissue was transferred to 30% (w/v) sucrose (Sigma; 84097) in PBS and incubated overnight at 4°C. To increase antibody permeability, retinas were frozen over dry-ice and thawed at room temperature for three cycles before starting immunostaining.

2.34 Immunohistochemistry

Retinas were incubated with blocking solution containing 1% (w/v) BSA (Sigma; A9418), 5% (v/v) Triton X-100 (Sigma; T8787), 0.5% (w/v) sodium azide (VWR; 786-299), and 10% (v/v) donkey serum (Millipore; S30) for 1 hour at room temperature on a shaker. Afterwards, the samples were immunostained with primary antibodies for 48 hours on a shaker at 4°C. Antibodies were diluted in antibody solution containing 1% (w/v) bovine serum albumin, 5% (v/v) Triton X-100, 0.5% (v/v) sodium azide, and 3% (v/v) donkey serum. The following primary antibodies were used: rat anti-CD68 (AbD Serotec; MCA1957; clone FA-11; LOT: 1807; 1:250); goat anti-Iba1 (Abcam; ab5076; LOT: FR3288145-1; 1:250); and rabbit anti-HA (Cell Signaling Technology; 3724T; LOT: 9; 1:500). Samples were then washed 3 times with PBS for 30 minutes each. Next, the tissue was incubated with secondary antibodies diluted in antibody solution for 2 hours at room temperature on a shaker and protected from light. The secondary antibodies raised in donkey were purchased from Thermo Fisher (Alexa Fluor 568; Alexa Fluor 647; Alexa Fluor 650; 1:2000). The tissue was again washed 3 times with PBS. Nuclei were labeled with Hoechst 33342 (Thermo Fisher; H3570; 1:5000) in PBS for 15 minutes. Retinas were briefly washed in PBS and mounted on microscope glass slides (Assistant; 42406020) with glass coverslips (#1.5) using antifade solution.
Images were subsequently acquired from the periphery of flat mounted retinas with an upright Zeiss LSM800 using a Plan-Apochromat 40x oil immersion objective (N.A. 1.4). A 2x2 tile scan was acquired with a resolution of 0.156 x 0.156 x 0.250µm in x, y, and z, respectively.

2.35 Microglial CD68 analysis through surface rendering

Confocal images were loaded into Fiji 1.52e (http://imagej.net/Fiji). The rolling ball algorithm was used for background removal with the radius set to 15 pixels for the CD68 channel, and 50 pixels for the Iba1 channel. Images were further processed with a 3x3x3 median filter. Image stacks were exported as .tif files, converted to .ims files using the Imaris converter, and imported into Imaris 8.4.2. (Bitplane Imaris). For each image, two separate surface renderings were generated on the microglia (Iba1) and CD68 channel using the Imaris surface rendering module. Surfaces were generated with the surface detail set to 0.2µm. The surface-surface coloc plugin was then used to obtain a third surface object of CD68 exclusively located within microglia. The total percentage of microglial CD68 per image was calculated from the surface volumes of the following renderings:

$$Microglial\ CD68\ (\%) = \frac{Total\ surface\ volume\ of\ CD68\ within\ microglia * 100}{Total\ surface\ volume\ of\ microglia}$$

2.36 List of reagents and antibodies

Detailed information on utilized reagents and antibodies is provided in **Table 4.**

Table 4: Reagents and antibodies.

Reagent	Manufacturer	Stock preparation
Protease inhibitor mix set 1	Calbiochem; 539131	100X stock in Milli-Q water; single-use aliquots; -20°C for 1 month maximum
Phosstop	Sigma; 4906845001	1 tablet per 10ml
NaF	Sigma; S7920	100mM stock in Milli-Q water; stored in plastic tubes; room temperature
Na_3VO_4	Sigma; 450243	100mM stock in Milli-Q water; activated and adjusted to pH 10; single-use aliquots; -20°C
IGEPAL CA-630	Sigma; I3021	Ready-to-use solution
Sodium dodecyl sulfate (SDS)	Sigma; 75746	10% (w/v) stock in Milli-Q water; room temperature
Ammonium persulfate (APS)	Sigma; A3678	10% (w/v) stock in Milli-Q water; single-use aliquots; -20°C
TEMED	Bio-Rad; 161-0800	Ready-to-use solution
Tween 20	Sigma; P9416	Ready-to-use solution
30% acrylamide mix	Bio-Rad; 1610154	Ready-to-use solution
Dithiothreitol (DTT)	Sigma; 10197777001	-
Tris base	Sigma; T1503	-
Glycine	Sigma; G8898	-
NaCl	Sigma; 793566	-
Bovine serum albumin (BSA)	Sigma; A9418	-
N-acetyl-L-cysteine	Sigma; A9165	5mg/ml stock in PBS; 0.22µm filtered; single-use aliquots; -20°C
Bovine Insulin	Sigma; I6634	2mg/ml stock in 0.01M HCl; 0.22µm filtered; 4°C
Human apo-transferrin	Sigma; T1147	2mg/ml stock in PBS, 0.22µm filtered; single-use aliquots; -20°C
Sodium selenite	Sigma; S5261	0.2mg/ml stock in PBS, 0.22µm filtered; single-use aliquots; -20°C
Human TGF-β2	PepoTech; 100-35B	0.02mg/ml stock in PBS with 0.1% (w/v) BSA; solvent 0.22µm filtered before reconstitution; single-use aliquots; -20°C
Murine IL34	R&D Systems; 5195-ML-010/CF	0.1mg/ml stock in Milli-Q water; solvent 0.22µm filtered before reconstitution; single-use aliquots; -20°C
Ovine wool cholesterol	Sigma; 700000P	1.5mg/ml stock in pure ethanol; single-use aliquots; -20°C
CNO	Abcam; ab141704	10mM stock in PBS; 0.22µm filtered; single-use aliquots; -20°C
Levalbuterol	Sigma; SML0138	10mM stock in PBS; 0.22µm filtered; single-use aliquots; -20°C
Forskolin	Sigma; F3917	10mM stock in DMSO; single-use aliquots; -20°C
NECA	Tocris; 1691	10mM stock in DMSO; single-use aliquots; -20°C
IFNγ	Sigma; SRP3058	10µg/ml stock in PBS with 1% (w/v) BSA; solvent 0.22µm filtered before reconstitution; single-use aliquots; -80°C
IL1β	Thermo Fisher; RIL1BI	10µg/ml stock in PBS with 1% (w/v) BSA; solvent 0.22µm filtered before reconstitution; single-use aliquots; -80°C
Tamoxifen	Sigma; T5648	-
Triton X-100	Sigma; T8787	Ready-to-use solution
Sodium azide	VWR; 786-299	Ready-to-use solution
Paraformaldehyde (PFA)	Sigma; P6148	4% (w/v) in PBS; adjusted to pH 7; 0.22µm filtered; -80°C for long-term storage; 4°C for short-term storage
Heparin	Sigma; H0878	-

Antibody	Manufacturer	Dilution
Mouse anti-VSV-G conjugated to Cy3	Sigma; C7706; LOT: 049M4837V	1:250
Rabbit anti-pERK1/2	Cell Signaling Technology; 9101S; LOT: 30	1:1,000
Rabbit anti-GAPDH	Sigma; ABS16; LOT: 3275069	1:1,000
Donkey anti-rabbit conjugated to HRP	GE Healthcare; NA934V; LOT: 16976257	1:10,000
Rat anti-CD68	AbD Serotec; MCA1957; clone FA-11; LOT: 1807	1:250

Antibody	Manufacturer	Dilution
Goat anti-Iba1	Abcam; ab5076; LOT: FR3288145-1	1:250
Rabbit anti-HA	Cell Signaling Technology; 3724T; LOT: 9	1:500
Donkey anti-goat conjugated to Alexa Fluor 568	Thermo Fisher; A11057	1:2,000
Donkey anti-rabbit conjugated to Alexa Fluor 647	Thermo Fisher; A31573	1:2,000
Donkey anti-rat conjugated to Alexa Fluor 650	Thermo Fisher; SA5-10029	1:2,000

2.37 Statistical analysis

All analyses were performed with *R*. Data were collected in excel files and imported into R via the *xlsx* or *readxl* package. Linear regression models were generated with the *lme4* package [67] and after changing the default contrast for unordered variables (*e.g.* experimental condition) to "contr.sum". This allows to run type III Anova on the model to evaluate the overall contribution of unordered effects on the response variable. Post-hoc tests were performed via the *multcomp* package [68] with default parameters. If not otherwise indicated, all possible pairwise comparisons were performed. Significance levels are indicated by asterisks ($p^{n.s.} > 0.05$; $p^{*} \leq 0.05$; $p^{**} \leq 0.01$; $p^{***} \leq 0.001$). Details about statistical models are provided in the individual sections below. **Supplementary Table S5** summarizes the test parameters for each graph. All graphs for data visualization were generated with the *ggplot2* package. Error bars or ribbons represent either standard error of the mean (SEM) calculated by the "mean_se" function (part of *hmisc* package; called through *ggplot2*) or show 95% confidence intervals around a smoothed line generated by the "geom_smooth" function (called through *ggplot2*; using the "loess" method for fitting).

2.37.1 Real-time measurement of increases in cAMP levels upon ligand treatment

We used linear regression to predict the log-transformed luminescence values (baseline-normalized) by an interaction of Time (repeated measurements at regular intervals) and Experimental condition, which is an interaction of Treatment period (Baseline or Ligand), Receptor (GPCR or Empty vector), Ligand (CNO or Levalbuterol) and Concentration (0.01µM, 0.1µM, 1µM or 10µM). A random effect (Experimental repetition) was included to account for the dependency of data, which results from repeated measurements within each individual experiment. This model was used to test whether ligand treatment of individual Receptor-Ligand-Concentration interactions results in significant differences from the baseline measurement.

Table 5: Statistical analysis of cAMP increase.

Real-time measurement of increases in cAMP levels upon ligand treatment	
Model	model <- lmer(log(Value) ~ Time * Experimental condition + (1|Experimental repetition), data = Data, REML = TRUE)
Value	Baseline-normalized luminescence values.
Time	Numerical variable representing time points of measurements. Time is given in minutes (*e.g.* for measurements with a 1min interval: 1, 2, 3, …).
Experimental condition	Interaction term of Treatment period (Baseline or Ligand), Receptor (GPCR or Empty vector), Ligand (CNO or Levalbuterol) and Concentration (0.01µM, 0.1µM, 1µM, or 10µM). This generates the following conditions: • Baseline:DREADD-β2AR_CNO_0.01µM • Ligand:DREADD-β2AR_CNO_0.01µM • Baseline:DREADD-β2AR_CNO_0.1µM • Ligand:DREADD-β2AR_CNO_0.1µM • Baseline:DREADD-β2AR_CNO_1µM • Ligand:DREADD-β2AR_CNO_1µM • Baseline:DREADD-β2AR_CNO_10µM • Ligand:DREADD-β2AR_CNO_10µM • Baseline:Empty vector_CNO_10µM • Ligand:Empty vector_CNO_10µM • Baseline:hM3Dq_CNO_10µM • Ligand:hM3Dq_CNO_10µM • Baseline:rM3Ds_CNO_10µM • Ligand:rM3Ds_CNO_10µM • Baseline:hM4Di_CNO_10µM • Ligand:hM4Di_CNO_10µM • Baseline:β2AR_Levalbuterol_10µM • Ligand:β2AR_Levalbuterol_10µM • Baseline:Empty vector_Levalbuterol_10µM • Ligand:Empty vector_Levalbuterol_10µM • Baseline:DREADD-GPR65_CNO_10µM • Ligand:DREADD-GPR65_CNO_10µM
Experimental repetition	Random effect accounting for the dependency of data due to repeated measurements.
Data	A single data frame containing all data recorded between time points 15 to 60 (minutes).
Posthoc contrasts	For each interaction of Receptor-Ligand-Concentration we separately compared the two Treatment periods with each other: • Baseline vs. Ligand

2.37.2 Baseline cAMP levels in the absence of ligand (constitutive activity)

We used a two-sided one-sample T-test to investigate whether ligand-treated conditions are significantly different from a value of 1, which represents the empty vector control of the respective experimental repetition.

Table 6: Statistical analysis of baseline cAMP.

Baseline cAMP levels in the absence of ligand (constitutive activity)	
Model	model <- t.test(Value, mu = 1, alternative = "two.sided", data = Subset)
Value	Average fold change between ligand treatment and empty vector control (which is 1) during 30 minutes of real-time baseline recording.
Subset	Data subset representing a certain GPCR. This includes the following subsets: • hM3Dq • rM3Ds • hM4Di • DREADD-β2AR • β2AR • DREADD-GPR65 • DREADD-GPR109A

2.37.3 SRE reporter assay

We used a two-sided one-sample T-test to investigate whether ligand-treated conditions are significantly different from a value of 1, which represents either the vehicle control or the empty vector control of the respective experimental repetition.

Table 7: Statistical analysis of SRE reporter activity.

SRE reporter assay with ligand treatment	
With ligand treatment	
Model	model <- t.test(Value, mu = 1, alternative = "two.sided", data = Subset)
Value	Fold change between ligand treatment and vehicle control (which is 1).
Subset	Data subset representing Receptor (GPCR or Empty vector) treated with a certain Ligand (CNO or Levalbuterol). This includes the following subsets: • hM3Dq_CNO • rM3Ds_CNO • hM4Di_CNO • DREADD-β2AR_CNO • Empty vector_CNO • β2AR_Levalbuterol • Empty vector_Levalbuterol • DREADD-GPR65_CNO • DREADD-GPR109A_CNO
Without ligand treatment (constitutive activity)	
Model	model <- t.test(Value, mu = 1, alternative = "two.sided", data = Subset)
Value	Fold change between ligand treatment and empty vector control (which is 1).
Subset	Data subset representing a certain GPCR. This includes the following subsets: • hM3Dq • rM3Ds • hM4Di • DREADD-β2AR • β2AR • DREADD-GPR65 • DREADD-GPR109A

2.37.4 Real-time assay measurement of β-arrestin 2 recruitment

We used linear regression to predict luminescence values (normalized to baseline and further to the respective vehicle control) by and interaction of Time (repeated measurements at regular intervals) and Experimental condition, which is an interaction of Treatment period (Baseline or Ligand) and Receptor (β2AR-SmBiT or DREADD-β2AR-SmBiT). A random effect (Experimental repetition) was included to account for the dependency of data, which results from repeated measurements within each individual experiment. This model was used to test whether ligand treatment of each Receptor results in significant differences from the baseline measurement.

Table 8: Statistical analysis of GPCR interaction with β-arrestin 2.

Real-time assay measurement of β-arrestin 2 recruitment upon ligand treatment	
Model	model <- lmer(Value ~ Time * Experimental condition + (1|Experimental repetition), data = Data, REML = TRUE)
Value	Baseline- and vehicle control-normalized luminescence values.
Time	Numerical variable representing time points of measurements. Time is given in minutes (*e.g.* for measurements with a 1min interval: 1, 2, 3, etc.)
Experimental condition	Interaction term of Treatment period (Baseline or Ligand) and Receptor (β2AR-SmBiT, DREADD-β2AR-SmBiT, DREADD-GPR65-SmBiT, or DREADD-GPR109A-SmBiT). This generates the following conditions: • Baseline:β2AR-SmBiT • Ligand:β2AR-SmBiT • Baseline:DREADD-β2AR-SmBiT • Ligand: DREADD-β2AR-SmBiT • Baseline:DREADD-GPR65-SmBiT • Ligand: DREADD-GPR65-SmBiT • Baseline:DREADD-GPR109A-SmBiT • Ligand: DREADD-GPR109A-SmBiT
Experimental repetition	Random effect accounting for the dependency of data due to repeated measurements.
Data	A single data frame containing all data.
Posthoc contrasts	For each Receptor we separately compared the two Treatment periods with each other: • Baseline vs. Ligand

2.37.5 Western blot to quantify ERK1/2 phosphorylation

We used linear regression to predict ratios between pERK1/2 and GAPDH by Experimental condition, which represents different treatment durations (untreated, 2min, 5min, or 15min). A random effect (Experimental repetition) was included to account for the dependency of data that are derived from the same experimental repetition.

To analyze basal ERK1/2 phosphorylation in untreated samples, we used a two-sided two-sample T-test and compared GPCR- with empty vector-transfected conditions.

Table 9: Statistical analysis of Western blots.

Western blot to quantify ERK1/2 phosphorylation	
Evaluating ERK1/2 phosphorylation after ligand treatment	
Model	model <- lmer(Value ~ Experimental condition + (1|Experimental repetition), data = Subset, REML = TRUE)
Value	Ratio between pERK1/2 and GAPDH.
Experimental condition	A factor with four levels (untreated, 2min, 5min, or 15min) describing the treatment duration.
Experimental repetition	Random effect accounting for the dependency of data within experimental repetitions.
Subset	Data subset containing all experiments of a certain receptor and ligand. This includes the following subsets: • β2AR_Levalbuterol • Empty vector_Levalbuterol • DREADD-β2AR_CNO • Empty vector_CNO
Posthoc contrasts	Each condition was compared with the untreated control condition. • untreated vs. 2min • untreated vs. 5min • untreated vs. 15min
Evaluating basal ERK1/2 phosphorylation in untreated samples	
Model	model <- t.test(Value ~ Experimental condition, alternative = "two.sided", data = Subset)
Value	Ratio between pERK1/2 and GAPDH.
Experimental condition	A factor with two levels (GPCR or Empty vector) describing whether cells have been transfected with GPCR or Empty vector.
Subset	Data subset of GPCR and Empty vector analysed with Western blot on the same gels. This includes the following subsets: • DREADD-β2AR and Empty vector • β2AR and Empty vector

2.37.6 GPCR internalization assay

We used linear regression to predict internalized area in μm^2 (measured individually per cell based on thresholded VSV-G signal) by Experimental condition, which is an interaction of Ligand (CNO or Vehicle) and Treatment period (0min, 15min, 30min or 60min). This model was used to test whether CNO treatment shows significant differences from vehicle controls at corresponding Treatment periods.

Table 10: Statistical analysis of ligand-induced GPCR internalization.

GPCR internalization assay	
Model	model <- lm(Value ~ Experimental condition, data = Data)
Value	Internalized area in μm^2 per cell based on thresholded VSV-G signal.
Experimental condition	Interaction term of Ligand (CNO or Vehicle) and Treatment period (Baseline, 15min, 30min or 60min). This generates the following conditions: • Baseline • Vehicle 15min • Vehicle 30min • Vehicle 60min • CNO 15min • CNO 30min • CNO 60min
Data	A single data frame containing all data.
Posthoc contrasts	We compared CNO and Vehicle treatment at matched Treatment periods: • CNO 15min vs. Vehicle 15min • CNO 30min vs. Vehicle 30min • CNO 60min vs. Vehicle 60min

2.37.7 Real-time measurement of decreases in cAMP levels upon ligand treatment

We used linear regression to predict the log-transformed luminescence values (normalized to baseline and further to the respective vehicle control) by Experimental condition, which is an interaction of Treatment period (Baseline, Ligand or Forskolin) and Receptor (GPCR or Empty vector). A random effect (Experimental repetition) was included to account for the dependency of data, which results from repeated measurements within each individual experiment. This model was used to test Receptor and Empty vector for significant differences between their three Treatment periods. The time intervals of repeated measurements were not included as a predictor in the model as it was not necessary to improve the fit. This is because measured values are rather uniformly distributed within the three different Treatment periods, meaning that this variably can already explain most of the variability in the data.

Table 11: Statistical analysis of cAMP decrease.

Real-time measurement of decreases in cAMP levels upon ligand treatment	
Model	model <- lmer(log(Value) ~ Experimental condition + (1|Experimental repetition), data = Data, REML = TRUE)
Value	Baseline- and vehicle control-normalized luminescence values.
Experimental condition	Interaction term of Treatment period (Baseline, Ligand, or Forskolin) and Receptor (GPCR or Empty vector). This generates the following conditions: • Baseline:DREADD-GPR109A • Ligand:DREADD-GPR109A • Forskolin:DREADD-GPR109A • Baseline:Empty vector • Ligand:Empty vector • Forskolin:Empty vector
Experimental repetition	Random effect accounting for the dependency of data due to repeated measurements.
Data	A single data frame containing all data.
Posthoc contrasts	For each Receptor we separately compared the three Treatment periods among each other: • Baseline vs. Ligand • Baseline vs. Forskolin • Ligand vs. Forskolin

2.37.8 CRE reporter assay

We used a two-sided one-sample T-test to investigate whether ligand-treated conditions are significantly different from a value of 1, which represents the vehicle control of the respective experimental repetition.

Table 12: Statistical analysis of CRE reporter activity.

CRE reporter assay with ligand treatment	
Model	model <- t.test(Value, mu = 1, alternative = "two.sided", data = Subset)
Value	Fold change between ligand-treatment and vehicle control (which is 1).
Subset	Data subset representing Receptor (GPCR or Empty vector) treated with a certain Ligand (CNO or Levalbuterol). This includes the following subsets: • DREADD-GPR109A • Empty vector

2.37.9 Live imaging of primary microglia

We used linear regression to model the change of total cell area in μm^2 by using an interaction of the two predictors Time and Experimental condition. Experimental condition itself is an interaction of Treatment period (Baseline or Ligand) and Experimental group (Non-transduced_Levalbuterol, DREADD-β2AR_CNO, Non-transduced_Vehicle, or Non-transduced_CNO). A random effect (Cell ID) was included to account for the dependency of data, which results from repeated measurements on individual cells. This random effect also accounts for size differences between cells. This model was used to test for significant differences between the two Treatment periods within each Experimental group.

Alternatively, we also compared Experimental groups with each other within designated Time points (1, 5, 10, 25, 40, 55min). For this, we used baseline-normalized values as response variable and an interaction of Time point and Experimental group as predictor. No random effect was included. This linear model was used to test for significant differences between the four Experimental groups within each Time point.

Table 13: Statistical analysis of filopodia induction in primary microglia.

Live imaging of primary microglia	
Model	model <- lmer(Value ~ Time * Experimental condition + (1|Cell ID), data = Data, REML = TRUE)
Value	Total cell area in μm^2.
Time	Numerical variable representing time points of measurements included in the analysis: 1, 5, 10, 25, 40, and 55min.
Experimental condition	Interaction term of Treatment period (Baseline or Ligand) and Experimental group (Non-transduced_Levalbuterol, DREADD-β2AR_CNO, Non-transduced_Vehicle, or Non-transduced_CNO). This generates the following conditions: • Baseline:Non-transduced_Levalbuterol • Ligand: Non-transduced_Levalbuterol • Baseline:DREADD-β2AR_CNO • Ligand:DREADD-β2AR_CNO • Baseline:Non-transduced_Vehicle • Ligand: Non-transduced_Vehicle • Baseline:Non-transduced_CNO • Ligand: Non-transduced_CNO
Cell ID	Random effect accounting for the dependency of data due to repeated measurements on the same cell. Also accounts for size differences between cells.
Data	A single data frame containing all data at the 1, 5, 10, 25, 40, and 55min time points.
Posthoc contrasts	Within each Experimental group we compared the two Treatment periods with each other: • Baseline vs. Ligand
Alternative comparison between experimental conditions within each time point	
Model	model <- lm(Value ~ Experimental group within time point, data = Data)
Value	Baseline-normalized cell area (measured in μm^2). Normalized values were obtained by dividing area of each cell through its mean during the baseline recording period.
Experimental group within time point	Interaction term of Time point (1, 5, 10, 25, 40, and 55min) and Experimental group (Non-transduced_Levalbuterol, DREADD-β2AR_CNO, Non-transduced_Vehicle, or Non-transduced_CNO). This generates the following conditions: • 1min:Non-transduced_Levalbuterol • 1min:DREADD-β2AR_CNO • 1min:Non-transduced_Vehicle • 1min:Non-transduced_CNO • 5min:Non-transduced_Levalbuterol • 5min:DREADD-β2AR_CNO • 5min:Non-transduced_Vehicle • 5min:Non-transduced_CNO • 10min:Non-transduced_Levalbuterol • 10min:DREADD-β2AR_CNO • 10min:Non-transduced_Vehicle • 10min:Non-transduced_CNO • 25min:Non-transduced_Levalbuterol • 25min:DREADD-β2AR_CNO • 25min:Non-transduced_Vehicle • 25min:Non-transduced_CNO • 40min:Non-transduced_Levalbuterol • 40min:DREADD-β2AR_CNO • 40min:Non-transduced_Vehicle • 40min:Non-transduced_CNO • 55min:Non-transduced_Levalbuterol • 55min:DREADD-β2AR_CNO • 55min:Non-transduced_Vehicle • 55min:Non-transduced_CNO
Data	A single data frame containing all data at the 1, 5, 10, 25, 40, and 55min time points.
Posthoc contrasts	Within each Time point we performed all pairwise comparisons between the four Experimental groups.

2.37.10 Gene expression profiling in HMC3 cells using RT-qPCR

We used a two-sided one-sample T-test to confirm that recombinant cytokine stimulation induces inflammatory gene expression. We compared the linear fold change of stimulated conditions to a value of 1, which represents the untreated control of the respective experimental repetition. For further comparison of different treatment conditions, we used linear regression. We predicted ddCq values for individual transcripts by Experimental condition, which represents the treatment with different compounds alone or in combination. A random effect (Experimental repetition) was included to account for the dependency of data derived from the same experimental repetition. Separate models were generated for each investigated transcript (IL6, TNF and IL1β) and cell line (non-transduced, DREADD-β2AR, DREADD-GPR65, and DREADD-GPR109A). These models were used to test for significant differences between different treatments.

Table 14: Statistical analysis of RT-qPCR data.

Gene expression profiling in HMC3 cells using RT-qPCR	
Confirming induction of inflammatory gene expression upon recombinant cytokine stimulation	
Model	model <- t.test(Value, mu = 1, alternative = "two.sided", data = Subset)
Value	Linear fold change compared to untreated control (which is 1).
Subset	Data subset for one transcript. This includes the following subsets: • IL6 • TNF • IL1β
Further comparison of different treatment conditions	
Model	model <- lmer(Value ~ Experimental condition + (1|Experimental repetition), data = Subset, REML = TRUE)
Value	ddCq values.
Experimental condition	A factor with three levels for each investigated combination of compounds. There are three treatment sets used to investigate the effect of either Levalbuterol (LB), CNO, or forskolin (FSK), on IFNγ/IL1β-induced gene expression:
	Treatment set 1: LB, IFNγ/IL1β, IFNγ/IL1β+LB
	Treatment set 2: CNO, IFNγ/IL1β, IFNγ/IL1β+CNO
	Treatment set 3: FSK, IFNγ/IL1β, IFNγ/IL1β+FSK
Experimental repetition	Random effect accounting for the dependency of data within experimental repetitions.
Subset	Data subset for one transcript, one cell line and one treatment set. This includes the following subsets: • IL6:Non-transduced_LB • TNF:Non-transduced_LB • IL1β:Non-transduced_LB • IL6:Non-transduced_CNO • TNF:Non-transduced_CNO • IL1β:Non-transduced_CNO • IL6:Non-transduced_FSK • TNF:Non-transduced_FSK • IL1β:Non-transduced_FSK • IL6:DREADD-β2AR_CNO • TNF:DREADD-β2AR_CNO • IL1β:DREADD-β2AR_CNO • IL6:DREADD-GPR65_CNO • TNF:DREADD-GPR65_CNO • IL1β:DREADD-GPR65_CNO • IL6:DREADD-GPR109A_CNO • TNF:DREADD-GPR109A_CNO • IL1β:DREADD-GPR109A_CNO
Posthoc contrasts	All pairwise comparisons within the respective treatment set were performed.

2.37.11 Next generation mRNA sequencing of HMC3 cells

We used *DESeq2* [63] to model gene expression and included Experimental repetition and Experimental condition as predictor variables. Experimental repetition accounts for sample dependencies and batch effects. Experimental condition is an interaction of cell line and treatment. One model was generated for the entire data set and desired comparisons were subsequently extracted by setting contrasts for the Experimental conditions to be tested against each other. The results are provided in **Supplementary Table S2**.

2.37.12 Microglial CD68 during optic nerve crush

We used linear regression to predict microglial CD68 (based on surface renderings) by Experimental condition, which is an interaction of Genotype (hM4Di or Wild type) and Treatment (CNO or saline). This model was used to test whether CNO treatment of hM4Di-expressing animals shows significant differences from saline-injected animals or CNO-treated wild types. Separate models were generated for the crushed and non-crushed retina.

Table 15: Statistical analysis of CD68 immunostainings.

Microglial CD68 after optic nerve crush	
Model	model <- lm(Value ~ Experimental condition, data = Subset)
Value	Percentage of CD68 in microglia based on surface renderings.
Experimental condition	Interaction term of Genotype (hM4Di or Wild type) and Treatment (CNO or saline). This generates the following conditions: • hM4Di:Saline • hM4Di:CNO • Wild type:CNO
Subset	Data subset representing the crushed or non-crushed retina. This includes the following subsets: • Crushed • Non-crushed
Posthoc contrasts	All pairwise comparisons within the respective subset were performed.

3 Results

3.1 Identifying GPCRs-of-interest in microglia

Microglia are tissue-resident macrophages of the central nervous system. They maintain homeostasis during physiological conditions and induce an inflammatory response upon tissue damage and pathogen encounter [69,70]. GPCRs are critical for these functions as they allow fast adaption to local perturbations. To identify which GPCRs are selectively enriched in microglia, we compared GPCR expression across different cell types in a previously established retina transcriptome database [46]. We found approximately one-third of the most abundant GPCRs enriched in microglia, which also included the well-defined β2-adrenergic receptor (β2AR) [9–11,44,45,71], making it a prime candidate for establishing our strategy (**Fig.2**).

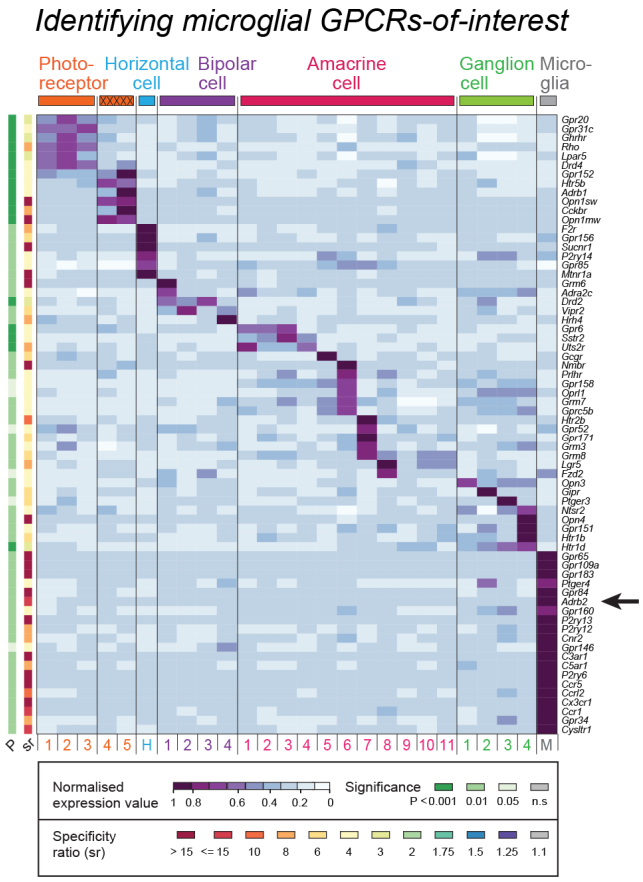

Figure 2: Discovering microglial GPCRs-of-interest.
a: GPCR gene expression analysis across different cell types in the mouse retina. Columns represent distinct cell types and show clusters of selectively enriched GPCRs. Purple indicates high gene expression. *P*-value and specificity ratio (s.r.) are color-coded as indicated in the figure and described in Siegert *et al.* [46]. Arrow points to β2AR/ADRB2.

3.2 Establishing a library for *in-silico* design of DREADD-based GPCR chimeras

To design DREADD-based chimeras, we first identified GPCR ligand binding domains, including N-terminus, extracellular loops (ECLs) and transmembrane helices (TMs), and GPCR signaling domains, comprising intracellular loops (ICLs) and C-terminus (**Fig.3a**). This allows us to generate CNO-responsive chimeras for a GPCR-of-interest by exchanging the corresponding ICLs and C-termini (**Fig.3b**, **Supplementary Table S1**). To accomplish this, we performed multiple protein sequence alignment using the established domains of bovine rhodopsin (RHO) from *Airan et al.* [27] as reference. We aligned rhodopsin with the CHRM3-based hM3Dq, human β2-adrenergic receptor (β2AR), and 292 other potential GPCRs-of-interest (**Fig.3c**). As internal controls, we included human α1-adrenergic receptor (hα1AR) and hamster β2-

adrenergic receptor (hamβ2AR) and confirmed that our alignment successfully reproduced the rhodopsin-based chimeras from *Airan et al.* [27]. To further verify alignment accuracy, we utilized the TMHMM algorithm, which predicts TM domains in a protein sequence [48]. We expected that predicted TMs will tightly flank the ICLs and C-termini identified by our alignment. Indeed, this was the case for all GPCRs shown in **Figure 3c** and **Figure 4**. The only exception was GPR109A, where TMHMM failed to identify the seventh TM with sufficient certainty. Occasionally, minor deviations from seamless flanking occurred but were within the observed range for the reference and internal controls (**Figure 4**).

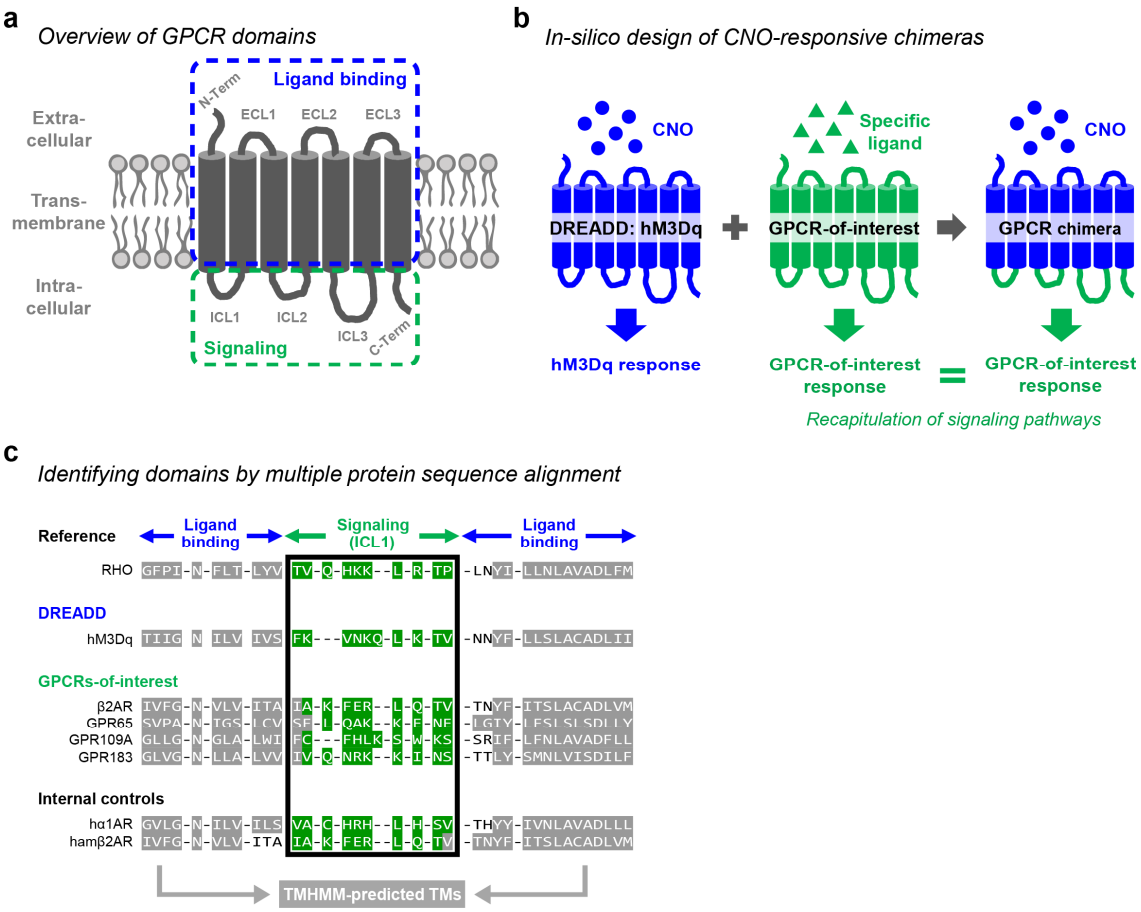

Figure 3: GPCR domains can be identified *in-silico* to engineer chimeric receptors.
a-b: Schematic of GPCR domains and chimera design. **a:** GPCRs consist of seven transmembrane domains, three extracellular loops (ECL1-3), three intracellular loops (ICL1-3), the N-terminus (N-Term) and C-terminus (C-Term). Ligand binding (blue) involves extracellular and transmembrane domains and consequently triggers conformational changes, which are transmitted to intracellular domains for induction of signaling cascades (green). **b:** The intracellular domains of hM3Dq (blue) are replaced with the intracellular domain of a GPCR-of-interest (green), generating a chimeric receptor that induces the signaling cascade of the GPCR-of-interest (green) upon CNO stimulation. **c:** Zoomed-in view on the multiple protein sequence alignment. Bovine rhodopsin (RHO) served as reference [27] to identify ligand binding and signaling domains of CHRM3-based hM3Dq, the human β2-adrenergic receptor (β2AR), three out of 292 GPCRs-of-interest (see **Supplementary Table S1**), human α1-adrenergic receptor (hα1AR) and hamster β2-adrenergic receptor (hamβ2AR). In grey: TMHMM-predicted transmembrane helices. In green: signaling domain for the first intracellular loop (ICL1).

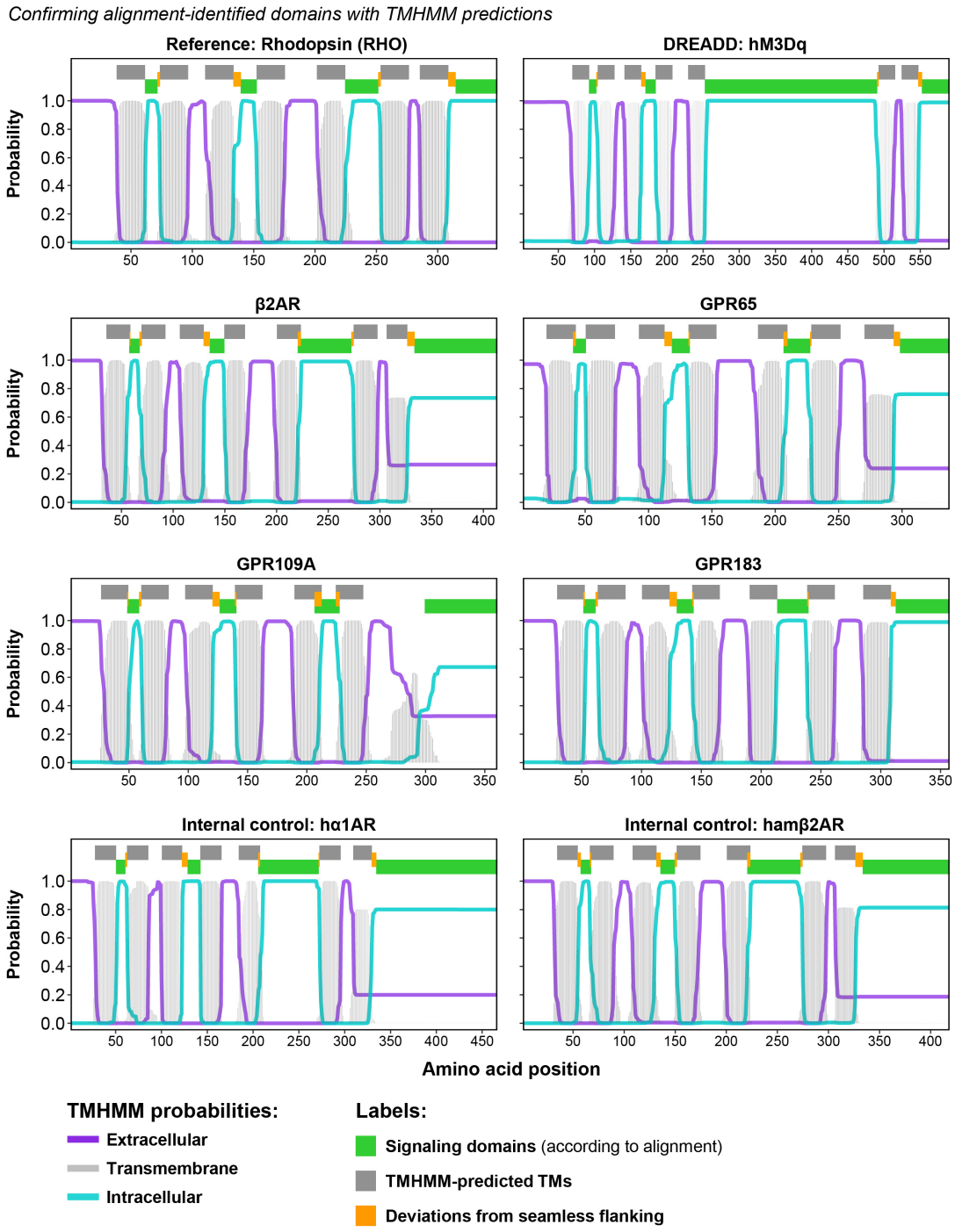

Figure 4: TMHMM-predictions support multiple protein sequence alignment accuracy.
TMHMM probability plots for rhodopsin (RHO), hM3Dq, four representative GPCRs-of-interest, human α1-adrenergic receptor (hα1AR), and hamster β2-adrenergic receptor (hamβ2AR). TMHMM reports the probability that a GPCR sequence is located in the extracellular (purple line), transmembrane (light grey line), or intracellular (light turquoise line) space. The top of each plot shows the results from multiple protein sequence alignment from N- to C-terminus. Alignment-identified intracellular signaling domains (green bars) were tightly flanked by TMHMM-predicted transmembrane domains (TMs; dark grey bars). Deviations from seamless flanking (orange bars) were minimal and comparable to deviations within the alignment reference (rhodopsin) and internal controls (hα1AR, hamβ2AR).

Finally, we exploited published crystal structures for three key GPCRs: the alignment reference RHO; the DREADD, for which we used rat CHRM3 as surrogate with over 90% sequence similarity; and our primary GPCR-of-interest β2AR. We mapped our identified ligand binding and signaling domains together with predicted TMs on these crystal structures and found that they closely matched the expected extracellular, transmembrane or intracellular locations (**Fig.5**). These results suggest that our alignment correctly predicts GPCR domains and serves as a library for generating DREADD-based GPCR chimeras.

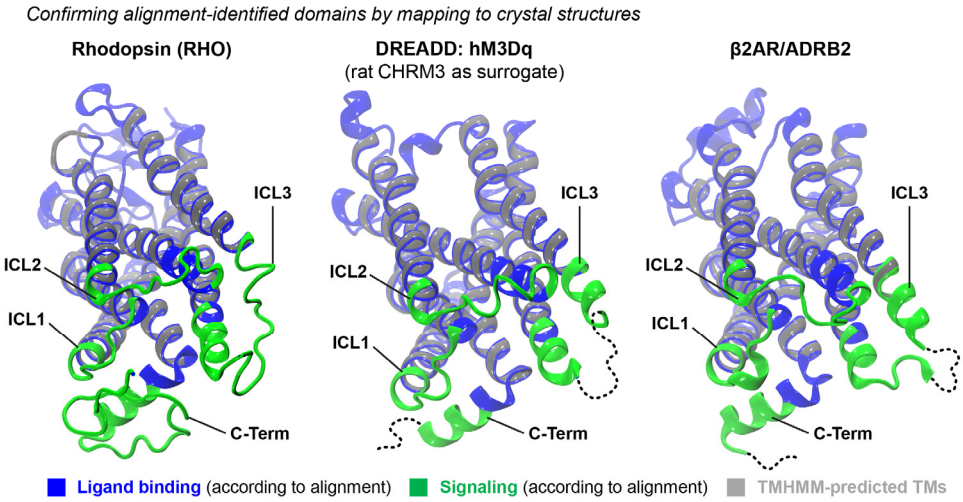

Figure 5: Confirming alignment accuracy on the structural level.
Crystal structures representing bovine RHO, rat CHRM3 as surrogate for hM3Dq, and human β2AR. Ligand binding domains (blue), signaling domains (green), and TMHMM-predicted sequences (grey) are highlighted. Structural representations are rotated with the intracellular domains facing the screen. Dotted lines: sequences not available within the crystal structures.

3.3 Engineering chimeric DREADD-β2AR

Next, we designed our first CNO-inducible GPCR chimera DREADD-β2AR *in-silico* by combining hM3Dq ligand binding and β2AR signaling domains (**Fig.6a**). Additionally, we introduced two modifications to the N-terminus: a hemagglutinin-derived signal peptide [50,51] followed by a VSV-G epitope [52] to probe for cell surface expression. The signal peptide supports co-translational import into the endoplasmic reticulum and subsequent plasma membrane incorporation [50,51]. Neither hM3Dq nor β2AR contain such a peptide sequence according to the SignalP algorithm [49] (**Fig.6b**). When we re-analyzed both GPCRs after introducing our N-terminal modifications *in-silico*, SignalP identified the signal peptide and its cleavage site upstream of the VSV-G tag (**Fig.S6c**).

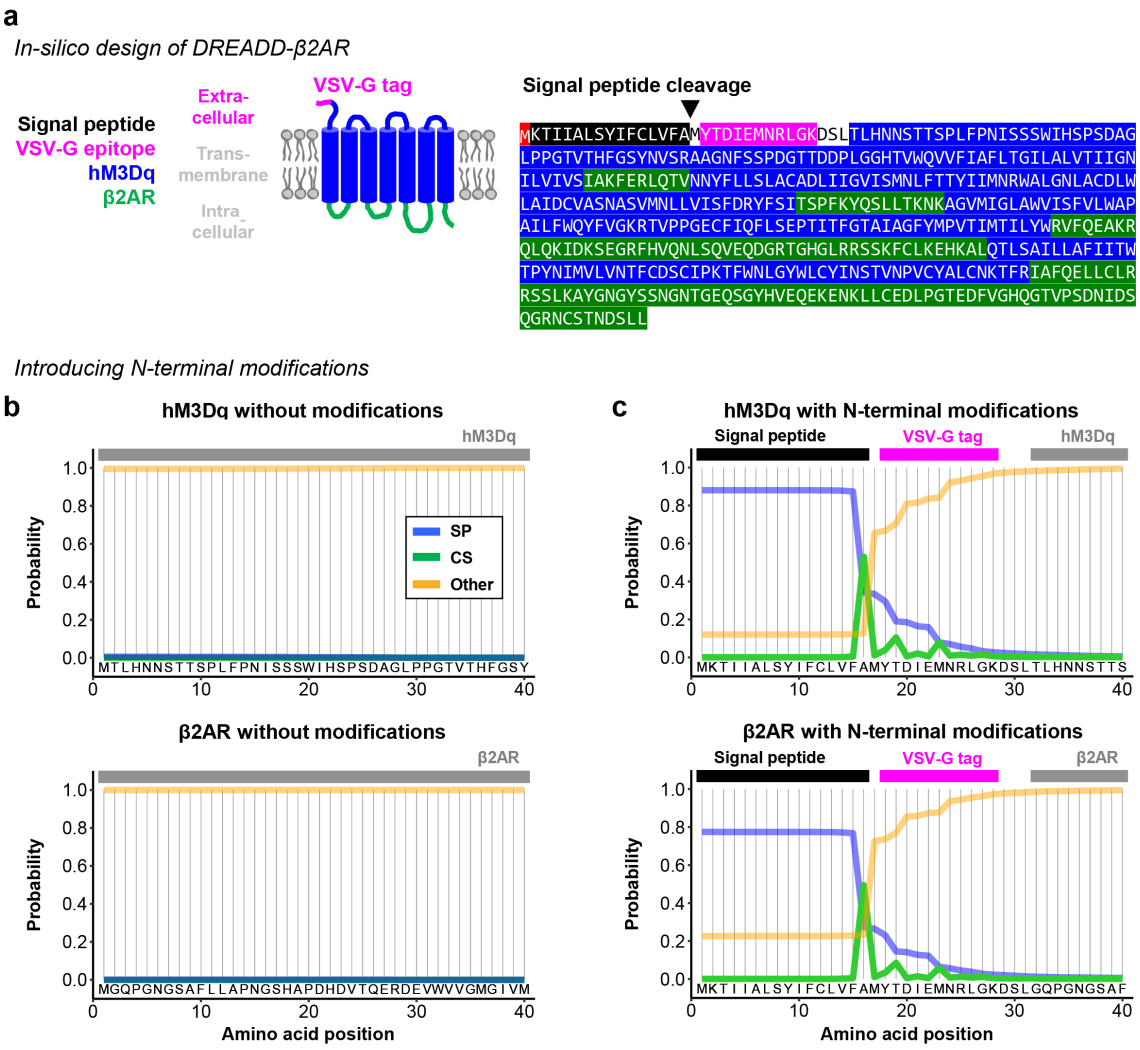

Figure 6: Generating chimeric DREADD-β2AR.
a: Schematic of DREADD-β2AR and corresponding protein sequence encoding for signal peptide (black), VSV-G epitope (magenta), hM3Dq ligand binding domains (blue), and β2AR signaling domains (green). Black arrow: start of the mature GPCR after post-translational cleavage of the signal peptide. **c-d:** SignalP probability plots for hM3Dq (top) and β2AR (below) without any modification (**c**) or with signal peptide and VSV-G epitope tag (**d**). Blue line (SP): probability that sequence belongs to a signal peptide. Green line (CS): probability of signal peptide cleavage. Orange line (Other): probability that sequence does not contain a signal peptide. Grey bar represents protein sequence of either hM3Dq or β2AR.

We synthesized the DREADD-β2AR coding sequence and cloned it into a mammalian expression vector utilizing the ubiquitous CMV promoter. Then, we transfected HEK cells and after 24 hours performed immunostaining for the VSV-G tag under non-permeabilizing conditions. We confirmed that DREADD-β2AR successfully incorporated into the cell membrane based on the strong VSV-G signal (**Fig.7a**), whereas non-transfected HEK cells lacked this staining (**Fig.7b**). For comparison, we also synthesized hM3Dq, non-chimeric β2AR, rM3Ds, and hM4Di containing the same N-terminal modifications. In all cases we detected successful surface expression (**Fig.7c-f**).

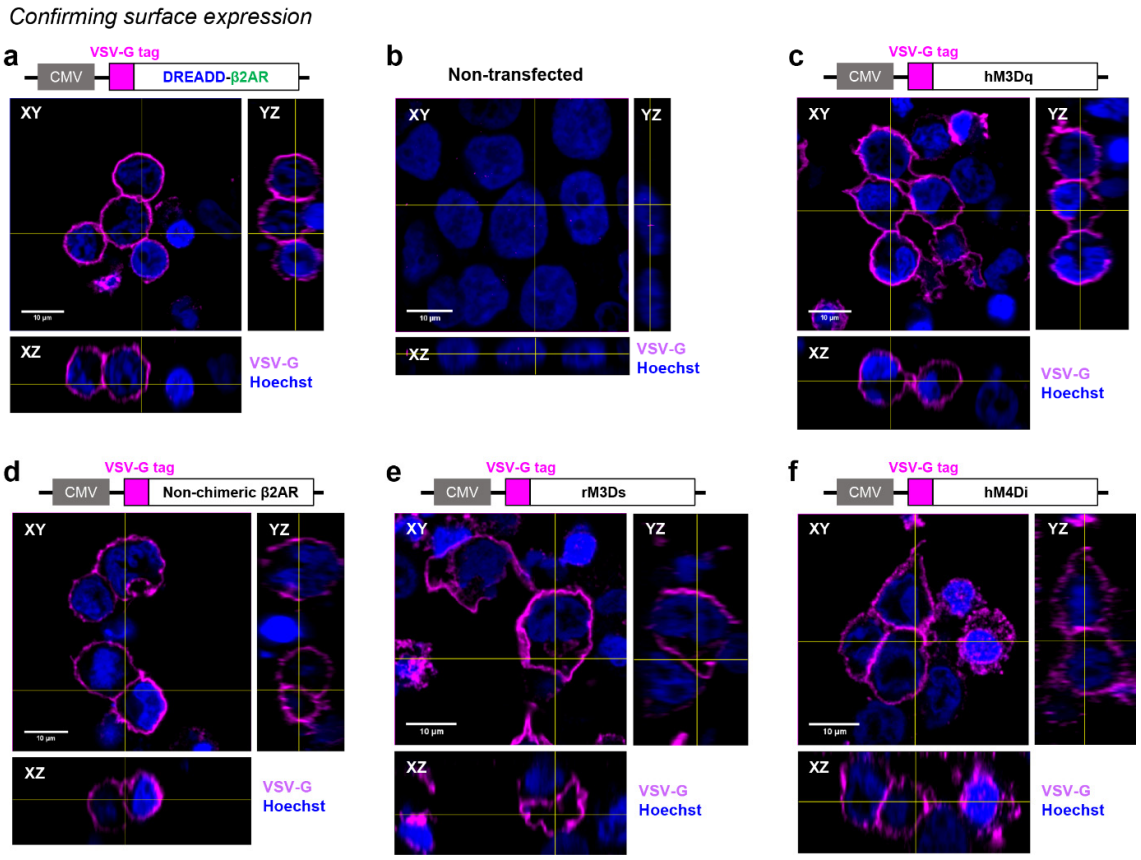

Figure 7: Confirming GPCR surface expression.
a-f: Orthogonal views of HEK cells immunostained for VSV-G tag under non-permeabilizing conditions. Panels show DREADD-β2AR-transfected cells (**a**), non-transfected cells (**b**), and cells transfected with hM3Dq (**c**), non-chimeric β2AR (**d**), rM3Ds (**e**), or hM4Di (**f**). Magenta: VSV-G tag. Blue: nuclear staining with Hoechst. CMV, human cytomegalovirus promoter.

3.4 Functional validation of chimeric DREADD-β2AR

To validate DREADD-β2AR functionality, we investigated whether CNO stimulation mimics the signaling pathways of non-chimeric β2AR as outlined in **Figure 8a**.

3.4.1 Second messenger cascades

First, we focused on the induction of second messenger cascades. β2AR is classically known to recruit $G\alpha_s$ upon ligand binding, resulting in an increase of cytoplasmic cAMP due to adenylyl cyclase (AC) activation [72] (**Fig.8b**). We co-transfected HEK cells with DREADD-β2AR and a modified firefly luciferase that increases luminescence in the presence of cAMP [56]. Indeed, we found a CNO-dose-dependent increase in cAMP with DREADD-β2AR (**Fig.8c**), which was not observed in cells transfected with empty vector backbone. For comparison, we transfected cells with non-chimeric β2AR and applied the selective β2AR-agonist levalbuterol [73,74]. DREADD-β2AR and non-chimeric β2AR elicited a similar fold change around 25 when stimulated with their respective ligand at a 10µM concentration (**Fig.8d**), which we subsequently used for all further assays unless specified otherwise. CNO stimulation of the $G\alpha_q$-coupled hM3Dq only triggered a comparatively minor 2.5-fold increase (**Fig.8e**). As a control, we also included chimeric rM3Ds, which was generated by replacing ICL2-3 of rat-

derived M3Dq with corresponding turkey β1-adrenergic receptor (β1AR) domains to facilitate strong $G\alpha_s$-coupling and induction of cAMP synthesis [43]. As expected, rM3Ds raised cAMP levels upon CNO application, resulting in a 12-fold increase that did not reach the extent of DREADD-β2AR or non-chimeric β2AR (**Fig.8g**). Surprisingly, hM4Di also significantly elevated cAMP by approximately 2.5-fold (**Fig.8e**), even though it is commonly described as $G\alpha_i$-coupled receptor expected to decrease cAMP [39]. Our data suggests that DREADD-β2AR successfully recapitulated the $G\alpha_s$-induced cAMP upregulation of non-chimeric β2AR. Importantly, hM3Dq alone was clearly distinguishable through its marginal impact on cAMP levels, indicating that the DREADD-β2AR response was mediated through properly identified β2AR signaling domains.

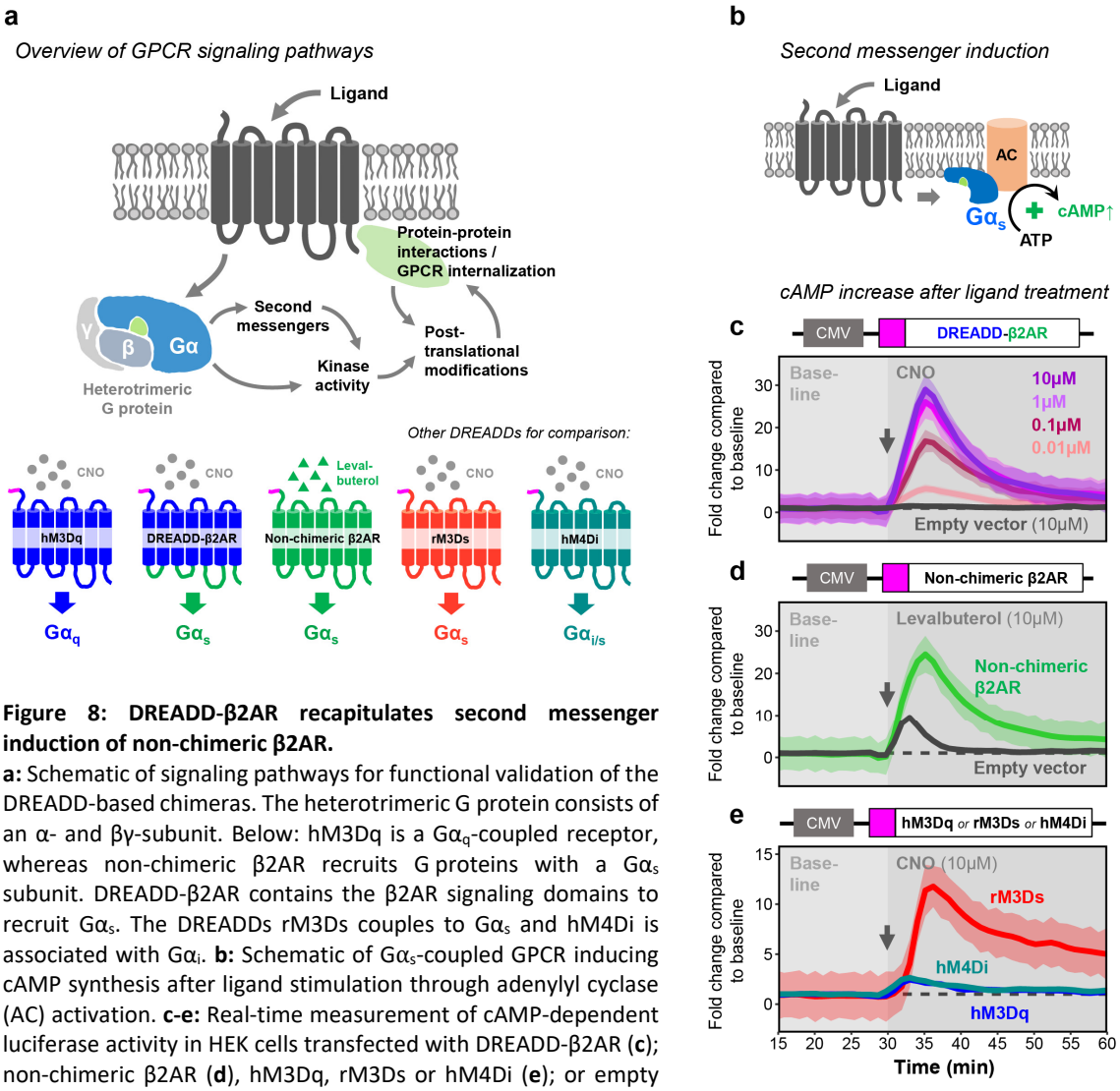

Figure 8: DREADD-β2AR recapitulates second messenger induction of non-chimeric β2AR.
a: Schematic of signaling pathways for functional validation of the DREADD-based chimeras. The heterotrimeric G protein consists of an α- and βγ-subunit. Below: hM3Dq is a $G\alpha_q$-coupled receptor, whereas non-chimeric β2AR recruits G proteins with a $G\alpha_s$ subunit. DREADD-β2AR contains the β2AR signaling domains to recruit $G\alpha_s$. The DREADDs rM3Ds couples to $G\alpha_s$ and hM4Di is associated with $G\alpha_i$. **b:** Schematic of $G\alpha_s$-coupled GPCR inducing cAMP synthesis after ligand stimulation through adenylyl cyclase (AC) activation. **c-e:** Real-time measurement of cAMP-dependent luciferase activity in HEK cells transfected with DREADD-β2AR (**c**); non-chimeric β2AR (**d**), hM3Dq, rM3Ds or hM4Di (**e**); or empty vector (**c-d**). Baseline measurements of 30 minutes (first 15 minutes not shown) followed by ligand application (grey arrow for onset) of either CNO or levalbuterol. Measure of center: Mean fold change compared to baseline mean (dashed line). Ribbons: 95% confidence intervals. N = four (DREADD-β2AR: CNO 0.1-10μM), seven (Empty vector: CNO), four (Non-chimeric β2AR: Levalbuterol; Empty vector: Levalbuterol; hM3Dq: CNO; hM4Di: CNO), or three (rM3Ds: CNO) experimental repetitions.

As a note, HEK cells endogenously express β2AR [75], which explains the partial response of empty vector-transfected cells to levalbuterol. **Figure 9a** shows that endogenous β2AR contributes to cAMP induction in a ligand dose-dependent manner. Additionally, we confirmed that the DREADD-β2AR and rM3Ds responses were both saturated at 10µM CNO (**Fig.9b**). This suggests that the data in **Figure 8c**, **e** reflect maximal cAMP induction capabilities which are higher for DREADD-β2AR when compared to rM3Ds.

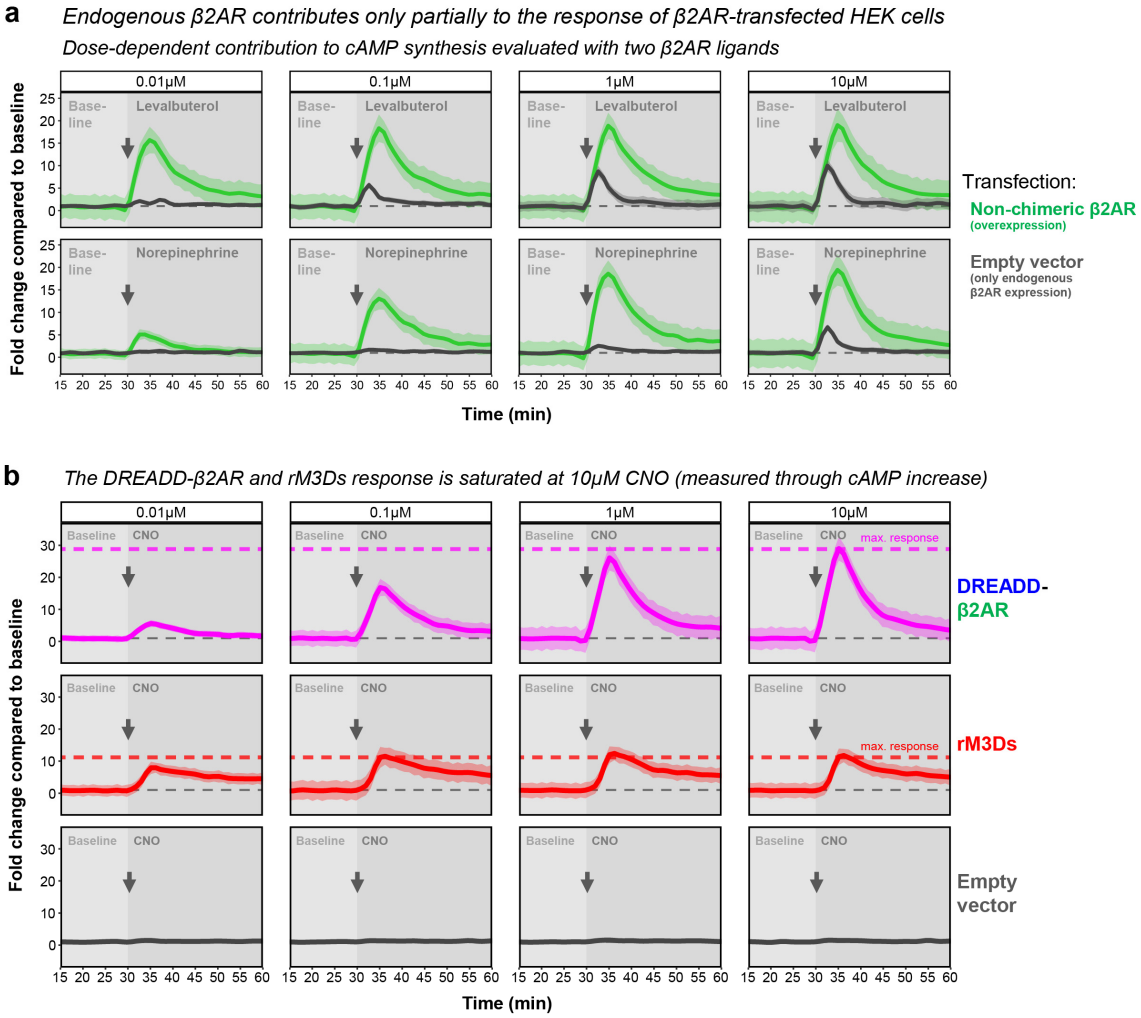

Figure 9: Endogenous β2AR contribution and CNO response of DREADD-β2AR and rM3Ds.
a: Real-time measurement of cAMP-dependent luciferase activity in HEK cells transfected with non-chimeric β2AR (green) or empty vector (grey). Baseline measurements of 30 minutes (first 15 minutes not shown) followed by application of β2AR agonists levalbuterol or norepinephrine (grey arrow for onset). Measure of center: Mean fold change compared to baseline mean (dashed line). Ribbons: 95% confidence intervals. N = three experimental repetitions. **b:** Real-time measurement of cAMP-dependent luciferase activity in HEK cells transfected with DREADD-β2AR (magenta), rM3Ds (red), or empty vector (grey). Baseline measurements of 30 minutes (first 15 minutes not shown) followed by CNO application (grey arrow for onset) at concentrations ranging from 0.01µM to 10µM. Measure of center: Mean fold change compared to baseline mean (grey dashed line). Maximum responses are indicated by magenta (DREADD-β2AR) and red (rM3Ds) dashed lines. Ribbons: 95% confidence intervals. N = four (DREADD-β2AR: all concentrations), three (rM3Ds, all concentrations), six (Empty vector: 0.01-1µM), or seven (Empty vector: 10µM) experimental repetitions.

3.4.2 Kinase activity

Next, we investigated kinase activity (**Fig.8a**). $G\alpha_q$-coupled GPCRs trigger the mitogen-activated protein kinase (MAPK) pathway and induce transcription through a serum responsive element (SRE) [58]. Therefore, we measured luciferase activity driven by an SRE reporter (**Fig.10a**). As anticipated, HEK cells transfected with hM3Dq increased luciferase activity 2.5-fold upon stimulation with CNO compared to vehicle (**Fig.10b**). We hypothesized that this effect would be absent in DREADD-β2AR-transfected HEK cells. Indeed, DREADD-β2AR did not increase luciferase activity; instead, the activity decreased more than 4-fold, which was similar to the non-chimeric β2AR response upon levalbuterol treatment. In empty vector-transfected cells, CNO had no impact on SRE-dependent reporter transcription, while levalbuterol reduced luciferase activity due to endogenous β2AR expression in HEK cells [75]. **Figure 10c** demonstrates the contribution of endogenous β2AR which depends on the ligand concentration. rM3Ds and hM4Di also inhibited the SRE reporter signal by 2-fold (**Fig.10b**). The opposing responses with DREADD-β2AR and hM3Dq further substantiate the correct identification of β2AR signaling domains.

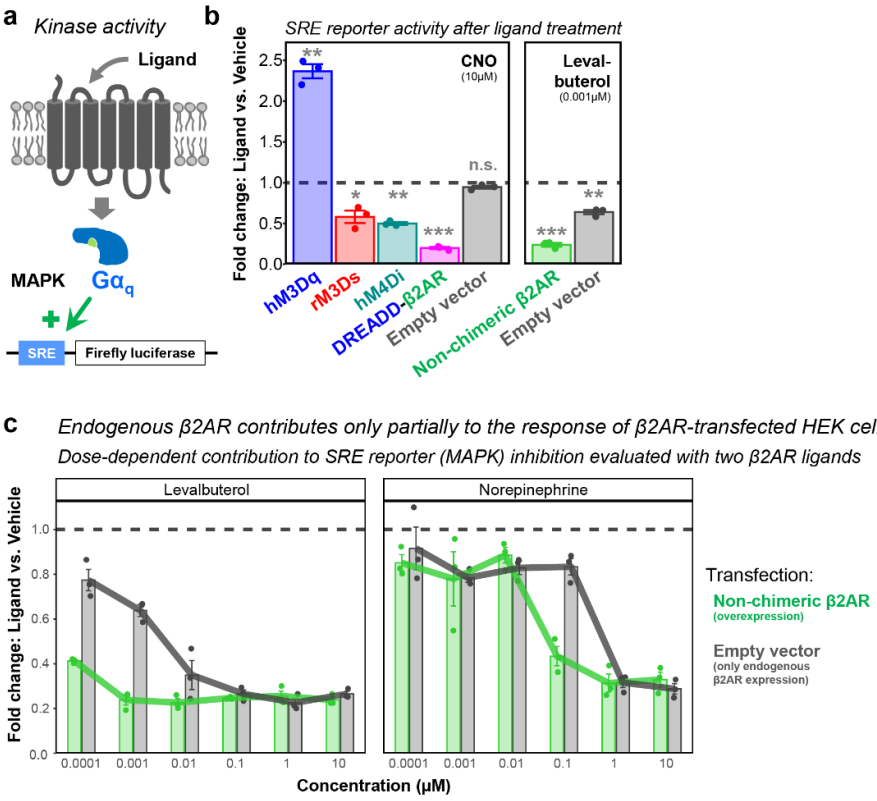

Figure 10: DREADD-β2AR recapitulates MAPK activity of non-chimeric β2AR.
a: Schematic of $G\alpha_q$-coupled GPCR engaging in the mitogen-activated protein kinase (MAPK) pathway which induces transcription of a firefly luciferase reporter from a serum responsive element (SRE). **b:** Endpoint measurement of SRE-dependent luciferase activity in HEK cells transfected with hM3Dq (blue), DREADD-β2AR (magenta), non-chimeric β2AR (green), rM3Ds (red), hM4Di (cyan), or empty vector (grey). Ligand stimulation either with 10μM CNO (left) or 0.001μM levalbuterol (right). Dashed line: level of vehicle control. Error bars: standard error of the mean. Two-sided one-sample T-test comparing to a mean of 1 which represents the vehicle control: $p^{***} < 0.001$; $p^{**} < 0.01$; $p^{n.s.} > 0.05$. Exact p-values: p = 0.004 (hM3Dq: CNO); p = 0.03 (rM3Ds: CNO); p = 0.001 (hM4Di: CNO); p < 0.002 (DREADD-β2AR: CNO); p = 0.09 (Empty vector: CNO); p < 0.001 (Non-chimeric β2AR: Levalbuterol); p = 0.01 (Empty vector: Levalbuterol). N = three experimental repetitions. **c:** Endpoint measurement of SRE-dependent luciferase activity in HEK cells transfected with non-chimeric β2AR (green) or

empty vector (grey). Dashed line: level of vehicle control. Error bars: standard error of the mean. N = three experimental repetitions.

3.4.3 Constitutive activity in the absence of ligand stimulation

Several GPCRs possess constitutive activity [76] and can initiate signaling pathways even in the absence of ligand stimulation (**Fig.11a**). To evaluate constitutive signaling, we used a cAMP-dependent luciferase assay suitable for measuring baseline activity [57] and recorded luminescence for 30 minutes. Consistent with previous reports [43], we found elevated cAMP levels in rM3Ds-transfected HEK cells compared to empty vector controls (**Fig.11b-c**). DREADD-β2AR only increased cAMP 3-fold, suggesting less constitutive activity. Notably, HEK cells transfected with non-chimeric β2AR also displayed baseline activity exceeding that of DREADD-β2AR. This is in accordance with previous studies that found constitutive signaling in several non-chimeric GPCRs [76]. hM3Dq and hM4Di did not impact the cAMP baseline.

We also evaluated constitutive activity on the MAPK pathway and compared baseline SRE reporter signals in GPCR-transfected HEK cells with empty vector controls (**Fig.11d**). Again, rM3Ds showed the most pronounced effect with a 15-fold decrease of SRE reporter activity (**Fig.11e**). In comparison, DREADD-β2AR and non-chimeric β2AR only moderately inhibited the SRE reporter by approximately 3- and 6-fold, respectively. Interestingly, hM3Dq also caused a small but significant 1.5-fold inhibition of baseline SRE activity while hM4Di had no impact. These results confirm the constitutive activity of rM3Ds [43] and indicate that DREADD-β2AR has a comparatively lower tendency to initiate signaling pathways in the absence of CNO stimulation.

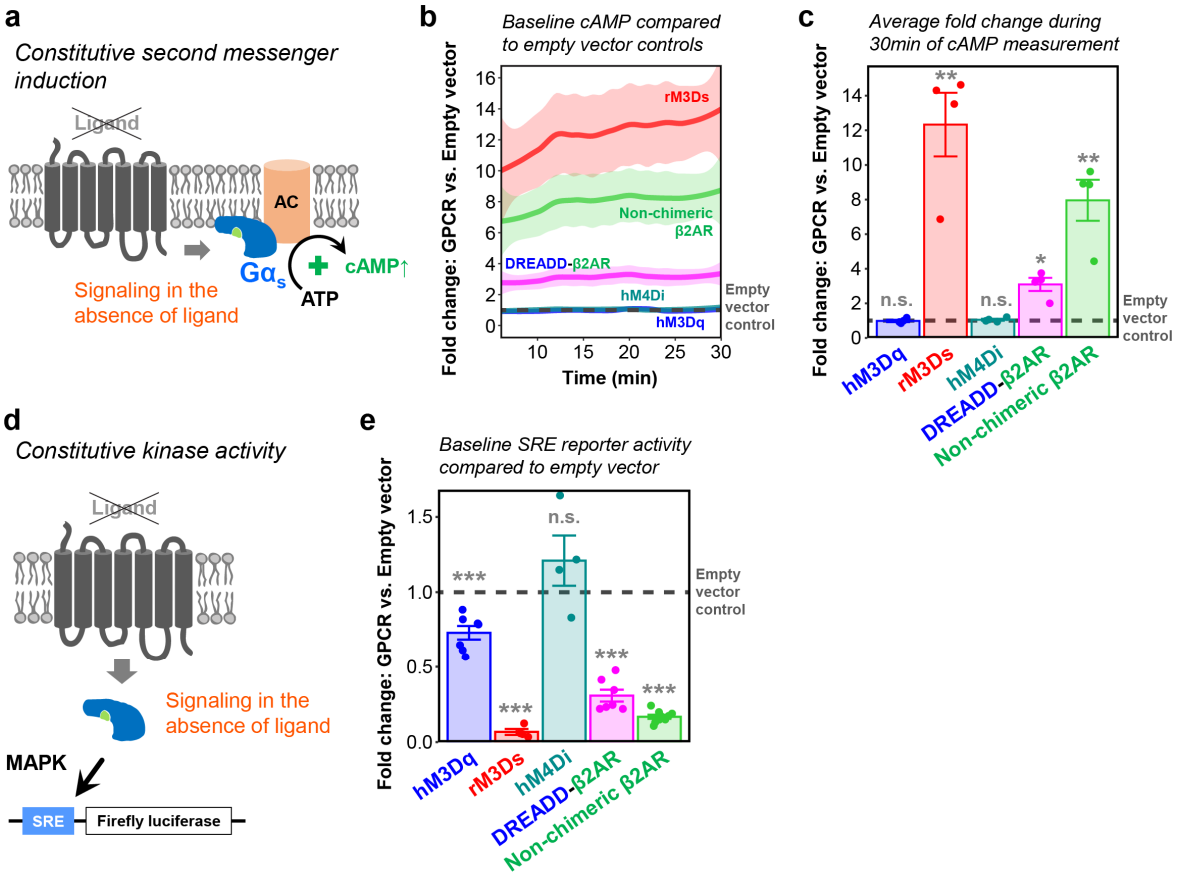

Figure 11: DREADD-β2AR displays lower constitutive activity compared to rM3Ds and non-chimeric β2AR. **a:** Schematic of GPCR increasing baseline cAMP levels through constitutive activity. **b:** Real-time measurement of cAMP-dependent luciferase activity during a 30min baseline in HEK cells transfected with hM3Dq (blue), rM3Ds (red), hM4Di (cyan), DREADD-β2AR (magenta), or non-chimeric β2AR (green). Measure of center: Mean fold change compared to empty vector (dashed line). Ribbons: 95% confidence intervals. N = four experimental repetitions. **c:** Graph shows average fold change compared to empty vector control during the 30min measurement in **b**. Dashed line: level of empty vector control. N = four experimental repetitions. Two-sided one-sample T-test comparing to a mean of 1 which represents the empty vector control: $p^{***} < 0.001$; $p^{**} < 0.01$; $p^{n.s.} > 0.05$. Exact p-values: p = 0.81 (hM3Dq); p = 0.009 (rM3Ds); p = 0.48 (hM4Di); p = 0.01 (DREADD-β2AR); p = 0.009 (Non-chimeric β2AR). **d:** Schematic of GPCR with constitutive activity impacting baseline MAPK signaling measured through an SRE reporter. **e:** Endpoint measurement of SRE-dependent luciferase activity in transfected HEK cells. Dashed line: level of empty vector control. Error bars: standard error of the mean. N = seven (hM3Dq, DREADD-β2AR), four (rM3Ds, hM4Di), or nine (Non-chimeric β2AR) experimental repetitions. Two-sided one-sample T-test comparing to a mean of 1 which represents the empty vector control: $p^{***} < 0.001$; $p^{**} < 0.01$; $p^{n.s.} > 0.05$. Exact p-values: p < 0.001 (hM3Dq); p < 0.001 (rM3Ds); p = 0.30 (hM4Di); p < 0.001 (DREADD-β2AR); p < 0.001 (Non-chimeric β2AR).

3.4.4 Protein-protein interaction

Next, we focused on protein-protein interactions and post-translational modifications regulated by β2AR signaling as outlined in **Figure 8a**. Ligand-activated β2AR recruits β-arrestin 2, which creates a scaffold for attracting signaling kinases [25] and further plays a role in receptor internalization [19]. To investigate the interaction between β-arrestin 2 and non-chimeric β2AR or DREADD-β2AR, we attached the complementary luciferase subunits LgBiT and SmBiT to their C-termini, respectively [77–79]. Upon β-arrestin 2 recruitment, both subunits are brought into close proximity, resulting in a bioluminescent signal (**Fig.12a**). Levalbuterol

stimulation of non-chimeric β2AR, as well as CNO stimulation of DREADD-β2AR, immediately increased bioluminescence compared to vehicle treatment (**Fig.12b**). This indicates that DREADD-β2AR recapitulates the fast β-arrestin 2 recruitment observed with non-chimeric β2AR.

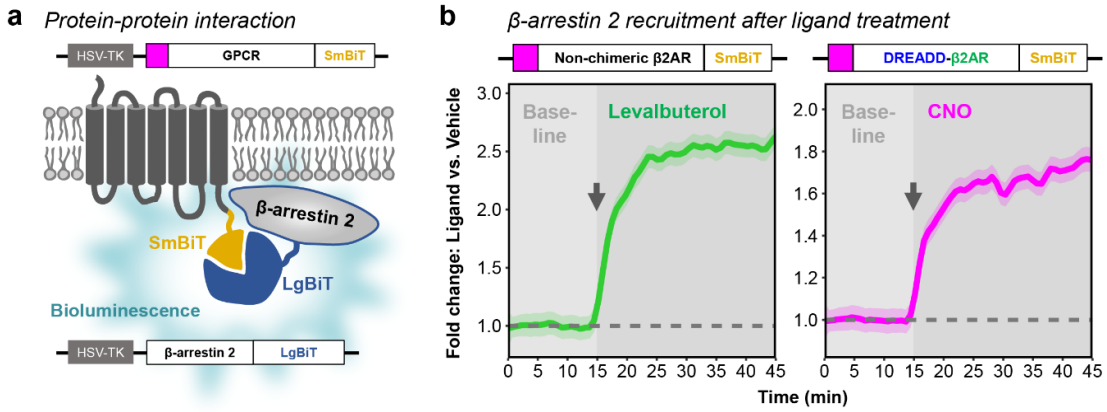

Figure 12: DREADD-β2AR recruits β-arrestin 2.
a: Schematic of induced bioluminescence upon GPCR-SmBiT and β-arrestin 2-LgBiT interaction. GPCR, G protein-coupled receptor. HSV-TK, herpes simplex virus thymidine kinase promoter. **b:** Real-time measurement of bioluminescence in HEK cells transfected with non-chimeric β2AR (left) or DREADD-β2AR (right). Baseline measurements followed by ligand application (grey arrow shows onset) of either levalbuterol (left) or CNO (right). Measure of center: Mean of baseline-normalized fold change compared to vehicle (dashed line) in the same experimental repetition. Ribbons: 95% confidence intervals. N = four (Non-chimeric β2AR) or five (DREADD-β2AR) experimental repetitions.

3.4.5 Post-translational modification

β2AR signaling also involves the rapid phosphorylation of extracellular signal-regulated kinases 1 and 2 (ERK1/2), which is partly mediated through recruitment of β-arrestins [25,72]. So, we investigated whether ERK1/2 phosphorylation occurred in HEK cells transfected with non-chimeric β2AR or DREADD-β2AR following treatment with levalbuterol or CNO, respectively. For both constructs, phosphorylation peaked two minutes after ligand stimulation and gradually declined after five minutes (**Fig.13a**), suggesting the recapitulation of post-translational modification dynamics. CNO exposure of empty vector-transfected HEK cells did not impact ERK1/2 phosphorylation. As a note, we also found constitutive ERK1/2 phosphorylation in the absence of ligand in both non-chimeric β2AR and DREADD-β2AR when compared to their empty vector controls (**Fig.13b**). Full scan Western blots for this experiment are provided in **Supplementary Figure S1.**

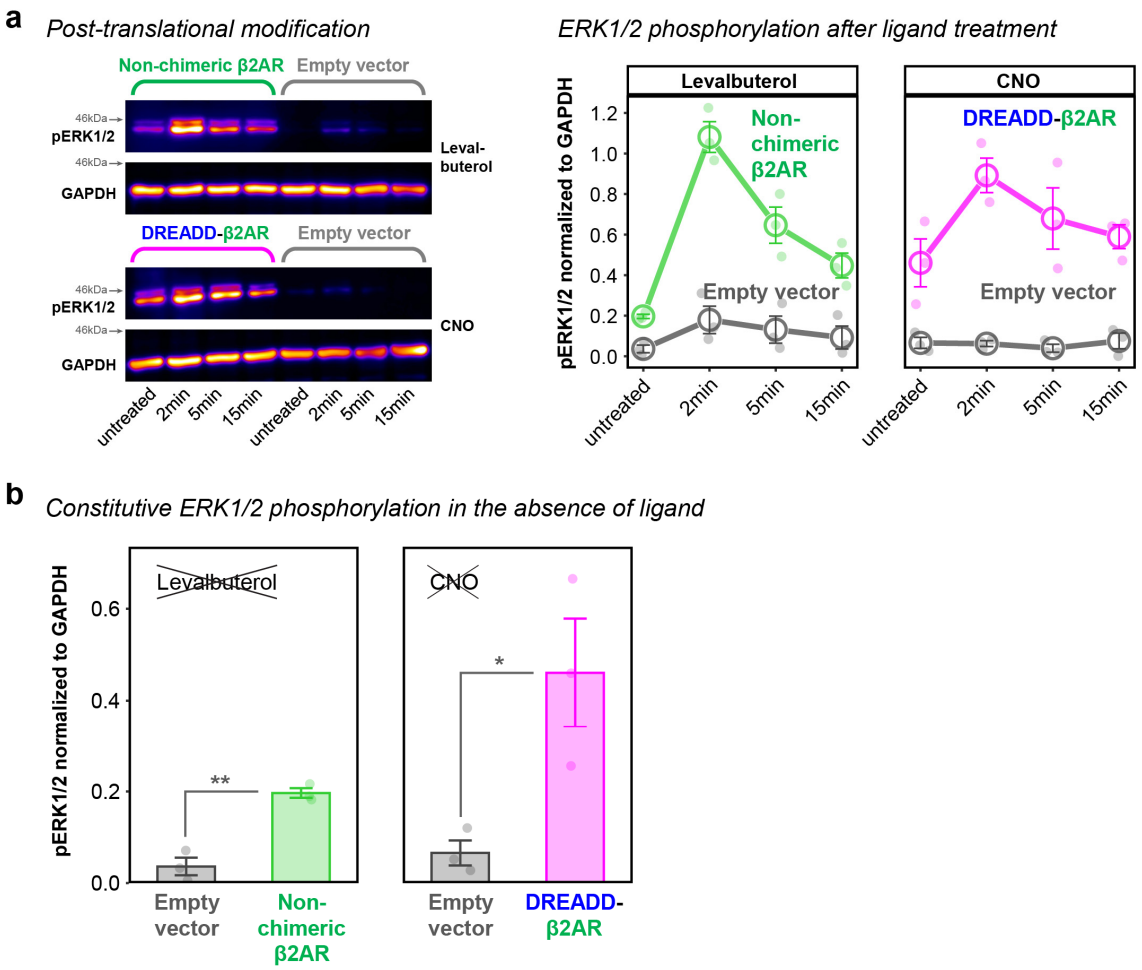

Figure 13: DREADD-β2AR phosphorylates ERK1/2.
a: Phosphorylation analysis of extracellular signal-regulated kinases 1 and 2 (ERK1/2) in untreated, levalbuterol- or CNO-treated HEK cells transfected with non-chimeric β2AR, DREADD-β2AR, or empty vector. Left: Western blot for pERK1/2 and GAPDH (loading control). The anti-pERK1/2 antibody results in an upper band for pERK1 (44kDa) and a lower band for pERK2 (42kDA). Right: Densitometry analysis of combined pERK1/2 normalized to GAPDH. Error bars: standard error of the mean. N = three experimental repetitions. **Supplementary Figure S1** shows full scan Western blot membranes from all repetitions. **b:** Comparison of pERK1/2 phosphorylation in untreated samples for evaluation of constitutive activity. Error bars: standard error of the mean. N = three experimental repetitions. Two-sided two-sample T-test: $p^{**} < 0.01$; $p^{*} < 0.05$. Exact p-values: p = 0.002 (Non-chimeric β2AR vs. Empty vector); p = 0.03 (DREADD-β2AR vs. Empty vector).

3.4.6 GPCR internalization

β-arrestin recruitment also mediates GPCR internalization [18–20], which provides a regulatory feedback loop for receptor activity after ligand stimulation (**Fig.8a**) [80,81]. To visualize receptor trafficking, we engineered DREADD-β2AR with EGFP attached at the C-terminus (**Fig.14a-b**). We transfected this construct into HEK cells and 24 hours later incubated them for 30 minutes with anti-VSV-G antibody to distinguish cell surface-incorporated DREADD-β2AR from receptors retained within the cell. Colocalization of VSV-G antibody and EGFP occurred on the cell surface. We barely found VSV-G signal within transfected cells suggesting that DREADD-β2AR internalization is largely absent without ligand stimulation (**Fig.14c**). In contrast, when we applied CNO for either 15, 30 or 60 minutes following VSV-G antibody labeling, VSV-G/EGFP signals colocalized within the cytoplasm. Internalization increased after 30 minutes

and became significantly higher after 60 minutes of CNO exposure compared to vehicle treatment (**Fig.14d-f**). We conclude that DREADD-β2AR can undergo ligand-induced receptor internalization.

Together, our results confirm that DREADD-β2AR successfully recapitulates the signaling cascades (**Fig.8a**) of non-chimeric β2AR with similar dynamics.

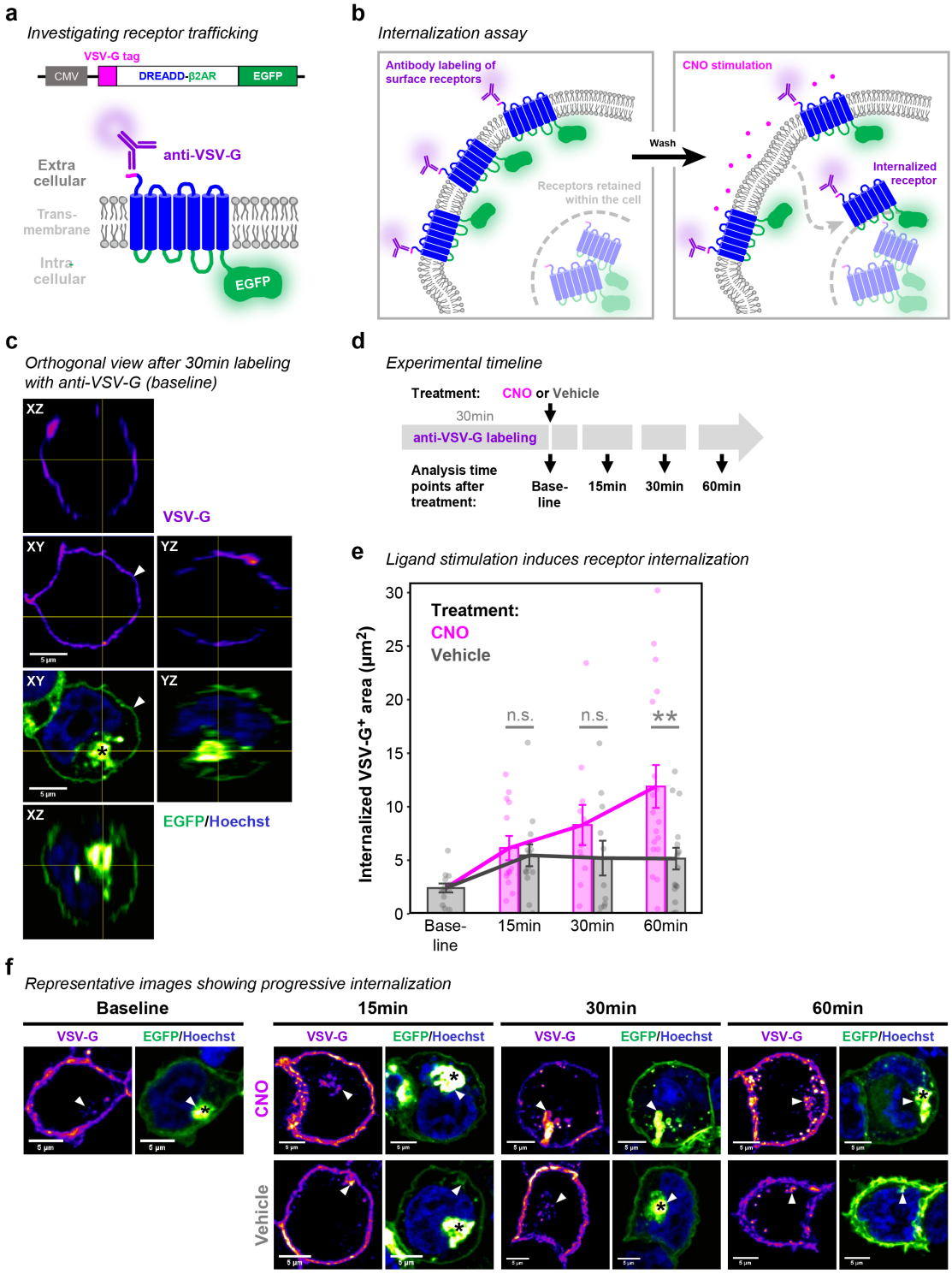

Figure 14: Internalization of DREADD-β2AR following CNO stimulation.

a: Schematic of the DREADD-β2AR-EGFP construct for internalization analysis. C-terminal EGFP visualizes receptor trafficking within the cell. Cell surface-expressed receptors are labeled with an antibody against the VSV-G epitope. CMV, human cytomegalovirus promoter. **b:** Schematic exemplifying the strategy for internalized receptor detection. **c:** Orthogonal view of DREADD-β2AR-EGFP-transfected HEK cell fixed immediately after 30 minutes of VSV-G antibody labeling. VSV-G signal visualized with an intensity-based color code (purple-red-yellow) to display signals of varying intensities. Green: EGFP visualized with intensity-based color code (green-

white). Blue: nuclear staining with Hoechst. White arrow head: VSV-G/EGFP signal at the cell surface. Black asterisk: accumulation of cytoplasmic EGFP indicating receptors retained within the cell. **d:** Schematic of experimental design. Following 30 minutes of antibody incubation, cells were fixed either immediately (baseline) or 15, 30 and 60 minutes after exposure to CNO or vehicle. **e:** Stimulation of DREADD-β2AR-EGFP-transfected HEK cells with CNO (magenta) or vehicle (grey). Each dot shows a single cell and its internalized VSV-G-positive area (μm^2). Error bars: standard error of the mean within each condition. Magenta and grey lines connect the mean values of CNO or vehicle exposure times, respectively. Linear regression analysis: $p^{**} < 0.01$; $p^{n.s.} > 0.05$. Two-sided post-hoc comparisons corrected for multiple testing: p = 0.98 (15min); p = 0.45 (30min); p = 0.001 (60min). N = 13 (Baseline), 13 (15min: CNO), 14 (15min: Vehicle), 11 (30min: CNO), 11 (30min: Vehicle), 18 (60min: CNO), 16 (60min: Vehicle) cells examined over one experiment. **f:** Representative maximum intensity projections of individual cells analyzed for internalized receptors confirmed by colocalizing VSV-G/EGFP signal (white arrow heads).

3.5 Chimeric DREADD-β2AR recapitulates β2AR-mediated effects on microglia motility

Microglia are highly motile cells that constantly scan their environment for signs of disrupted tissue homeostasis. Activation of β2AR signaling was recently shown to rapidly induce filopodia formation as a consequence of elevated cAMP levels [45].

To recapitulate this phenotype with our DREADD-β2AR, we first generated a bicistronic GPCR-P2A-EGFP vector containing a self-cleaving P2A peptide site [82] that allows simultaneous GPCR and cytoplasmic EGFP expression (**Fig.15a**). We transfected HEK cells with this DREADD-β2AR-P2A-EGFP vector and confirmed the expected cytoplasmic EGFP localization co-existing with anti-VSV-G immunostaining on the cell membrane (**Fig.15b**). Subsequently, we packaged our DREADD-β2AR-P2A-EGFP construct into lentiviral vectors and transduced primary microglia. Successful transduction was sparse but individual cells could be clearly identified by their EGFP expression (**Fig.15c**).

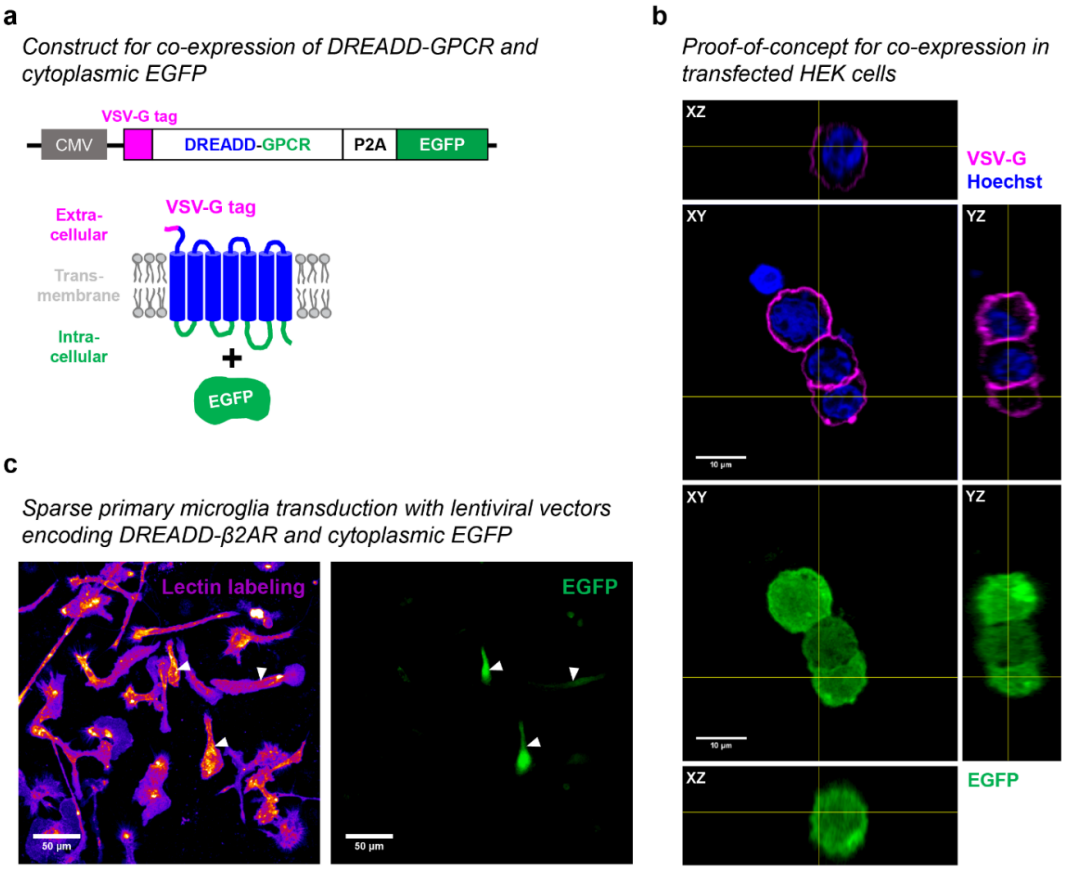

Figure 15: Vector validation for bicistronic expression of DREADD-GPCRs and EGFP.
a: Schematic of a bicistronic vector with human cytomegalovirus (CMV) promoter, VSV-G epitope, DREADD-GPCR, the self-cleaving P2A peptide sequence, and EGFP. Transfected cells express the GPCR on the cell surface and EGFP in the cytoplasm. **b:** Orthogonal view of HEK cells transfected with DREADD-β2AR-P2A-EGFP immunostained for the VSV-G tag under non-permeabilizing conditions. Magenta: VSV-G tag. Green: EGFP. Blue: nuclear staining with Hoechst. **c:** Unstained primary microglia seven days after transduction with a lentiviral vector encoding DREADD-β2AR-P2A-EGFP at a multiplicity of infection (MOI) of 3. Left: labeling with fluorophore-conjugated tomato lectin, displayed with intensity-based color code (purple-red-yellow). Right: EGFP.

Next, we performed live-imaging of primary microglia cultures and confirmed filopodia extension and an increase in total microglia area after endogenous β2AR stimulation through levalbuterol (**Fig.16**). During the first 10 minutes of baseline recordings, microglia were motile and changed their area only marginally. After levalbuterol application, the cell area significantly increased throughout the following 45 minutes of imaging compared to the baseline (**Fig.16a**, **e**). To mimic this effect through DREADD-β2AR, we imaged EGFP-positive cells approximately one week after lentiviral transduction. We found that in these cells CNO application induced filopodia formation (**Fig.16b**, **e**) similar to levalbuterol. Non-transduced microglia stimulated with either vehicle or CNO did not significantly increase their area (**Fig.16c-e**).

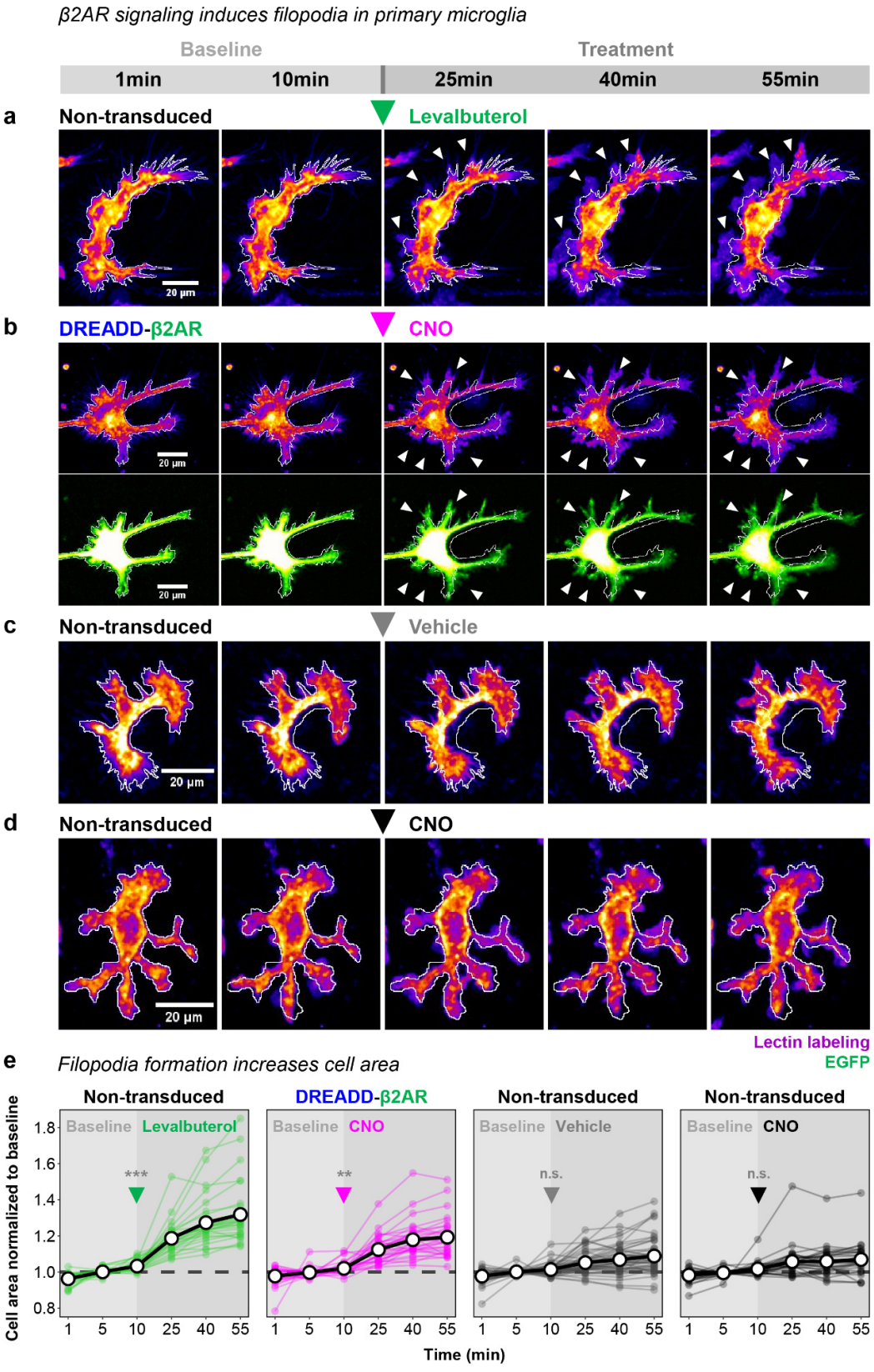

Figure 16: Stimulation of DREADD-β2AR induces filopodia formation in primary microglia.
a-d: Representative images of primary microglia during 55 minutes of live imaging. After a 10 minutes baseline, non-transduced cells were stimulated with either levalbuterol (**a**), vehicle (**c**), or CNO (**d**). Cells transduced with

DREADD-β2AR-P2A-EGFP (**b**) were treated with CNO after 10 minutes of baseline recording. Lectin labeling visualized with an intensity-based color code (purple-red-yellow) to display signals of varying intensities. Green: EGFP visualized with intensity-based color code (green-white). White outline: cell area perimeter at 1 minute projected on all other shown time points. White arrow heads: filopodia formation. **e:** Quantification of cell area changes throughout 55 minutes of live imaging. A 10 minutes baseline was followed by ligand application (arrow heads for onset) of either levalbuterol, CNO, or vehicle. Graphs show the fold change of individual cells normalized to their baseline mean at selected time points of 1, 5, 10, 25, 40, and 55 minutes. Thick black lines: mean of all cells (30-50 per experimental group). Thin colored lines: individual cells. Dashed lines: baseline mean. Linear regression analysis modeling cell area (μm^2) of individual cells across time to compare baseline with treatment period: $p^{***} < 0.001$; $p^{**} < 0.01$; $p^{n.s.} > 0.05$. Two-sided post-hoc comparisons corrected for multiple testing: $p < 0.001$ (Non-transduced: Levalbuterol); $p = 0.004$ (DREADD-β2AR: CNO); $p = 0.58$ (Non-transduced: Vehicle); $p = 0.84$ (Non-transduced: CNO). N = 30 (Non-transduced: Levalbuterol), 32 (DREADD-β2AR: CNO), 50 (Non-transduced: Vehicle), 30 (Non-transduced: CNO) cells examined over three, ten, nine, and eight experiments, respectively.

Figure 17 provides a statistical comparison across all experimental groups at each indicated time point and confirms that levalbuterol treatment and DREADD-β2AR are significantly different from the control conditions. It is worth mentioning that filopodia extension in cultured microglia does not present the complexity of microglial process dynamics observed *in-vivo* [45,71]. Yet, given the difficulty of microglial transduction *in-vivo* [83], our simpler but more accessible *in-vitro* system suggests that DREADD-β2AR successfully mimics β2AR signaling in microglia and modulates their function.

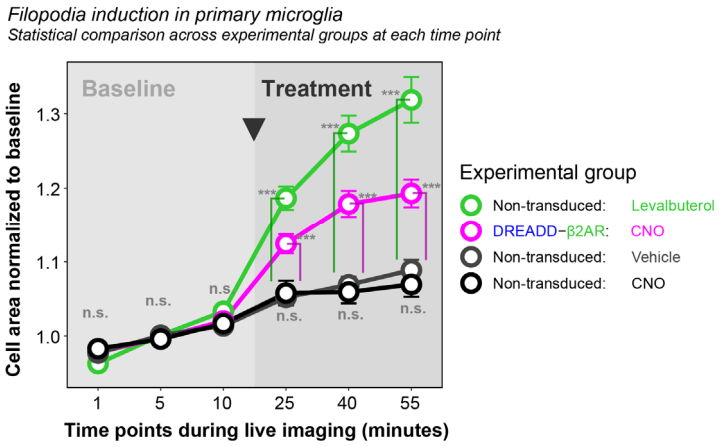

Figure 17: Comparison of filopodia induction.
Analysis of filopodia formation in primary microglia using lentiviral expression of DREADD-β2AR-P2A-EGFP. Graph combines all panels from **Figure 16e** and shows statistical comparison between experimental groups within each time point. Error bars: standard error of the mean. Linear regression analysis with two-sided post-hoc comparisons corrected for multiple testing: $p^{***} < 0.001$; $p^{n.s.} > 0.05$. Exact p-values for selected comparisons at the 25min time point: p = 1,00 (Non-transduced: Vehicle vs. Non-transduced: CNO); p < 0.001 (Non-transduced: Vehicle vs. Non-transduced: Levalbuterol); p < 0.001 (Non-transduced: Vehicle vs. DREADD-β2AR:CNO). Selected comparisons at the 40min time point: p = 0.99 (Non-transduced: Vehicle vs. Non-transduced: CNO); p < 0.001 (Non-transduced: Vehicle vs. Non-transduced: Levalbuterol); p < 0.001 (Non-transduced: Vehicle vs. DREADD-β2AR: CNO). Selected comparisons at the 55min time point: p = 0.99 (Non-transduced: Vehicle vs. Non-transduced: CNO); p < 0.001 (Non-transduced: Vehicle vs. Non-transduced: Levalbuterol); p < 0.001 (Non-transduced: Vehicle vs. DREADD-β2AR: CNO). See **Supplementary Table S5** for exact p-values of all comparisons. N = 30 (Non-transduced: Levalbuterol), 32 (DREADD-β2AR: CNO), 50 (Non-transduced: Vehicle), 30 (Non-transduced: CNO) cells examined over three, ten, nine, and eight experiments, respectively.

3.6 Generating DREADD-based chimeras for additional microglial GPCRs-of-interest

After confirming the functionality of our strategy with DREADD-β2AR, we decided to extend our approach to GPR65 and GPR109A/HCAR2, which like β2AR, showed microglia-enriched gene expression (see **Fig.2**). GPR65 and GPR109A respond to protons [84] and ketone bodies [85], respectively, and were shown to modulate inflammatory responses such as cytokine expression in microglia *in-vitro* systems [86,87]. Both of their ligands are prone to cause off-target effects as acidic environments trigger various unpredictable responses in immune cells [88,89], and the ketone β-hydroxybutyrate can impact histone modification in a GPCR-independent manner [90,91]. This makes GPR65 and GPR109A interesting candidates for DREADD-based chimeras to dissect their inflammatory role with a well-defined ligand.

Thus, we designed DREADD-GPR65 and DREADD-GPR109A with the same N-terminal modifications as DREADD-β2AR (**Fig.6a**). First, we transfected HEK cells with these chimeras and confirmed successful cell membrane incorporation through immunostaining for the VSV-G tag (**Fig.18a-b**). Then, we investigated whether both chimeras triggered their expected second messenger cascades and kinase activity. Like β2AR, GPR65 belongs to the $G\alpha_s$-coupling family [84]. Therefore, we applied our previously established validation strategy for second messenger induction (**Fig.8b-e**). We measured cAMP levels in HEK cells transfected with DREADD-GPR65 and found a significant increase after CNO stimulation, which was not detected in empty vector-transfected cells (**Fig.18c**). Stimulation of DREADD-GPR65 also impacted the MAPK pathway and reduced SRE-mediated reporter expression, similar to β2AR (**Fig.18d**, see **Fig.10a-b** for comparison).

In contrast to GPR65 and β2AR, GPR109A couples to $G\alpha_i$ and suppresses cAMP synthesis by inhibiting adenylyl cyclase (AC) [85] and therefore competes with the AC activator forskolin [92,93] (**Fig.18e**). To measure $G\alpha_i$-mediated decreases in cAMP, we adapted a cAMP-dependent luciferase assay with kinetics suitable for $G\alpha_i$-signaling [57]. Within 10 minutes following CNO stimulation, DREADD-GPR109A-transfected HEK cells decreased cAMP levels by approximately 15% compared to vehicle (**Fig.18e**). After 30 minutes of CNO exposure, we added forskolin as a competing component to induce cAMP synthesis. DREADD-GPR109A-transfected cells exposed to CNO kept their cAMP signal approximately 15% below the vehicle control suggesting robust AC inhibition. Empty vector-transfected HEK cells did not respond to CNO, and their cAMP levels always remained at vehicle control levels (**Fig.18e**, see **Fig.18f** for non-normalized values demonstrating the prominent cAMP increase upon forskolin application).

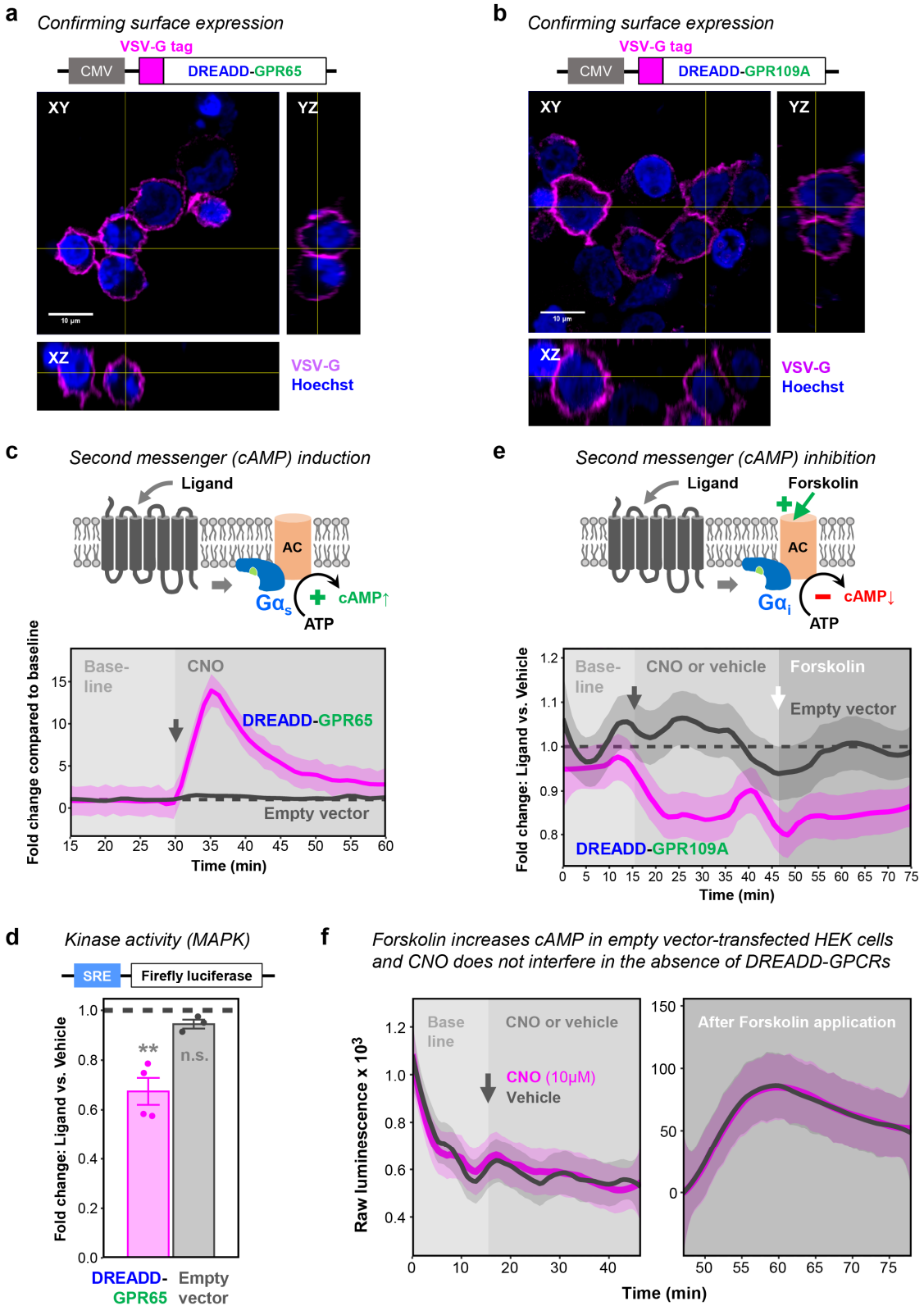

Figure 18: DREADD-GPR65 and DREADD-GPR109A respond with their expected signaling cascades.
a-b: Orthogonal view of HEK cells transfected with DREADD-GPR65 (**a**) or DREADD-GPR109A (**b**) immunostained for the VSV-G tag under non-permeabilizing conditions. Magenta: VSV-G tag. Blue: nuclear staining with Hoechst. CMV, human cytomegalovirus promoter. **c:** Top: Schematic of $G\alpha_s$-coupled GPCR inducing cAMP

synthesis after ligand stimulation through adenylyl cyclase (AC) activation. Below: Real-time measurement of cAMP-dependent luciferase activity in HEK cells transfected with DREADD-GPR65 (magenta) or empty vector (grey). Baseline measurement of 30 minutes (first 15 minutes not shown) followed by CNO application (grey arrow for onset). Measure of center: Mean fold change compared to baseline mean (dashed line). Ribbons: 95% confidence intervals. N = four (DREADD-GPR65) or seven (Empty vector) experimental repetitions. **d:** Endpoint measurement of serum responsive element (SRE)-dependent luciferase activity in HEK cells transfected with DREADD-GPR65 (magenta) or empty vector (grey). Ligand stimulation with CNO. Dashed line: level of the respective vehicle control. Error bars: standard error of the mean. N = four (DREADD-GPR65) or three (Empty vector) experimental repetitions. Two-sided one-sample T-test comparing to a mean of 1 which represents the vehicle control: $p^{*} < 0.05$; $p^{n.s.} > 0.05$. Exact p-values: p = 0.009 (DREADD-GPR65); p = 0.09 (Empty vector). **e:** Top: Schematic of $G\alpha_i$-coupled GPCR reducing cAMP levels after ligand stimulation through adenylyl cyclase (AC) inhibition. Forskolin induces cAMP synthesis through AC activation. Below: Real-time measurement of cAMP-dependent luciferase activity in HEK cells transfected with DREADD-GPR109A (magenta) or empty vector (grey). Baseline measurements followed by application of CNO or vehicle (grey arrow for onset) and forskolin (white arrow for onset). Measure of center: Mean fold change compared to vehicle (dashed line) in the same experimental repetition. Ribbons: 95% confidence intervals. N = five experimental repetitions. **f:** Real-time measurement of cAMP-dependent luciferase activity in HEK cells transfected with empty vector. Baseline measurements followed by application of CNO or vehicle (grey arrow for onset) and forskolin (second panel). Graph shows raw luminescence units of cells treated with CNO (magenta) or vehicle (grey). Measure of center: Mean raw luminescence units. Non-normalized raw values are used for this visualization to exemplify the strong signal increase upon forskolin application. Ribbons: 95% confidence intervals. N = five experimental repetitions.

To further substantiate the $G\alpha_i$ effect, we tested for the ability of DREADD-GPR109A to compete with $G\alpha_s$ signaling (**Fig.19a**). For this, we used a reporter that drives luciferase expression through a cAMP-responsive element (CRE) [58], which is induced by $G\alpha_s$ activity. First, we confirmed successful $G\alpha_s$ induction in empty vector-transfected HEK cells through stimulation with 5'-N-ethylcarboxamidoadenosine (NECA), a potent agonist of the endogenously expressed $G\alpha_s$-coupled A2B adenosine receptor (A2BAR) [94]. The expression of the CRE reporter was NECA dose-dependent and reached saturation at 5µM, while concomitant CNO application did not interfere (**Fig.19b**). Subsequently, we transfected HEK cells with DREADD-GPR109A and applied CNO together with 5µM NECA. As anticipated, CNO significantly inhibited $G\alpha_s$-mediated transcription from the CRE reporter by approximately 20% when compared to vehicle (**Fig.19c**). As a note, CNO stimulation of DREADD-GPR109A did not dampen CRE reporter activity without simultaneous induction through NECA (**Fig.19d**), possibly because the assay is not suitable for detecting rather minor reductions from baseline levels [57]. In addition, stimulation of DREADD-GPR109A had no impact on the MAPK pathway measured through SRE reporter activity (**Fig.19e**).

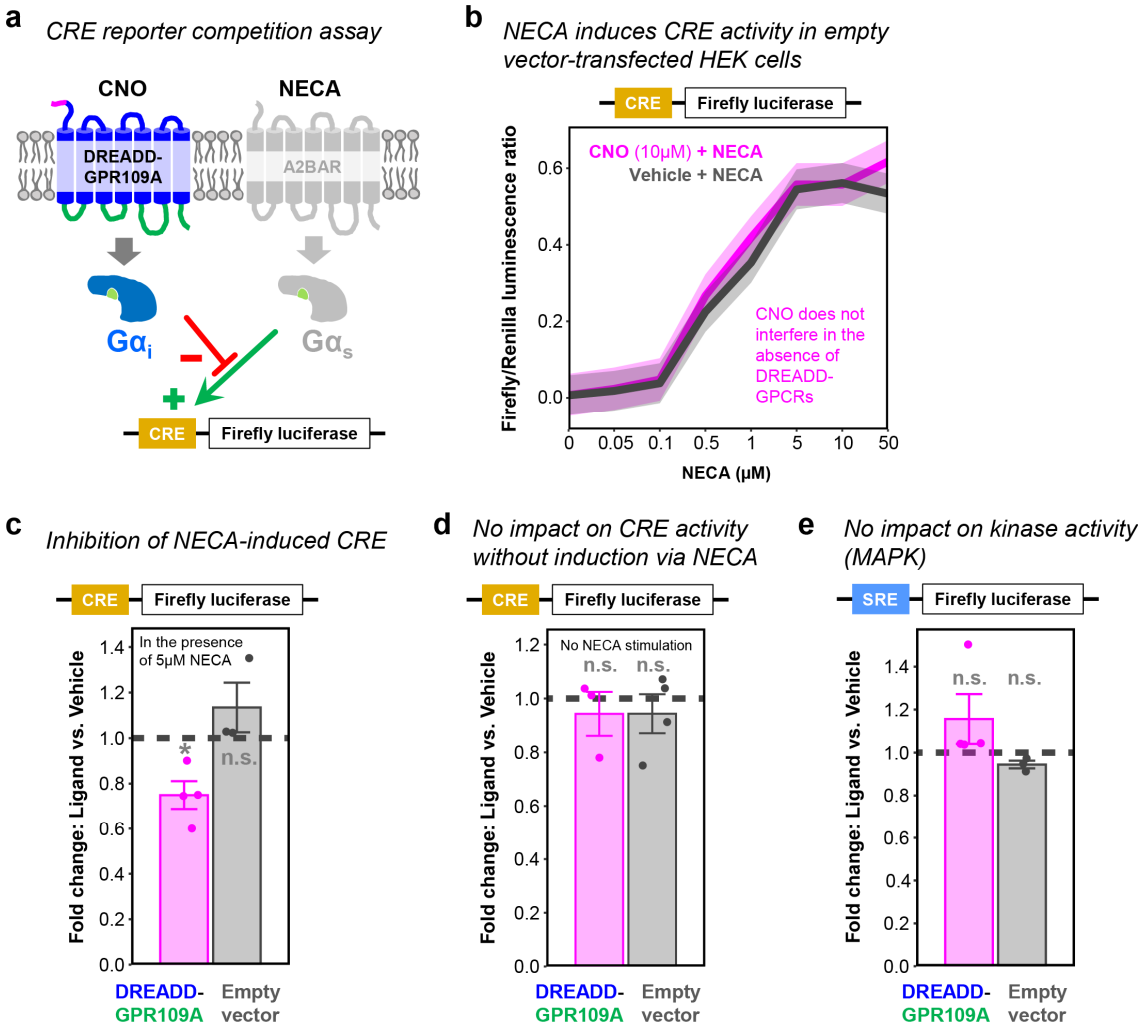

Figure 19: DREADD-GPR109A induces Gαi signaling but does not impact the MAPK pathway.
a: Schematic of competition assay between Gαi-coupled DREADD-GPR109A and Gαs-coupled A2B adenosine receptor (A2BAR). Simultaneous stimulation of Gαi through CNO and Gαs through NECA prevents cAMP responsive element (CRE)-mediated luciferase reporter activity. **b:** Endpoint measurement of cAMP responsive element (CRE)-dependent firefly luciferase activity in HEK cells transfected with empty vector. Treatment with increasing concentrations of NECA in presence of either CNO (magenta) or vehicle (grey). Graph shows non-normalized firefly/renilla luciferase luminescence ratios to exemplify the signal increase upon NECA application. Ribbons: standard error of the mean. N = three technical replicates from one experiment. **c:** Endpoint measurement of CRE-dependent luciferase activity in HEK cells transfected with DREADD-GPR109A (magenta) or empty vector (grey). Simultaneous stimulation with CNO and 5µM NECA. Dashed line: level of the respective vehicle control. Error bars: standard error of the mean. N = four (DREADD-GPR109A) or three (Empty vector) experimental repetitions. Two-sided one-sample T-test comparing to a mean of 1 which represents the vehicle control: $p^{*} < 0.05$; $p^{n.s.} > 0.05$. Exact p-values: p = 0.03 (DREADD-GPR109A); p = 0.34 (Empty vector). **d:** Endpoint measurement of CRE-dependent luciferase activity in HEK cells transfected with DREADD-GPR109A (magenta) or empty vector (grey). Ligand stimulation with CNO. Dashed line: level of the respective vehicle control. Error bars: standard error of the mean. N = three (DREADD-GPR109A) or four (Empty vector) experimental repetitions. One-sample T-test as described in **c**. **e:** Endpoint measurement of serum responsive element (SRE)-dependent luciferase activity in HEK cells transfected with DREADD-GPR109A (magenta) or empty vector (grey). Ligand stimulation with CNO. Dashed line: level of the respective vehicle control. Error bars: standard error of the mean. N = four (DREADD-GPR109A) or three (Empty vector) experimental repetitions. One-sample T-test as described in **c**.

Even though DREADD-GPR65 and DREADD-GPR109A differed in their second messenger and kinase activity, both GPCRs were able to recruit β-arrestin 2 upon CNO application (**Fig.20a-b**), emphasizing that individual GPCRs can display diverse signaling patterns.

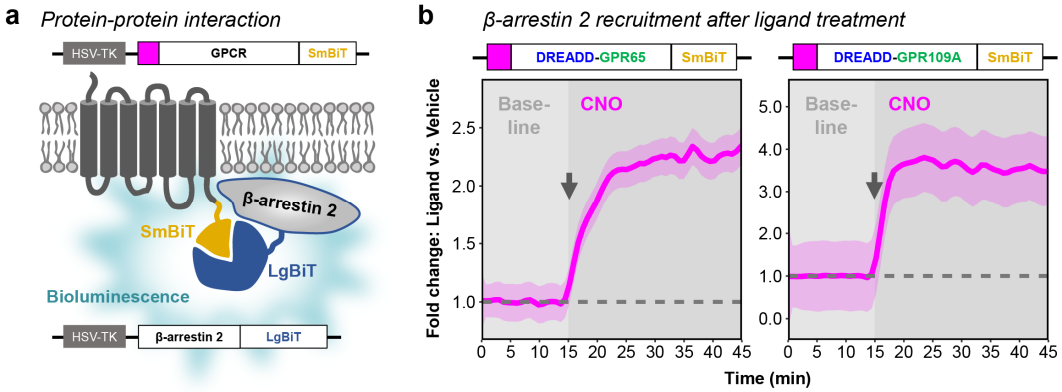

Figure 20: β-arrestin 2 recruitment of DREADD-GPR65 and DREADD-GPR109A.
a: Schematic of induced bioluminescence upon GPCR-SmBiT and β-arrestin 2-LgBiT interaction. GPCR, G protein-coupled receptor. HSV-TK, herpes simplex virus thymidine kinase promoter. **b:** DREADD-GPR65 and GPR109A recruit β-arrestin 2 upon CNO stimulation. Real-time measurement of β-arrestin 2 recruitment in HEK cells transfected with DREADD-GPR65 (left) or DREADD-GPR109A (right). Baseline measurements followed by CNO application (grey arrow shows onset). Measure of center: Mean of baseline-normalized fold change compared to vehicle (dashed line) in the same experimental repetition. Ribbons: 95% confidence intervals. N = three experimental repetitions.

Lastly, we evaluated constitutive signaling of both chimeras as previously done in **Figure 11** by measuring baseline cAMP levels and MAPK activity in the absence of CNO. DREADD-GPR65 increased baseline cAMP comparable to rM3Ds, while DREADD-GPR109A was indistinguishable from empty vector controls (**Fig.21a-c**). When assessing constitutive MAPK signaling, DREADD-GPR65 performed similarly to DREADD-β2AR and induced less SRE reporter inhibition than rM3Ds, while DREADD-GPR109A displayed no activity when compared to empty vector controls (**Fig.21d-e**). In conclusion, the results suggest that our DREADD-based strategy is reproducible and can be extended to other GPCRs-of-interest.

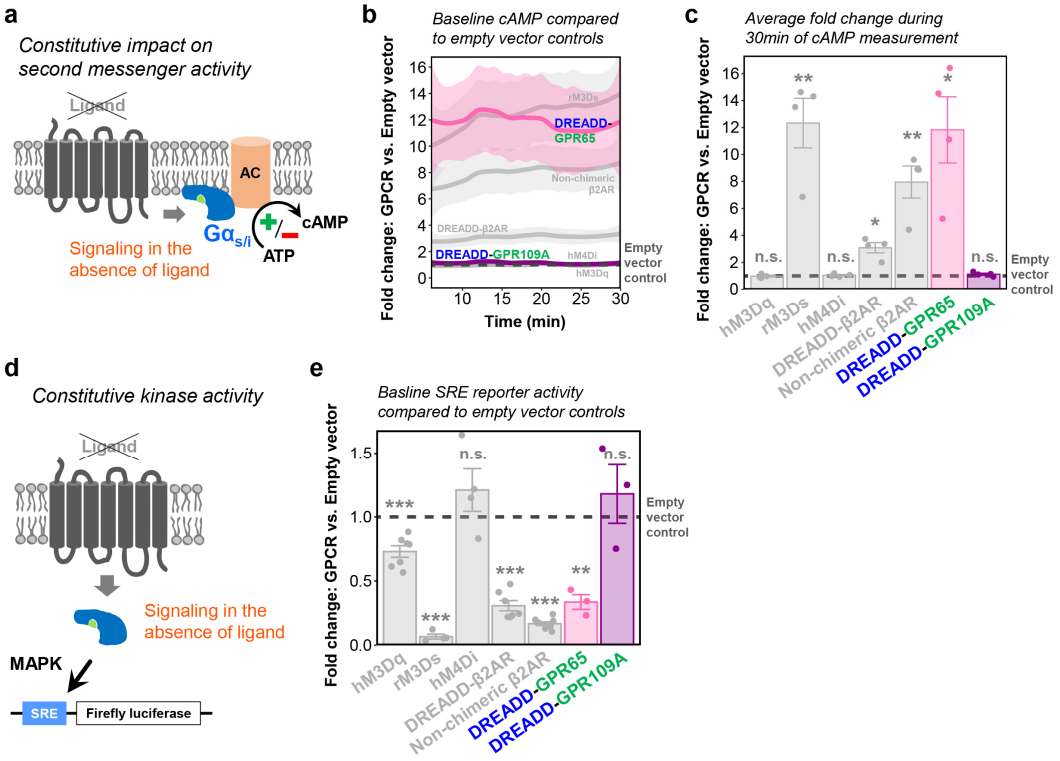

Figure 21: Constitutive activity of DREADD-GPR65 and DREADD-GPR109A.
a: Schematic of GPCR impacting baseline cAMP levels through constitutive activity. **b:** Real-time measurement of cAMP-dependent luciferase activity during a 30min baseline in HEK cells transfected with DREADD-GPR65 (pink) and DREADD-GPR109A (purple). Previously evaluated GPCRs (light grey) from **Figure 11** are included for comparison. Measure of center: Mean fold change compared to empty vector (dashed line) in the same experimental repetition. Ribbons: 95% confidence intervals. N = four experimental repetitions. **c:** Graph shows average fold change compared to empty vector control during the 30min measurement in **b**. Dashed line: level of empty vector control. Error bars: standard error of the mean. N = four experimental repetitions. Two-sided one-sample T-test comparing to a mean of 1 which represents the empty vector control: $p^{***} < 0.001$; $p^{**} < 0.01$; $p^{n.s.} > 0.05$. Exact p-values: p = 0.81 (hM3Dq); p = 0.009 (rM3Ds); p = 0.48 (hM4Di); p = 0.01 (DREADD-β2AR); p = 0.009 (Non-chimeric β2AR); p = 0.02 (DREADD-GPR65); p = 0.20 (DREADD-GPR109A). **d:** Schematic of GPCR with constitutive activity impacting baseline MAPK signaling measured through an SRE reporter. **e:** Endpoint measurement of SRE-dependent luciferase activity in transfected HEK cells. Dashed line: level of empty vector control. Error bars: standard error of the mean. N = seven (hM3Dq, DREADD-β2AR), four (rM3Ds, hM4Di), nine (Non-chimeric β2AR), or three (DREADD-GPR65, DREADD-GPR109A) experimental repetitions. One-sample T-test as described in **c**. Exact p-values: p < 0.001 (hM3Dq); p < 0.001 (rM3Ds); p = 0.30 (hM4Di); p < 0.001 (DREADD-β2AR); p < 0.001 (Non-chimeric β2AR); p = 0.007 (DREADD-GPR65); p = 0.52 (DREADD-GPR109A).

3.7 Using DREADD-GPCRs to investigate microglia function

Finally, we utilized our DREADD-based chimeras to investigate functional consequences of GPCR signaling in a microglia context. We took advantage of the microglia-like cell line HMC3 [95], which allows generation of cell lines with stable DREADD-GPCR expression. This provides a homogeneous cell population and is advantageous for reliable quantification of GPCR responses, which cannot be achieved in primary microglia due to suboptimal transduction efficiencies with available vectors [96] (see **Fig.15c**). Thus, we cloned and packaged each DREADD-GPCR-P2A-EGFP construct into genome-integrating lentiviral vectors, transduced HMC3 cells, and fluorescence-activated cell sorted for EGFP-positive cells. We confirmed

successful incorporation of GPCR chimeras in EGFP-expressing HMC3 cells through VSV-G immunostaining under non-permeabilizing conditions (**Fig.22a-c**).

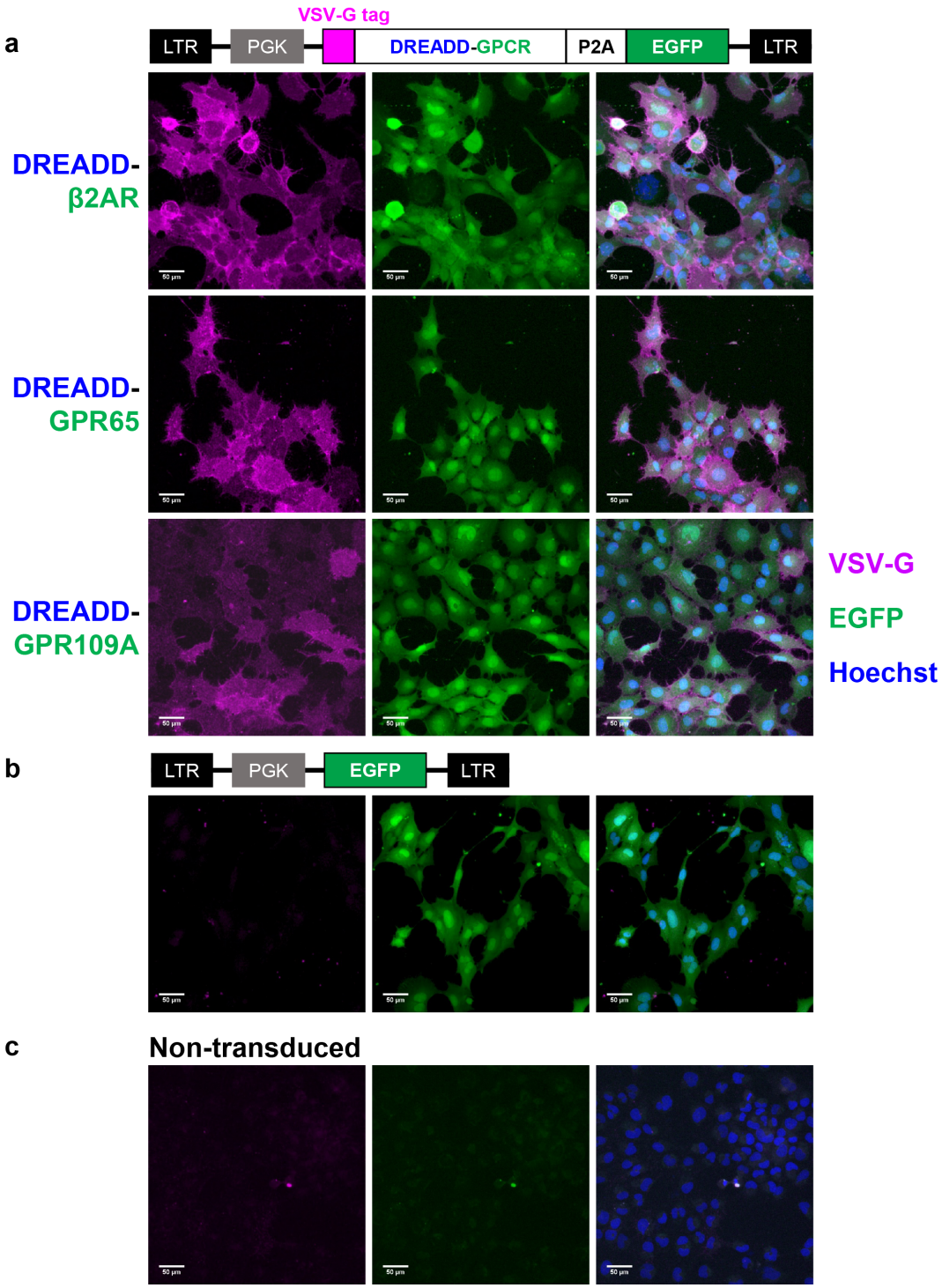

Figure 22: Stable DREADD-GPCR expression in HMC3 cells through lentiviral vectors.
a: Schematic of lentiviral vector with DREADD-GPCR-P2A-EGFP flanked by long terminal repeats (LTRs) and expression driven by the phosphoglycerate kinase (PGK) promoter. Images show maximum intensity projections

of HMC3 cells immunostained for the VSV-G tag under non-permeabilizing conditions. Cells were either transduced with DREADD-β2AR, DREADD-GPR65, or DREADD-GPR109A (**a**); a control vector encoding only EGFP (**b**); or remained non-transduced (**c**). Magenta: VSV-G. Green: EGFP. Blue: nuclear staining with Hoechst.

In parallel, we also confirmed with quantitative reverse transcription PCR (RT-qPCR) that β2AR endogenously occurs in HMC3 cells at moderate mRNA levels (**Fig.23**), allowing stimulation with the selective β2AR agonist levalbuterol.

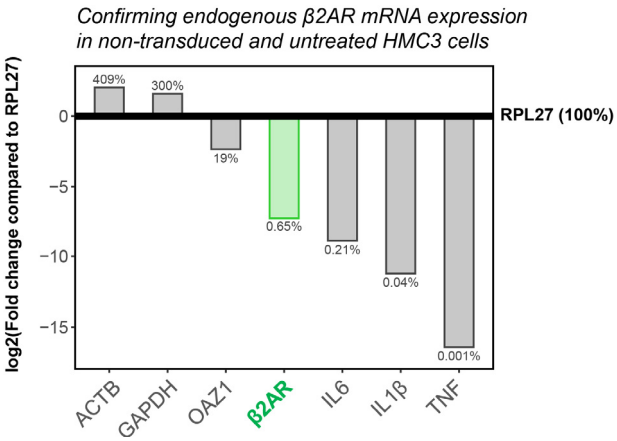

Figure 23: HMC3 cells endogenously express β2AR.
RT-qPCR-based comparison of gene expression. Bars: log2-fold changes compared to RPL27 and are based on the mean of three technical replicates from a representative experiment. Relative transcript abundance is additionally shown as a percentage of RPL27 (100%). ACTB, β-actin. GAPDH, glyceraldehyde-3-phosphate dehydrogenase. OAZ1, ornithine decarboxylase antizyme 1. RPL27, ribosomal protein L27.

Subsequently, we investigated whether our GPCRs can induce Ca^{2+} signaling, which occurs in microglia upon sensing perturbations in their neuronal tissue environment [97]. We imaged HMC3 cell lines after incubation with a Ca^{2+}-sensitive fluorescent dye and applied either levalbuterol, CNO, vehicle, or ATP as positive control, which is known to trigger Ca^{2+} transients in microglia [97]. During six minutes of recording, HMC3 cells commonly displayed spontaneous Ca^{2+} currents (**Fig.24a**), evidenced by fluctuations in fluorescence intensity and software-based [61] Ca^{2+} peak detection. ATP treatment resulted in rapid and synchronized accumulation of Ca^{2+} events (**Fig.24b**, **i**). This was not observed with levalbuterol stimulation of endogenous β2AR (**Fig.24c**, **i**) and neither with DREADD-β2AR (**Fig.24f**, **i**), DREADD-GPR65 (**Fig.24g**, **i**), or DREADD-GPR109A (**Fig.24h-i**) upon CNO application. Thus, we conclude that these GPCRs are not mediators of Ca^{2+} signaling in the microglia-like cell line HMC3.

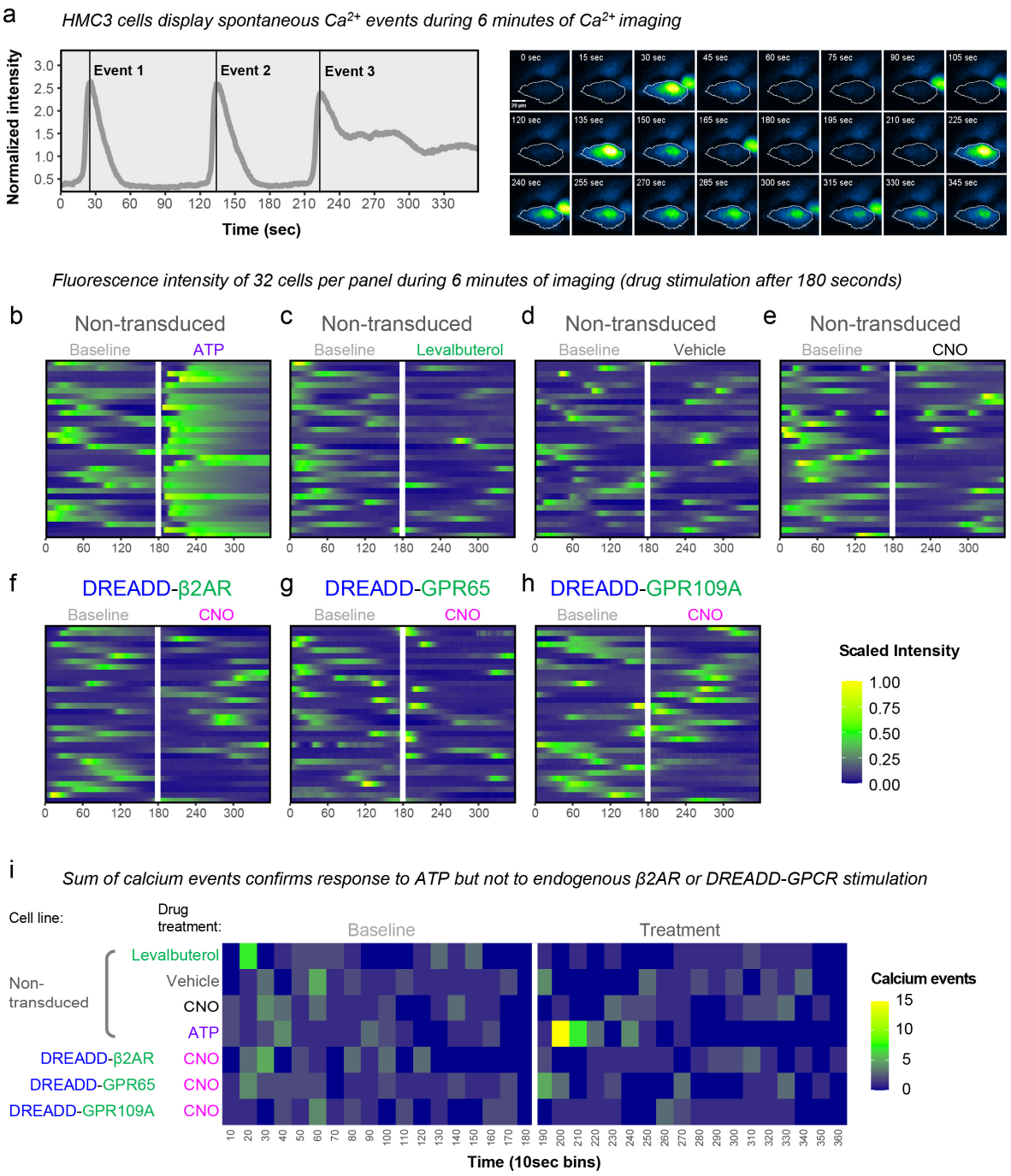

Figure 24: β2AR and DREADD-GPCRs do not induce Ca^{2+} signaling in HMC3 cells.
a: Example of HMC3 cells displaying spontaneous Ca^{2+} events during six minutes of Ca^{2+} imaging. Left: graph shows Ca^{2+}-dependent fluorescence intensity normalized to the mean intensity of the cell throughout the recording. Ca^{2+} events are software-detected. Right: consecutive images of the analyzed cell at representative time points. Ca^{2+}-dependent fluorescence is displayed through an intensity-based color code (blue-green-yellow). **b-h:** Each panel shows an HMC3 cell line treated with either ATP (positive control), levalbuterol, vehicle, or CNO. Each row in a panel is an individual cell. Ca^{2+}-dependent fluorescence intensity is scaled per panel. White vertical line indicates drug application time point after three minutes baseline. **i:** Graph shows sum of software-detected Ca^{2+} events from all cells per condition (panels in **b-h**) across time in 10 second-bins. White vertical line indicates drug application time point.

3.8 DREADD-based chimeras modulate microglial inflammatory gene expression

Next, we investigated immunomodulatory consequences of GPCR signaling and induced inflammation by exposing HMC3 cells to recombinant interferon γ (IFNγ) and interleukin 1β (IL1β). Both cytokines can trigger the transcription of inflammatory genes such as interleukin 6 (IL6) [98]. Tumor necrosis factor (TNF) and IL1β expression are also part of the HMC3 cell inflammatory signature [99]. RT-qPCR confirmed that IFNγ/IL1β stimulation increased the expression of these three inflammatory genes (**Fig.25**).

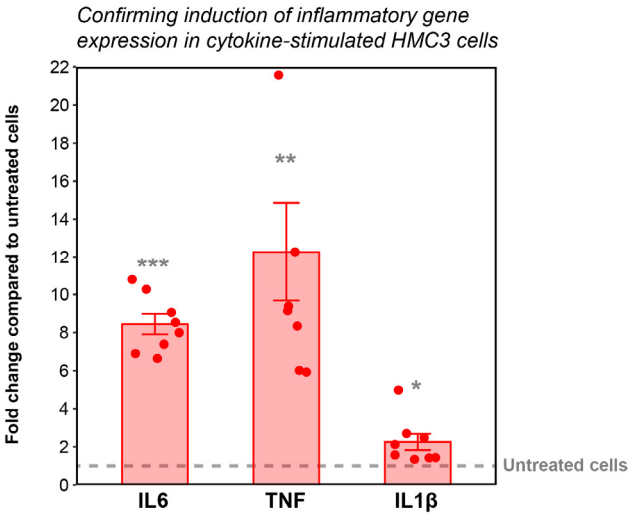

Figure 25: HMC3 cells respond to the cytokines IFNγ and IL1β.
RT-qPCR of HMC3 cells exposed to recombinant IFNγ and IL1β. Expression values of IL6, TNF, and IL1β shown as fold change compared to untreated cells (dashed line). Error bars: standard error of the mean. N = eight experimental repetitions. Two-sided one-sample T-test comparing to a mean of 1 which represents untreated cells: $p^{***} < 0.001$; $p^{*} < 0.01$; $p^{*} < 0.05$. Exact p-values: $p < 0.001$ (IL6); $p = 0.003$ (TNF); $p = 0.02$ (IL1β).

When we treated non-transduced HMC3 cells with levalbuterol and compared IL6, TNF, and IL1β transcript abundance to the mean of untreated samples, we did not observe a response. However, when we combined levalbuterol with IFNγ/IL1β, we found significant changes compared to IFNγ/IL1β stimulation alone. Transcript levels of IL6 increased and TNF decreased, while at the same time IL1β stayed unaltered (**Fig.26a**). Strikingly, we recapitulated the same response pattern with DREADD-β2AR-expressing cells upon CNO application (**Fig.26b**). Importantly, CNO did not impact the inflammatory response in the absence of GPCR chimeras. (**Fig.26c**). We repeated this experiment with the DREADD-GPR65 cell line and found a similar effect with increased IL6 and dampened TNF expression (**Fig.26d**). In contrast, DREADD-GPR109A did not significantly modify inflammatory gene expression induced by IFNγ/IL1β stimulation (**Fig.26e**).
Since all three $G\alpha_s$-coupled receptors modulated gene expression in the same manner, and we have previously shown their ability to induce the second messenger cAMP (see **Fig.8c-d** and **Fig.18c**), we hypothesized that elevated cAMP levels during IFNγ/IL1β exposure are responsible for the shared gene expression signature. To test this, we performed IFNγ/IL1β stimulation in the presence of forskolin, which induces cAMP synthesis in a GPCR-independent manner [92,93]. Indeed, we observed a significant increase of IL6 and decrease of TNF compared to IFNγ/IL1β treatment alone (**Fig.26f**). Interestingly, forskolin prevented the IFNγ/IL1β-mediated upregulation of IL1β mRNA levels, which we did not observe with endogenous β2AR, DREADD-β2AR, or DREADD-GPR65. These results suggest that our DREADD-based strategy provides the means to mimic GPCR signaling with high fidelity, which is not achieved solely by triggering the underlying second messenger cascade with forskolin.

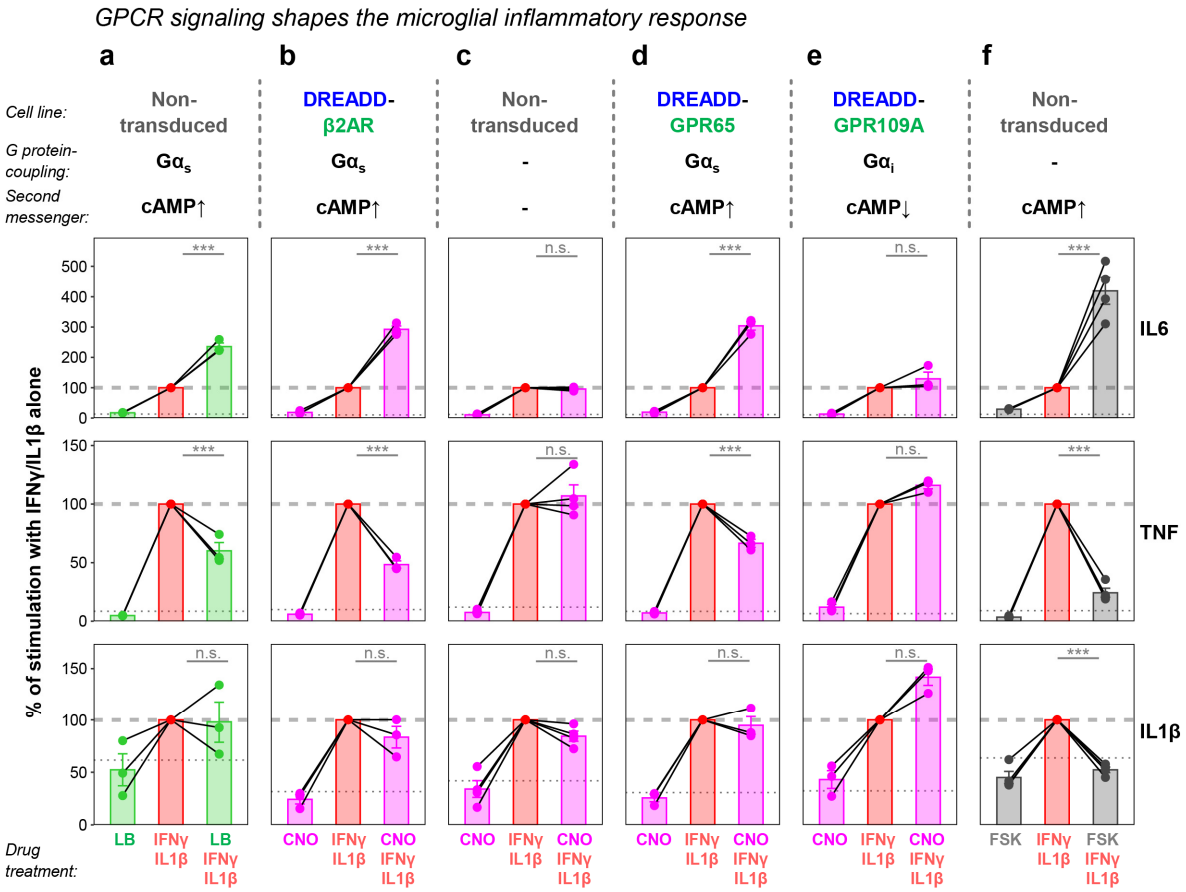

Figure 26: DREADD-based chimeras modulate expression of key inflammatory genes.
a-f: RT-qPCR for IL6 (top row), TNF (middle row), and IL1β (bottom row). Different HMC3 cell lines simultaneously treated with recombinant IFNγ and IL1β, and combinations of levalbuterol (LB, **a**), CNO (**b-e**), or forskolin (FSK, **f**). Graphs show fold changes compared to untreated cells with the IFNγ/IL1β treatment set to 100% within each repetition (dashed line). Dotted line: level of untreated controls. Lines connecting dots: dependent samples within experimental repetitions. Error bars: standard error of the mean. N = three (a, b, d, e) or four (c, f) experimental repetitions. Linear regression analysis with two-sided post-hoc comparisons corrected for multiple testing: $p^{***} < 0.001$; $p^{n.s.} > 0.05$. Exact p-values: $p < 0.001$ (a, IL6); $p < 0.001$ (a, TNF); $p = 0.96$ (a, IL1β); $p < 0.001$ (b, IL6); $p < 0.001$ (b, TNF); $p = 0.62$ (b, IL1β); $p = 0.94$ (c, IL6); $p = 0.79$ (c, TNF); $p = 0.60$ (c, IL1β); $p < 0.001$ (d, IL6); $p < 0.001$ (d, TNF); $p = 0.93$ (d, IL1β); $p = 0.22$ (e, IL6); $p = 0.64$ (e, TNF); $p = 0.18$ (e, IL1β); $p < 0.001$ (f, IL6); $p < 0.001$ (f, TNF); $p < 0.001$ (f, IL1β). See **Supplementary Table S5** for exact p-values of all comparisons.

To substantiate that DREADD-β2AR recapitulates the endogenous β2AR response, we performed next generation mRNA sequencing of our HMC3 cell lines with GPCR signaling under inflammatory conditions (**Fig.27a**). Principal component analysis and hierarchical clustering of sample-to-sample distances resulted in three clusters (**Fig.27b-c**, respectively): Cluster 1 summarized the biological triplicate of non-transduced HMC3 cells without exposure to inflammatory cytokines. Cluster 2 contained all cell lines that have been treated with IFNγ/IL1β but without simultaneous GPCR stimulation. The only exception is DREADD-GPR109A. Ligand stimulation of DREADD-β2AR, DREADD-GPR65, and endogenous β2AR in non-transduced cells altered the inflammatory signature and formed Cluster 3. CNO-treated DREADD-GPR109A stayed in Cluster 2, supporting the previous RT-qPCR data (see **Fig.26e**) and indicating that this receptor is not involved in modulating inflammation in HMC3 cells.

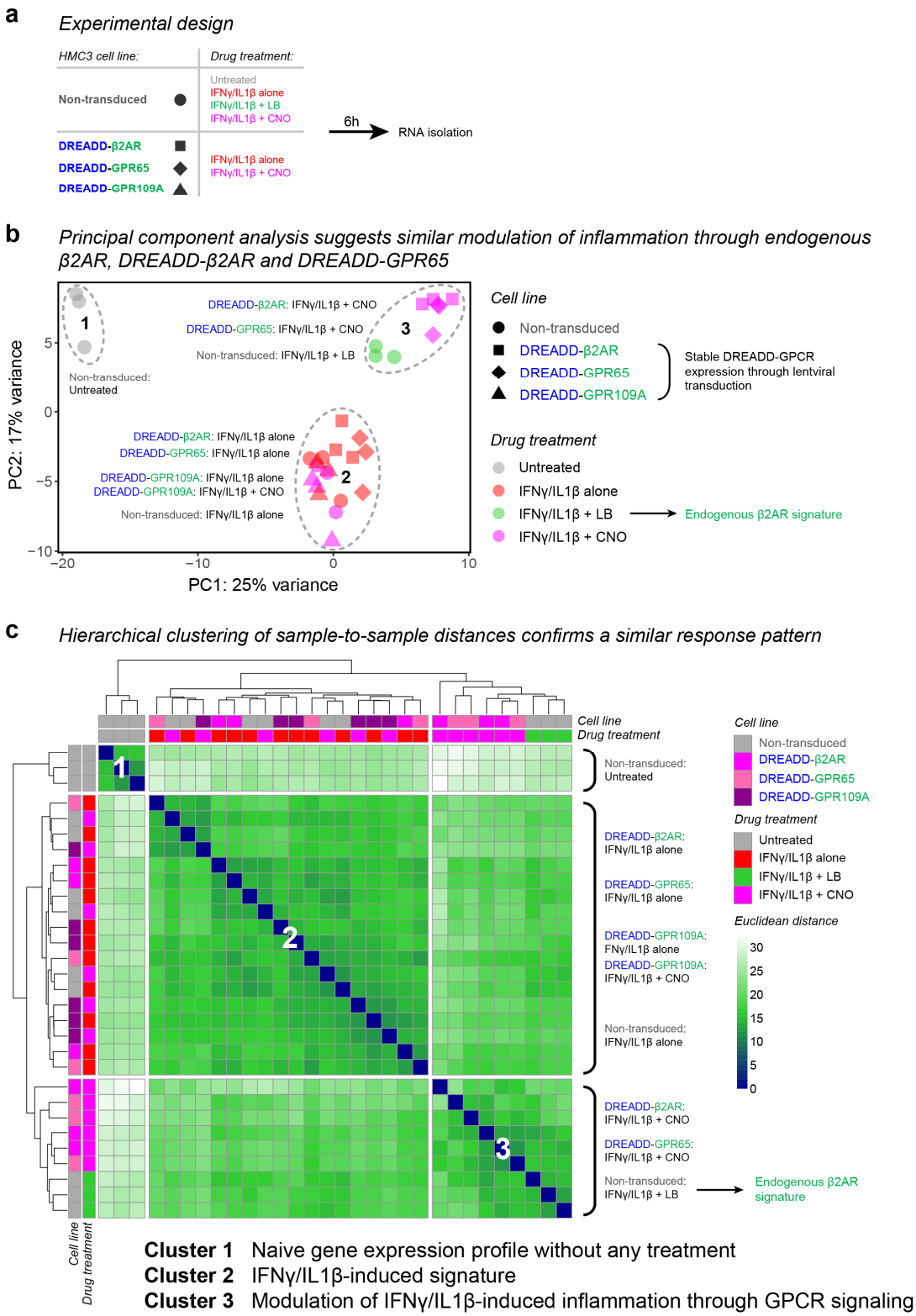

Figure 27: Principal component analysis and hierarchical clustering reveal similar response patterns.
a: Experimental layout for next generation mRNA sequencing of HMC3 cell lines. IFNγ: interferon γ. IL1β: interleukin 1β. LB: levalbuterol. **b:** Principal component analysis including all genes. **c:** Hierarchical clustering of Euclidean sample-to-sample distances based on all genes. Cluster numbers correspond to clusters in the principal component analysis (**a**).

Subsequently, we performed differential expression analysis and first compared non-transduced untreated with IFNγ/IL1β-treated cells. We found 420 differentially expressed genes (**Fig.28a-b**, **Supplementary Table S2**), which we confirmed with gene ontology enrichment analysis to be associated with inflammation (**Fig.28c**).

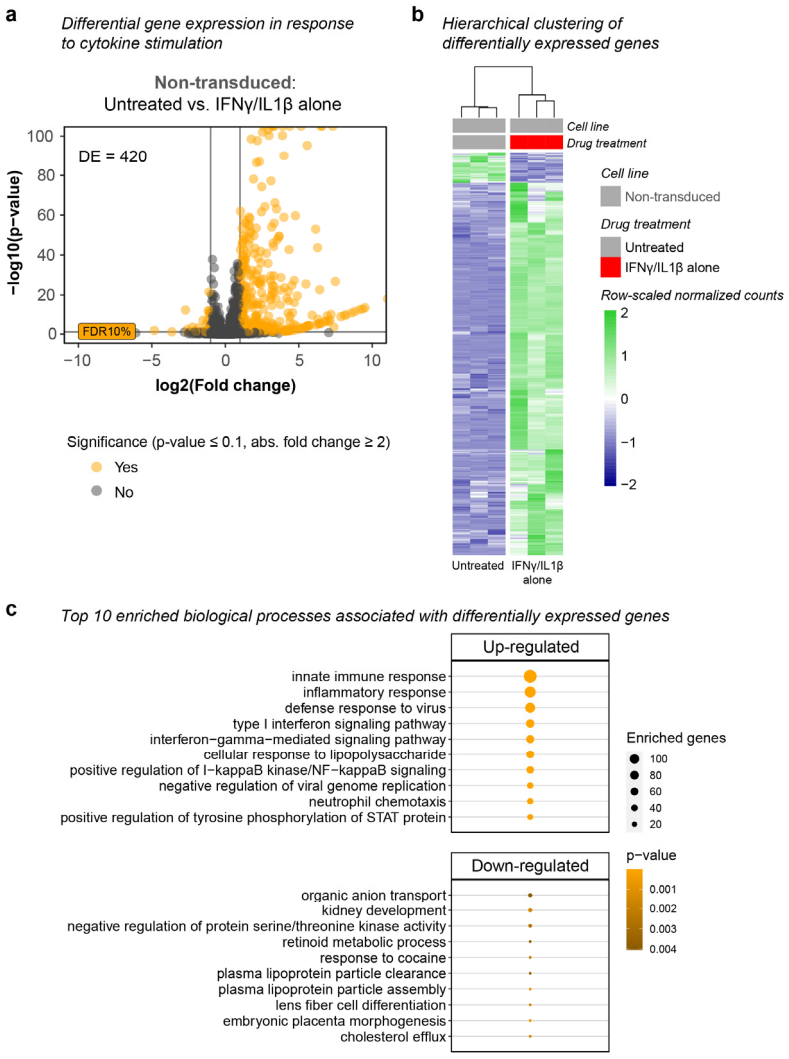

Figure 28: Confirming induction of inflammation through IFNγ and IL1β treatment.
a: Vulcano plot of next generation mRNA sequencing data comparing non-transduced and untreated HMC3 cells to stimulation with IFNγ/IL1β alone. Graph shows individual genes (points), their log2 fold change and p-value. DE: number of differentially expressed genes (orange data points) defined by $p < 0.1$ and absolute linear fold change > 2. Horizontal lines: false discovery rate (FDR) cutoff of 10% ($p < 0.1$). Vertical lines: linear fold change cutoff for downregulation (< -2) and upregulation (> 2), respectively. **b:** Hierarchical clustering of samples (columns) across all differentially expressed genes (rows) based on row-scaled normalized counts. **c:** Gene ontology enrichment analysis showing the top 10 biological processes associated with differentially expressed up- and downregulated genes. Dot size: number of enriched genes associated with a biological process. Dot color: p-value of enrichment analysis (Fisher test).

Next, we were interested to identify genes that are modulated by GPCR signaling during the inflammatory response. Levalbuterol stimulation of endogenous β2AR (**Fig.29a**) resulted in 79 differentially expressed genes while DREADD-β2AR (**Fig.29b**) and DREADD-GPR65 (**Fig.29c**) altered 164 and 99 genes, respectively. We did not find any differentially expressed genes with DREADD-GPR109A (**Fig.29d**), and CNO proved to be largely inert in the absence of DREADD-GPCRs (**Fig.29e**).
To compare the signatures of ligand-stimulated endogenous β2AR, DREADD-β2AR and DREADD-GPR65, we calculated fold changes to the respective IFNγ/IL1β alone treatments for the differentially expressed genes identified in **Figure 29a-c**. The Pearson's coefficient showed a high correlation of approximately 0.8 between endogenous β2AR, DREADD-β2AR and DREADD-GPR65 (**Fig.29f**). Hierarchical clustering organized the genes in three groups (**Fig.29g**,

Supplementary Table S3) which we analyzed through gene ontology enrichment. Whereas gene cluster 2 and 3 indicate biologically diverse processes, gene cluster 1 pointed towards MAPK and cAMP activity (**Fig.29h**), which we earlier identified as downstream targets in our HEK cell assays (see **Fig.8b-d**, **Fig.10a-b** and **Fig.18c-d**).

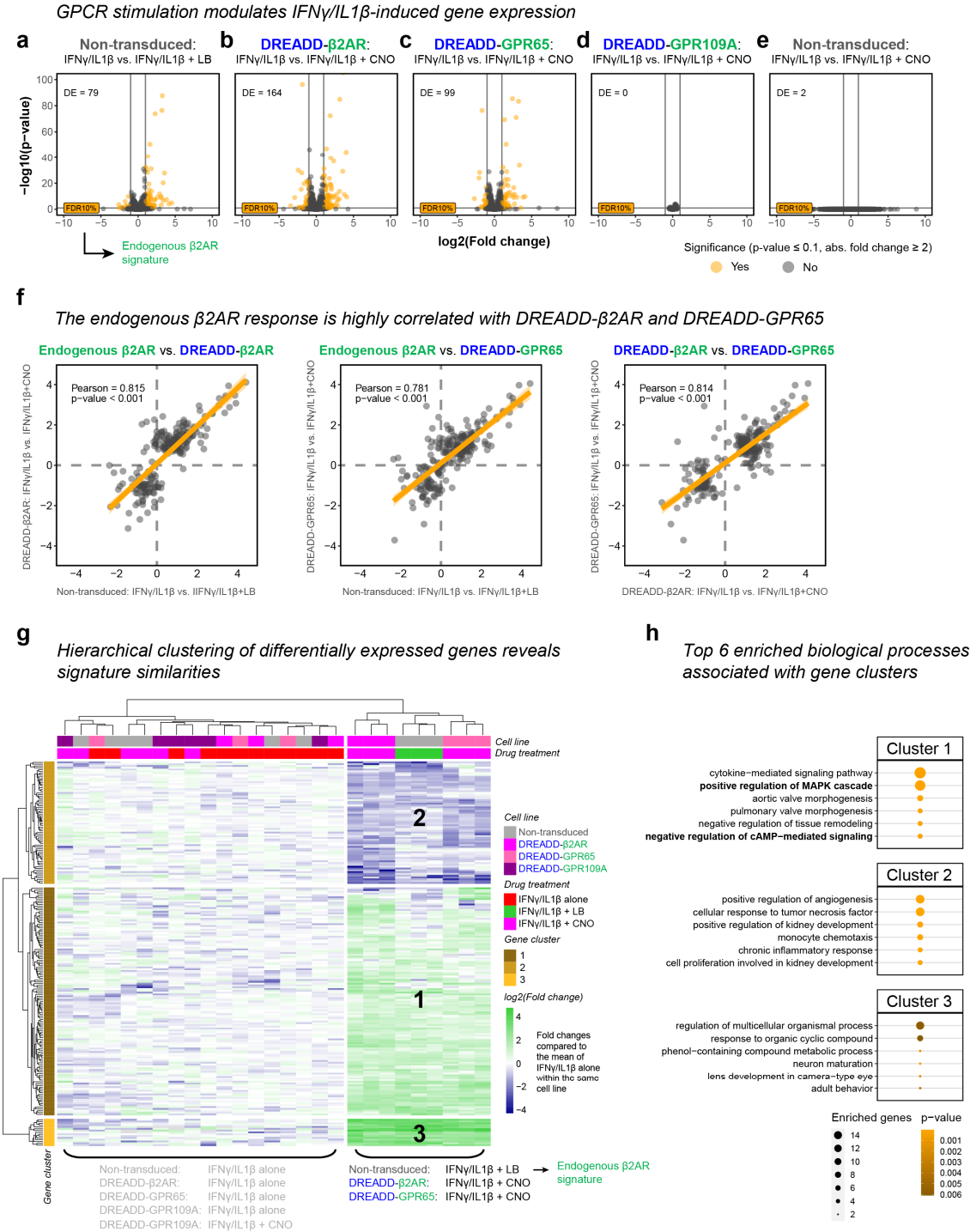

Figure 29: DREADD-GPCRs shape the inflammatory response and recapitulate the β2AR signature.
a-e: Vulcano plots of next generation mRNA sequencing data from different HMC3 cell lines simultaneously treated with IFNγ/IL1β, and either levalbuterol (LB) or CNO. Graphs show individual genes (points), their log2

fold change and p-value in comparison to IFNγ/IL1β alone in the same cell line. DE: number of differentially expressed genes (orange data points) defined by $p < 0.1$ and absolute linear fold change > 2. Horizontal lines: false discovery rate (FDR) cutoff of 10% ($p < 0.1$). Vertical lines: linear fold change cutoff for downregulation (< -2) and upregulation (> 2), respectively. **f:** Pearson correlation of GPCR signatures across all differentially expressed genes (dots) shown in **a-c** based on their log2 fold change compared to IFNγ/IL1β alone in the same cell line. Orange line and ribbon: fitted linear model with 95% confidence intervals. **g:** Hierarchical clustering of samples (columns) and all differentially expressed genes (rows) shown in **a-c** based on log2 fold changes. Green: upregulation compared to IFNγ/IL1β alone in the same cell line. Blue: downregulation compared to IFNγ/IL1β alone in the same cell line. Numbers indicate gene clusters. **h:** Gene ontology enrichment analysis showing the top 6 biological processes associated with gene clusters indicated by the numbers in **g**. Dot size: number of enriched genes associated with a biological process. Dot color: p-value of enrichment analysis (Fisher test).

Figure 30 highlights the response similarity of the $G\alpha_s$-coupled receptors across the topmost differentially expressed genes with one exception: regulator of G protein signaling 2 (RGS2), which was selectively upregulated upon DREADD-β2AR and DREADD-GPR65 stimulation. Since $G\alpha_s$ activity induces RGS2 and provides negative feedback regulation on cAMP synthesis [100], the overexpression of our DREADD-GPCRs might have triggered a stronger response compared to endogenous β2AR.

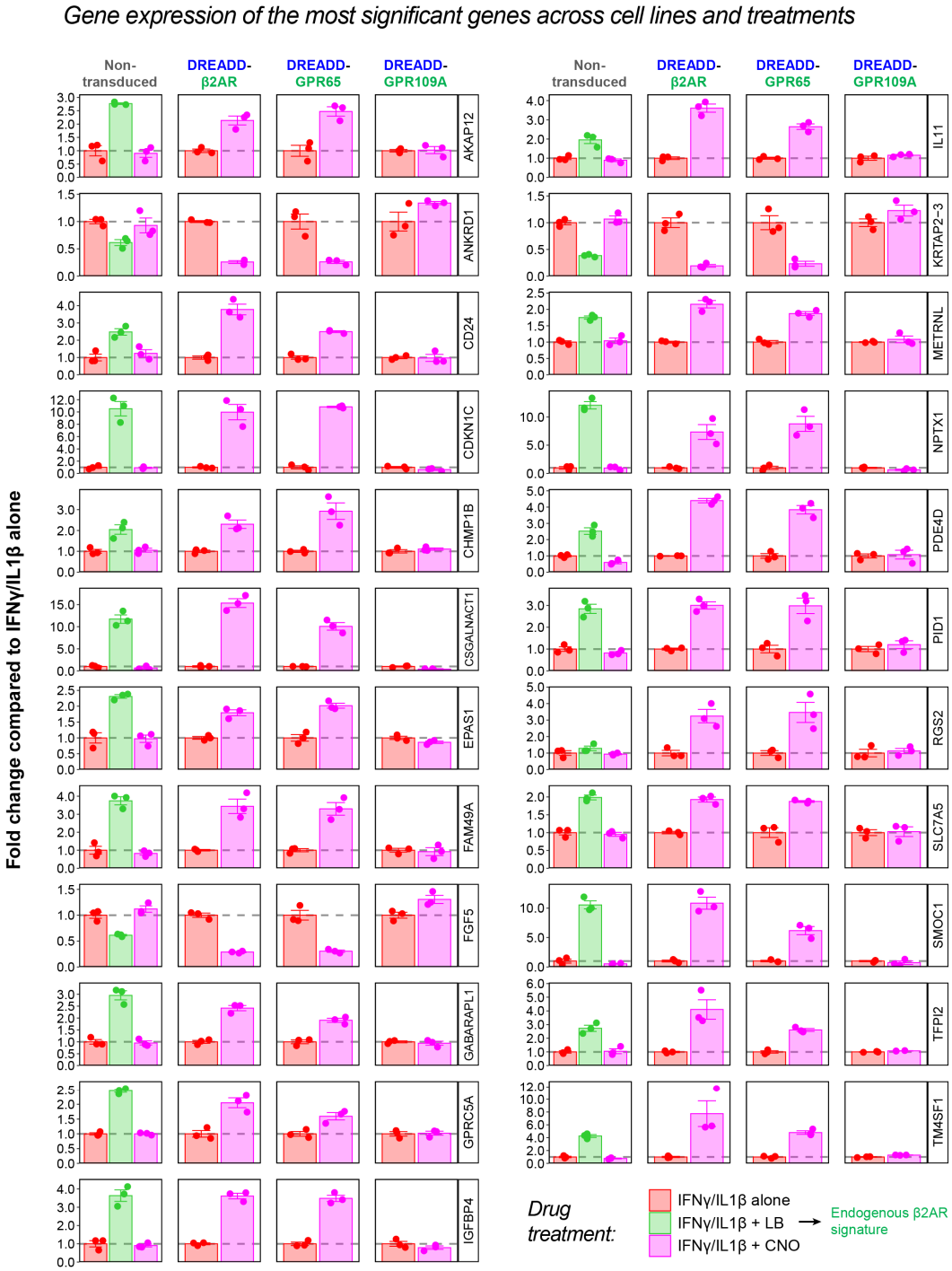

Figure 30: Bar graphs for comparison of the top differentially expressed genes.
Graphs show linear fold changes compared to IFNγ/IL1β alone within the same HMC3 cell line. Genes are selected based on smallest adjusted p-values from comparisons in **Figure 29a-c**. Dashed line: level of IFNγ/IL1β alone. Error bars: standard error of the mean. N = three experimental repetitions.

Even though DREADD-β2AR and DREADD-GPR65 had highly correlated signatures due to canonical $G\alpha_s$-coupling, we found unique features upon hierarchical clustering of their respective response signatures (**Fig.31a**, **Supplementary Table S4**). A small set of genes located in cluster A and C exhibited a distinct expression pattern but was not overall enriched

in distinct biological pathways (**Fig.31b**). To compare this unique response with another $G\alpha_s$-coupled GPCR, we generated stable rM3Ds-expressing HMC3 cells (**Fig.31c**) and performed RT-qPCR on cluster A and C genes. In addition, we also included the three inflammatory genes IL6, TNF and IL1β, which we have quantified in our previously established HMC3 cell lines (see **Fig.26**). We found that the rM3Ds response was distinguished from endogenous β2AR, DREADD-β2AR and DREADD-GPR65 based on principal component analysis (**Fig.31d**) and hierarchical clustering (**Fig.31e**). At the same time, DREADD-β2AR intermingled with endogenous β2AR and was separated from DREADD-GPR65 (**Fig.31d-e**). Notably, rM3Ds also differed in the expression pattern of TNF and IL1β. rM3Ds did not induce the robust downregulation of TNF but instead increased IL1β, which was not affected by β2AR and our DREADD-GPCRs (**Fig.31e**). Upregulation of IL6 was similar between rM3Ds and the other receptors, indicating that this might be a more conserved feature of $G\alpha_s$ signaling. Our data suggest that $G\alpha_s$-driven modulation of gene expression can display subtle differences depending on individual GPCRs and show that DREADD-β2AR successfully mimics endogenous β2AR more closely compared to rM3Ds.

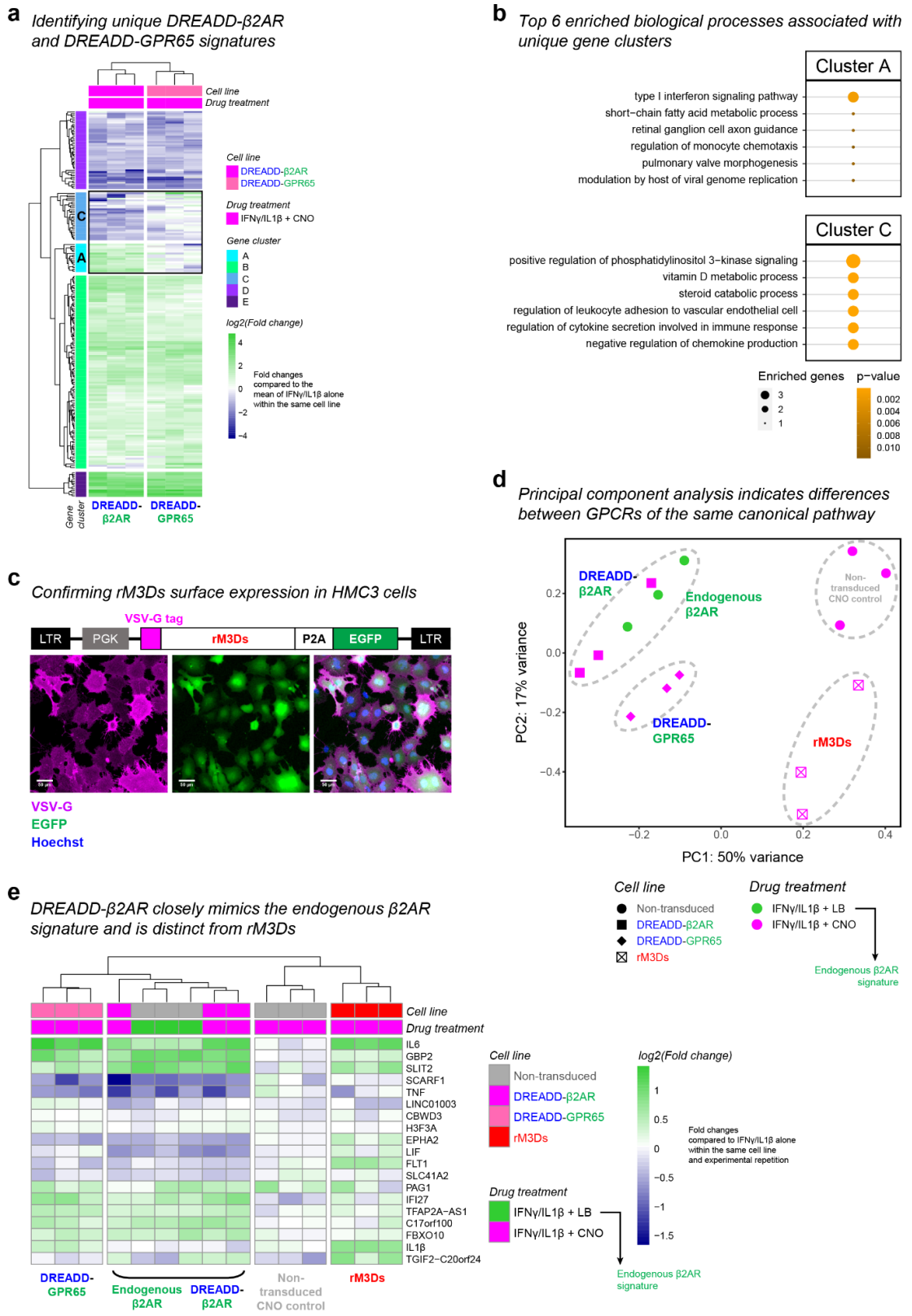

Figure 31: GPCRs of the same canonical pathway can induce subtle but distinct transcriptional patterns.
a: mRNA sequencing-based identification of five gene clusters through hierarchical clustering of HMC3 cell samples (columns) across all differentially expressed genes (rows) in **Figure 29a-c** based on their log2 fold

changes. Upregulation (green) and downregulation (blue) compared to IFNγ/IL1β alone in the same cell line. Black rectangle highlights gene clusters A and C suggestive of a unique pattern between DREADD-β2AR and DREADD-GPR65. **b:** Gene ontology enrichment analysis of the top 6 biological processes associated with genes in cluster A and C. Dot size: number of enriched genes associated with a biological process. Dot color: p-value of enrichment analysis (Fisher test). **c:** Schematic of lentiviral vector used for generating HMC3 cells with stable expression of rM3Ds-P2A-EGFP. LTR: long terminal repeat. PGK: phosphoglycerate kinase promoter. Images show maximum intensity projections of HMC3 cells immunostained for the VSV-G tag under non-permeabilizing conditions. Magenta: VSV-G. Green: EGFP. Blue: nuclear staining with Hoechst. **d-e:** RT-qPCR for genes derived from cluster A and C. HMC3 cell lines simultaneously treated with IFNγ/IL1β and combinations of levalbuterol (LB) or CNO. **d:** Principal component analysis based on log2 fold changes compared to IFNγ/IL1β alone in the same cell line. **e:** Hierarchical clustering of HMC3 cell samples (columns) and genes (rows). Upregulation (green) and downregulation (blue) compared to IFNγ/IL1β alone in the same cell line.

3.9 Investigating the impact of GPCR signaling on microglia function *in-vivo*

Finally, we were interested to study whether GPCRs can influence the ability of microglia to respond to tissue environment perturbations *in-vivo*. However, microglia *in-vivo* manipulation through DREADD-based chimeras is currently hindered by a shortage of efficient and specific vectors [83]. Therefore, we took advantage of a transgenic mouse line with microglia-specific expression of hM4Di to gain general insight through the classical DREADD system (**Fig.32a**). First, we confirmed hM4Di-expression in retinal microglia through immunostaining for an N-terminally attached HA epitope (**Fig.32b-c**).

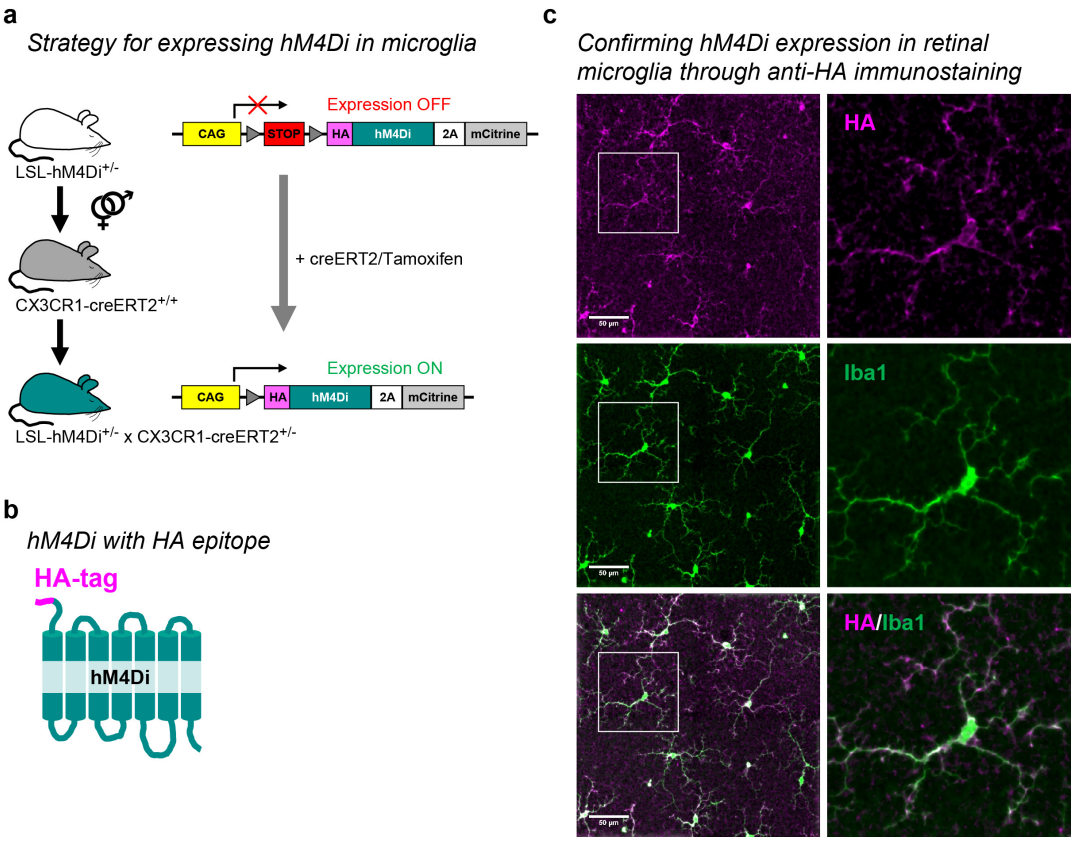

Figure 32: Confirmation of hM4Di expression in microglia.
a: Schematic of obtaining mice with microglial hM4Di expression. A tamoxifen-inducible creERT2 driver line using the CX3CR1 promoter allows excision of the floxed (grey triangles) stop cassette in microglia. **b:** Schematic of

hM4Di N-terminally tagged with an HA-epitope. **c:** Maximum intensity projections of the retinal inner plexiform layer (IPL) from an hM4Di-expressing mouse, immunostained for the HA-tag and microglia (Iba1). Right panels provide a zoomed-in view of the area indicated by the respective white squares.

To induce tissue perturbation, we performed optic nerve crush, a surgical procedure damaging retinal ganglion cell axons which subsequently leads to neurodegeneration (**Fig.33a**) [101]. Microglia located in the inner plexiform layer (IPL) of the crushed retina are close to these dying neurons and will transition to an alarmed state upon sensing the progressing tissue damage [101]. We injected animals with CNO or saline immediately before optic nerve damage and once every 24 hours for the next five days to continuously trigger hM4Di signaling in microglia as they respond to the degenerating environment (**Fig.33b**). To assess the activation state of IPL microglia, we sacrificed animals one hour after the last injection, immnostained for the commonly used activation marker CD68 [102,103], and quantified its expression through surface renderings (**Fig.33c**). In crushed retinas, we observed significantly increased microglial CD68 in CNO-treated hM4Di-expressing mice compared to saline-injected animals of the same genotype or CNO-injected wild type mice. Interestingly, this effect was absent in non-crushed retinas of the same animals (**Fig.33d-e**), indicating that hM4Di signaling enhanced microglia reactivity only when induced in a degenerating environment. These data therefore show that GPCR signaling has the ability to modulate the microglial response *in-vivo* and shape their activation state. Yet, the precise signaling events downstream of hM4Di stimulation in microglia are unknown. hM4Di is a $G\alpha_i$-coupled GPCR and is therefore expected to decrease cAMP synthesis through adenylyl cyclase (AC) inhibition (see **Fig.18e** for schematic) [104]. Surprisingly, we found the exact opposite in HEK cells transfected with hM4Di, where CNO application increased cAMP levels instead (see **Fig.8e**). This suggests that using hM4Di to draw general conclusions about the impact of other $G\alpha_i$-coupled receptors might not be appropriate. In this context, DREADD-based GPCR chimers could offer an interesting alternative to individually investigate specific GPCRs-of-interest.

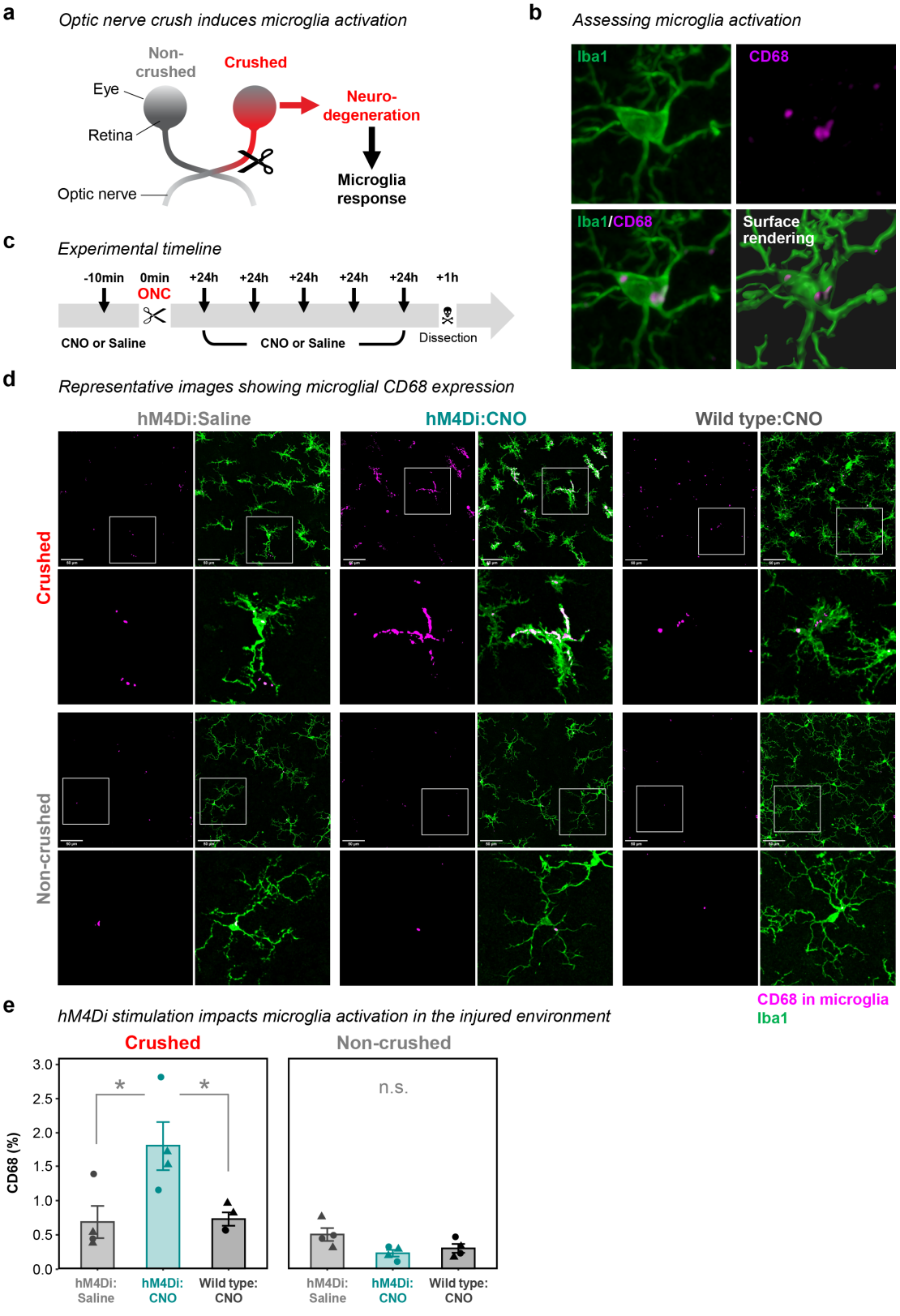

Figure 33: Microglia activation is modulated by hM4Di signaling during optic nerve crush.
a: Schematic showing how optic nerve crush serves as a model for microglia activation. **b:** Experimental timeline and injection paradigm. ONC, optic nerve crush. **c:** Example images showing the quantification of microglial CD68 expression through surface renderings. Microglia are immunostained with the macrophage marker Iba1. **d:**

Representative maximum intensity projections of retinal microglia in the inner plexiform layer (IPL). Bottom panels provide a zoomed-in view of the area indicated by the respective white squares. The CD68 channel has been masked through surface rendering to only show signal within microglia. **e:** Quantification of microglial CD68. Graph shows percentage of total microglia surface volume occupied by CD68. Circles and triangles indicate male and female animals, respectively. Error bars: standard error of the mean. N = four animals. Linear regression analysis with two-sided post-hoc comparisons corrected for multiple testing: $p^{*} < 0.05$; $p^{n.s.} > 0.05$. Exact p-values of comparisons within the crushed eye: p = 0.031 (hM4Di: Saline vs. hM4Di: CNO); p = 0.037 (hM4Di: CNO vs. Wild type: CNO); p = 0.99 (hM4Di: Saline vs. Wild type: CNO). Exact p-values of comparisons within the non-crushed eye: p = 0.06 (hM4Di: Saline vs. hM4Di: CNO); p = 0.77 (hM4Di: CNO vs. Wild type: CNO); p = 0.17 (hM4Di: Saline vs. Wild type: CNO).

4 Discussion

Here, we illustrate the utility of a DREADD-based GPCR chimera strategy to selectively dissect the impact of GPCR activation in microglia. DREADD-based chimeras exploit the advantages of the DREADD system, which responds to CNO with high affinity and in a concentration range that minimizes potential off-target effects [39–41]. This strategy complements existing light-inducible GPCR chimera approaches [26–30] and overcomes two main caveats associated with light stimulation such as phototoxicity [32–35] and the necessity for invasive surgical procedures for deep tissue light delivery [36]. Not only can CNO be administered intraperitoneally and pass the blood brain barrier [42], but it also provides future opportunities to manipulate cells outside of light-accessible tissues such as circulating T-cells, B-cells, monocytes and granulocytes.

Even though our study focuses on immune cell function, GPCRs modulate a wide range of biological processes in other cell types as well. We generated a table with the protein sequences of putative signaling domains for all 292 GPCRs-of-interest included in our alignment, separated into ICL1-3 and C-terminus (**Supplementary Table S1**). These sequences can be inserted in-between the hM3D ligand binding domains as outlined in **Figure 34** to generate a CNO-responsive chimera mimicking a GPCR-of-interest, which provides a framework for straightforward *in-silico* design. Thereby, our approach also complements the previously published DREADD chimera rM3Ds [43], which has been generated by combining the rat equivalent of hM3Dq with ICL2-3 from turkey β1AR to achieve canonical $G\alpha_s$-coupling. Our design strategy utilizes all signaling domains including ICL1-3 and C-terminus for high fidelity recapitulation of a GPCR-of-interest. Our library of signaling domains (**Supplementary Table S1**) also offers the means to create a large variety of possible chimeras and to evaluate the contribution of different ICLs and C-termini to certain pathways.

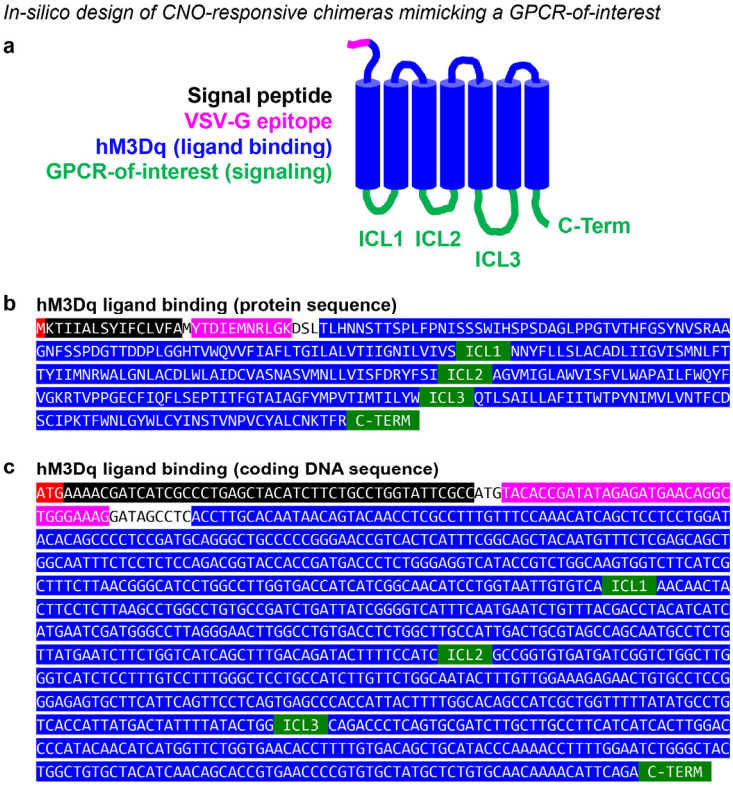

Figure 34: Straightforward *in-silico* design of DREADD-based chimeras. **a:** Schematic of a DREADD-based GPCR chimera containing signal peptide (black) and VSV-G epitope tag (magenta) at the N-terminus. Blue: ligand binding domains of hM3Dq. Green: signaling domains of a GPCR-of-interest. **b-c:** Protein (**b**) and corresponding coding DNA sequence (**c**) of the hM3Dq ligand binding domains. To generate a DREADD-based chimera for a specific GPCR-of-interest, sequences encoding for the respective signaling domains (green) are inserted in the designated fields. ICL1-3, intracellular loops 1-3. C-Term, C-terminus. Protein sequences of putative signaling domains of 292 GPCRs-of-interest are available in **Supplementary Table S1**.

4.1 DREADD-based GPCR chimeras successfully mimic a GPCR-of-interest

Our engineering approach utilized multiple protein sequence alignment to identify CNO-binding DREADD domains and signaling domains of potential GPCRs-of-interest rather than protein domain identification on crystal structures; the latter are not available for most GPCRs. We used published crystal structures for RHO, CHRM3, and β2AR, and confirmed alignment accuracy by comparing our identified domains with these structural representations (**Fig.5**). To validate our strategy, we focused on β2AR, given the extensive literature sources on its function and importance for the immune system [9–11,44,45,71]. Indeed, we found that CNO stimulation of DREADD-β2AR in HEK cells successfully mimicked β2AR signaling and induced cAMP synthesis (**Fig.8b-e**), acted on the MAPK pathway by suppressing transcription from an SRE reporter (**Fig.10a-b**), recruited β-arrestin 2 (**Fig.12a-b**), and phosphorylated ERK1/2 (**Fig.13a**). This suggests that we properly identified ligand binding and signaling domains in DREADD and β2AR. Additionally, we compared DREADD-β2AR with rM3Ds and found that our construct imitated the cAMP and MAPK activity of β2AR with higher fidelity (**Fig.8b-e**, **Fig.10a-b**) and displayed lower constitutive activity (**Fig.11**). We also found that DREADD-β2AR-expressing primary microglia responded to CNO with filopodia formation, replicating previously reported effects of endogenous β2AR activation (**Fig.16**) [45]. This underlines that our chimeric approach is able to modulate microglia function in primary culture systems.

4.2 DREADD-based GPCR chimeras modulate microglia inflammatory gene expression

To dissect immunomodulatory properties of GPCR activation, we utilized the HMC3 microglia-like cell line and established cultures with stable DREADD-GPCR expression to reliably quantify the impact on inflammation. We challenged these cells with the inflammation mediators IFNγ and IL1β, which can induce prominent inflammatory gene expression in the HMC3 line [98] in contrast to commonly used lipopolysaccharide (LPS) [95]. Using RT-qPCR, we found that, in the presence of IFNγ/IL1β, β2AR activation with levalbuterol induced pro- and anti-inflammatory properties reflected by enhanced IL6 and reduced TNF expression, respectively (**Fig.26a**). We successfully mimicked this response with DREADD-β2AR upon CNO stimulation (**Fig.26b**). These findings are in line with studies reporting similar pro- and anti-inflammatory effects of β2AR in different *in-vitro* systems [44,105,106]. In our study, we also generated DREADD-based chimeras imitating the proton-sensing GPR65 and ketone-binding GPR109A. Following CNO stimulation, DREADD-GPR65 modified inflammatory gene expression similar to β2AR (**Fig.26d**), whereas DREADD-GPR109A did not alter IL6, TNF, or IL1β mRNA levels during IFNγ/IL1β-induced inflammation (**Fig.26e**). A previous study [86] observed an anti-inflammatory effect of GPR65 in primary mouse microglia by inhibiting LPS-induced IL1β expression after acidification of the culture medium. Our results suggest that this effect is not present in HMC3 cells when using the cytokines IFNγ/IL1β to trigger inflammation. Another study [87] reported an anti-inflammatory role of GPR109A in the murine N9 microglia-like cell line by downregulating LPS-induced TNF and IL1β after dimethyl fumarate treatment, an immunomodulatory drug and GPR109A agonist. Such discrepancies highlight the response diversity with different *in vitro* systems and inflammatory mediators [86,87].

To further support that DREADD-β2AR can replicate β2AR, we used next generation mRNA sequencing and confirmed a strong correlation between the two responses across

approximately 200 differentially expressed genes (**Fig.29f-g**). This analysis also confirmed that DREADD-GPR65 modulated inflammation in a highly similar manner and gene ontology enrichment hinted that cAMP and MAPK activity are partly responsible for the shared gene expression pattern (**Fig.29h**). The highly correlated signatures of β2AR/DREADD-β2AR and DREADD-GPR65 suggest that canonical $G\alpha_s$-coupling modulates IFNγ/IL1β-mediated inflammation in a similar manner. Nevertheless, we identified a unique transcriptional signature across a small number of genes and confirmed with RT-qPCR that this expression pattern is distinct from $G\alpha_s$-coupled rM3Ds (**Fig.31d-e**). Our data thus show that DREADD-based chimeras coupled to the same canonical pathway are capable of recapitulating unique transcriptional profiles.

4.3 Outlook and future perspectives

Recently, the DREADD system has been explored for selective microglia manipulation *in-vivo* to study their role during neuropathic pain in mice [107]. This study exploited a transgenic mouse line to achieve microglia-specific expression of the $G\alpha_i$-coupled hM4Di in order to shed light on this broad signaling pathway. By using the same mouse model, we found that hM4Di signaling enhanced microglial activation during optic nerve crush-induced neurodegeneration (**Fig.33**). This highlights the impact of GPCRs on modulating microglial responses. However, microglia might express $G\alpha_i$-coupled receptors with non-canonical signaling cascades that are not captured by this DREADD approach. Moreover, our HEK cell data showed that hM4Di was capable of inducing cAMP synthesis (**Fig.8e**) despite being expected to do the opposite [39], which stresses the importance of potential cell type-specific consequences. In this context, DREADD-based chimeras could offer a strategy for a more fine-tuned dissection of specific GPCRs and their role in regulating microglia function.

While microglia *in-vitro* models are critical for neuroimmunological research, it is important to note that different culture systems display distinct genetic signatures and only partially reflect the phenotype of microglia *in-vivo* [108]. Therefore, it would be ultimately desirable to apply DREADD-chimeras in an *in-vivo* context. Currently, *in-vivo* targeting of microglia is a major challenge within the field due to a current lack of efficient and specific vectors [83]. Yet there is ongoing effort within the microglia community to optimize viral vectors and the development of improved targeting strategies might allow *in-vivo* manipulation through DREADD-GPCR in the future.

Yet, GPCR signaling is also critical for many other cell types that are more accessible for chimeric GPCR expression. For example, recent advances with human induced pluripotent stem (hiPS) cells enable researchers to generate complex *in-vitro* models such as microglia-neuron-astrocyte co-cultures [109,110]. It would be interesting to establish stable hiPS cell lines for several DREADD-GPCRs, which can subsequently be differentiated into different cell types. In this context, our DREADD-based chimeras would be an attractive tool for inducing distinct signaling pathways in individual cell types and dissecting the consequences. Thus, our strategy complements existing methods for GPCR investigation and offers an alternative approach to study GPCR signaling in various model systems.

5 Supplementary Figures

Images of Western blot membranes

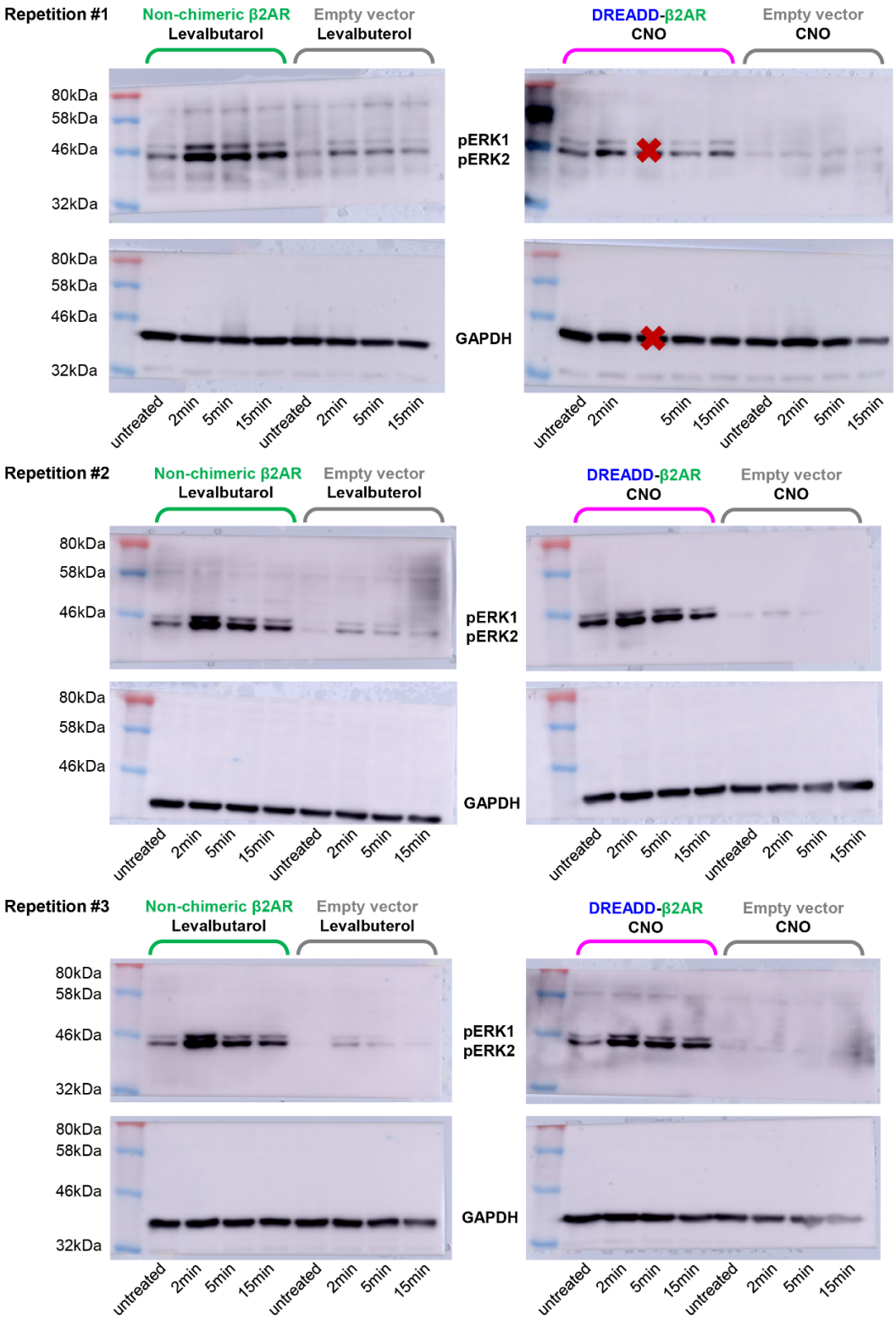

Supplementary Figure S1: Western blot analysis of ERK1/2 phosphorylation.
Summary of all Western blots for phosphorylation analysis of extracellular signal-regulated kinases 1 and 2 (ERK1/2) in untreated, levalbuterol- or CNO-treated HEK cells transfected with non-chimeric β2AR (green), DREADD-β2AR (magenta), or empty vector (grey). Densitometry analysis shown in **Figure 13**. Red cross: lanes excluded due to incorrect sample loading.

6 Supplementary Tables

Supplementary Table S1: Library of putative GPCR signaling domains.
Species indicators (italic lowercase letters before GPCR name): *b*, bovine; *ham*, hamster; *h*, human; m, mouse; r, rat. All GPCRs without a species indicator are human. *, DREADDs. **, GPCRs used for chimeras. ICL1-3, intracellular loops 1-3. C-Term, C-terminus.

GPCR	ICL1	ICL2	ICL3	C-Term
*b***RHO**	TVQHKKLRTP	CKPMSNFRFGENH	QLVFTVKEAAAQQQESATTQKAEKEVT	NCMVTTLCCGKNPLGDDEASTTVSKTETSQVAPA
*h***α1AR**	VACHRHLHSV	SYPLRYPTIVTQRR	RVYVVAKRESRGLKSGLKTDKSDSEQVTLRIHRKNAPAGGSGMASAKT KTHFSVRLLKFSREKKAA	KAFQNVLRIQCLCRKQSSKHALGYTLHPPSQAVEGQHKDMVRIPVGSRETFYRISKTDGVC EWKFFSSMPRGSARITVSKDQSSCTTARVRSKSFLQVCCCVGPSTPSLDKNHQVPTIKVHTI SLSENGEEV
*ham***β2AR**	IAKFERLQTV	TSPFKYQSLLTKNK	RVFQVAKRQLQKIDKSEGRFHSPNLGQVEQDGRSGHGLRRSSKFCLKE HKAL	IAFQELLCLRRSSSKAYGNGYSSNSNGKTDYMGEASGCQLGQEKESERLCEDPPGTESFVN CQGTVPSLSLDSQGRNCSTNDSPL
*h***β2AR****	IAKFERLQTV	TSPFKYQSLLTKNK	RVFQEAKRQLQKIDKSEGRFHVQNLSQVEQDGRTGHGLRRSSKFCLKE HKAL	IAFQELLCLRRSSLKAYGNGYSSNGNTGEQSGYHVEQEKENKLLCEDLPGTEDFVGHQGTV PSDNIDSQGRNCSTNDSLL
*h***CX3CR1b**	LTNSKKPKSV	VLAANSMNNRTVQH	RIIQTLFSCKNHKKAKAI	RYLYHLYGKCLAVLCGRSVHVDFSSSESQRSRHGSVLSSNFTYHTSDGDALLLL
*h***DRD2**	VSREKALQTT	AMPMLYNTRYSSKRR	KIYIVLRRRRKRVNTKRSSRAFRAHLRAPLKGNCTHPEDMKLCTVIMKS NGSFPVNRRRVEAARRAQELEMEMLSSTSPPERTRYSPIPPSHHQLTLP DPSHHGLHSTPDSPAKPEKNGHAKDHPKIAKIFEIQTMPNGKTRTSLKT MSRRKLSQQKEKKAT	KAFLKILHC
*h***GPR109A**	FCFHLKSWKS	VHPHHALNKISNRT	RIIWSLRQRQMDRHAKIKRAI	NFFSTLINRCLQRKMTGEPDNNRSTSVELTGDPNKTRGAPEALMANSGEPWSPSYLGPTS P
*h***GPR183**	IVQNRKKINS	VHPLRYNKIKRIEH	QICCKLFRTAKQNPLTEKSGVNKKAL	RKVMRMLKRQVSVSISSAVKSAPEENSREMTETQMMIHSKSSNGK
*h***GPR65**	SFLQAKKESE	VYPLKFFFLRTRRF	KVYQAVRHNKATENKEKKRII	YDMWNILKFCTGRCNTSQRQRKRILSVSTKDTMELEVLE
*h***GPR84**	LAIQPKLRTR	AHPKLFPQVFSAKG	LIHRQVKRAAQALDQYKLRQASIHSNHVARTDEAMPGRFQELDSRLAS GGPSEGISSEPVSAATTQTLEGDSSEVGDQINSKRAKQMAEKSPPEAS AKAQPIKGARRAPDSSSEFGKVT	QAYGSILKRGPRSFHRLH
*h***M3Dq***	FKVNKQLKTV	TRPLTYRAKRTTKR	RIYKETEKRTKELAGLQASGTEAETENFVHPTGSSRSCSSYELQQQSMK RSNRRKYGRCHFWFTTKSWKPSSEQMDQDHSSSDSWNNNDAAASL ENSASSDEEDIGSETRAIYSIVLKLPGHSTILNSTKLPSSDNLQVPEEELG MVDLERKADKLQAQKSVDDGGSFPKSFSKLPIQLESAVDTAKTSDVNS SVGKSTATLPLSFKEATLAKRFALKTRSQITKRKRMSLVKEKKAA	TTFKMLLLCQCDKKKRRKQQYQQRQSVIFHKRAPEQAL
*h***M4Di***	IKVNRQLQTV	TKPLTYPARRTTKM	HISLASRSRVHKHRPEGPKEKKAKTLAFLKSPLMKQSVKKPPPGEAARE ELRNGKLEEAPPPALPPPPRPVADKDTSNESSSGSATQNTKERPATELS TTEATTPAMPAPPLQPRALNPASRWSKIQIVTKQTGNECVTAIEIVPAT PAGMRPAANVARKFASIARNQVRKKRQMAARERKVT	KTFRHLLLCQYRNIGTAR
*h***RHO**	TVQHKKLRTP	CKPMSNFRFGENH	QLVFTVKEAAAQQQESATTQKAEKEVT	NCMLTTICCGKNPLGDDEASATVSKTETSQVAPA
*m***CX3CR1**	LTNSRKPKSI	VLAANSMNNRTVQH	RIIQTLFSCKNRKKARAV	RYLGHLYRKCLAVLCGHPVHTGFSPESQRSRQDSILSSFTHYTSEGDGSLLL
*m***GPR109A****	FCFHLKSWKS	VHPHHFLNKISNRT	RIIWSLRQRQMDRHAKIKRAI	NFFSTCINRCLRKKTLGEPDNNRSTSVELTGDPSTTRSIPGALMADPSEPGSPPYLASTSR
*m***GPR183**	IVQNRKKINS	VHPLRYNKIKRIEY	QICCKLFRTAKQNPLTEKSGVNKKAL	RKVMKMLKRQVSVSISSAVRSAPEENSREMTESQMMIHSKASNGR
*m***GPR65****	SFLQAKKENE	VYPLKFSFLRTRRF	KVYRAVRHNQATENSEKRRII	ADMWNILKLCTRKHNRHQGKKRDILSVSTRDAVELEIID

GPCR	ICL1	ICL2	ICL3	C-Term
***m*GPR84**	LAIRPKLRTR	AHPKLFPQVFSAKG	LIHRQVKRAARALDQYGLHQASIRSHQVAGTQEAMPGHFQELDSGVASRGPSEGISSEPVSAATTQTLEGDSSEAGGQGIRKAAQQIAERSLPEVHRKPRETAGARRATDAPSEFGKVT	HAYGSILKRGPQSFRRFH
***m*RHO**	TVQHKKLRTP	CKPMSNFRFGENH	QLVFTVKEAAAQQQESATTQKAEKEVT	NCMLTTLCCGKNPLGDDDASATASKTETSQVAPA
rα1AR	VACHRHLHSV	SYPLRYPTIVTQRR	RVYVVAKRESRGLKSGLKTDKSDSEQVTLRIHRKNVPAEGGGVSSAKNKTHFSVRLLKFSREKKAA	KAFQNVLRIQCLRRRQSSKHALGYTLHPPSQALEGQHRDMVRIPVGSGETFYKISKTDGVCEWKFFSSMPQGSARITVPKDQSACTTARVRSKSFLQVCCCVGSSAPRPEENHQVPTIKIHTISLGENGEEV
ACKR1	LFRPLFRWQLCPGWPV	GHRLGAGQVPGL	LKKALGMGPGPW	RTLLPSLPLPEGWSSHLDTLGSKS
ACKR2	LLRYVPRRRM	VHAQPYHRLRTRAK	RIGCVLVRLRPAGQGRAL	QYLKAFLAAVLGWHLAPGTAQASLSSCSESSILTAQEEMTGMNDLGERQSENYPNKEDVGNKSA
ACKR3	NIQAKTTGYD	TYFTNTPSSRKKMV	LLARAISASSDQEKHSSR	YELMKAFIFKYSAKTGLTKLIDASRVSETEYSALEQSTK
ACKR4	YAYYKKQRTK	KVPSQSGVGKPC	ITARTLMKMPNIKISRPL	NYVMKVAKKYGSWRRQRQSVEEFPFDSEGPTEPTSTFSI
ADORA1	VKVNQALRDA	KIPLRYKMVVTPRR	EVFYLIRKQLNKKVSASSGDPQKYYGKELKIA	VTFLKIWNDHFRCQPAPPIDEDLPEERPDD
ADORA2A	VWLNSNLQNV	RIPLRYNGLVTGTR	RIFLAARRQLKQMESQPLPGERARSTLQKEVHAA	QTFRKIIRSHVLRQQEPFKAAGTSARVLAAHGSDGEQVSLRLNGHPPGVWANGSAPHPERRPNGYALGLVSGGSAQESQGNTGLPDVELLSHELKGVCPEPPGLDDPLAQDGAGVS
ADORA2B	VGTANTLQTP	CVPLRYKSLVTGTR	KIFLVACRQLQRTELMDHSRTTLQREIHAA	YTFHKIISRYLLCQADVKSGNGQAGVQPALGVGL
ADRA1B	VACNRHLRTP	RYSLQYPTLVTRRK	RVYIVAKRTTKNLEAGVMKEMSNSKELTLRIHSKNFHEDTLSSTKAKGHNPRSSIAVKLFKFSREKKAA	RAFVRILGCQCRGRGRRRRRRRRRLGGCAYTYRPWTRGGSLERSQSRKDSLDDSGSCLSGSQRTLPSASPSPGYLGRGAPPPVELCAFPEWKAPGALLSLPAPEPPGRRGRHDSGPLFTFKLLTEPESPGTDGGASNGGCEAAADVANGQPGFKSNMPLAPGQF
ADRA1D	VACNRHLQTV	RHSLKYPAIMTERK	RVYVVARSTTRSLEAGVKRERGKASEVVLRIHCRGAATGADGAHGMRSAKGHTFRSSLSVRLLKFSREKKAA	RAFLRLLRCQCRRRRRRRPLWRVYGHHWRASTSGLRQDCAPSSGDAPPGAPLALTALPDPDPEPPGTPEMQAPVASRRKPPSAFREWRLLGPFRRPTTQLRAKVSSLSHKIRAGGAQRAEAACAQRSEVEAVSLGVPHEVAEGATCQAYELADYSNLRETDI
ADRA2A	VFTSRALKAP	TQAIEYNLKRTPRR	RIYQIAKRRTRVPPSRRGPDAVAAPPGGTERRPNGLGPERSAGPGGAEAEPLPTQLNGAPGEPAPAGPRDTDALDLEESSSSDHAERPPGPRRPERGPRGKGKARASQVKPGDSLPRRGPGATGIGTPAAGPGEERVGAAKASRWRGRQNREKRFT	RAFKKILCRGDRKRIV
ADRA2B	VLTSRSLRAP	SRALEYNSKRTPRR	RIYLIAKRSNRRGPRAKGGPGQGESKQPRPDHGGALASAKLPALASVASAREVNGHSKSTGEKEEGETPEDTGTRALPPSWAALPNSGQGQKEGVCGASPEDEAEEEEEEEECEPQAVPVSPASACSPPLQQPQGSRVLATLRGQVLLGRGVGAIGGQWWRRRAQLTREKRFT	RAFRRILCRPWTQTAW
ADRA2C	VLTSRALRAP	TQAVEYNLKRTPRR	RIYRVAKLRTRTLSEKRAPVGPDGASPTTENGLGAAAGAGENGHCAPPPADVEPDESSAAAERRRRRGALRRGGRRRAGAEGGAGGADGQGAGPGAAESGALTASRSPGPGGRLSRASSRSVEFFLSRRRRARSSVCRRKVAQAREKRFT	RSFKHILFRRRRRGFRQ
ADRB1	IAKTPRLQTL	TSPFRYQSLLTRAR	RVFREAQKQVKKIDSCERRFLGGPARPPSPSPSPVPAPAPPPGPPRPAAAAATAPLANGRAGKRRPSRLVALREQKAL	KAFQRLLCCARRAARRRHATHGDRPRASGCLARPGPPPSPGAASDDDDDDVVGATPPARLLEPWAGCNGGAAADSDSSLDEPCRPGFASESKV
ADRB3	IAWTPRLQTM	TNPLRYGALVTKRC	RVFVVATRQLRLLRGELGRFPPEESPPAPSRSLAPAPVGTCAPPEGVPACGRRPARLLPLREHRAL	SAFRRLLCRCGRRLPPEPCAAARPALFPSGVPAARSSPAQPRLCQRLDGASWGVS
AGTR1	IYFYMKLKTV	VHPMKSRLRRTMLV	LIWKALKKAYEIQKNKPRNDDIF	RYFLQLLKYIPPKAKSHSNLSTKMSTLSYRPSDNVSSSTKKPAPCFEVE
AGTR2	FCCQKGPKKV	IYPFLSQRRNPWQ	GIRKHLLKTNSYGKNRITRDQVL	QKLRSVFRVPITWLQGKRESMSCRKSSSLREMETFVS
APLNR	VFRSSREKRRS	VRPVANARLRLRVS	FIAQTIAGHFRKERIEGLRKRRRLL	QACTSMLCCGQSRCAGTSHSSSGEKSASYSSGHSQGPGPNMGKGGEQMHEKSIPYSQETLVVD

GPCR	ICL1	ICL2	ICL3	C-Term
AVPR1A	LHRTPRKTSR	CHPLKTLQQPARR	FICYNIWCNVRGKTASRQSKGAEQAGVAFQKGFLLAPCVSSVKSISRAKIRTV	QDCVQSFPCCQNMKEKFNKEDTDSMSRRQTFYSNNRSPTNSTGMWKDSPKSSKSIKFIPVST
AVPR1B	LGQLGRKRSR	CHPLRSLQQPGQS	LICHEICKNLKVKTQAWRVGGGGWRTWDRPSPSTLAATTRGLPSRVSSINTISRAKIRTV	RPLRHLACCGGPQPRMRRRLSDGSLSSRHTTLLTRSSCPATLSLSLSLTLSGRPRPEESPRDLELADGEGTAETIIF
AVPR2	LARRGRRGHWAP	CRPMLAYRHGSGAH	LIFREIHASLVPGPSERPGGRRRGRRTGSPGEGAHVSAAVAKTV	SELRSLLCCARGRTPPSLGPQDESCTTASSSLAKDTSS
BDKRB1	FLLPRRQLNV	VHPMASRRQQRRRQ	HILASLRTREEVSRTRCGGRKDSKTT	TKVWELYKQCTPKSLAPISSSHRKEIFQLFWRN
BDKRB2	FCLHKSSCTV	VKTMSMGRMRGVRW	QIMQVLRNNEMQKFKEIQTERRAT	KKSWEVYQGVCQKGGCRSEPIQMENSMGTLRTSISVERQIHKLQDWAGSRQ
BRS3	FFKTKSMQTV	VKPLERQPSNAILK	LIARTLYKSTLNIPTEEQSHARKQIESRKRIA	KHFKAQLFCCKAERPEPPVADTSLTTLAVMGTVPGTGSIQMSEISVTSFTGCSVKQAEDRF
C3AR1	AGLKMQRTV	FKPIWCQNHRNVGM	FIVFRMQRGRFAKSQSKTF	KKARQSIQGILEAAFSEELTRSTHCPSNNVISERNSTTV
C5AR1	TAFEAKRTI	FKPIWCQNFRGAGL	FILLRTWSRRATRSTKTL	GRLRKSLPSLLRNVLTEESVVRESKSFTRSTVDTMAQKTQAV
C5AR2	AGKVARRRV	LGPAWWSTVQRACG	ALLCWAARRCR	RSLPAACHWALRESQGQDESVDSKKSTSHDLVSEMEV
CCKAR	LIRNKRMRTV	CKPLQSRVWQTKSH	LISLELYQGIKFEASQKKSAKERKPSTTSSGKYEDSDGCYLQKTRPPRKLELRQLSTGSSSRANRIRSNSSAANLMAKKRVI	LGFMATFPCCPNPGPPGARGEVGEEEEGGTTGASLSRFSYSHMSASVPPQ
CCKBR	LGLSRRLRTV	CRPLQARVWQTRSH	LISRELYLGLRFDGDSDSDSQSRVRNQGGLPGAVHQNGRCRPETGAVGEDSDGCYVQLPRSRPALELTALTAPGPGSGSRPTQAKLLAKKRVV	QACLETCARCCPRPPRARPRALPDEDPPTPSIASLSRLSYTTISTLGPG
CCR1	LVQYKRLKNM	VHAVFALRARTVTF	GIIKILLRRPNEKKSKAV	KYLRQLFHRRVAVHLVKWLPFLSVDRLERVSSTSPSTGEHELSAGF
CCR10	HLAARRAARSP	ARALPAGPRPSTPGR	LLGRTLLAARGPERRRAL	QDLRRLLRGGSCPSGPQPRRGCPRRPRLSSCSAPTETHSLSWDN
CCR2	LINCKKLKCL	VHAVFALKARTVTF	GILKTLLRCRNEKKRHRAV	SLFHIALGCRIAPLQKPVCGGPGVRPGKNVKVTTQGLLDGRGKGKSIGRAPEASLQDKEGA
CCR3	LIKYRRLRIM	VHAVFALRARTVTF	GIIKTLLRCPSKKKYKAI	KYLRHFFHRHLLMHLGRYIPFLPSEKLERTSSVSPSTAEPELSIVF
CCR4	LFKYKRLRSM	VHAVFSLRARTLTY	MIIRTLQHCKNEKKNKAV	KYILQLFKTCRGLFVLCQYCGLLQIYSADTPSSSYTQSTMDHDLHDAL
CCR5	LINCKRLKSM	VHAVFALKARTVTF	GILKTLLRCRNEKKRHRAV	NYLLVFFQKHIAKRFCKCCSIFQQEAPERASSVYTRSTGEQEISVGL
CCR6	FAFYKKARSM	VQATKSFRLRSRTLPR	FIVKTLVQAQNSKRHKAI	NYFLKILKDLWCVRRKYKSSGFSCAGRYSENISRQTSETADNDNASSFTM
CCR7	YIYFKRLKTM	VQAVSAHRHRARVL	VIIRTLLQARNFERNKAI	NDLFKLFKDLGCLSQEQLRQWSSCRHIRRSSMSVEAETTTTFSP
CCR8	LVVCKKLRSI	VHAVYALKVRTIRM	KILHQLKRCQNHNKTKAI	KHLSEIFQKSCSQIFNYLGRQMPRESCEKSSSCQQHSSRSSSVDYIL
CCR9	YWYCTRVKTM	AQAMRAHTWREKRL	IIIHTLIQAKKSSKHKAL	RDLVKTLKNLGCISQAQWVSFTRREGSLKLSSMLLETTSGALSL
CCRL2	LVKYKGLKRV	LHKGNFFSARRRVPC	QMRKTLRFREQRYSLF	KYLCRCFHLRSNTPLQPRGQSAQGTSREEPDHSTEV
CHRM1	FKVNTELKTV	TRPLSYRAKRTPRR	RIYRETENRARELAALQGSETPGKGGGSSSSSERSQPGAEGSPETPPGRCCRCCRAPRLLQAYSWKEEEEEDEGSMESLTSSEGEEPGSEVVIKMPMVDPEAQAPTKQPPRSSPNTVKRPTKKGRDRAGKGQKPRGKEQLAKRKTFSLVKEKKAA	DTFRLLLLCRWDKRRWRKIPKRPGSVHRTPSRQC
CHRM2	IKVNRHLQTV	TKPLTYPVKRTTKM	HISRASKSRIKKDKKEPVANQDPVSPSLVQGRIVKPNNNNMPSSDDGLEHNKIQNGKAPRDPVTENCVQGEEKESSNDSTSVSAVASNMRDDEITQDENTVSTSLGHSKDENSKQTCIRIGTKTPKSDSCTPTNTTVEVVGSSGQNGDEKQNIVARKIVKMTKQPAKKKPPPSREKKVT	KTFKHLLMCHYKNIGATR
CHRM3	FKVNKQLKTV	TRPLTYRAKRTTKR	RIYKETEKRTKELAGLQASGTEAETENFVHPTGSSRSCSSYELQQQSMKRSNRRKYGRCHFWFTTKSWKPSSEQMDQDHSSSDSWNNNDAAASLENSASSDEEDIGSETRAIYSIVLKLPGHSTILNSTKLPSSDNLQVPEEELGMVDLERKADKLQAQKSVDDGGSFPKSFSKLPIQLESAVDTAKTSDVNSSVGKSTATLPLSFKEATLAKRFALKTRSQITKRKRMSLVKEKKAA	TTFKMLLLCQCDKKKRRKQQYQQRQSVIFHKRAPEQAL

GPCR	ICL1	ICL2	ICL3	C-Term
CHRM4	IKVNRQLQTV	TKPLTYPARRTTKM	HISLASRSRVHKHRPEGPKEKKAKTLAFLKSPLMKQSVKKPPPGEAARE ELRNGKLEEAPPPALPPPPRPVADKDTSNESSSGSATQNTKERPATELS TTEATTPAMPAPPLQPRALNPASRWSKIQIVTKQTGNECVTAIEIVPAT PAGMRPAANVARKFASIARNQVRKKRQMAARERKVT	KTFRHLLLCQYRNIGTAR
CHRM5	FKVNSQLKTV	TRPLTYRAKRTPKR	RIYRETEKRTKDLADLQGSDSVTKAEKRKPAHRALFRSCLRCPRPTLAQR ERNQASWSSSRRSTSTTGKPSQATGPSANWAKAEQLTTCSSYPSSEDE DKPATDPVLQVVYKSQGKESPGEEFSAEETEETFVKAETEKSDYDTPNY LLSPAAAHRPKSQKCVAYKFRLVVKADGNQETNNGCHKVKIMPCPFP VAKEPSTKGLNPNPSHQMTKRKRVVLVKERKAA	KTFKMLLLCRWKKKKVEEKLYWQGNSKLP
CMKLR1	ATFKMKKTV	LLPVWSQNHRSVRL	TIVCKLQRNRLAKTKKPF	KFKVALFSRLVNALSEDTGHSSYPSHRSFTKMSSMNERTSMNERETGML
CNR1	ILHSRSLRCRP	HRPLAYKRIVTRPK	ILWKAHSHAVRMIQRGTQKSIIIHTSEDGKVQVTRPDQARMDIRLA	HAFRSMFPSCEGTAQPLDNSMGDSDCLHKHANNAASVHRAAESCIKSTVKIAKVTMSVS TDTSAEAL
CNR2	ILSSHQLRRKP	RYPPSYKALLTRGR	HVLWKAHQHVASLSGHQDRQVPGMARMRLDVRLA	SSAHHCLAHWKKCVRGLGSEAKEEAPRSSVTETEADGKITPWPDSRDLDLSDC
CXCR1	ILYSRVGRSV	VHATRTLTQKRH	FTLRTLFKAHMGQKHRAM	HGFLKILAMHGLVSKEFLARHRVTSYTSSSVNVSSNL
CXCR2	ILYSRVGRSV	VHATRTLTQKRYL	FTLRTLFKAHMGQKHRAM	HGLLKILAIHGLISKDSLPKDSRPSFVGSSSGHTSTTL
CXCR3	LLSRRTALSS	VHATQLYRRGPPAR	HILAVLLVSRGQRRLRAM	ERMWMLLLRLGCPNQRGLQRQPSSSRRDSSWSETSEASYSGL
CXCR4	MGYQKKLRSM	VHATNSQRPRKLLA	IIISKLSHSKGHQKRKAL	TSAQHALTSVSRGSSLKILSKGKRGGHSSVSTESESSSFHSS
CXCR5	LERHRQTRSS	VHAVHAYRHRRLLS	GVVHRLRQAQRRPQRQKAV	SDLSRLLTKLGCTGPASLCQLFPSWRRSSLSESENATSLTTF
CXCR6	SIFYHKLQSL	VKATKAYNQQAKRM	VIIKTLLHAGGFQKHRSL	KNFWKLVKDIGCLPYLGVSHQWKSSEDNSKTFSASHNVEATSMFQL
CYSLTR1	LIKTYHKKSA	VFPVQNINLVTQKK	MIILTLLKKSMKKNLSSHKKAI	KRLSTFRKHSLSSVTYVPRKKASLPEKGEEICKV
CYSLTR2	FLQPYKKSTS	VHPFRLLHVTSIRS	LIIRVLLKVEVPESGLRVSHRKAL	DRLKSALRKGHPQKAKTKCVFPVSVWLRKETRV
DRD1	VIRFRHLRSKV	SSPFRYERKMTPKA	RIYRIAQKQIRRIAALERAAVHAKNCQTTTGNGKPVECSQPESSFKMSF KRETKVL	KAFSTLLGCYRLCPATNNAIETVSINNNGAAMFSSHHEPRGSISKECNLVYLIPHAVGSSEDL KKEEAAGIARPLEKLSPALSVILDYDTDVSLEKIQPITQNGQHPT
DRD3	VLKERALQTT	VMPVHYQHGTGQSSC RR	RIYVVLKQRRRKRILTRQNSQCNSVRPGFPQQTLSPDPAHLELKRYYSIC QDTALGGPGFQERGGELKREEKTRNSLSPTIAPKLSLEVRKLSNGRLSTS LKLGPLQPRGVPLREKKAT	KAFLKILSC
DRD4	VATERALQTP	AVPLRYNRQGGSRR	ATFRGLQRWEVARRAKLHGRAPRRPSGPGPPSPTPPAPRLPQDPCGP DCAPPAPGLPRGPCGPDCAPAAPGLPPDPCGPDCAPPAPGLPQDPCG PDCAPPAPGLPRGPCGPDCAPPAPGLPQDPCGPDCAPPAPGLPPDPC GSNCAPPDAVRAAALPPQTPPQTRRRRRAKITGRERKAM	NVFRKALRACC
DRD5	IVRSRHLRANM	SRPFRYKRKMTQRM	RIYRIAQVQIRRISSLERAAEHAQSCRSSAACAPDTSLRASIKKETKVL	KVFAQLLGCSHFCSRTPVETVNISNELISYNQDIVFHKEIAAAYIHMMPNAVTPGNREVDN DEEEGPFDRMFQIYQTSPDGDPVAESVWELDCEGEISLDKITPFTPNGFH
EDNRA	IYQNKCMRNG	ASWSRVQGIGIPLV	LMTCEMLNRRNGSLRIALSEHLKQRREVA	NCFQSCLCCCCYQSKSLMTSVPMNGTSIQWKNHDQNNHNTDRSSHKDSMN
EDNRB	IYKNKCMRNG	ASWSRIKGIGVPKW	LMTCEMLRKKSGMQIALNDHLKQRREVA	NCFKSCLCCWCQSFEEKQSLEEKQSCLKFKANDHGYDNFRSSNKYSSS
F2R	FILKMKVKKP	VYPMQSLSWRTLGR	SIIRCLSSSAVANRSKKSRAL	RYVYSILCCKESSDPSSYNSSGQLMASKMDTCSSNLNNSIYKKLLT
F2RL1	FLFRTKKKHP	VNPMGHSRKKANIA	LMIRMLRSSAMDENSEKKRKRAI	DHAKNALLCRSVRTVKQMQVSLTSKKHSRKSSSYSSSSTTVKTSY
F2RL2	LFFRTRSIC	VHPFTYRGLPKHTY	AIIRTLNAYDHRWLWYV	HSTAYLTK
F2RL3	LATQAPRLP	VHPLRARALRGRRL	ATLHTLAASGRRYGHALRLT	DKVRAGLFQRSPGDTVASKASAEGGSRGMGTHSSLLQ
FFAR1	TAHARLRLTP	AFPLGYQAFRRPCY	GCLRALARSGLTHRRKLRAA	PGLKTVCAARTQGGKSQK
FFAR2	FVGRIRQPQPAP	AFPVQYKLSRRPLY	RFVWIMLSQPLVGAQRRRRAV	RAFGRGLQVLRNQGSSLLGRRGKDTAEGTNEDRGVGQGEGMPSSDFTTE
FFAR3	FVGKLQRRPVA	AHPLWYKTRPRLGQ	RLVWILGRGGSHRRQRRVA	ADFHELLRRLCGLWGQWQQESSMELKEQKGGEEQRADRPAERKTSEHSQGCGTGGQV ACAES
FFAR4	VARRRRRGA	VHLQRGVRGPGRRA	KILQTSEHLLDARAVVTHSEITKASRKRLTVSLAYSESHQIRVSQQDFRLF	NEWKKIFCCFWFPEKGAILTDTSVKRNDLSIISG

GPCR	ICL1	ICL2	ICL3	C-Term
FPR1	AGFRMTHTV	LHPVWTQNHRTVSL	LIATKIHKQGLIKSSRPL	ERLIHALPASLERALTEDSTQTSDTATNSTLPSAEVELQAK
FPR2	AGFRMTRTV	LHPVWAQNHRTVSL	LIAAKIHKKGMIKSSRPL	ERLIHSLPTSLERALSEDSAPTNDTAANSASPPAETELQAM
FPR3	AGFRMTRTV	LHPAWAQNHRTMSL	IIAAKIHRNHMIKSSRPL	ERLIRSLPTSLERALTEVPDSAQTSNTDTTSASPPEETELQAM
FSHR	LTTSQYKLTV	THAMQLDCKVQLRH	HIYLTVRNPNIVSSSSDTRIA	RDFFILLSKCGCYEMQAQIYRTETSSTVHNTHPRNGHCSSAPRVTNGSTYILVPLSHLAQN
GALR1	LARSKPGKPRST	VHSRRSSSLRVSRN	KVLNHLHKKLKNMSKKSEASKKKTA	KAYKQVFKCHIRKDSHLSDTKESKSRIDTPPSTNCTHV
GALR2	LLRGGQAVST	RYPLHSRELRTPRN	RTLRYLWRAVDPVAAGSGARRAKRKVT	KGFRTICAGLLGRAPGRASGRVCAAARGTHSGSVLERESSDLLHMSEAAGALRPCPGASQ PCILEPCPGPSWQGPKAGDSILTVDVA
GALR3	LLQPGPSAWQE	RHPLRSRALRTPRN	RTLRFLWAAVGPAGAAAAEARRRATGRAG	ARFRRLWPCGRRRRHRARRALRRVRPASSGPPGCPGDARPSGRLLAGGGQGPEPREGPV HGGEAARGPE
GHSR	VSRFRELRTT	CFPLRAKVVVTKGR	LIGRKLWRRRRGDAVVGASLRDQNHKQTV	VAVFRLLGFEPFSQRKLSTLKDESSRAWTESSINT
GNRHR	LQKWTQKKEKG KKLSR	TRPLALKSNSKV	KIIFTLTRVLHQDPHELQLNQSKNNIPRARLKTL	
GNRHR2	GT	LNPLGSRSG	RIVLSVSRPQTRKGSHAPAGEFALPRSFDNCPRVRLRAL	RGHQELSIDSSKEGSGRMLQEEIHAFRQLEVQKTVTSRRAGETKGISITSI
GPBAR1	IAWDRRLRSPP	LRPLQPPGS	RVLATAHRQLQDICRLERAVCRDEPSALARALTWRQA	APWRAAAQRCLQGLWGRASRDSPGPSIAYHPSSQSSVDLDLN
GPER1	NISFREKMTI	ARAMRCSLFRTKHH	LIVRVLVRAHRHRGLRPRRQKAL	DKLRLYIEQKTNLPALNRFCHAALKAVIPDSTEQSDVRFSSAV
GPR1	TGFKWKKTV	IHPVLSHRHRTLKN	CLIFKVKKRSILISSRHF	ARFRSSVAEILKYTLWEVSCSGTVSEQLRNSETKNLCLLETAQ
GPR101	LQRKPQLLQV	IHPLSYPSKMTQRR	VVFCAARRQHALLYNVKRHSLEVRVKDCVENEDEEGAEKKEEFQDESE FRRQHEGEVKAKEGRMEAKDGSLKAKEGSTGTSESSVEARGSEEVRES STVASDGSMEGKEGSTKVEENSMKADKGRTEVNQCSIDLGEDDMEF GEDDINFSEDDVEAVNIPESLPPSRRNSNSNPPLPRCYQCKAA	KEIQDMLKKFFCKEKPPKEDSHPDLPGTEGGTEGKIVPSYDSATFP
GPR119	IHKNDGV	KQPFRYLKIMSGFV	DMLKIASMHSQQIRKMEHAGAMAGGYRSPRTPSDFKAL	LQLYHMALGVKKVLTSFLLFLSARNCGPERPRESSCHIVTISSSEFDG
GPR12	IFHNPSLRAP	YYALTYHSERTVTF	QICKIVMRHAHQIALQHHFLATSHYVTTRKGV	KALCLICCGCIPSSLAQRARSPSDV
GPR132	ALLQVLQGNV	VYALESRGRRRRRT	RIFRSIKQSMGLSAAQKAKVK	QEVSRIHKGWKEWSMKTDVTRLTHSRDTEELQSPVALADHYTFSRPVHPPGSPCPAKRLI EESC
GPR135	IVKHRQLRTV	VRPPREKIGRRR	HICKTVRLSDVRVRPVNTYARVLRFFSEVRTA	MLLGRNREEGYRTRNVDAFLPSQGPGLQARSRSRLRNRYANRLGACNRMSSSNPASGVA GDVAMWARKNPVVLFCREGPPEPVTAVTKQPKSEAGDTSL
GPR139	LSQLVARRQKS	CHPLKYHTVSYPAR	IIVYKLRRKSNFRLRGYSTGKTT	TMAAATLKAFFKCQKQPVQFYTNHNFSITSSPWISPANSHCIKMLVYQYDKNGKPIKVSP
GPR141	LVKMNTRSV	FKCKDKVEFYRKLH	VFIIMLMVQKLRHSLLSHQEFWAQ	QKIIGLWNCVLCR
GPR142	LARLATRTRRP	CHPLHHRAASSPGR	AIIHRLRRRGRSGLQPRVGKST	ATVRQVIHDAYLPCTLASQPEGMAAKPVMEPPGLPTGAEV
GPR146	NLHSKASMTM	ALPRTYMASVYN	LLSRVRREDTPLDRDTGRLEPSAH	SKLQRLMKKLPCGDRHCSPDHMGVQQVLA
GPR148	LRNQRLRQEP	IHPLRYLSFMSHGA	RIYAEAKTSGIWGQGYSRARGT	QLLGMVRGHLPSRRHQAIFTIS
GPR149	LLKMQNRTV	HRGVGSQTASRRSGQ	PRLHSNYQEISRGASIPGTPPTAGRVVSLSPEDAPGPSLRRSGGCSPSSD TVFGPGAPAAAGAEACRRENRGTLYGTRSFTVSVAQ	RKGFEFNLSFQKSYGIYKIAHEDYYDDDENSIFYHNLMNSECETTKDPQRDNRNIFNAIKVE ISTTPSLDSSTQRGINKCTNTDITEAKQDSNNKKDAFSDKTGGDINYEETTFSEGPERRLSHE ESQKPDLSDWEWCRSKSERTPRQRSGYALAIPLCAFQGTVSLHAPTGKTLSLSTYEVSAEG QKITPASKKIEVYRSKSVGHEPNSEDSSSTFVDTSVKIHLEVLEICDNEEALDTVSIISNISQSST QVRSPSLRYSRKENRFVSCDLGETASYSLFLPTSNPDGDINISIPDTVEAHRQNSKRQHQER DGYQEEIQLLNKAYRKREEESKGS
GPR15	LHFKPGSRRL	VWPVVSRKFRRTDC	CIARKLCAHYQQSGKHNKKLKKSI	RAIVHCLCPCLKNYDFGSSTETSDSHLTKALSTFIHAEDFARRRKRSVSL
GPR150	LCGGGGPWAGP KRRK	RLPHGRPLP	HLLSVWWRHRPQAPAAAAPWSASPGRAPAPSALPRAKVQSL	RQLRKRLGSLCCAPQGGAEDEEGPRGHQALYRQRWPHPHYHHARREPLDEGGLRPPPP RPRPLPCSCESAF
GPR151	LLHNAWKGKPS M	SDPAKQVSIHNYTI	RAYDQCKKRGTKTQNLRNQIRSKQVT	EGLKGVWKWMITKKPPTVSESQETPAGNSEGLPDKVPSPESPASIPEKEKPSSPSSGKGKT EKAEIPILPDVEQFWHERDTVPSVQDNDPIPWEHEDQETGEGVK

GPCR	ICL1	ICL2	ICL3	C-Term
GPR152	AGSQARHGAGTR	LCPHWYPGHRPVRL	LTQATACRTCHRQQQPAACRGFA	TLLRSVLSSFAAALCEERPGSFTPTEPQTQLDSEGPTLPEPMAEAQSQMDPVAQPQVNPTLQPRSDPTAQPQLNPTAQPQSDPTAQPQLNLMAQPQSDSVAQPQADTNVQTPAPAASSVPSPCDEASPTPSSHPTPGALEDPATPPASEGESPSSTPPEAAPGAGPT
GPR153	VGAKQKKWKP	CWPVNYRLSNAKKQ	ALFQTLAVQVGRQADRRAFTVPTIVVEDAQGKRRSSIDGSEPAKTSLQTT	HDDADVWAAVPLPAFLPRWGSGEDLAALAHLVLPAGPERRRASLLAFAEDAPPSRARRRSAESLLSLRPSALDSGPRGARDSPPGSPRRRPGPGPRSASASLLPDAFALTAFECEPQALRRPPGPFPAAPAAPDGADPGEAPTPPSSAQRSPGPRPSAHSHAGSLRPGLSASWGEPGGLRAAGGGGSTSSFLSSPSESSGYATLHSDSLGSAS
GPR160	LGMRRKNTCQNF	SKTTKLSFKCQKLF	TLVQAIRITSYMNETILYFPFSSHSSYTVRSKK	LKDIGLPLDPFVNWKCCFIPLTIPNLEQIEKPISIMIC
GPR161	LYKKSYLLTL	LYPMVYPMKITGNR	FIFRVARVKARKVHCGTVVIVEEDAQRTGRKNSSTSTSSSGSRRNAFQGVVYSANQCKAL	KELLGMCFGDRYYREPFVQRQRTSRLFSISNRITDLGLSPHLTALMAGGQPLGHSSSTGDTGFSCSQDSGTDMMLLEDYTSDDNPPSHCTCPPKRRSSVTFEDEVEQIKEAAKNSILHVKAEVHKSLDSYAASLAKAIEAEAKINLFGEEALPGVLVTARTVPGGGFGGRRGSRTLVSQRLQLQSIEEGDVLAAEQR
GPR162	ISAKQQKHKP	RWPVNYRLSNAKKQ	TFYQTLWARPRRARQARRVGGGGGTKAGGPGALGTRPAFEVPAIVVEDARGKRRSSLDGSESAKTSLQVT	HDETNIFSTPREPGSFLHKWSSSDDIRVLPAQSRALGGPPEYLGQRHRLEDEEDEEEAEGGGLASLRQFLESGVLGSGGGPPRGPGFFREEITTFIDETPLPSPTASPGHSPRRPRPLGLSPRRLSLGSPESRAVGLPLGLSAGRRCSLTGGEESARAWGGSWGPGNPIFPQLTL
GPR17	FIRDHKSGTP	VHPVKSLKLRRPLY	LIIRSLRQGLRVEKRLKTKAV	HALCNLLCGKRLKGPPPSFEGKTNESSLSAKSEL
GPR171	FIQKNTNHRC	THSCKIYRIQEPGF	LVIRQLYRNKDNENYPNVKKAL	SKVTETFASPKETKAQKEKLRCENNA
GPR173	VLKERALHKA	AHHRFYAKRMTLWT	KLLLFEYRHRKMKPVQMVPAISQNWTFHGPGATGQAAANWIAGFGRGPMPPTLLGIRQNGHAASRRLLGMDEVKGEKQLG	KCLRTHAPCWGTGGAPAPREPYCVM
GPR174	FYGYMKETKR	MYPFRFHDCKQKYD	KTVLSLQDKYPMAQDLGEKQKAL	RRLSRQDLHDSIQLHAKSFVSNHTASTMTPELC
GPR176	TCRTTVFKSV	LYPLERKISDAK	LIRRALSASQKKKVIIAALRTPQNTISIPYASQREAELH	KCLIGTLVQLHHRYSRRNVVSTGSGMAEASLEPSIRSGSQLLEMFHIGQQQIFKPTEDEEESEAKYIGSADFQAKEIFSTCLEGEQGPQFAPSAPPLSTVDSVSQVAPAAPVEPETFPDKYSLQFGFGPFELPPQWLSETRNSKKRLLPPLGNTPEELIQTKVPKVGRVERKMSRNNKVSIFPKVDS
GPR18	FSCTTKKRTT	VQPKYAKELKNTCK	VIIHNLLHGRTSKLKPKVKEKSI	ARVISVMLYRNYLRSMRRKSFRSGSLRSLSNINSEML
GPR182	NWRGSGRAGL	TSASPSWQRYQHRV	LTACRLRQPGQPKSRRHC	GRLLNAVVHYLPKDQTKAGTCASSSSCSTQHSIIITKGDSQPAAAAPHPEPSLSFQAHHLLPNTSPISPTQPLTPS
GPR19	IHRSRRTQST	VYPLSFKVSREK	KVIKYIWRIGTDGRTVRRTMNIVPRTKVKTI	RGMKETFCMSSMKCYRSNAYTITTSSRMAKKNYVGISEIPSMAKTITKDSIYDSFDREAKEKKLAWPINSNPPNTFV
GPR20	FCCRTRAKTP	VRPEGSRRCRQPAC	RIMCALSRPGLLHQGRQRRVRAM	ATVRGLFGQHGEREPSSGDVVSMHRSSKGSGRHHILSAGPHALTQALANGPEA
GPR21	FHCAPLLNHHT	TKPLTYNTLVTPWR	NIFRICQQHTKDISERQARFSSQSGETGEVQACPDKRYA	RGLKRLSGAMCTSCASQTTANDPYTVRSKGPLNGCHI
GPR22	YCMKSNLINSV	VKPANRILTMGR	KILQALNIRIGTRFSTGQKKKARKKKTISLTTQHEATDMSQSSGGRNVVFGVRTSVSVIIALRRAVKRHRERRERQKRVF	KVLKSKMKKRVVSIVEADPLPNNAVIHNSWIDPKRNKKITFEDSEIREKCLVPQVVTD
GPR25	LAGRRGPRRL	VKLLEARPLRTPRC	RISRRLRRPPHVGRARRNSL	ARALDGACGRTGRLARRISSASSLSRDDSSVFRCRAQAANTASASW
GPR26	LLHSADIRRQA	VFPLSYRAKMRLRD	KVLKVARFHCKRIDVITMQTLVLLVDLHPSVRERCLEEQKRRRQRAT	KSCKEILNRLLHRRSIHSSGLTGDSHSQNILPVSE
GPR27	IVRERSLHRA	HHRFYAERLAGWPC	RLLFFIHDRRKMRPARLVPAVSHDWTFHGPGATGQAAANWTAGFGRGPTPPALVGIRPAGPGRGARRLLVLEEFKTEKRLC	DCFRAQFPCCQSPRTTQATHPCDLKGIGL
GPR3	IVGTPAFRAP	YNALTYYSETTVTR	QICRIVCRHAQQIALQRHLLPASHYVATRKGI	KVLWAVCCCCSSSKIPFRSRSPSDV
GPR31	FLFRVRVWKP	VHPRLKVNLLSPQA	GIIRALQKRLREPEKQPKLQRAQ	SSYRRVFHTLRGKGQAAEPPDFNPRDSYS
GPR32	TVFRMARTV	LYPVWALNHRTVQR	LIRAKLLREGWVHANRPK	EKFFQSLTSALARAFGEEEFLSSCPRGNAPRE
GPR33	LRFKMKQTV	LHPVWSQQHRTPRW	RVASKVKERSLFKSSKPF	KVFKKSILALFESTFSEDSSVERTQT
GPR34	FLGIHRKRNS	NRSIQQRKAITTKQ	KIGKNLLRISKRRSKFPNSGKYATTA	KIMCQLLFRRFQGEPSRSESTSEFKPGYSLHDTSVAVKIQSSSKST

GPCR	ICL1	ICL2	ICL3	C-Term
GPR35	FCCRMQQWTE	RHPLRARGLRSPRQ	KVVTALAQRPPTDVGQAEATRKAA	EASALAVAPSAKAHKSQDSLCVTLA
GPR37	VCHNYYMRSI	NVQMYYEMIENCSS	VTARKIRKAEKACTRGNKRQIQLESQMN	RAFMECCCCCCEECIQKSSTVTSDDNDNEYTTELELSPFSTIRREMSTFASVGTHC
GPR37L1	VWHSYYLKSA	STLPKVRPIERCQS	VTWRVRGPPGRKSECRASKHEQCESQLN	QAFLDCCCCCCCEECGGASEASAANGSDNKLKTEVSSSIYFHKPRESPPLLPLGTPC
GPR39	VLQKKGYLQKE	CHPFRYKAVSGPCQ	NMMQVLMKSQKGSLAGGTRPPQLRKSESEESRTARRQTI	RVFVQVLCCRLSLQHANHEKRLRVHAHSTTDSARFVQRPLLFASRRQSSARRTEKIFLSTFQ SEAEPQSKSQSLSLESLEPNSGAKPANSAAENGFQEHEV
GPR4	AYRQVQQRNE	AHPLRFARLRRVKT	GILRAVRGSVSTERQEKAKIK	SDVAKALHNLLRFLASDKPQEMANASLTLETPLTSKRNSTAKAMTGSWAATPPSQGDQV QLKMLPPAQ
GPR42	FVGKLRCRPVA	AHPLWYKTRPRLGQ	RLVWILGRGGSHRRQRRVA	ADFHELLRRLCGLWGQWQQESSMELKEQKGGEEQRADRPAERKTSEHSQGCGTGGQV ACAEN
GPR45	VYQRPAMRSA	VQRQDKLNPRR	CILNTVRKNAVRVHNQSDSLDLRQLTRAGLRRLQRQQQVSVDLSFKTK AF	EACIELLPQTFQILPKVPERIRRRIQPSTVYVCNENQSAV
GPR50	VTKNKKLRNS	CHSLQYERIFSVRN	RIWTKVLAARDPAGQNPDNQLAEVRNF	REYWTIFHAMRHPIIFFSGLISDIREMQEARTLARARAHARDQAREQDRAHACPAVEETP MNVRNVPLPGDAAAGHPDRASGHPKPHSRSSSAYRKSASTHHKSVFSHSKAASGHLKPV SGHSKPASGHPKSATVYPKPASVHFKADSVHFKGDSVHFKPDSVHFKPASSNPKPITGHH VSAGSHSKSAFSAATSHPKPTTGHIKPATSHAEPTTADYPKPATTSHPKPTAADNPELSASH CPEIPAIAHPVSDDSDLPESASSPAAGPTKPAASQLESDTIADLPDPTVVTTSTNDYHDVVVI DVEDDPDEMAV
GPR52	FHCAPLLHHYT	TKPLSYNQLVTPCR	HIFKICRQHTKEINDRRARFPSHEVDSSRETGHSPDRRYA	LGLRRLSETMCTSCMCVKDQEAQEPKPRKRANSCSI
GPR55	FSTFLKNRWP	RYPLLVSHLRSPRK	RSIHILLGRRDHTQDWVQQKACI	MNIRAHRPSRVQLVLQDTTISRG
GPR6	IASTPALRTP	YNALTYYSRRTLLG	RICQVVWRHAHQIALQQHCLAPPHLAATRKGV	RALWLLLCGCFQSKVPFRSRSPSEV
GPR61	IAKTPALR	VHPMRYEVRMTLGL	SMFRVARVAAMQHGPLPTWMETPRQRSESLSSRSTMVTSSGAPQTT PHRTFGGGKAA	GELSKQFVCFFKPAPEEELRLPSREGSIEENFLQFLQGTGCPSESWVSRPLPSPKQEPPAVD FRIPGQIAEETSEFLEQQLTSDIIMSDSYLRPAASPRLES
GPR62	VLRTPGLR	VHPLRPGSRPP	GIFVVARRAALRPPRPARGSRLHSDSLDSRLSILPPLRPRLPGGKAA	LALGRLSRRALPGPVRACTPQAWHPRALLQCLQRPPEGPAVGPSEAPEQTPELAGGRSPA YQGPPESSLS
GPR63	VYQKAAMRSA	VQRQDKLNPYR	GILNTLRHNALRIHSYPEGICLSQASKLGLMSLQRPFQMSIDMGFKTRA F	DACLDMMPKSFKFLPQLPGHTKRRIRPSAVYVCGEHRTVV
GPR68	LYFGYLQIKARNE	AHPFRFHQFRTLKA	GILRAVRRSHGTQKSRKDQIQ	RDLARLRGACLAFLTCSRTGRAREAYPLGAPEASGKSGAQGEEPELLTKLHPAFQTPNSPG SGGFPTGRLA
GPR75	FFDPAFRKFRTN	LGKQPNRTASF	MIAQTLRKNAQVRKCPPVITVDASRPQPFMGVPVQGGGDPIQCAMP ALYRNQNYNKLQHVQTRGYTKSPNQLVTPAASRLQLVSAINLSTAKDS KAV	RKVLWCLQYIGLGFFCCKQKTRLRAMGKGNLEVNRNKSSHHETNSAYMLSPKPQKKFVD QACGPSHSKESMVSPKISAGHQHCGQSSSTPINTRIEPYYSIYNSSPSQEESSPCNLQPVNS FGFANSYIAMHYHTTNDLVQEYDSTSAKQIPVPSV
GPR78	CAYSAELRTRA	GFPLRYAGRLRPRY	QVHRVARRHCQRMDTVTMKALALLADLHPSVRQRCLIQQKRRRHRA T	QVLAGMVHRLLKRTPRPASTHDSSLDVAGMVHQLLKRTPRPASTHNGSVDTENDSCLQQ TH
GPR82	FLTKIGKKTS	MQKDSSQETTSCYEKIF YGHLLKKFRQPNF	SFVSHLRKIRTCTSIMEKDLTYSSVK	KTLYNLFTKSNSAHMQSYG
GPR83	IFKNQRMHSA	MHPLKPRISITK	RVAKKLWLCNMIGDVTTEQYFALRRKKKKTI	IELKALLSMCQRPPKPQEDRPPSPVPSFRVAWTEKNDGQRAPLANNLLPTSQLQSGKTDL SSVEPIVTMS
GPR85	LVKDKTLHRA	AHHRFYTKRLTFWT	KLIFFVHDRRKMKPVQFVAAVSQNWTFHGPGASGQAAANWLAGFG RGPTPPTLLGIRQNANTTGRRRLLVLDEFKMEKRIS	RCFSTTLLYCRKSRLPREPYCVI
GPR87	FFHIRNKTS	VKPFGDSRMYSITF	AISRYIHKSSRQFISQSSRKRKHN	RRLFKKSNIRTRSESIRSLQSVRRSEVRIYYDYTDV
GPR88	VSSFRKLQTT	RAPATYQALYQRRH	GIVRRVRVSVKRVS	RSVRSVLPGVGDAAAAAVAATAVPAVSQAQLGTRAAGQHW
GRPR	FCTVKSMRNV	VRPMDIQASHALMK	FIAKNLIQSAYNLPVEGNIHVKKQIESRKRLA	KQFNTQLLCCQPGLIIRSHSTGRSTTCMTSLKSTNPSVATFSLINGNICHERYV
HCAR1	FCFHMKTWKP	VHPHHAVNTISTRV	KIVWSLRRRQQLARQARMKKAT	KFYNKLKICSLKPKQPGHSKTQRPEEMPISNLGRRSCISVANSFQSQSDGQWDPHIVEWH

GPCR	ICL1	ICL2	ICL3	C-Term
HCAR3	FCFHLKSWKS	VHPHHALNKISNWT	RIIWSLRQRQMDRHAKIKRAI	NFFSTLINRCLQRKITGEPDNNRSTSVELTGDPNKTRGAPEALIANSGEPWSPSYLGPTSNNHSKKGHCHQEPASLEKQLGCCIE
HCRTR1	VWRNHHMRTV	CHPLLFKSTARR	QIFRKLWGRQIPGTTSALVRNWKRPSDQLGDLEQGLSGEPQPRARAFLAEVKQMRARRKTA	EQFKAAFSCCLPGLGPCGSLKAPSPRSSASHKSLSLQSRCSISKISEHVVLTSVTTVLP
HCRTR2	VWKNHHMRTV	CHPLMFKSTAKR	QIFRKLWCRQIPGTSSVVQRKWKPLQPVSQPRGPGQPTKSRMSAVAAEIKQIRARRKTA	EEFKAAFSCCCLGVHHRQEDRLTRGRTSTESRKSLTTQISNFDNISKLSEQVVLTSISTLPAANGAGPLQNW
HRH1	VRSERKLHTV	QQPLRYLKYRTKTR	KIYKAVRQHCQHRELINRSLPSFSEIKLRPENPKGDAKKPGKESPWEVLKRKPKDAGGGSVLKSPSQTPKEMKSPVVFSQEDDREVDKLYCFPLDIVHMQAAAEGSSRDYVAVNRSHGQLKTDEQGLNTHGASEISEDQMLGDSQSFSRTDSDTTTETAPGKGKLRSGSNTGLDYIKFTWKRLRSHSRQYVSGLHMNRERKAA	KTFKRILHIRS
HRH2	VGLNRRLRNL	MDPLRYPVLVTPVR	RIFKVARDQAKRINHISSWKAATIREHKAT	TGYQQLFCCRLANRNSHKTSLRSNASQLSRTQSREPRQQEEKPLKLQVWSGTEVTAPQGATDR
HRH3	FVADSSLRTQ	TRAVSYRAQQGDTRR	SIYLNIQRRTRLRLDGAREAAGPEPPPEAQPSPPPPPGCWGCWQKGHGEAMPLHRYGVGEAAVGAEAGEATLGGGGGGGSVASPTSSSGSSSRGTERPRSLKRGSKPSASSASLEKRMKMVSQSFTQRFRLSRDRKVA	RAFTKLLCPQKLKIQPHSSLEHCWK
HRH4	FVVDKNLRHR	SNAVSYRTQHTGVLK	NIYWSLWKRDHLSRCQSHPGLTAVSSNICGHSFRGRLSSRRSLSASTEVPASFHSERQRRKSSLMFSSRTKMNSNTIASKMGSFSQSDSVALHQREHVELLRARRLA	KAFLKIFCIKKQPLPSQHSRSVSS
HTR1A	IALERSLQNV	TDPIDYVNKRTPRR	RIFRAARFRIRKTVKKVEKTGADTRHGASPAPQPKKSVNGESGSRNWRLGVESKAGGALCANGAVRQGDDGAALEVIEVHRVGNSKEHLPLPSEAGPTPCAPASFERKNERNAEAKRKMALARERKTV	NAFKKIIKCKFCRQ
HTR1B	VYRTRKLHTP	TDAVEYSAKRTPKR	RIYVEARSRILKQTPNRTGKRLTRAQLITDSPGSTSSVTSINSRVPDVPSESGSPVYVNQVKVRVSDALLEKKKLMAARERKAT	QAFHKLIRFKCTS
HTR1D	ILLTRKLHTP	TDALEYSKRRTAGH	RIYRAARNRILNPPSLYGKRFTTAHLITGSAGSSLCSLNSSLHEGHSHSAGSPLFFNHVKIKLADSALERKRISAARERKAT	QAFQKIVPFRKAS
HTR1E	IGTTKKLHQP	TNAIEYARKRTAKR	RIYHAAKSLYQKRGSSRHLSNRSTDSQNSFASCKLTQTFCVSDFSTSDPTTEFEKFHASIRIPPFDNDLDHPGERQQISSTRERKAA	LAFKKLIRCREHT
HTR1F	IIVTRKLHHP	TDAVEYARKRTPKH	KIYRAAKTLYHKRQASRIAKEEVNGQVLLESGEKSTKSVSTSYVLEKSLSDPSTDFDKIHSTVRSLRSEFKHEKSWRRQKISGTRERKAA	KAFQKLVRCRC
HTR2A	VSLEKKLQNA	QNPIHHSRFNSRTK	LTIKSLQKEATLCVSDLGTRAKLASFSFLPQSSLSSEKLFQRSIHREPGSYTGRRTMQSISNEQKAC	SAFSRYIQCQYKENKKPLQLILVNTIPALAYKSSQLQMGQKKNSKQDAKTTDNDCSMVALGKQHSEEASKDNSDGVNEKVSCV
HTR2B	VSLEKKLQYA	KKPIQANQYNSRAT	LTIHALQKKAYLVKNKPPQRLTWLTVSTVFQRDETPCSSPEKVAMLDGSRKDKALPNSGDETLMRRTSTIGKKSVQTISNEQRAS	DAFGRYITCNYRATKSVKTLRKRSSKIYFRNPMAENSKFFKKHGIRNGINPAMYQSPMRLRSSTIQSSSIILLDTLLLTENEGDKTEEQVSYV
HTR2C	VSMEKKLHNA	RNPIEHSRFNSRTK	LTIYVLRRQALMLLHGHTEEPPGLSLDFLKCCKRNTAEEENSANPNQDQNARRRKKKERRPRGTMQAINNERKAS	RAFSNYLRCNYKVEKKPPVRQIPRVAATALSGRELNVNIYRHTNEPVIEKASDNEPGIEMQVENLELPVNPSSVVSERISSV
HTR4	VCWDRQLRKI	CQPLVYRNKMTPLR	RIYVTAKEHAHQIQMLQRAGASSESRPQSADQHSTHRMRTETKAA	RAFLIILCCDDERYRRPSILGQTVPCSTTTINGSTHVLRDAVECGGQWESQCHPPATSPLVAAQPSDT
HTR5A	ILRVRTFHRV	TRHMEYTLRTRKCV	KIYKAAKFRVGSRKTNSVSPISEAVEVKDSAKQPQMVFTVRHATVTFQPEGDTWREQKEQRAA	SAFKNFFSRQH
HTR6	ICTQPALRNT	LSPLRYKLRMTPLR	RILLAARKQAVQVASLTTGMASQASETLQVPRTPRPGVESADSRRLATKHSRKALKAS	RALGRFLPCPRCPRERQASLASPSLRTSHSGPRPGLSLQQVLPLPLPPDSDSDSDAGSGGSSGLRLTAQLLLPGEATQDPPLPTRAAAAVNFFNIDPAEPELRPHPLGIPTN

GPCR	ICL1	ICL2	ICL3	C-Term
HTR7	VCFVKKLRQP	TRPLTYPVRQNGKC	QIYKAARKSAAKHKFPGFPRVEPDSVIALNGIVKLQKEVEECANLSRLLKHERKNISIFKREQKAA	TTYRSLLQCQYRNINRKLSAAGMHEALKLAERPERPEFVLRACTRRVLLRPEKRPPVSVWVLQSPDHHNWLADKMLTTVEKKVMIHD
KISS1R	ICRHKPMRTV	VFPLRALHRRTPRL	AMLRHLGRVAVRPAPADSALQGQVLAERAGAVRAKVS	QAFRRVCPCAPRRPRRPRRPGPSDPAAPHAELLRLGSHPAPARAQKPGSSGLAARGLCVLGEDNAPL
LGR4	LHLHNNKIRSLSQHCFDGL	QFPNLTGTVHLESLTLTGTKISSI	CTSLPSSKLFIGLISVSNLFMGIYTGILTFLDAVSWGRFAEFGIWWETGSGCKVAGFLAVFSSESAIFLLMLATVERSLSAKDIMKNGKSNHLKQFRVA	EDWKLLKRRVTKKSGSVSVSISSQGGCLEQDFYYDCGMYSHLQGNLTVCDCCESFLLTKPVSCKHLIKSHSCPALAVASCQRPEGYWSDCGTQSAHSDYADEEDSFVSDSSDQVQACGRACFYQSRGFPLVRYAYNLPRVKD
LGR5	LHLHNNRIHSLGKKCFDGL	EFPDLTGTANLESLTLTGAQISSL	PLYISPIKLLIGVIAAVNMLTGVSSAVLAGVDAFTFGSFARHGAWWENGVGCHVIGFLSIFASESSVFLLTLAALERGFSVKYSAKFETKAPFSSLKVI	EDLVSLRKQTYVWTRSKHPSLMSINSDDVEKQSCDSTQALVTFTSSSITYDLPPSSVPSPAYPVTESCHLSSVAFVPCL
LGR6	LHLHNNRIQHLG	EFPDLKGTTSLEILTLTR	PVPLPPVKFVVGAIAGANTLTGISCGLLASVDALTFGQFSEYGARWETGLGCRATGFLAVLGSEASVLLLTLAAVQCSVSVSCVRAYGKSPSLGSVRAG	DDLRRLRPRAGDSGPLAYAAAGELEKSSCDSTQALVAFSDVDLILEASEAGRPPGLETYGFPSVTLISCQQPGAPRLEGSHCVEPEGNHFGNPQPSMDGELLLRAEGSTPAGGGLSGGGGFQPSGLAFASHV
LHCGR	LLTSRYKLTV	TYAIHLDQKLRLRH	KIYFAVRNPELMATNKDTKIA	RDFFLLLSKFGCCKRRAELYRRKDFSAYTSNCKNGFTGSNKPSQSTLKLSTLHCQGTALLDKTRYTEC
LPAR1	IYVNRRFHFP	FRMQLHTRMSNRR	HIFGYVRQRTMRMSRHSSGPRRNRDTMMSLL	ATFRQILCCQRSENPTGPTEGSDRSASSLNHTILAGVHSNDHSVV
LPAR2	IASNRRFHQP	MAVQLHSRLPRGR	RIFFYVRRRVQRMAEHVSCHPRYRETTLSLV	RTFRRLLCCACLRQSTRESVHYTSSAQGGASTRIMLPENGHPLMDSTL
LPAR3	VIKNRKFHFP	MRMRVHSNLTKKR	RIYVYVKRKTNVLSPHTSGSISRRRTPMKLM	GTMKKMICCFSQENPERRPSRIPSTVLSRSDTGSQYIEDSISQGAVCNKSTS
LPAR4	FCFRMKMRSE	VYPFRSRTIRTRRN	VVLRTLRKPATLSQIGTNKKKVL	KSFYINAHIRMESLFKTETPLTTKPSLPAIQEEVSDQTTNNGGELMLESTF
LPAR5	FLRALRVHSV	VHPLRLRHLRRPRV	RVFWTLARPDATQSQRRRKTV	NTLRGLGTPHRARTSATNGTRAALAQSERSAVTTDATRPDAASQGLLRPSDSHSLSSFTQCPQDSAL
LPAR6	FICVLKVRNE	VYPFKSKTLRTKRN	MVLKTLTKPVTLSRSKINKTKVL	NSIKMKNWSVRRSDFRFSEVHGAENFIQHNLQTLKSKIFDNESAA
LTB4R	ILKRMQKRSV	ARPFVSQKLRTKAM	DIGRRLQARRFRRSRRTG	SAGVGFVAKLLEGTGSEASSTRRGGSLGQTARSGPAALEPGPSESLTASSPLKLNELN
LTB4R2	LAGWRPARGRPL	TRPFLAPRLRSPAL	VTLARLRGARWGSGRHGARVG	RAGPRFLTRLFEGSGEARGGGRSREGTMELRTTPQLKVVGQGRGNGDPGGGMEKDGPEWDL
MAS1	LCFRMRRNP	LYPIWYRCHRPKYQ	LVVKIRKNTWASHSSKLY	KRFKESLKVVLTRAFKDEMQPRRQKDNCNTVTVETVV
MAS1L	LCCGATNP	LFPIWYRCHRPKYT	LLIRFLCCSQQQKATRVY	KRLKESLRVILQRALADKPEVGRNKKAAGIDPMEQPHSTQHVENLLPREHRVDVET
MC1R	IAKNRNLHSP	FYALRYHSIVTLPR	QGIARLHKRQRPVHQGFGLKGA	RTLKEVLTCSW
MC2R	VFKNKNLQAP	FHALRYHSIVTMRR	RKISTLPRANMKGA	DAFKKMIFCSRYW
MC3R	VVRNGNLHSP	FYALRYHSIMTVRK	KRIAALPPADGVAPQQHSCMKGA	NTFREILCGCNGMNLG
MC4R	IAKNKNLHSP	FYALQYHNIMTVKR	KRIAVLPGTGAIRQGANMKGA	KTFKEIICCYPLGGLCDLSSRY
MC5R	IVKNKNLHSP	FYALRYHHIMTARR	KRIAALPGASSARQRTSMQGA	KTFKEIICCRGFRIACSFPRRD
MCHR1	VVKKSKLHWCNNV	VHPISSTKFRKPSV	RILQRMTSSVAPASQRSIRLRTKRVT	KRLVLSVKPAAQGQLRAVSNAQTADEERTESKGT
MCHR2	IIRSRKKTV	VQPFRLTRWRTRYK	LILCYTWEMYQQNKDARCCNPSVPKQRVMKLT	KRLPQIQRRATEKEINNMGNTLKSHF
MLNR	IGRYRDMRTT	CRPLRARVLVTRRR	LIGRELWSSRRPLRGPAASGRERGHRQTV	AAAFKLLLARKSRPRGFHRSRDTAGEVAGDTGGDTVGYTETSANVKTMG
MRGPRD	LGFRMHRNP	LFPIWFKCHRPRHL	LFVWVRRSSQQWRRQPTRLF	RSHRLPTRSLGTVLQQALREEPELEGGETPTVGTNEMGA
MRGPRE	LSSNVYRNP	LFPAWYSCRRPRHL	LLLRVERGPQRPPPRGFP	RRLPLRLVLQRALGDEAELGAVRETSRRGLVDIAA
MRGPRF	FGFSIKRNP	IFPAWYWRRRPKRL	LILHVECRARRRQRSAKLN	QRLWEPLRVVFQRALRDGAELGEAGGSTPNTVTMEMQCPPGNAS
MRGPRG	LGFRIKKGP	LFPACYQGCRPRHA	VLFVWVTCCSTRPRPRLY	EPLRSVLRRALGEGAELGARGQSLPMGLL
MRGPRX1	LGCRMRRNA	LWPIWYRCHRPTHL	LLIRILCGSRKIPLTRLY	QRQNRQNLKLVLQRALQDASEVDEGGGQLPEEILELSGSRLEQ
MRGPRX2	LGFRMRRNA	LWPIWYRCRRPRHL	LLVRILCGSRGLPLTRLY	KQWRLQQPILKLALQRALQDIAEVDHSEGCFRQGTPEMSRSSLV
MRGPRX3	LGCRMRRNA	LWPIWYHCRRPRYL	LLVRILCGSRKMPLTRLY	QRQNRQNLKLVLQRALQDTPEVDEGGGWLPQETLELSGSRLEQ

GPCR	ICL1	ICL2	ICL3	C-Term
MRGPRX4	LGYRMRRNA	LWPIWYRCRRPTHL	LLVRILCGSRKMPLTRLY	QRQNRQNLKLVLQRALQDKPEVDKGEGQLPEESLELSGSRLGP
MTNR1A	VYRNKKLRNA	CHSLKYDKLYSSKN	RIWILVLQVRQRVKPDRKPKLKPQDFRNF	KEYRRIIVSLCTARVFFVDSSNDVADRVKWKPSPLMTNNNVVKVDSV
MTNR1B	VLRNRKLRNA	CHSMAYHRIYRRWH	RIWVLVLQARRKAKPESRLCLKPSDLRSF	REYKRILLALWNPRHCIQDASKGSHAEGLQSPAPPIIGVQHQADAL
NMBR	FITNSAMRSV	VNPMDMQTSGALLR	HIAKTLIKSAHNLPGEYNEHTKKQMETRKRLA	RHFNSQLCCGRKSYQERGTSYLLSSSAVRMTSLKSNAKNMVTNSVLLNGHSMKQEMAL
NMUR1	ILRHKAMRTP	VHPLQARSMVTRAH	LIGLRLRRERLLLMQEAKGRGSAAARSRYTCRLQQHDRGRRQVT	ETFQEALCLGACCHRLRPRHSSHSLSRMTTGSTLCDVGSLGSWVHPLAGNDGPEAQQET DPS
NMUR2	ILQHQAMKTP	LHPFRAKLQSTRRR	LMALRLKKDKSLEADEGNANIQRPCRKSVN	AAFQNVISSFHKQWHSQHDPQLPPAQRNIFLTECHFVELTEDIGPQFPCQSSMHNSHLPA ALSSEQMSRTNYQSFHFNKT
NPBWR1	LLRAPRMKTV	LATAESRRVAGRTY	TLLCRLHAMRLDSHAKALERAKKRVT	RNLRQLITCRAAA
NPBWR2	ILRAPKMKTV	LATVRSRHMPWRTYRG	DLLRRLRAVRLRSGAKALGKARRKVT	KNFRSILRC
NPFFR1	VLKNRHMHTV	VHPFREKLTLRK	RIARKLCQAPGPAPGGEEAADPRASRRRARVV	RGFQAAFRARLCPRPSGSHKEAYSERPGGLLHRRVFVVVRPSDSGLPSESGPSSGAPRPGR LPLRNGRVAHHGLPREGPGCSHLPLTIPAWDI
NPFFR2	VMRNKHMHTV	VYPFKPKLTIKT	RIGISLFRAAVPHTGRKNQEQWHVVSRKKQKII	RGFQEAFQLQLCQKRAKPMEAYALKAKSHVLINTSNQLVQESTFQNPHGETLLYRKSAEK PQQELVMEELKETTNSSEI
NPSR1	TWRRKKKSR	VYPMKFLQGEKQ	IVIRTIWIKSKTYETVISNCSDGKLCSSYNRGLISKAKIKAI	SISFPCREQRSQDSRMTFRERTERHEMQILSKPEFI
NPY1R	ILKQKEMRNV	INPRGWRPNNRH	KIYIRLKRRNNMMDKMRDNKYRSSETKRIN	RDLQFFFNFCDFRSRDDDYETIAMSTMHTDVSKTSLKQASPVAFKKINNNDDNEKI
NPY2R	VIKFKSMRTV	VYHLESKISKRI	RIWSKLKNHVSPGAANDHYHQRRQKTT	KAFLSAFRCEQRLDAIHSEVSVTFKAKKNLEVRKNSGPNDSFTEATNV
NPY4R	VRQKEKANV	INPTGWKPSISQ	RIYRRLQRQGRVFHKGTYSLRAGHMKQVN	KEIKALVLTCQQSAPLEESEHLPLSTVHTEVSKGSLRLSGRSNPI
NPY5R	LMKKRNQKTT	KHPISNNLTANH	SVCRSISCGLSNKENRLEENEMINLTLHPSKKSGPQVKLSGSHKWSYSFI KKHRRRYSKKTACVLPAPERPSQENHSRILPENFGSVRSQLSSSSKFIPG VPTCFEIKPEENSDVHELRVKRSVTRIKKRSRSVF	ADLVSLIHCLHM
NPY6R	FKKQRKAQNF	VNPRGWKPSVTH	KIVICLRRRNAKVDKKKENEGRLNENKRIN	RC
NTSR1	LARKKSLQSLQS T	CHPFKAKTLMSRSR	IIANKLTVMVRQAAEQGQVCTVGGEHSTFSMAIEPGRVQALRHGV	HIFLATLACLCPVWRRRRKRPAFSRKADSVSSNHTLSSNATRETLY
NTSR2	VLKARAGRAGR	CQPLRARSLLTPRR	VTVSHLLALCSQVPSTSTPGSSTPSRLELLSEEGLLSFIVWKKTFIQGGQV SLVRHKDVRRIRSLQRSV	KLFLEAVSSLCGEHHPMKRLPPKPQSPTLMDTASGFGDPPETRT
OPN3	YYKFQRLRTP	VHARVINFSW	HILYSIRMLRCVEDLQTIQVIKILKYEKKLA	RSLLQLLCLRLLRCQRPAKDLPAAGSEMQIRPIVMSQKDGDRPKKKVTFNSSSIIFIITSDESL SVDDSDKTNGSKVDVIQVRPL
OPN4	FCRSRSLRTP	TRPLATFGVASKRR	FIFRAIRETGRALQTFGACKGNGESLWQRQRLQSECKMA	VAIAQHLPCLGVLLGVSRRHSRPYPSYRSTHRSTLTSHTSNLSWISIRRRQESLGSESEVGW THMEAAAVWGAAQQANGRSLYGQGLEDLEAKAPPRPQGHEAETPGKTKGLIPSQDPR M
OPN5	SSRRKKKLRP	CYLSYGVWLKRKH	KIIAKVKSSSKEVAHFDSRIHSSHVLEMKLT	KFACCQTGGLKATKKKSLEGFRLHTVTTVRKSSAVLEIHEEWE
OPRD1	IVRYTKMKTA	CHPVKALDFRTPAK	LMLLRLRSVRLLSGSKEKDRSLRRIT	RCFRQLCRKPCGRPDPSSFSRAREATARERVTACTPSDGPGGGAAA
OPRK1	IIRYTKMKTA	CHPVKALDFRTPLK	LMILRLKSVRLLSGSREKDRNLRRIT	RCFRDFCFPLKMRMERQSTSRVRNTVQDPAYLRDIDGMNKPV
OPRL1	ILRHTKMKTA	CHPIRALDVRTSSK	LMIRRLRGVRLLSGSREKDRNLRRIT	ACFRKFCCASALRRDVQVSDRVRSIAKDVALACKTSETVPRPA
OPRM1	IVRYTKMKTA	CHPVKALDFRTPRN	LMILRLKSVRMLSGSKEKDRNLRRIT	RCFREFCIPTSSNIEQQNSTRIRQNTRDHPSTANTVDRTNHQLENLEAETAPLP
OXER1	FCIHTRPWTS	VQPHHVLSRASVGA	SIGLTIRNRGLGGQAGPQRAM	HQSRALLGLTRGRQGPVSDESSYQPSRQWRYREASRKAEAIGKLKVQGEVSLEKEGSSQG
OXGR1	YIFKMRPWKS	IHPMSCFSIHKTRC	TIIHTLTHGLQTDSCLKQKAR	QAVCSTVRCKVSGNLEQAKKISYSNNP
OXTR	LRTTRQKHSR	CQPLRSLRRRT	LISFKIWQNLRLKTAAAAAAEAPEGAAAGDGGRVALARVSSVKLISKAK IRTV	ELVQRFLCCSASYLKGRRLGETSASKKSNSSSFVLSHRSSSQRSCSQPSTA
P2RY1	FVFHMKPWSG	VYPLKSLGRLKKKN	LIVRALIYKDLDNSPLRRKSI	RRLSRATRKASRRSEANLQSKSEDMTLNILPEFKQNGDTSL
P2RY10	LCRFISKKNK	LKPFRARDWKRRYD	KTTISLRQPPMAFQGISERQKAL	DQLSRHGSSVTRSRLMSKESGSSMIG
P2RY11	FSIRKQRPWHP	VHPFFARSHLRPKH	ALGRAVLRSPGMTVAEKLRVA	SLGCCCRHCPGYRDSWNPEDAKSTGQALPLNATAAPKPSEPQSRELSQ

GPCR	ICL1	ICL2	ICL3	C-Term
P2RY12	FFQIRSKSN	TRPFKTSNPKNLLG	LITKELYRSYVRTRGVGKVPRKKVN	NSLISMLKCPNSATSLSQDNRKKEQDGGDPNEETPM
P2RY13	FVHIPSSSTF	IRPLRNIFLKKPVF	VIAKKVYDSYRKSKSKDRKNNKKLE	EKLPCMQGRKTTASSQENHSSQTDNITLG
P2RY14	FFYVPSSKS	VKPLWTSFIQSVSY	AITKKIFKSHLKSSRNSTSVKKKSS	EILCKKLHIPLKAQNDLDISRIKRGNTTLESTDTL
P2RY2	FLCRLKTWNA	LRPLRSLRWGRARY	LMARRLLKPAYGTSGGLPRAKRKSV	RDAKPPTGPSPATPARRRLGLRRSDRTDMQRIEDVLGSSEDSRRTESTPAGSENTKDIRL
P2RY4	FIFRLRPWDA	CHPLRALRWGRPRL	LMARRLYQPLPGSAQSSSRLRSL	RQLRQLCGGGKPQPRTAASSLALVSLPEDSSCRWAATPQDSSCSTPRADRL
P2RY6	ICTSRRALTR	CHPLAPWHKRGGRR	LLACRLCRQDGPAEPVAQERRGKAA	RRPHELLQKLTAKWQRQGR
P2RY8	LCRRMGPRSP	LYPLSSKRWRRRRY	ATILKLLRTEEAHGREQRRRAV	LRLREYLGCRRVPRDTLDTRRESLFSARTTSVRSEAGAHPEGMEGATRPGLQRQESVF
PRLHR	IARVRRLHNV	VHPLRRRISLRL	RVSVKLRNRVVPGCVTQSQADWDRARRRRTF	EELRKLLVAWPRKIAPHGQNMTVSVVI
PROKR1	LVRYKKLRNL	VHPLRPRMKCQT	RISRELWFKAVPGFQTEQIRKRLRCRRKTV	KYFKKIMLLHWKASYNGGKSSADLDLKTIGMPATEEVDCIRLK
PROKR2	LTRYKKLRNL	VHPLKPRMNYQT	RISRELWFKAVPGFQTEQIRKRLRCRRKTV	KYFKKMMLLHWRPSQRGSKSSADLDLRTNGVPTTEEVDCIRLK
PTAFR	FARLYPCKKFNE	TRPIKTAQANTRKR	VIIRTLLMQPVQQQRNAEVKRRAL	KHLTEKFYSMRSSRKCSRATTDTVTEVVVPFNQIPGNSLKN
PTGDR	LARSGLGWCSRRP	GHPFFYRRHITLRL	RNLYAMHRRLQRHPRSCTRDCAEPRADGREASPQPLEELDHL	IFFHKIFIRPLRYRSRCSNSTNMESSL
PTGDR2	VGCRMRQTV	VRPVWAQNHRTVAA	AVSLRLQHRGRRRPGRFV	RKLRRSLRTVLESVLVDDSELGGAGSSRRRRTSSTARSASPLALCSRPEEPRGPARLLGWLLGSCAASPQTGPLNRALSSTSS
PTGER1	LAQAAGRLRRRRSAAT	TRPLLHAARVSVAR	ALLRARWRRRSRRPPPASGPDSRRRWGAHGPRSASASSASSIASASTFFGGSRSSGSARRARAHDVEMV	RQLLRLLPPRAGAKGGPAGLGLTPSAWEASSLRSSRHSGLSHF
PTGER2	LARRWRGDVGCSAGRRSSLSL	GHPYFYQRRVSRSG	LNLIRMHRRSRRSRCGPSLGSGRGGPGARRRGERVSMAEETDHL	RLMRSVLCCRISLRTQDATQTSCSTQSDASKQADL
PTGER3	VSRSYRRRESKR	RAPHWYASHMKTRA	ATIKALVSRCRAKATASQSSAQWGRITTETA	ILLRKFCQIRYHTNNYASSSTSLPCQCSSTLMWSDHLER
PTGER4	LCKSRKEQKE	NHAYFYSHYVDKRL	RMHRQFMRRTSLGTEQHHAAAAASVASRGHPAASPALPRLSDFRRRRSFRRIAGAEIQMV	KAIEKIKCLFCRIGGSRRERSGQHCSDSQRTSSAMSGHSRSFISRELKEISSTSQTLLPDLSLPDLSENGLGGRNLLPGVPGMGLAQEDTTSLRTLRISETSDSSQGQDSESVLLVDEAGGSGRAGPAPKGSSLQVTFPSETLNLSEKCI
PTGFR	LMKAYQRFRQKS	TKPIFHSTKITSKH	TLLRVKFKSQQHRQGRSHHLEMV	KNLYKLASQCCGVHVISLHIWELSSIKNSLKVAAISESPVAEKSAST
PTGIR	LSARRPAR	SHPYLYAQLDGPRC	LSLCRMYRQQKRHQGSLGPRPRTGEDEVDHL	QRLKLWVCCLCLGPAHGDSQTPLSQLASGRRDPRAPSAPVGKEGSCVPLSAWGEGQVEPLPPTQQSSGSAVGTSSKAEASVACSLC
QRFPR	VTRSKAMRTV	VHPFKMKWQYTNRR	KIGYELWIKKRVGDGSVLRTIHGKEMSKIARKKKRAV	KNVLSAVCYCIVNKTFSPAQRHGNSGITMMRKKAKFSLRENPVEETKGEAFSDGNIEVKLCEQTEEKKKLKRHLALFRSELAENSPLDSGH
RXFP1	VSAVTCFGNIFVICMRPYIRSE	VYPFRCVRPGKCR	SMFYSVHQSAITATEIRNQVKKEMILA	EMIHRFWYNYRQRKSMDSKGQKTYAPSFIWVEMWPLQEMPPELMKPDLFTYPCEMSLISQSTRLNSYS
RXFP2	RSFIKAENTT	VFPFSNIRPGKRQ	TMFCSIQKTALQTTEVRNCFGREVAVA	DKLKQLLHKHQRKSIFKIKKKSLSTSIVWIEDSSSLKLGVLNKITLGDSIMKPVS
RXFP3	MKSMQGWRKSS	ASALKSHRTRGHGR	LLVRFIADRRAAGTKGGAAVAGGRPTGASARRLSKVT	KALKSLLWRIASPSITSMRPFTATTKPEHEDQGLQAPAPPHAAAEPDLLYYPPGVVVYSGGRYDLLPSSSAY
RXFP4	LSNCARRAPGPP	AMAAGPGTHLSLFW	LLLAFLQRRQRRRQDSRVVA	QALAGTFRDLRLRLWPQGGGWVQQVALKQVGRRWVASNPRESRPSTLLTNLDRGTPG
S1PR1	IWKTKKFHRP	LKMKLHNGSNNFR	RIYSLVRTRSRRLTFRKNISKASRSSEKSLALL	RAFIRIMSCCKCPSGDSAGKFKRPIIAGMEFSRSKSDNSSHPQKDEGDNPETIMSSGNVNSSS
S1PR2	VARNSKFHSA	AKVKLYGSDKSCR	RIYCVVRSSHADMAAPQTLALL	REVLRPLQCWRPGVGVQGRRRGGTPGHHLLPLRSSSSLERGMHMPTSPTFLEGNTVV
S1PR3	IWKNNKFHNR	IKMRPYDANKRHR	RIYFLVKSSSRKVANHNNSERSMALL	RAFFRLVCNCLVRGRGARASPIQPALDPSRSKSSSSNNSSHSPKVKEDLPHTAPSSCIMDKNAALQNGIFCN
S1PR4	ITSHMRSRRW	VRPVAESGATKTSR	AIFRLVQASGQKAPRPAARRKARRLL	RAVLSFLCCGCLRLGMRGPGDCLARAVEAHSGASTTDSSLRPRDSFRGSRSLSFRMREPLSSISSVRSI

GPCR	ICL1	ICL2	ICL3	C-Term
S1PR5	LGRHPRFHAP	ARRGPAPVSSRGR	RIYCQVRANARRLPARPGTAGTTSTRARRKPRSLALL	HALLRLVCCGRHSCGRDPSGSQQSASAAEASGGLRRCLPPGLDGSFSGSERSSPQRDGLD TSGSTGSPGAPTAARTLVSEPAAD
SSTR1	ILRYAKMKTA	VHPIKAARYRRPTV	LIIAKMRMVALKAGWQQRKRSERKIT	RSFQRILCLSWMDNAAEEPVDYYATALKSRAYSVEDFQPENLESGGVFRNGTCTSRITTL
SSTR2	ILRYAKMKTI	VHPIKSAKWRRPRT	FIIIKVKSSGIRVGSSKRKKSEKKVT	KSFQNVLCLVKVSGTDDGERSDSKQDKSRLNETTETQRTLLNGDLQTSI
SSTR3	VLRHTASPSV	VHPTRSARWRTAPV	LIVVKVRSAGRRVWAPSCQRRRRSERRVT	QGFRRVLLRPSRRVRSQEPTVGPPEKTEEEDEEEEDGEESREGGKGKEMNGRVSQITQPG TSGQERPPSRVASKEQQLLPQEASTGEKSSTMRISYL
SSTR4	ILRYAKMKTA	VHPLRAATYRRPSV	LIVGKMRAVALRAGWQQRRRSEKKIT	RFFQRVLCLRCCLLEGAGGAEEEPLDYYATALKSKGGAGCMCPPLPCQQEALQPEPGRKRI PLTRTTTF
SSTR5	VLRFAKMKTV	VHPLSSARWRRPRV	LIVVKVRAAGVRVGCVRRRSERKVT	QSFQKVLCLRKGSGAKDADATEPRPDRIRQQQEATPPAHRAAANGLMQTSKL
SUCNR1	YIFSLKNWNS	KYPFREHLLQKKEF	KIALFLKQRNRQVATALPLEKPL	DMLMNQLRHNFKSLTSFSRWAHELLLSFREK
TAAR1	ISHFKQLHTP	CDPLRYKAKMNILV	RIYLIAKEQARLISDANQKLQIGLEMKNGISQSKERKAV	KALKMMLFGKIFQKDSSRCKLFLELSS
TAAR2	ISYFKQLHTP	CYPLLYSTKITIPV	KIFAVSRKHAHAINNLRENQNNQVKKDKKAA	RALKYILLGKIFSSCFHNTILCMQKESE
TAAR3	ISHFKQLHSP	CYPLHYTTKMTNST	KIFIVSKQHARVISHVPENTKGAVKKHLSKKKDRKAA	KAFKYIVSGKIFSSHSETANLFPEAH
TAAR5	VSYFKALHTP	CDPLLYPSKFTVRV	KIFVVATRQAQQITTLSKSLAGAAKHERKAA	KALKLTLSQKVFSPQTRTVDLYQE
TAAR6	ILHFKQLHSP	TDPLVYPTKFTVSV	NIFLVARRQAKKIENTGSKTESSSESYKARVARRERKAA	KAIKVIVTGQVLKNSSATMNLFSEHI
TAAR8	VLHFKQLHSP	TDPLVYATKFTVSV	KIFLIAKQQAIKIETTSSKVESSSESYKIRVAKRERKAA	KAIKLILSGDVLKASSSTISLFLE
TAAR9	ILHFKQLHTP	TDPLTYPTKFTVSV	KIFLVAKHQARKIESTASQAQSSSESYKERVAKRERKAA	KAIKLIVSGKVLRTDSSTTNLFSEEVETD
TACR1	ILAHKRMRTV	IHPLQPRLSATA	VVGITLWASEIPGDSSDRYHEQVSAKRKVV	LGFKHAFRCCPFISAGDYEGLEMKSTRYLQTQGSVYKVSRLETTISTVVGAHEEEPEDGPKA TPSSLDLTSNCSSRSDSKTMTESFSFSSNVLS
TACR2	ILAHRRMRTV	VHPFQPRLSAPST	VIGLTLWRRAVPGHQAHGANLRHLQAMKKFV	SGFRLAFRCCPWVTPTKEDKLELTPTTSLSTRVNRCHTKETLFMAGDTAPSEATSGEAGRP QDGSGLWFGYGLLAPTKTHVEI
TACR3	ILAHKRMRTV	IDPLKPRLSATA	IVGITLWGGEIPGDTCDKYHEQLKAKRKVV	AGFKRAFRWCPFIKVSSYDELELKTTRFHPNRQSSMYTVTRMESMTVVFDPNDADTTRSS RKKRATPRDPSFNGCSRRNSKSASATSSFISSPYTSVDEYS
TBXA2R	LAGARQGGSHT RSS	TRPFSRPAVASQRR	TLCHVYHGQEAAQQRPRDSEVEMM	AVLRRLQPRLSTRPRSLSLQPQLTQRSGLQ
TRHR	VMRTKHMRTP	CHPIKAQFLCTFSR	FIARILFLNPIPSDPKENSKTWKNDSTHQNTNLNVNTSNRCFNSTVSSR KQVT	AAFRKLCNCKQKPTEKPANYSVALNYSVIKESDHFSTELDDITVTDTYLSATKVSFDDTCLAS EVSFSQS
TSHR	LLTSHYKLNV	TFAMRLDRKIRLRH	KIYITVRNPQYNPGDKDTKIA	RDVFILLSKFGICKRQAQAYRGQRVPPKNSTDIQVQKVTHDMRQGLHNMEDVYELIENSH LTPKKQGQISEEYMQTVL
UTS2R	TCRSLRAVAS	LRPLDTVQRPKGY	RLARAYRRSQRASFKRARRPGARAL	DHLRGRVRGPGSGGGRGPVPSLQPRARFQRCSGRSLSSCSPQPTDSLVLAPAAPARPAPE GPRAPA
XCR1	LVKYESLESL	VSPLSTLRVPTLRC	EILRTLFRSRSKRRHRTV	THLKHVLRQFWFCRLQAPSPASIPHSPGAFAYEGASFY

Supplementary Table S2: Differential gene expression results.

Comparison: statistical comparison between indicated treatments, where either Untreated or IFNγ/IL1β within the same cell line serves as baseline. *baseMean:* Average read counts. *log2FoldChange:* log2-transformed fold change in the respective comparison (in relation to baseline). *lfcSE:* Standard error of the log2-transformed fold change. *Statistic:* Wald test statistic. *p-value:* p-value before adjustment. *padj:* p-value after "Benjamini-Hochberg" adjustment with an alpha of 0.1. *Direction:* up- or downregulation in the respective comparison.

Gene	Cell line	Comparison	baseMean	log2FoldChange	lfcSE	Statistic	p-value	padj	Direction
Figure 28a									
CXCL1	Non-transduced	Untreated vs. IFNγ/IL1β	4647.5125	7.3186	0.1721	42.5217	0.0000	0.0000	Up
DTX3L	Non-transduced	Untreated vs. IFNγ/IL1β	3206.9456	3.9149	0.0898	43.5766	0.0000	0.0000	Up
GBP1	Non-transduced	Untreated vs. IFNγ/IL1β	5589.8012	6.5287	0.1263	51.7068	0.0000	0.0000	Up
IFIT3	Non-transduced	Untreated vs. IFNγ/IL1β	2457.6883	5.1560	0.1216	42.3987	0.0000	0.0000	Up
IRF1	Non-transduced	Untreated vs. IFNγ/IL1β	5735.8477	6.5561	0.1266	51.7913	0.0000	0.0000	Up
PARP14	Non-transduced	Untreated vs. IFNγ/IL1β	3210.8707	4.3919	0.0957	45.8973	0.0000	0.0000	Up
SOD2	Non-transduced	Untreated vs. IFNγ/IL1β	3501.9008	3.3563	0.0708	47.3884	0.0000	0.0000	Up
STAT1	Non-transduced	Untreated vs. IFNγ/IL1β	5049.7848	3.2387	0.0661	48.9970	0.0000	0.0000	Up
WARS	Non-transduced	Untreated vs. IFNγ/IL1β	6346.2407	3.1775	0.0674	47.1544	0.0000	0.0000	Up
ZC3HAV1	Non-transduced	Untreated vs. IFNγ/IL1β	7554.5074	2.6090	0.0569	45.8905	0.0000	0.0000	Up
APOL6	Non-transduced	Untreated vs. IFNγ/IL1β	2624.0080	7.0163	0.1947	36.0418	0.0000	0.0000	Up
TAP1	Non-transduced	Untreated vs. IFNγ/IL1β	1696.3720	5.8025	0.1648	35.2006	0.0000	0.0000	Up
NFKBIA	Non-transduced	Untreated vs. IFNγ/IL1β	3723.2041	2.6544	0.0760	34.9386	0.0000	0.0000	Up
TRIM25	Non-transduced	Untreated vs. IFNγ/IL1β	2107.6833	2.3878	0.0705	33.8468	0.0000	0.0000	Up
CCL2	Non-transduced	Untreated vs. IFNγ/IL1β	2912.7026	6.7796	0.2079	32.6101	0.0000	0.0000	Up
TAP2	Non-transduced	Untreated vs. IFNγ/IL1β	3139.8605	2.8450	0.0899	31.6580	0.0000	0.0000	Up
NFKBIZ	Non-transduced	Untreated vs. IFNγ/IL1β	1131.9308	3.7592	0.1189	31.6132	0.0000	0.0000	Up
HLA-E	Non-transduced	Untreated vs. IFNγ/IL1β	1701.6339	2.4989	0.0800	31.2360	0.0000	0.0000	Up
IFI16	Non-transduced	Untreated vs. IFNγ/IL1β	1105.4200	3.3546	0.1145	29.3075	0.0000	0.0000	Up
PMAIP1	Non-transduced	Untreated vs. IFNγ/IL1β	1370.8289	2.6536	0.0906	29.2744	0.0000	0.0000	Up
PARP9	Non-transduced	Untreated vs. IFNγ/IL1β	840.4886	4.5570	0.1590	28.6630	0.0000	0.0000	Up
CLDN1	Non-transduced	Untreated vs. IFNγ/IL1β	2289.9252	1.7397	0.0618	28.1529	0.0000	0.0000	Up
CXCL8	Non-transduced	Untreated vs. IFNγ/IL1β	7683.6672	5.8377	0.2076	28.1204	0.0000	0.0000	Up
GBP3	Non-transduced	Untreated vs. IFNγ/IL1β	717.8437	3.9920	0.1430	27.9196	0.0000	0.0000	Up
PTX3	Non-transduced	Untreated vs. IFNγ/IL1β	4240.9542	2.5067	0.0927	27.0480	0.0000	0.0000	Up
GRAMD3	Non-transduced	Untreated vs. IFNγ/IL1β	835.2520	2.5219	0.0955	26.3946	0.0000	0.0000	Up
DRAM1	Non-transduced	Untreated vs. IFNγ/IL1β	1375.3505	1.9096	0.0737	25.9248	0.0000	0.0000	Up
B2M	Non-transduced	Untreated vs. IFNγ/IL1β	19232.0340	1.4275	0.0555	25.7001	0.0000	0.0000	Up
PSMB9	Non-transduced	Untreated vs. IFNγ/IL1β	776.8089	4.9050	0.1911	25.6639	0.0000	0.0000	Up
RIPK2	Non-transduced	Untreated vs. IFNγ/IL1β	863.7223	2.8171	0.1101	25.5829	0.0000	0.0000	Up
SOCS3	Non-transduced	Untreated vs. IFNγ/IL1β	1885.3959	3.0360	0.1211	25.0744	0.0000	0.0000	Up
ZNFX1	Non-transduced	Untreated vs. IFNγ/IL1β	2961.6681	1.8764	0.0763	24.5944	0.0000	0.0000	Up
TNFAIP2	Non-transduced	Untreated vs. IFNγ/IL1β	3020.8680	3.7945	0.1573	24.1204	0.0000	0.0000	Up
UBD	Non-transduced	Untreated vs. IFNγ/IL1β	4045.0961	10.3008	0.4443	23.1827	0.0000	0.0000	Up
UBE2L6	Non-transduced	Untreated vs. IFNγ/IL1β	657.6368	2.7234	0.1189	22.9124	0.0000	0.0000	Up
IFIT5	Non-transduced	Untreated vs. IFNγ/IL1β	723.5877	2.3086	0.1012	22.8093	0.0000	0.0000	Up
CD274	Non-transduced	Untreated vs. IFNγ/IL1β	867.6037	2.4141	0.1063	22.7092	0.0000	0.0000	Up
HELZ2	Non-transduced	Untreated vs. IFNγ/IL1β	521.8066	3.0811	0.1359	22.6648	0.0000	0.0000	Up
EFNA1	Non-transduced	Untreated vs. IFNγ/IL1β	2968.1900	3.1957	0.1434	22.2859	0.0000	0.0000	Up
TNFAIP3	Non-transduced	Untreated vs. IFNγ/IL1β	580.6892	2.9234	0.1335	21.8975	0.0000	0.0000	Up
SP110	Non-transduced	Untreated vs. IFNγ/IL1β	752.7121	2.5212	0.1157	21.7869	0.0000	0.0000	Up
DDX58	Non-transduced	Untreated vs. IFNγ/IL1β	472.9837	3.8908	0.1801	21.6030	0.0000	0.0000	Up
IRF2	Non-transduced	Untreated vs. IFNγ/IL1β	461.5672	2.9730	0.1376	21.6023	0.0000	0.0000	Up
CASP7	Non-transduced	Untreated vs. IFNγ/IL1β	1137.9572	1.7672	0.0825	21.4105	0.0000	0.0000	Up
SBNO2	Non-transduced	Untreated vs. IFNγ/IL1β	1062.6699	2.1855	0.1025	21.3220	0.0000	0.0000	Up
CSF1	Non-transduced	Untreated vs. IFNγ/IL1β	720.7486	5.5736	0.2646	21.0656	0.0000	0.0000	Up
APOL2	Non-transduced	Untreated vs. IFNγ/IL1β	1134.4073	3.9965	0.1953	20.4638	0.0000	0.0000	Up
TRIB1	Non-transduced	Untreated vs. IFNγ/IL1β	490.5769	2.3256	0.1156	20.1193	0.0000	0.0000	Up
PDCD1LG2	Non-transduced	Untreated vs. IFNγ/IL1β	619.7959	2.1256	0.1059	20.0663	0.0000	0.0000	Up
LYN	Non-transduced	Untreated vs. IFNγ/IL1β	688.9566	1.9233	0.1008	19.0870	0.0000	0.0000	Up
TRIM21	Non-transduced	Untreated vs. IFNγ/IL1β	350.3354	3.1099	0.1638	18.9849	0.0000	0.0000	Up
NNMT	Non-transduced	Untreated vs. IFNγ/IL1β	4876.2039	2.4807	0.1332	18.6176	0.0000	0.0000	Up
NMI	Non-transduced	Untreated vs. IFNγ/IL1β	356.7689	3.3787	0.1921	17.5917	0.0000	0.0000	Up
PLSCR1	Non-transduced	Untreated vs. IFNγ/IL1β	1380.8839	2.6954	0.1555	17.3365	0.0000	0.0000	Up
IRF9	Non-transduced	Untreated vs. IFNγ/IL1β	254.4583	3.4845	0.2027	17.1880	0.0000	0.0000	Up
ADAR	Non-transduced	Untreated vs. IFNγ/IL1β	1680.3969	1.0367	0.0609	17.0251	0.0000	0.0000	Up
BIRC3	Non-transduced	Untreated vs. IFNγ/IL1β	414.6550	2.4658	0.1451	16.9944	0.0000	0.0000	Up
SECTM1	Non-transduced	Untreated vs. IFNγ/IL1β	392.0935	4.7742	0.2855	16.7212	0.0000	0.0000	Up
LAP3	Non-transduced	Untreated vs. IFNγ/IL1β	675.3819	1.6169	0.0972	16.6359	0.0000	0.0000	Up
IL32	Non-transduced	Untreated vs. IFNγ/IL1β	257.0740	3.9925	0.2403	16.6175	0.0000	0.0000	Up
CD40	Non-transduced	Untreated vs. IFNγ/IL1β	671.9037	1.6818	0.1018	16.5224	0.0000	0.0000	Up
PRRG1	Non-transduced	Untreated vs. IFNγ/IL1β	1438.8928	1.2628	0.0768	16.4393	0.0000	0.0000	Up
HAPLN3	Non-transduced	Untreated vs. IFNγ/IL1β	244.7788	3.3267	0.2053	16.2039	0.0000	0.0000	Up
STAT3	Non-transduced	Untreated vs. IFNγ/IL1β	785.6401	1.3807	0.0853	16.1944	0.0000	0.0000	Up
SP100	Non-transduced	Untreated vs. IFNγ/IL1β	1239.5842	1.6087	0.0998	16.1130	0.0000	0.0000	Up
MAFF	Non-transduced	Untreated vs. IFNγ/IL1β	944.8039	1.6328	0.1020	16.0023	0.0000	0.0000	Up
IFI30	Non-transduced	Untreated vs. IFNγ/IL1β	239.5922	3.1590	0.1985	15.9149	0.0000	0.0000	Up
LZTS1	Non-transduced	Untreated vs. IFNγ/IL1β	1084.2959	2.1052	0.1329	15.8390	0.0000	0.0000	Up
KLF6	Non-transduced	Untreated vs. IFNγ/IL1β	2017.8423	1.1469	0.0725	15.8143	0.0000	0.0000	Up
PSMB8-AS1	Non-transduced	Untreated vs. IFNγ/IL1β	307.5754	6.1531	0.3904	15.7620	0.0000	0.0000	Up
STAT2	Non-transduced	Untreated vs. IFNγ/IL1β	580.9366	1.6660	0.1071	15.5571	0.0000	0.0000	Up
TRIM56	Non-transduced	Untreated vs. IFNγ/IL1β	563.7014	1.7547	0.1130	15.5260	0.0000	0.0000	Up
OGFR	Non-transduced	Untreated vs. IFNγ/IL1β	330.9041	1.9538	0.1278	15.2877	0.0000	0.0000	Up
TBX3	Non-transduced	Untreated vs. IFNγ/IL1β	2443.2017	1.2332	0.0809	15.2469	0.0000	0.0000	Up
PSMB8	Non-transduced	Untreated vs. IFNγ/IL1β	212.5152	3.6746	0.2412	15.2349	0.0000	0.0000	Up
EPSTI1	Non-transduced	Untreated vs. IFNγ/IL1β	252.5794	3.6377	0.2396	15.1843	0.0000	0.0000	Up
NAMPT	Non-transduced	Untreated vs. IFNγ/IL1β	2825.0717	1.4332	0.0946	15.1461	0.0000	0.0000	Up
OPTN	Non-transduced	Untreated vs. IFNγ/IL1β	592.6861	1.6613	0.1107	15.0130	0.0000	0.0000	Up
ZC3H12A	Non-transduced	Untreated vs. IFNγ/IL1β	252.9153	3.5376	0.2364	14.9658	0.0000	0.0000	Up
TMEM158	Non-transduced	Untreated vs. IFNγ/IL1β	1660.4133	1.2552	0.0839	14.9536	0.0000	0.0000	Up
IFITM3	Non-transduced	Untreated vs. IFNγ/IL1β	1525.2199	1.1804	0.0799	14.7790	0.0000	0.0000	Up
NRP2	Non-transduced	Untreated vs. IFNγ/IL1β	224.8808	3.2467	0.2209	14.6981	0.0000	0.0000	Up
IL6ST	Non-transduced	Untreated vs. IFNγ/IL1β	2307.8338	1.1520	0.0789	14.6010	0.0000	0.0000	Up
GCLM	Non-transduced	Untreated vs. IFNγ/IL1β	1043.0873	1.6056	0.1101	14.5889	0.0000	0.0000	Up
CXCL5	Non-transduced	Untreated vs. IFNγ/IL1β	210.9604	3.2894	0.2280	14.4274	0.0000	0.0000	Up
IDO1	Non-transduced	Untreated vs. IFNγ/IL1β	464.5613	6.2800	0.4381	14.3350	0.0000	0.0000	Up
COL27A1	Non-transduced	Untreated vs. IFNγ/IL1β	385.5061	2.0282	0.1420	14.2835	0.0000	0.0000	Up
PPIF	Non-transduced	Untreated vs. IFNγ/IL1β	2951.7528	1.0331	0.0729	14.1787	0.0000	0.0000	Up
APOL1	Non-transduced	Untreated vs. IFNγ/IL1β	204.7781	4.3383	0.3061	14.1752	0.0000	0.0000	Up
BBC3	Non-transduced	Untreated vs. IFNγ/IL1β	760.7439	1.2973	0.0920	14.0964	0.0000	0.0000	Up

Gene	Cell line	Comparison	baseMean	log2FoldChange	lfcSE	Statistic	p-value	padj	Direction
IKZF2	Non-transduced	Untreated vs. IFNγ/IL1β	277.6139	2.3994	0.1709	14.0375	0.0000	0.0000	Up
NFKB1	Non-transduced	Untreated vs. IFNγ/IL1β	764.4594	1.4615	0.1053	13.8785	0.0000	0.0000	Up
PML	Non-transduced	Untreated vs. IFNγ/IL1β	183.9057	2.7980	0.2016	13.8781	0.0000	0.0000	Up
FZD5	Non-transduced	Untreated vs. IFNγ/IL1β	355.6888	1.9421	0.1401	13.8654	0.0000	0.0000	Up
IL7R	Non-transduced	Untreated vs. IFNγ/IL1β	1749.8384	1.1663	0.0853	13.6789	0.0000	0.0000	Up
CFLAR	Non-transduced	Untreated vs. IFNγ/IL1β	3191.7710	1.3345	0.0988	13.5030	0.0000	0.0000	Up
ERAP2	Non-transduced	Untreated vs. IFNγ/IL1β	316.7212	2.2420	0.1664	13.4716	0.0000	0.0000	Up
ZNF267	Non-transduced	Untreated vs. IFNγ/IL1β	442.4498	1.3885	0.1039	13.3685	0.0000	0.0000	Up
SLC2A3	Non-transduced	Untreated vs. IFNγ/IL1β	896.9065	1.2771	0.0958	13.3315	0.0000	0.0000	Up
TAPBP	Non-transduced	Untreated vs. IFNγ/IL1β	1009.8211	1.1321	0.0852	13.2945	0.0000	0.0000	Up
TNIP1	Non-transduced	Untreated vs. IFNγ/IL1β	579.4375	1.3169	0.1007	13.0836	0.0000	0.0000	Up
ATF3	Non-transduced	Untreated vs. IFNγ/IL1β	200.7206	2.4310	0.1861	13.0618	0.0000	0.0000	Up
C5orf56	Non-transduced	Untreated vs. IFNγ/IL1β	220.4816	2.9039	0.2233	13.0023	0.0000	0.0000	Up
TNFRSF1A	Non-transduced	Untreated vs. IFNγ/IL1β	770.2530	1.2450	0.0959	12.9805	0.0000	0.0000	Up
PDP1	Non-transduced	Untreated vs. IFNγ/IL1β	907.8438	1.1360	0.0897	12.6698	0.0000	0.0000	Up
RNF213	Non-transduced	Untreated vs. IFNγ/IL1β	510.9443	1.2586	0.0998	12.6149	0.0000	0.0000	Up
TNFAIP8	Non-transduced	Untreated vs. IFNγ/IL1β	589.1154	1.3550	0.1077	12.5852	0.0000	0.0000	Up
JAK2	Non-transduced	Untreated vs. IFNγ/IL1β	460.2117	1.4205	0.1129	12.5783	0.0000	0.0000	Up
IL15	Non-transduced	Untreated vs. IFNγ/IL1β	249.8648	2.2265	0.1796	12.3963	0.0000	0.0000	Up
CDC42EP4	Non-transduced	Untreated vs. IFNγ/IL1β	227.5225	1.8356	0.1487	12.3476	0.0000	0.0000	Up
LMCD1	Non-transduced	Untreated vs. IFNγ/IL1β	1090.5605	1.1825	0.0962	12.2888	0.0000	0.0000	Up
LDLR	Non-transduced	Untreated vs. IFNγ/IL1β	936.5613	1.1099	0.0910	12.1998	0.0000	0.0000	Up
NKX3-1	Non-transduced	Untreated vs. IFNγ/IL1β	288.6385	1.7337	0.1440	12.0362	0.0000	0.0000	Up
LONRF1	Non-transduced	Untreated vs. IFNγ/IL1β	215.6773	2.1034	0.1757	11.9702	0.0000	0.0000	Up
PSME1	Non-transduced	Untreated vs. IFNγ/IL1β	1121.0910	1.0272	0.0859	11.9521	0.0000	0.0000	Up
PSME2	Non-transduced	Untreated vs. IFNγ/IL1β	669.8873	1.6413	0.1382	11.8755	0.0000	0.0000	Up
C15orf48	Non-transduced	Untreated vs. IFNγ/IL1β	192.3965	3.3090	0.2797	11.8298	0.0000	0.0000	Up
DDX60	Non-transduced	Untreated vs. IFNγ/IL1β	141.4244	3.1015	0.2622	11.8275	0.0000	0.0000	Up
TMEM51	Non-transduced	Untreated vs. IFNγ/IL1β	699.3551	1.0822	0.0917	11.8035	0.0000	0.0000	Up
C1S	Non-transduced	Untreated vs. IFNγ/IL1β	135.3869	3.7884	0.3245	11.6753	0.0000	0.0000	Up
IFI35	Non-transduced	Untreated vs. IFNγ/IL1β	150.5608	2.6169	0.2272	11.5173	0.0000	0.0000	Up
GCH1	Non-transduced	Untreated vs. IFNγ/IL1β	169.0549	2.4146	0.2105	11.4728	0.0000	0.0000	Up
BATF3	Non-transduced	Untreated vs. IFNγ/IL1β	167.3901	1.9455	0.1704	11.4139	0.0000	0.0000	Up
BIRC2	Non-transduced	Untreated vs. IFNγ/IL1β	1957.3326	1.0629	0.0932	11.4009	0.0000	0.0000	Up
SSTR2	Non-transduced	Untreated vs. IFNγ/IL1β	144.7604	4.6904	0.4125	11.3716	0.0000	0.0000	Up
C1R	Non-transduced	Untreated vs. IFNγ/IL1β	131.4034	3.0866	0.2720	11.3474	0.0000	0.0000	Up
CEBPD	Non-transduced	Untreated vs. IFNγ/IL1β	277.4483	2.1530	0.1907	11.2915	0.0000	0.0000	Up
CXCL2	Non-transduced	Untreated vs. IFNγ/IL1β	324.8618	7.4899	0.6645	11.2708	0.0000	0.0000	Up
DDX60L	Non-transduced	Untreated vs. IFNγ/IL1β	165.2520	2.3543	0.2117	11.1209	0.0000	0.0000	Up
MIR155HG	Non-transduced	Untreated vs. IFNγ/IL1β	133.2689	2.2972	0.2072	11.0878	0.0000	0.0000	Up
CXCL3	Non-transduced	Untreated vs. IFNγ/IL1β	138.5374	5.4890	0.4987	11.0077	0.0000	0.0000	Up
RELB	Non-transduced	Untreated vs. IFNγ/IL1β	162.0174	2.4065	0.2205	10.9159	0.0000	0.0000	Up
FST	Non-transduced	Untreated vs. IFNγ/IL1β	2700.1030	1.1125	0.1020	10.9019	0.0000	0.0000	Up
DNPEP	Non-transduced	Untreated vs. IFNγ/IL1β	383.0187	1.3230	0.1216	10.8824	0.0000	0.0000	Up
SOCS1	Non-transduced	Untreated vs. IFNγ/IL1β	119.1141	4.5371	0.4175	10.8685	0.0000	0.0000	Up
AIM1	Non-transduced	Untreated vs. IFNγ/IL1β	100.9556	3.1986	0.2944	10.8665	0.0000	0.0000	Up
LRRTM2	Non-transduced	Untreated vs. IFNγ/IL1β	123.4545	3.2971	0.3052	10.8036	0.0000	0.0000	Up
PSMB10	Non-transduced	Untreated vs. IFNγ/IL1β	373.2284	1.3993	0.1307	10.7047	0.0000	0.0000	Up
PARP8	Non-transduced	Untreated vs. IFNγ/IL1β	209.5914	1.6536	0.1554	10.6409	0.0000	0.0000	Up
IFIH1	Non-transduced	Untreated vs. IFNγ/IL1β	117.1257	4.0341	0.3808	10.5950	0.0000	0.0000	Up
SAMD9L	Non-transduced	Untreated vs. IFNγ/IL1β	160.3539	6.4263	0.6185	10.3902	0.0000	0.0000	Up
IL1B	Non-transduced	Untreated vs. IFNγ/IL1β	92.0404	3.7314	0.3607	10.3445	0.0000	0.0000	Up
IFIT2	Non-transduced	Untreated vs. IFNγ/IL1β	121.2378	3.1865	0.3082	10.3381	0.0000	0.0000	Up
SQRDL	Non-transduced	Untreated vs. IFNγ/IL1β	317.2573	1.2172	0.1184	10.2786	0.0000	0.0000	Up
PTPN12	Non-transduced	Untreated vs. IFNγ/IL1β	968.0349	1.0261	0.1000	10.2566	0.0000	0.0000	Up
CCL11	Non-transduced	Untreated vs. IFNγ/IL1β	187.2876	4.2964	0.4218	10.1862	0.0000	0.0000	Up
TNFRSF10D	Non-transduced	Untreated vs. IFNγ/IL1β	1866.4327	-1.1149	0.1100	-10.1385	0.0000	0.0000	Down
TNFRSF9	Non-transduced	Untreated vs. IFNγ/IL1β	95.8090	3.2904	0.3259	10.0968	0.0000	0.0000	Up
SAMD9	Non-transduced	Untreated vs. IFNγ/IL1β	178.4347	1.7912	0.1776	10.0843	0.0000	0.0000	Up
CD47	Non-transduced	Untreated vs. IFNγ/IL1β	330.3841	1.2631	0.1257	10.0494	0.0000	0.0000	Up
IFIT1	Non-transduced	Untreated vs. IFNγ/IL1β	122.6468	2.4631	0.2454	10.0386	0.0000	0.0000	Up
ETV6	Non-transduced	Untreated vs. IFNγ/IL1β	477.4634	1.4339	0.1438	9.9718	0.0000	0.0000	Up
NAB1	Non-transduced	Untreated vs. IFNγ/IL1β	358.6691	1.2562	0.1263	9.9490	0.0000	0.0000	Up
BCL2A1	Non-transduced	Untreated vs. IFNγ/IL1β	78.3154	3.1923	0.3240	9.8525	0.0000	0.0000	Up
IL18BP	Non-transduced	Untreated vs. IFNγ/IL1β	94.0180	4.9046	0.5069	9.6756	0.0000	0.0000	Up
BCL3	Non-transduced	Untreated vs. IFNγ/IL1β	105.3852	3.1079	0.3246	9.5735	0.0000	0.0000	Up
ETS1	Non-transduced	Untreated vs. IFNγ/IL1β	2714.1997	1.0046	0.1051	9.5585	0.0000	0.0000	Up
IFNAR2	Non-transduced	Untreated vs. IFNγ/IL1β	169.4656	1.6942	0.1774	9.5519	0.0000	0.0000	Up
RHBDF2	Non-transduced	Untreated vs. IFNγ/IL1β	442.0697	1.0287	0.1092	9.4195	0.0000	0.0000	Up
BTN3A1	Non-transduced	Untreated vs. IFNγ/IL1β	89.4480	2.6493	0.2820	9.3951	0.0000	0.0000	Up
TIFA	Non-transduced	Untreated vs. IFNγ/IL1β	254.7216	1.4537	0.1547	9.3956	0.0000	0.0000	Up
ETV7	Non-transduced	Untreated vs. IFNγ/IL1β	95.1564	4.1879	0.4465	9.3784	0.0000	0.0000	Up
CXCL10	Non-transduced	Untreated vs. IFNγ/IL1β	346.8163	11.0449	1.1866	9.3080	0.0000	0.0000	Up
TRIM22	Non-transduced	Untreated vs. IFNγ/IL1β	72.6928	3.4439	0.3709	9.2860	0.0000	0.0000	Up
NCOA7	Non-transduced	Untreated vs. IFNγ/IL1β	325.1693	1.3547	0.1463	9.2590	0.0000	0.0000	Up
JUNB	Non-transduced	Untreated vs. IFNγ/IL1β	157.1301	1.8386	0.2005	9.1683	0.0000	0.0000	Up
OAS3	Non-transduced	Untreated vs. IFNγ/IL1β	59.6136	3.0988	0.3399	9.1162	0.0000	0.0000	Up
LTB	Non-transduced	Untreated vs. IFNγ/IL1β	44.9479	4.3162	0.4799	8.9941	0.0000	0.0000	Up
FAM46A	Non-transduced	Untreated vs. IFNγ/IL1β	191.8147	1.3943	0.1557	8.9535	0.0000	0.0000	Up
PANX1	Non-transduced	Untreated vs. IFNγ/IL1β	205.3219	1.3810	0.1549	8.9136	0.0000	0.0000	Up
PARP12	Non-transduced	Untreated vs. IFNγ/IL1β	87.3281	2.2210	0.2528	8.7866	0.0000	0.0000	Up
RARRES3	Non-transduced	Untreated vs. IFNγ/IL1β	106.4087	4.7042	0.5391	8.7255	0.0000	0.0000	Up
SP140L	Non-transduced	Untreated vs. IFNγ/IL1β	238.5343	1.1672	0.1351	8.6373	0.0000	0.0000	Up
STARD8	Non-transduced	Untreated vs. IFNγ/IL1β	89.5790	2.4381	0.2859	8.5273	0.0000	0.0000	Up
RNU6-7	Non-transduced	Untreated vs. IFNγ/IL1β	20.4597	57.2759	6.7230	8.5194	0.0000	0.0000	Up
POU2F2	Non-transduced	Untreated vs. IFNγ/IL1β	79.2126	2.1569	0.2542	8.4854	0.0000	0.0000	Up
ARHGAP31	Non-transduced	Untreated vs. IFNγ/IL1β	108.8090	1.8290	0.2157	8.4776	0.0000	0.0000	Up
USP18	Non-transduced	Untreated vs. IFNγ/IL1β	93.5704	2.1789	0.2573	8.4687	0.0000	0.0000	Up
VEGFC	Non-transduced	Untreated vs. IFNγ/IL1β	248.4504	1.7684	0.2094	8.4435	0.0000	0.0000	Up
IL15RA	Non-transduced	Untreated vs. IFNγ/IL1β	61.5114	3.7613	0.4463	8.4278	0.0000	0.0000	Up
CA13	Non-transduced	Untreated vs. IFNγ/IL1β	59.6991	3.1804	0.3830	8.3036	0.0000	0.0000	Up
TRIB2	Non-transduced	Untreated vs. IFNγ/IL1β	216.5206	1.2557	0.1521	8.2562	0.0000	0.0000	Up
IFNGR2	Non-transduced	Untreated vs. IFNγ/IL1β	308.7735	1.0081	0.1225	8.2281	0.0000	0.0000	Up
NAV2	Non-transduced	Untreated vs. IFNγ/IL1β	349.2689	1.0085	0.1242	8.1169	0.0000	0.0000	Up
BTN3A2	Non-transduced	Untreated vs. IFNγ/IL1β	100.5133	1.8503	0.2299	8.0467	0.0000	0.0000	Up
XAF1	Non-transduced	Untreated vs. IFNγ/IL1β	135.7300	9.5131	1.1919	7.9813	0.0000	0.0000	Up
BLOC1S5-TXNDC5	Non-transduced	Untreated vs. IFNγ/IL1β	131.2452	22.3882	2.8356	7.8954	0.0000	0.0000	Up
NUAK2	Non-transduced	Untreated vs. IFNγ/IL1β	234.6206	1.2396	0.1578	7.8565	0.0000	0.0000	Up
RBCK1	Non-transduced	Untreated vs. IFNγ/IL1β	227.2871	1.0249	0.1305	7.8556	0.0000	0.0000	Up
LOC100419583	Non-transduced	Untreated vs. IFNγ/IL1β	64.3825	2.6036	0.3347	7.7782	0.0000	0.0000	Up
CCL20	Non-transduced	Untreated vs. IFNγ/IL1β	264.1183	9.3605	1.2039	7.7754	0.0000	0.0000	Up
CIITA	Non-transduced	Untreated vs. IFNγ/IL1β	131.8554	9.1644	1.1873	7.7187	0.0000	0.0000	Up
SAMHD1	Non-transduced	Untreated vs. IFNγ/IL1β	193.1479	1.3174	0.1715	7.6813	0.0000	0.0000	Up
RGS4	Non-transduced	Untreated vs. IFNγ/IL1β	44.7108	-2.7076	0.3543	-7.6422	0.0000	0.0000	Down

Gene	Cell line	Comparison	baseMean	log2FoldChange	lfcSE	Statistic	p-value	padj	Direction
ST6GAL2	Non-transduced	Untreated vs. IFNγ/IL1β	180.8638	-1.1085	0.1465	-7.5670	0.0000	0.0000	Down
ARNTL2	Non-transduced	Untreated vs. IFNγ/IL1β	340.5390	1.0697	0.1416	7.5549	0.0000	0.0000	Up
CD83	Non-transduced	Untreated vs. IFNγ/IL1β	228.1403	1.1113	0.1483	7.4960	0.0000	0.0000	Up
HIVEP2	Non-transduced	Untreated vs. IFNγ/IL1β	216.4067	1.0897	0.1454	7.4938	0.0000	0.0000	Up
OSR2	Non-transduced	Untreated vs. IFNγ/IL1β	237.1459	-1.1506	0.1535	-7.4942	0.0000	0.0000	Down
BATF2	Non-transduced	Untreated vs. IFNγ/IL1β	81.7551	8.8215	1.1929	7.3948	0.0000	0.0000	Up
NRP1	Non-transduced	Untreated vs. IFNγ/IL1β	199.8826	1.1758	0.1598	7.3574	0.0000	0.0000	Up
CFH	Non-transduced	Untreated vs. IFNγ/IL1β	53.1626	4.5720	0.6322	7.2316	0.0000	0.0000	Up
SGK223	Non-transduced	Untreated vs. IFNγ/IL1β	176.7447	1.2012	0.1663	7.2212	0.0000	0.0000	Up
IL4R	Non-transduced	Untreated vs. IFNγ/IL1β	263.0001	1.0290	0.1426	7.2162	0.0000	0.0000	Up
ITK	Non-transduced	Untreated vs. IFNγ/IL1β	94.1036	8.6067	1.1941	7.2077	0.0000	0.0000	Up
BST2	Non-transduced	Untreated vs. IFNγ/IL1β	44.9042	4.2719	0.5958	7.1700	0.0000	0.0000	Up
DMD	Non-transduced	Untreated vs. IFNγ/IL1β	219.9432	1.0359	0.1447	7.1582	0.0000	0.0000	Up
NFE2L3	Non-transduced	Untreated vs. IFNγ/IL1β	231.7092	1.1615	0.1636	7.0985	0.0000	0.0000	Up
DNAJB4	Non-transduced	Untreated vs. IFNγ/IL1β	155.6385	-1.0944	0.1547	-7.0759	0.0000	0.0000	Down
LGALS3BP	Non-transduced	Untreated vs. IFNγ/IL1β	262.3453	1.0065	0.1423	7.0718	0.0000	0.0000	Up
ARID5A	Non-transduced	Untreated vs. IFNγ/IL1β	207.4449	1.0606	0.1506	7.0425	0.0000	0.0000	Up
ADAMTS5	Non-transduced	Untreated vs. IFNγ/IL1β	218.3167	-1.0459	0.1499	-6.9766	0.0000	0.0000	Down
CTSS	Non-transduced	Untreated vs. IFNγ/IL1β	83.9670	7.1945	1.0386	6.9269	0.0000	0.0000	Up
LOC154761	Non-transduced	Untreated vs. IFNγ/IL1β	48.3701	2.1978	0.3204	6.8586	0.0000	0.0000	Up
GBP4	Non-transduced	Untreated vs. IFNγ/IL1β	50.8447	8.2351	1.2067	6.8246	0.0000	0.0000	Up
SLAMF8	Non-transduced	Untreated vs. IFNγ/IL1β	44.2368	5.9100	0.8688	6.8021	0.0000	0.0000	Up
CXCL11	Non-transduced	Untreated vs. IFNγ/IL1β	76.1308	8.0987	1.1947	6.7790	0.0000	0.0000	Up
MOB3C	Non-transduced	Untreated vs. IFNγ/IL1β	51.4316	2.0836	0.3090	6.7438	0.0000	0.0000	Up
NLRC5	Non-transduced	Untreated vs. IFNγ/IL1β	93.4035	6.9507	1.0354	6.7128	0.0000	0.0000	Up
TRIM38	Non-transduced	Untreated vs. IFNγ/IL1β	145.1085	1.2192	0.1821	6.6957	0.0000	0.0000	Up
TGM2	Non-transduced	Untreated vs. IFNγ/IL1β	69.0524	2.1234	0.3182	6.6736	0.0000	0.0000	Up
KIAA1217	Non-transduced	Untreated vs. IFNγ/IL1β	68.3466	2.0667	0.3104	6.6585	0.0000	0.0000	Up
MX1	Non-transduced	Untreated vs. IFNγ/IL1β	48.8640	2.9452	0.4440	6.6328	0.0000	0.0000	Up
SLC25A28	Non-transduced	Untreated vs. IFNγ/IL1β	134.2056	1.1315	0.1716	6.5954	0.0000	0.0000	Up
TANC1	Non-transduced	Untreated vs. IFNγ/IL1β	309.0109	1.0594	0.1609	6.5843	0.0000	0.0000	Up
APOL4	Non-transduced	Untreated vs. IFNγ/IL1β	53.8488	7.8630	1.1974	6.5665	0.0000	0.0000	Up
IL6	Non-transduced	Untreated vs. IFNγ/IL1β	210.3710	4.3931	0.6698	6.5593	0.0000	0.0000	Up
SH3BP2	Non-transduced	Untreated vs. IFNγ/IL1β	191.0858	1.0060	0.1552	6.4797	0.0000	0.0000	Up
MDGA1	Non-transduced	Untreated vs. IFNγ/IL1β	179.4939	1.0649	0.1651	6.4492	0.0000	0.0000	Up
TCAF2	Non-transduced	Untreated vs. IFNγ/IL1β	146.8043	1.1674	0.1813	6.4387	0.0000	0.0000	Up
SLC25A37	Non-transduced	Untreated vs. IFNγ/IL1β	187.2497	1.0323	0.1621	6.3699	0.0000	0.0000	Up
SCN9A	Non-transduced	Untreated vs. IFNγ/IL1β	148.3896	1.0779	0.1695	6.3580	0.0000	0.0000	Up
ZC3H12C	Non-transduced	Untreated vs. IFNγ/IL1β	116.3872	1.2052	0.1916	6.2897	0.0000	0.0000	Up
ISG15	Non-transduced	Untreated vs. IFNγ/IL1β	129.0865	1.3131	0.2100	6.2528	0.0000	0.0000	Up
CXCL6	Non-transduced	Untreated vs. IFNγ/IL1β	56.5270	6.3137	1.0410	6.0652	0.0000	0.0000	Up
CREBRF	Non-transduced	Untreated vs. IFNγ/IL1β	195.2768	1.0446	0.1727	6.0475	0.0000	0.0000	Up
PRRT2	Non-transduced	Untreated vs. IFNγ/IL1β	42.9484	2.0892	0.3523	5.9297	0.0000	0.0000	Up
GBP5	Non-transduced	Untreated vs. IFNγ/IL1β	50.1979	7.1173	1.2036	5.9132	0.0000	0.0000	Up
C8orf46	Non-transduced	Untreated vs. IFNγ/IL1β	74.4262	1.5023	0.2543	5.9081	0.0000	0.0000	Up
S1PR1	Non-transduced	Untreated vs. IFNγ/IL1β	48.9510	-1.5117	0.2577	-5.8660	0.0000	0.0000	Down
BAK1	Non-transduced	Untreated vs. IFNγ/IL1β	137.9703	1.1186	0.1918	5.8320	0.0000	0.0000	Up
ADAMTSL1	Non-transduced	Untreated vs. IFNγ/IL1β	78.5607	-1.2099	0.2077	-5.8249	0.0000	0.0000	Down
PLAU	Non-transduced	Untreated vs. IFNγ/IL1β	237.1552	1.1117	0.1911	5.8180	0.0000	0.0000	Up
CDKN1C	Non-transduced	Untreated vs. IFNγ/IL1β	1154.7312	-1.0112	0.1739	-5.8143	0.0000	0.0000	Down
CISH	Non-transduced	Untreated vs. IFNγ/IL1β	42.0978	2.1397	0.3714	5.7614	0.0000	0.0000	Up
GBP2	Non-transduced	Untreated vs. IFNγ/IL1β	60.4148	6.8895	1.1959	5.7609	0.0000	0.0000	Up
CDCP1	Non-transduced	Untreated vs. IFNγ/IL1β	131.3198	1.0515	0.1853	5.6732	0.0000	0.0000	Up
FLT3LG	Non-transduced	Untreated vs. IFNγ/IL1β	25.5621	2.7445	0.4852	5.6564	0.0000	0.0000	Up
IFITM1	Non-transduced	Untreated vs. IFNγ/IL1β	39.6581	3.7112	0.6561	5.6567	0.0000	0.0000	Up
TNC	Non-transduced	Untreated vs. IFNγ/IL1β	740.3523	1.1880	0.2104	5.6473	0.0000	0.0000	Up
TRAFD1	Non-transduced	Untreated vs. IFNγ/IL1β	103.1478	1.1481	0.2040	5.6285	0.0000	0.0000	Up
ISG20	Non-transduced	Untreated vs. IFNγ/IL1β	64.1414	2.0200	0.3593	5.6223	0.0000	0.0000	Up
XIRP1	Non-transduced	Untreated vs. IFNγ/IL1β	34.9002	6.7733	1.2080	5.6071	0.0000	0.0000	Up
CXCL9	Non-transduced	Untreated vs. IFNγ/IL1β	21.4658	7.0464	1.2595	5.5947	0.0000	0.0000	Up
ELF3	Non-transduced	Untreated vs. IFNγ/IL1β	38.8246	4.4061	0.7946	5.5453	0.0000	0.0000	Up
USP43	Non-transduced	Untreated vs. IFNγ/IL1β	108.4040	1.2955	0.2357	5.4954	0.0000	0.0000	Up
FAS	Non-transduced	Untreated vs. IFNγ/IL1β	38.3345	2.3013	0.4206	5.4718	0.0000	0.0000	Up
IFI6	Non-transduced	Untreated vs. IFNγ/IL1β	159.3681	1.9608	0.3613	5.4266	0.0000	0.0000	Up
HDAC9	Non-transduced	Untreated vs. IFNγ/IL1β	59.4177	1.6072	0.2968	5.4151	0.0000	0.0000	Up
LINC00312	Non-transduced	Untreated vs. IFNγ/IL1β	141.2250	1.3174	0.2440	5.3993	0.0000	0.0000	Up
RNF19B	Non-transduced	Untreated vs. IFNγ/IL1β	151.0534	1.2043	0.2242	5.3722	0.0000	0.0000	Up
BTN3A3	Non-transduced	Untreated vs. IFNγ/IL1β	38.9327	2.5420	0.4757	5.3441	0.0000	0.0000	Up
NOCT	Non-transduced	Untreated vs. IFNγ/IL1β	69.0613	1.3604	0.2557	5.3213	0.0000	0.0000	Up
NLRP3	Non-transduced	Untreated vs. IFNγ/IL1β	40.3348	2.0268	0.3866	5.2433	0.0000	0.0000	Up
FLT1	Non-transduced	Untreated vs. IFNγ/IL1β	21.9174	3.1844	0.6119	5.2041	0.0000	0.0000	Up
APOL3	Non-transduced	Untreated vs. IFNγ/IL1β	14.4057	6.3780	1.2392	5.1467	0.0000	0.0000	Up
TDRD7	Non-transduced	Untreated vs. IFNγ/IL1β	36.4303	1.8280	0.3563	5.1299	0.0000	0.0000	Up
CD74	Non-transduced	Untreated vs. IFNγ/IL1β	19.0303	6.3890	1.2493	5.1140	0.0000	0.0000	Up
PDZK1IP1	Non-transduced	Untreated vs. IFNγ/IL1β	12.3959	6.5051	1.2729	5.1105	0.0000	0.0000	Up
ANXA2R	Non-transduced	Untreated vs. IFNγ/IL1β	49.0230	1.7737	0.3487	5.0861	0.0000	0.0000	Up
CBR3	Non-transduced	Untreated vs. IFNγ/IL1β	97.0644	1.0833	0.2149	5.0406	0.0000	0.0000	Up
FIGN	Non-transduced	Untreated vs. IFNγ/IL1β	49.1910	-1.3027	0.2587	-5.0361	0.0000	0.0000	Down
LINC00623	Non-transduced	Untreated vs. IFNγ/IL1β	14.8865	3.1928	0.6380	5.0047	0.0000	0.0000	Up
VCAM1	Non-transduced	Untreated vs. IFNγ/IL1β	14.4034	4.6797	0.9437	4.9590	0.0000	0.0000	Up
TNF	Non-transduced	Untreated vs. IFNγ/IL1β	10.5056	6.2157	1.2683	4.9009	0.0000	0.0000	Up
SLC2A6	Non-transduced	Untreated vs. IFNγ/IL1β	88.2271	1.1224	0.2294	4.8928	0.0000	0.0000	Up
GSAP	Non-transduced	Untreated vs. IFNγ/IL1β	19.3570	2.6441	0.5475	4.8299	0.0000	0.0000	Up
SNAI2	Non-transduced	Untreated vs. IFNγ/IL1β	506.8612	1.0329	0.2144	4.8181	0.0000	0.0000	Up
HAS3	Non-transduced	Untreated vs. IFNγ/IL1β	73.3930	1.1152	0.2337	4.7717	0.0000	0.0000	Up
PLEKHA4	Non-transduced	Untreated vs. IFNγ/IL1β	50.7855	1.2912	0.2708	4.7688	0.0000	0.0000	Up
OAS2	Non-transduced	Untreated vs. IFNγ/IL1β	23.5984	5.6281	1.1906	4.7272	0.0000	0.0001	Up
REC8	Non-transduced	Untreated vs. IFNγ/IL1β	27.9235	2.2975	0.4875	4.7128	0.0000	0.0001	Up
SAA2	Non-transduced	Untreated vs. IFNγ/IL1β	27.6438	5.7667	1.2287	4.6933	0.0000	0.0001	Up
KLF13	Non-transduced	Untreated vs. IFNγ/IL1β	76.6752	1.0615	0.2264	4.6877	0.0000	0.0001	Up
MAFB	Non-transduced	Untreated vs. IFNγ/IL1β	25.5464	2.5540	0.5450	4.6860	0.0000	0.0001	Up
CD70	Non-transduced	Untreated vs. IFNγ/IL1β	139.1203	1.0201	0.2180	4.6788	0.0000	0.0001	Up
C1QTNF1	Non-transduced	Untreated vs. IFNγ/IL1β	24.8840	5.6704	1.2212	4.6433	0.0000	0.0001	Up
RHEBL1	Non-transduced	Untreated vs. IFNγ/IL1β	107.1586	1.0269	0.2237	4.5897	0.0000	0.0001	Up
IFI27	Non-transduced	Untreated vs. IFNγ/IL1β	29.4840	2.5639	0.5613	4.5678	0.0000	0.0001	Up
SETBP1	Non-transduced	Untreated vs. IFNγ/IL1β	50.9396	1.3227	0.2906	4.5508	0.0000	0.0001	Up
C19orf66	Non-transduced	Untreated vs. IFNγ/IL1β	42.8827	1.3895	0.3076	4.5178	0.0000	0.0001	Up
IRF7	Non-transduced	Untreated vs. IFNγ/IL1β	66.5785	1.0899	0.2419	4.5054	0.0000	0.0001	Up
IFI44	Non-transduced	Untreated vs. IFNγ/IL1β	29.2324	2.8554	0.6342	4.5026	0.0000	0.0001	Up
SLC15A3	Non-transduced	Untreated vs. IFNγ/IL1β	21.4198	4.8447	1.0834	4.4717	0.0000	0.0002	Up
NAPB	Non-transduced	Untreated vs. IFNγ/IL1β	62.4078	1.0760	0.2407	4.4709	0.0000	0.0002	Up
TRAF1	Non-transduced	Untreated vs. IFNγ/IL1β	11.6483	3.1838	0.7132	4.4642	0.0000	0.0002	Up
ICAM1	Non-transduced	Untreated vs. IFNγ/IL1β	15.2021	5.5147	1.2379	4.4547	0.0000	0.0002	Up
CCDC125	Non-transduced	Untreated vs. IFNγ/IL1β	82.2915	1.0293	0.2320	4.4370	0.0000	0.0002	Up

Gene	Cell line	Comparison	baseMean	log2FoldChange	lfcSE	Statistic	p-value	padj	Direction
MAP3K8	Non-transduced	Untreated vs. IFNγ/IL1β	15.7382	3.6185	0.8164	4.4320	0.0000	0.0002	Up
TNFSF10	Non-transduced	Untreated vs. IFNγ/IL1β	14.3998	5.5401	1.2589	4.4008	0.0000	0.0002	Up
KCTD14	Non-transduced	Untreated vs. IFNγ/IL1β	45.1653	7.3835	1.7268	4.2759	0.0000	0.0004	Up
SIM1	Non-transduced	Untreated vs. IFNγ/IL1β	39.8334	1.5534	0.3633	4.2754	0.0000	0.0004	Up
WNT7B	Non-transduced	Untreated vs. IFNγ/IL1β	12.9244	-2.2361	0.5246	-4.2621	0.0000	0.0004	Down
TMEM173	Non-transduced	Untreated vs. IFNγ/IL1β	55.2632	1.0824	0.2558	4.2319	0.0000	0.0005	Up
DUSP10	Non-transduced	Untreated vs. IFNγ/IL1β	48.4369	1.2936	0.3061	4.2268	0.0000	0.0005	Up
SPSB1	Non-transduced	Untreated vs. IFNγ/IL1β	44.6562	1.3349	0.3169	4.2125	0.0000	0.0005	Up
CTSO	Non-transduced	Untreated vs. IFNγ/IL1β	51.3638	1.3101	0.3117	4.2030	0.0000	0.0005	Up
CD34	Non-transduced	Untreated vs. IFNγ/IL1β	31.0346	1.7046	0.4059	4.1992	0.0000	0.0005	Up
C10orf10	Non-transduced	Untreated vs. IFNγ/IL1β	23.9024	1.9607	0.4700	4.1717	0.0000	0.0006	Up
MYD88	Non-transduced	Untreated vs. IFNγ/IL1β	46.8298	1.2255	0.2945	4.1608	0.0000	0.0006	Up
TEX19	Non-transduced	Untreated vs. IFNγ/IL1β	49.6278	1.3445	0.3241	4.1487	0.0000	0.0006	Up
TRIM55	Non-transduced	Untreated vs. IFNγ/IL1β	18.6986	-1.8298	0.4410	-4.1488	0.0000	0.0006	Down
TBX21	Non-transduced	Untreated vs. IFNγ/IL1β	7.9719	5.3621	1.2977	4.1320	0.0000	0.0007	Up
RGPD6	Non-transduced	Untreated vs. IFNγ/IL1β	4.7591	27.8573	6.7608	4.1204	0.0000	0.0007	Up
KLF4	Non-transduced	Untreated vs. IFNγ/IL1β	36.1976	1.7117	0.4155	4.1196	0.0000	0.0007	Up
PPAP2B	Non-transduced	Untreated vs. IFNγ/IL1β	81.8155	1.3587	0.3298	4.1195	0.0000	0.0007	Up
BANCR	Non-transduced	Untreated vs. IFNγ/IL1β	12.8834	5.2684	1.2832	4.1056	0.0000	0.0007	Up
CASP4	Non-transduced	Untreated vs. IFNγ/IL1β	18.6234	2.8137	0.7095	3.9660	0.0001	0.0013	Up
STBD1	Non-transduced	Untreated vs. IFNγ/IL1β	40.7847	1.3151	0.3330	3.9490	0.0001	0.0014	Up
NIPAL4	Non-transduced	Untreated vs. IFNγ/IL1β	42.5678	1.1641	0.2956	3.9379	0.0001	0.0014	Up
IFI44L	Non-transduced	Untreated vs. IFNγ/IL1β	8.8447	5.1419	1.3108	3.9228	0.0001	0.0015	Up
MMP3	Non-transduced	Untreated vs. IFNγ/IL1β	16.1315	3.3702	0.8653	3.8947	0.0001	0.0017	Up
CLIC5	Non-transduced	Untreated vs. IFNγ/IL1β	13.1540	2.9802	0.7658	3.8914	0.0001	0.0017	Up
ROBO4	Non-transduced	Untreated vs. IFNγ/IL1β	15.0735	2.1480	0.5702	3.7674	0.0002	0.0027	Up
SLC12A7	Non-transduced	Untreated vs. IFNγ/IL1β	10.8228	4.3485	1.1707	3.7146	0.0002	0.0033	Up
HLA-DRA	Non-transduced	Untreated vs. IFNγ/IL1β	12.7895	4.6637	1.2609	3.6988	0.0002	0.0035	Up
NFKB2	Non-transduced	Untreated vs. IFNγ/IL1β	20.0689	1.9320	0.5267	3.6685	0.0002	0.0039	Up
BDKRB1	Non-transduced	Untreated vs. IFNγ/IL1β	11.6771	3.1372	0.8579	3.6569	0.0003	0.0040	Up
TNFRSF1B	Non-transduced	Untreated vs. IFNγ/IL1β	13.4818	4.1963	1.1517	3.6434	0.0003	0.0042	Up
TRPC4	Non-transduced	Untreated vs. IFNγ/IL1β	34.4902	-1.1990	0.3310	-3.6219	0.0003	0.0045	Down
MX2	Non-transduced	Untreated vs. IFNγ/IL1β	4.4174	5.0068	1.3830	3.6203	0.0003	0.0045	Up
S100A3	Non-transduced	Untreated vs. IFNγ/IL1β	24.5496	1.5750	0.4351	3.6196	0.0003	0.0045	Up
SLFN5	Non-transduced	Untreated vs. IFNγ/IL1β	27.6494	1.3111	0.3636	3.6054	0.0003	0.0047	Up
CYP26B1	Non-transduced	Untreated vs. IFNγ/IL1β	9.4412	-2.5715	0.7134	-3.6046	0.0003	0.0048	Down
ITGB6	Non-transduced	Untreated vs. IFNγ/IL1β	9.6708	3.4980	0.9747	3.5887	0.0003	0.0050	Up
STAT5A	Non-transduced	Untreated vs. IFNγ/IL1β	10.5904	3.4683	0.9708	3.5727	0.0004	0.0053	Up
ICOSLG	Non-transduced	Untreated vs. IFNγ/IL1β	29.6039	1.3492	0.3779	3.5703	0.0004	0.0053	Up
PLSCR4	Non-transduced	Untreated vs. IFNγ/IL1β	22.3399	1.8120	0.5082	3.5655	0.0004	0.0054	Up
SLC4A4	Non-transduced	Untreated vs. IFNγ/IL1β	33.6943	-1.2278	0.3443	-3.5657	0.0004	0.0054	Down
VAMP5	Non-transduced	Untreated vs. IFNγ/IL1β	22.1806	1.6391	0.4616	3.5507	0.0004	0.0056	Up
KIAA1644	Non-transduced	Untreated vs. IFNγ/IL1β	42.7071	1.2042	0.3407	3.5350	0.0004	0.0059	Up
MUC1	Non-transduced	Untreated vs. IFNγ/IL1β	37.1448	1.1661	0.3307	3.5261	0.0004	0.0061	Up
NCKAP5	Non-transduced	Untreated vs. IFNγ/IL1β	52.2899	2.8072	0.8005	3.5069	0.0005	0.0065	Up
SAA1	Non-transduced	Untreated vs. IFNγ/IL1β	11.2584	3.9822	1.1434	3.4828	0.0005	0.0071	Up
AMER1	Non-transduced	Untreated vs. IFNγ/IL1β	35.2880	1.1362	0.3274	3.4709	0.0005	0.0074	Up
PHF11	Non-transduced	Untreated vs. IFNγ/IL1β	33.3470	1.3069	0.3804	3.4353	0.0006	0.0082	Up
GFPT2	Non-transduced	Untreated vs. IFNγ/IL1β	32.7279	1.2249	0.3582	3.4194	0.0006	0.0087	Up
LIF	Non-transduced	Untreated vs. IFNγ/IL1β	63.0252	1.1499	0.3369	3.4133	0.0006	0.0089	Up
DPY19L2	Non-transduced	Untreated vs. IFNγ/IL1β	41.4965	1.2191	0.3597	3.3893	0.0007	0.0095	Up
PDZD2	Non-transduced	Untreated vs. IFNγ/IL1β	37.1459	1.0164	0.3001	3.3870	0.0007	0.0096	Up
MLKL	Non-transduced	Untreated vs. IFNγ/IL1β	22.2650	1.5959	0.4713	3.3860	0.0007	0.0096	Up
TLR3	Non-transduced	Untreated vs. IFNγ/IL1β	18.5547	2.1539	0.6439	3.3450	0.0008	0.0110	Up
LOC101927204	Non-transduced	Untreated vs. IFNγ/IL1β	36.1047	1.1791	0.3528	3.3420	0.0008	0.0111	Up
SERPING1	Non-transduced	Untreated vs. IFNγ/IL1β	13.7581	2.5109	0.7600	3.3040	0.0010	0.0125	Up
SCARF1	Non-transduced	Untreated vs. IFNγ/IL1β	10.1398	2.3635	0.7166	3.2981	0.0010	0.0127	Up
NOS1AP	Non-transduced	Untreated vs. IFNγ/IL1β	4.2623	4.6939	1.4383	3.2635	0.0011	0.0141	Up
CRHBP	Non-transduced	Untreated vs. IFNγ/IL1β	8.6280	-2.0771	0.6448	-3.2213	0.0013	0.0160	Down
TMEM191C	Non-transduced	Untreated vs. IFNγ/IL1β	4.1563	-4.8228	1.4981	-3.2192	0.0013	0.0160	Down
RBM47	Non-transduced	Untreated vs. IFNγ/IL1β	11.4821	2.7464	0.8533	3.2186	0.0013	0.0160	Up
GJD3	Non-transduced	Untreated vs. IFNγ/IL1β	4.8899	4.4246	1.3858	3.1928	0.0014	0.0173	Up
TMEM229B	Non-transduced	Untreated vs. IFNγ/IL1β	6.7472	4.1611	1.3140	3.1667	0.0015	0.0186	Up
MMP25-AS1	Non-transduced	Untreated vs. IFNγ/IL1β	18.0490	1.7016	0.5375	3.1659	0.0015	0.0186	Up
PRDM1	Non-transduced	Untreated vs. IFNγ/IL1β	9.8086	4.1410	1.3182	3.1414	0.0017	0.0200	Up
RASGRP3	Non-transduced	Untreated vs. IFNγ/IL1β	18.0722	1.4834	0.4724	3.1403	0.0017	0.0200	Up
OAS1	Non-transduced	Untreated vs. IFNγ/IL1β	9.5779	3.1630	1.0212	3.0972	0.0020	0.0228	Up
ANKRD20A1	Non-transduced	Untreated vs. IFNγ/IL1β	4.3271	20.8835	6.7528	3.0925	0.0020	0.0230	Up
GIMAP2	Non-transduced	Untreated vs. IFNγ/IL1β	4.6420	4.2727	1.3825	3.0905	0.0020	0.0232	Up
IKBKE	Non-transduced	Untreated vs. IFNγ/IL1β	35.9759	1.0285	0.3336	3.0830	0.0020	0.0236	Up
NEK5	Non-transduced	Untreated vs. IFNγ/IL1β	16.0186	1.6558	0.5394	3.0695	0.0021	0.0245	Up
ENOX1	Non-transduced	Untreated vs. IFNγ/IL1β	38.9068	1.0011	0.3282	3.0502	0.0023	0.0257	Up
RTP4	Non-transduced	Untreated vs. IFNγ/IL1β	4.2602	4.3564	1.4292	3.0480	0.0023	0.0259	Up
TET1	Non-transduced	Untreated vs. IFNγ/IL1β	35.4007	-1.0547	0.3470	-3.0392	0.0024	0.0265	Down
LOC101928674	Non-transduced	Untreated vs. IFNγ/IL1β	8.3274	2.2965	0.7558	3.0385	0.0024	0.0265	Up
CASP1	Non-transduced	Untreated vs. IFNγ/IL1β	7.7081	4.0958	1.3558	3.0211	0.0025	0.0278	Up
SELPLG	Non-transduced	Untreated vs. IFNγ/IL1β	9.9617	2.5630	0.8514	3.0103	0.0026	0.0286	Up
C11orf91	Non-transduced	Untreated vs. IFNγ/IL1β	53.4012	1.1935	0.3969	3.0073	0.0026	0.0288	Up
IRAK2	Non-transduced	Untreated vs. IFNγ/IL1β	28.0312	1.2390	0.4164	2.9753	0.0029	0.0316	Up
SPTLC3	Non-transduced	Untreated vs. IFNγ/IL1β	45.2938	1.4478	0.4883	2.9648	0.0030	0.0325	Up
CPNE5	Non-transduced	Untreated vs. IFNγ/IL1β	9.1323	1.8714	0.6318	2.9620	0.0031	0.0327	Up
TESK2	Non-transduced	Untreated vs. IFNγ/IL1β	23.9305	1.1812	0.4002	2.9517	0.0032	0.0336	Up
ELOVL7	Non-transduced	Untreated vs. IFNγ/IL1β	17.8255	1.5620	0.5326	2.9328	0.0034	0.0354	Up
FIBCD1	Non-transduced	Untreated vs. IFNγ/IL1β	19.8047	-1.2848	0.4396	-2.9227	0.0035	0.0362	Down
CPEB3	Non-transduced	Untreated vs. IFNγ/IL1β	31.1919	1.1372	0.3892	2.9218	0.0035	0.0363	Up
USP30-AS1	Non-transduced	Untreated vs. IFNγ/IL1β	5.3868	4.0164	1.3747	2.9216	0.0035	0.0363	Up
FAM86C1	Non-transduced	Untreated vs. IFNγ/IL1β	29.7058	-1.0287	0.3530	-2.9143	0.0036	0.0369	Down
IL7	Non-transduced	Untreated vs. IFNγ/IL1β	4.3520	4.1531	1.4277	2.9091	0.0036	0.0375	Up
APOC1	Non-transduced	Untreated vs. IFNγ/IL1β	18.0796	-1.3308	0.4600	-2.8932	0.0038	0.0390	Down
IGIP	Non-transduced	Untreated vs. IFNγ/IL1β	21.9219	-1.0767	0.3724	-2.8915	0.0038	0.0392	Down
HLA-C	Non-transduced	Untreated vs. IFNγ/IL1β	27.1556	1.1105	0.3844	2.8887	0.0039	0.0395	Up
GLP2R	Non-transduced	Untreated vs. IFNγ/IL1β	6.5762	3.9580	1.3751	2.8784	0.0040	0.0404	Up
TMEFF2	Non-transduced	Untreated vs. IFNγ/IL1β	17.1757	1.5848	0.5508	2.8770	0.0040	0.0406	Up
ELOVL2-AS1	Non-transduced	Untreated vs. IFNγ/IL1β	23.6483	1.1378	0.3979	2.8598	0.0042	0.0422	Up
LOC105274304	Non-transduced	Untreated vs. IFNγ/IL1β	14.8033	-1.3866	0.4849	-2.8598	0.0042	0.0422	Down
ZNF469	Non-transduced	Untreated vs. IFNγ/IL1β	11.7973	1.5919	0.5569	2.8583	0.0043	0.0424	Up
GAS1	Non-transduced	Untreated vs. IFNγ/IL1β	37.4107	1.0307	0.3616	2.8505	0.0044	0.0431	Up
TNFRSF14	Non-transduced	Untreated vs. IFNγ/IL1β	9.8473	1.8331	0.6489	2.8248	0.0047	0.0459	Up
CARD6	Non-transduced	Untreated vs. IFNγ/IL1β	9.9191	2.1838	0.7815	2.7943	0.0052	0.0496	Up
CSGALNACT1	Non-transduced	Untreated vs. IFNγ/IL1β	88.8010	1.2475	0.4493	2.7766	0.0055	0.0519	Up
HIPK1-AS1	Non-transduced	Untreated vs. IFNγ/IL1β	9.7679	1.7442	0.6297	2.7700	0.0056	0.0527	Up
ZBED2	Non-transduced	Untreated vs. IFNγ/IL1β	5.8831	-2.0041	0.7266	-2.7583	0.0058	0.0541	Down
BIK	Non-transduced	Untreated vs. IFNγ/IL1β	11.1692	1.6746	0.6100	2.7452	0.0060	0.0560	Up
CAND2	Non-transduced	Untreated vs. IFNγ/IL1β	21.8520	1.1867	0.4333	2.7391	0.0062	0.0569	Up

Gene	Cell line	Comparison	baseMean	log2FoldChange	lfcSE	Statistic	p-value	padj	Direction
ZDHHC14	Non-transduced	Untreated vs. IFNγ/IL1β	17.4349	1.5337	0.5623	2.7277	0.0064	0.0584	Up
APOM	Non-transduced	Untreated vs. IFNγ/IL1β	8.8662	-2.0253	0.7472	-2.7103	0.0067	0.0610	Down
PPP2R3B	Non-transduced	Untreated vs. IFNγ/IL1β	25.5450	-1.0757	0.4000	-2.6890	0.0072	0.0641	Down
LOC100499489	Non-transduced	Untreated vs. IFNγ/IL1β	19.0474	1.1214	0.4206	2.6661	0.0077	0.0677	Up
RUNX3	Non-transduced	Untreated vs. IFNγ/IL1β	19.2637	1.4359	0.5417	2.6510	0.0080	0.0702	Up
CDH6	Non-transduced	Untreated vs. IFNγ/IL1β	10.1759	1.7209	0.6566	2.6210	0.0088	0.0752	Up
ZNF577	Non-transduced	Untreated vs. IFNγ/IL1β	11.4440	-1.3337	0.5095	-2.6176	0.0089	0.0758	Down
KDR	Non-transduced	Untreated vs. IFNγ/IL1β	5.9576	3.1001	1.1999	2.5836	0.0098	0.0819	Up
PALMD	Non-transduced	Untreated vs. IFNγ/IL1β	4.9086	-2.0806	0.8070	-2.5782	0.0099	0.0830	Down
SPDYE8P	Non-transduced	Untreated vs. IFNγ/IL1β	15.5263	1.7034	0.6608	2.5778	0.0099	0.0830	Up
CHMP4C	Non-transduced	Untreated vs. IFNγ/IL1β	4.3474	-3.6354	1.4106	-2.5771	0.0100	0.0831	Down
LGALS9	Non-transduced	Untreated vs. IFNγ/IL1β	10.1656	2.0630	0.8021	2.5719	0.0101	0.0841	Up
SERPINB2	Non-transduced	Untreated vs. IFNγ/IL1β	7.2384	3.3416	1.3085	2.5537	0.0107	0.0876	Up
CLIP2	Non-transduced	Untreated vs. IFNγ/IL1β	5.5886	1.9912	0.7882	2.5263	0.0115	0.0929	Up
HERC6	Non-transduced	Untreated vs. IFNγ/IL1β	9.4482	2.1320	0.8467	2.5179	0.0118	0.0946	Up
PKIA	Non-transduced	Untreated vs. IFNγ/IL1β	4.7055	-2.5663	1.0201	-2.5157	0.0119	0.0950	Down
MPND	Non-transduced	Untreated vs. IFNγ/IL1β	11.0006	-1.3808	0.5505	-2.5080	0.0121	0.0966	Down
PLEKHA7	Non-transduced	Untreated vs. IFNγ/IL1β	11.5946	-1.4677	0.5861	-2.5042	0.0123	0.0972	Down
Figure 29a									
NPTX1	Non-transduced	IFNγ/IL1β vs. IFNγ/IL1β + LB	1334.7631	3.2626	0.1600	20.3924	0.0000	0.0000	Up
CDKN1C	Non-transduced	IFNγ/IL1β vs. IFNγ/IL1β + LB	1154.7312	3.2175	0.1689	19.0544	0.0000	0.0000	Up
TM4SF1	Non-transduced	IFNγ/IL1β vs. IFNγ/IL1β + LB	1253.7217	2.2998	0.1229	18.7178	0.0000	0.0000	Up
TFPI2	Non-transduced	IFNγ/IL1β vs. IFNγ/IL1β + LB	1461.2215	1.6146	0.1036	15.5805	0.0000	0.0000	Up
AKAP12	Non-transduced	IFNγ/IL1β vs. IFNγ/IL1β + LB	3243.4861	1.3029	0.0925	14.0790	0.0000	0.0000	Up
IL11	Non-transduced	IFNγ/IL1β vs. IFNγ/IL1β + LB	1307.1058	1.0119	0.0801	12.6277	0.0000	0.0000	Up
IGFBP4	Non-transduced	IFNγ/IL1β vs. IFNγ/IL1β + LB	245.4927	1.7724	0.1433	12.3688	0.0000	0.0000	Up
EPAS1	Non-transduced	IFNγ/IL1β vs. IFNγ/IL1β + LB	1164.3497	1.1154	0.0907	12.2912	0.0000	0.0000	Up
GPRC5A	Non-transduced	IFNγ/IL1β vs. IFNγ/IL1β + LB	1020.0468	1.3069	0.1107	11.8011	0.0000	0.0000	Up
CSGALNACT1	Non-transduced	IFNγ/IL1β vs. IFNγ/IL1β + LB	88.8010	3.5611	0.3048	11.6823	0.0000	0.0000	Up
SMOC1	Non-transduced	IFNγ/IL1β vs. IFNγ/IL1β + LB	86.2921	3.3834	0.3352	10.0927	0.0000	0.0000	Up
GABARAPL1	Non-transduced	IFNγ/IL1β vs. IFNγ/IL1β + LB	209.8672	1.4766	0.1496	9.8699	0.0000	0.0000	Up
CD24	Non-transduced	IFNγ/IL1β vs. IFNγ/IL1β + LB	155.3958	1.5031	0.1714	8.7701	0.0000	0.0000	Up
FAM49A	Non-transduced	IFNγ/IL1β vs. IFNγ/IL1β + LB	88.1571	1.8219	0.2150	8.4732	0.0000	0.0000	Up
PID1	Non-transduced	IFNγ/IL1β vs. IFNγ/IL1β + LB	95.9266	1.4765	0.1857	7.9511	0.0000	0.0000	Up
IDO1	Non-transduced	IFNγ/IL1β vs. IFNγ/IL1β + LB	464.5613	1.1299	0.1424	7.9335	0.0000	0.0000	Up
NHS	Non-transduced	IFNγ/IL1β vs. IFNγ/IL1β + LB	43.7281	2.8991	0.3684	7.8684	0.0000	0.0000	Up
ADARB1	Non-transduced	IFNγ/IL1β vs. IFNγ/IL1β + LB	131.8997	1.3275	0.1728	7.6829	0.0000	0.0000	Up
CHMP1B	Non-transduced	IFNγ/IL1β vs. IFNγ/IL1β + LB	296.9243	1.0513	0.1369	7.6774	0.0000	0.0000	Up
STC1	Non-transduced	IFNγ/IL1β vs. IFNγ/IL1β + LB	97.7202	1.6377	0.2159	7.5850	0.0000	0.0000	Up
CRISPLD2	Non-transduced	IFNγ/IL1β vs. IFNγ/IL1β + LB	92.2008	1.6657	0.2270	7.3376	0.0000	0.0000	Up
KRTAP2-3	Non-transduced	IFNγ/IL1β vs. IFNγ/IL1β + LB	225.3629	-1.3060	0.1801	-7.2526	0.0000	0.0000	Down
NR4A3	Non-transduced	IFNγ/IL1β vs. IFNγ/IL1β + LB	28.2325	3.1143	0.4331	7.1903	0.0000	0.0000	Up
GREM1	Non-transduced	IFNγ/IL1β vs. IFNγ/IL1β + LB	909.7217	1.2151	0.1721	7.0615	0.0000	0.0000	Up
NCKAP5	Non-transduced	IFNγ/IL1β vs. IFNγ/IL1β + LB	52.2899	2.6130	0.3712	7.0389	0.0000	0.0000	Up
PTGES	Non-transduced	IFNγ/IL1β vs. IFNγ/IL1β + LB	23.0019	3.1218	0.4562	6.8436	0.0000	0.0000	Up
CREM	Non-transduced	IFNγ/IL1β vs. IFNγ/IL1β + LB	79.4316	1.6987	0.2518	6.7461	0.0000	0.0000	Up
FAM167A	Non-transduced	IFNγ/IL1β vs. IFNγ/IL1β + LB	73.9400	1.6961	0.2591	6.5468	0.0000	0.0000	Up
WDR66	Non-transduced	IFNγ/IL1β vs. IFNγ/IL1β + LB	134.5781	1.4355	0.2202	6.5201	0.0000	0.0000	Up
SPTLC3	Non-transduced	IFNγ/IL1β vs. IFNγ/IL1β + LB	45.2938	2.2298	0.3464	6.4374	0.0000	0.0000	Up
PDE7B	Non-transduced	IFNγ/IL1β vs. IFNγ/IL1β + LB	21.5652	3.8412	0.6016	6.3844	0.0000	0.0000	Up
DIO2	Non-transduced	IFNγ/IL1β vs. IFNγ/IL1β + LB	37.4922	2.2955	0.3644	6.2990	0.0000	0.0000	Up
PDE4D	Non-transduced	IFNγ/IL1β vs. IFNγ/IL1β + LB	195.3763	1.2618	0.2031	6.2130	0.0000	0.0000	Up
PDE3A	Non-transduced	IFNγ/IL1β vs. IFNγ/IL1β + LB	22.5278	3.4277	0.5643	6.0739	0.0000	0.0000	Up
IGFN1	Non-transduced	IFNγ/IL1β vs. IFNγ/IL1β + LB	68.1654	1.4169	0.2368	5.9836	0.0000	0.0000	Up
LTB	Non-transduced	IFNγ/IL1β vs. IFNγ/IL1β + LB	44.9479	-1.7387	0.2998	-5.7990	0.0000	0.0000	Down
STAMBPL1	Non-transduced	IFNγ/IL1β vs. IFNγ/IL1β + LB	113.6935	1.0225	0.1763	5.8008	0.0000	0.0000	Up
GPRC5C	Non-transduced	IFNγ/IL1β vs. IFNγ/IL1β + LB	44.3908	1.7278	0.3038	5.6881	0.0000	0.0000	Up
GBP2	Non-transduced	IFNγ/IL1β vs. IFNγ/IL1β + LB	60.4148	1.2419	0.2279	5.4499	0.0000	0.0000	Up
AVPI1	Non-transduced	IFNγ/IL1β vs. IFNγ/IL1β + LB	69.8208	1.2392	0.2292	5.4066	0.0000	0.0000	Up
LINC00473	Non-transduced	IFNγ/IL1β vs. IFNγ/IL1β + LB	18.7203	4.5378	0.8506	5.3350	0.0000	0.0000	Up
CCL20	Non-transduced	IFNγ/IL1β vs. IFNγ/IL1β + LB	264.1183	1.2977	0.2547	5.0959	0.0000	0.0000	Up
PPAP2B	Non-transduced	IFNγ/IL1β vs. IFNγ/IL1β + LB	81.8155	1.2635	0.2528	4.9991	0.0000	0.0001	Up
SLC7A8	Non-transduced	IFNγ/IL1β vs. IFNγ/IL1β + LB	8.2984	4.1678	0.8427	4.9460	0.0000	0.0001	Up
MAP2K6	Non-transduced	IFNγ/IL1β vs. IFNγ/IL1β + LB	52.5561	1.4022	0.2852	4.9170	0.0000	0.0001	Up
EPHA5	Non-transduced	IFNγ/IL1β vs. IFNγ/IL1β + LB	37.8641	1.6000	0.3399	4.7078	0.0000	0.0002	Up
VCAM1	Non-transduced	IFNγ/IL1β vs. IFNγ/IL1β + LB	14.4034	-2.5808	0.5535	-4.6626	0.0000	0.0003	Down
NFATC2	Non-transduced	IFNγ/IL1β vs. IFNγ/IL1β + LB	17.1329	2.0876	0.4505	4.6338	0.0000	0.0003	Up
NR4A2	Non-transduced	IFNγ/IL1β vs. IFNγ/IL1β + LB	12.2332	3.1227	0.6916	4.5153	0.0000	0.0005	Up
LRRC4C	Non-transduced	IFNγ/IL1β vs. IFNγ/IL1β + LB	40.6439	1.6128	0.3635	4.4362	0.0000	0.0007	Up
C11orf96	Non-transduced	IFNγ/IL1β vs. IFNγ/IL1β + LB	13.1747	2.2456	0.5097	4.4059	0.0000	0.0008	Up
EBF1	Non-transduced	IFNγ/IL1β vs. IFNγ/IL1β + LB	39.9057	1.3251	0.3020	4.3871	0.0000	0.0009	Up
LINC00673	Non-transduced	IFNγ/IL1β vs. IFNγ/IL1β + LB	34.8490	1.3557	0.3165	4.2833	0.0000	0.0014	Up
PLXNA2	Non-transduced	IFNγ/IL1β vs. IFNγ/IL1β + LB	34.5028	-1.6155	0.3848	-4.1985	0.0000	0.0019	Down
CITED4	Non-transduced	IFNγ/IL1β vs. IFNγ/IL1β + LB	17.7002	1.9692	0.4706	4.1841	0.0000	0.0020	Up
SLC28A3	Non-transduced	IFNγ/IL1β vs. IFNγ/IL1β + LB	45.4368	-1.1392	0.2818	-4.0423	0.0001	0.0034	Down
C8orf31	Non-transduced	IFNγ/IL1β vs. IFNγ/IL1β + LB	13.4365	2.1436	0.5367	3.9938	0.0001	0.0041	Up
ISG20	Non-transduced	IFNγ/IL1β vs. IFNγ/IL1β + LB	64.1414	1.0008	0.2551	3.9225	0.0001	0.0050	Up
TRPC4	Non-transduced	IFNγ/IL1β vs. IFNγ/IL1β + LB	34.4902	1.2951	0.3315	3.9071	0.0001	0.0052	Up
LYPD1	Non-transduced	IFNγ/IL1β vs. IFNγ/IL1β + LB	38.2942	1.7889	0.4643	3.8530	0.0001	0.0061	Up
SERPINB7	Non-transduced	IFNγ/IL1β vs. IFNγ/IL1β + LB	31.9771	-1.5479	0.4074	-3.7991	0.0001	0.0074	Down
GNG4	Non-transduced	IFNγ/IL1β vs. IFNγ/IL1β + LB	26.9602	1.3582	0.3632	3.7400	0.0002	0.0088	Up
PDGFB	Non-transduced	IFNγ/IL1β vs. IFNγ/IL1β + LB	31.0992	-1.2354	0.3305	-3.7386	0.0002	0.0088	Down
BTN3A3	Non-transduced	IFNγ/IL1β vs. IFNγ/IL1β + LB	38.9327	1.1796	0.3177	3.7129	0.0002	0.0095	Up
PDZD2	Non-transduced	IFNγ/IL1β vs. IFNγ/IL1β + LB	37.1459	-1.1141	0.3038	-3.6669	0.0002	0.0111	Down
SLIT2	Non-transduced	IFNγ/IL1β vs. IFNγ/IL1β + LB	193.2624	1.0123	0.2835	3.5707	0.0004	0.0153	Up
WNT10B	Non-transduced	IFNγ/IL1β vs. IFNγ/IL1β + LB	12.4779	1.9541	0.5547	3.5227	0.0004	0.0177	Up
NIPAL4	Non-transduced	IFNγ/IL1β vs. IFNγ/IL1β + LB	42.5678	-1.0136	0.2904	-3.4907	0.0005	0.0191	Down
NFATC1	Non-transduced	IFNγ/IL1β vs. IFNγ/IL1β + LB	40.5734	1.0430	0.2992	3.4864	0.0005	0.0193	Up
HIVEP3	Non-transduced	IFNγ/IL1β vs. IFNγ/IL1β + LB	37.7180	1.0644	0.3056	3.4826	0.0005	0.0194	Up
LTBP2	Non-transduced	IFNγ/IL1β vs. IFNγ/IL1β + LB	29.2988	-1.2646	0.3713	-3.4056	0.0007	0.0248	Down
ATOH8	Non-transduced	IFNγ/IL1β vs. IFNγ/IL1β + LB	22.2405	1.3681	0.4080	3.3535	0.0008	0.0290	Up
SNAP25	Non-transduced	IFNγ/IL1β vs. IFNγ/IL1β + LB	20.4236	1.4206	0.4361	3.2573	0.0011	0.0378	Up
ARHGAP6	Non-transduced	IFNγ/IL1β vs. IFNγ/IL1β + LB	9.8162	2.0668	0.6352	3.2539	0.0011	0.0381	Up
SCARF1	Non-transduced	IFNγ/IL1β vs. IFNγ/IL1β + LB	10.1398	-2.1284	0.6634	-3.2083	0.0013	0.0431	Down
F2RL1	Non-transduced	IFNγ/IL1β vs. IFNγ/IL1β + LB	10.5223	-2.1808	0.7098	-3.0723	0.0021	0.0616	Down
FIBCD1	Non-transduced	IFNγ/IL1β vs. IFNγ/IL1β + LB	19.8047	1.3112	0.4420	2.9666	0.0030	0.0806	Up
PCDHGA10	Non-transduced	IFNγ/IL1β vs. IFNγ/IL1β + LB	11.7677	-2.5255	0.8667	-2.9138	0.0036	0.0914	Down
FBXL2	Non-transduced	IFNγ/IL1β vs. IFNγ/IL1β + LB	29.1102	-1.0583	0.3677	-2.8785	0.0040	0.0995	Down
Figure 29b									
IL11	DREADD-β2AR	IFNγ/IL1β vs. IFNγ/IL1β + CNO	1307.1058	1.9113	0.0753	25.3856	0.0000	0.0000	Up
TM4SF1	DREADD-β2AR	IFNγ/IL1β vs. IFNγ/IL1β + CNO	1253.7217	2.7945	0.1205	23.1856	0.0000	0.0000	Up
CDKN1C	DREADD-β2AR	IFNγ/IL1β vs. IFNγ/IL1β + CNO	1154.7312	3.6250	0.1630	22.2383	0.0000	0.0000	Up

Gene	Cell line	Comparison	baseMean	log2FoldChange	lfcSE	Statistic	p-value	padj	Direction
FGF5	DREADD-β2AR	IFNγ/IL1β vs. IFNγ/IL1β + CNO	1727.1772	-1.8789	0.0883	-21.2788	0.0000	0.0000	Down
NPTX1	DREADD-β2AR	IFNγ/IL1β vs. IFNγ/IL1β + CNO	1334.7631	3.1486	0.1574	20.0029	0.0000	0.0000	Up
TFPI2	DREADD-β2AR	IFNγ/IL1β vs. IFNγ/IL1β + CNO	1461.2215	1.8772	0.1015	18.4964	0.0000	0.0000	Up
AKAP12	DREADD-β2AR	IFNγ/IL1β vs. IFNγ/IL1β + CNO	3243.4861	1.3723	0.0914	15.0073	0.0000	0.0000	Up
CSGALNACT1	DREADD-β2AR	IFNγ/IL1β vs. IFNγ/IL1β + CNO	88.8010	4.0208	0.2760	14.5663	0.0000	0.0000	Up
IGFBP4	DREADD-β2AR	IFNγ/IL1β vs. IFNγ/IL1β + CNO	245.4927	1.9425	0.1405	13.8265	0.0000	0.0000	Up
PDE4D	DREADD-β2AR	IFNγ/IL1β vs. IFNγ/IL1β + CNO	195.3763	2.3296	0.1739	13.3929	0.0000	0.0000	Up
METRNL	DREADD-β2AR	IFNγ/IL1β vs. IFNγ/IL1β + CNO	579.4857	1.0357	0.0840	12.3349	0.0000	0.0000	Up
KRTAP2-3	DREADD-β2AR	IFNγ/IL1β vs. IFNγ/IL1β + CNO	225.3629	-2.4395	0.2016	-12.1004	0.0000	0.0000	Down
SMOC1	DREADD-β2AR	IFNγ/IL1β vs. IFNγ/IL1β + CNO	86.2921	3.5592	0.2984	11.9279	0.0000	0.0000	Up
ANKRD1	DREADD-β2AR	IFNγ/IL1β vs. IFNγ/IL1β + CNO	1877.2006	-1.9681	0.1682	-11.7034	0.0000	0.0000	Down
SLC7A5	DREADD-β2AR	IFNγ/IL1β vs. IFNγ/IL1β + CNO	752.7291	1.0814	0.0954	11.3393	0.0000	0.0000	Up
EPAS1	DREADD-β2AR	IFNγ/IL1β vs. IFNγ/IL1β + CNO	1164.3497	1.0033	0.0893	11.2395	0.0000	0.0000	Up
CD24	DREADD-β2AR	IFNγ/IL1β vs. IFNγ/IL1β + CNO	155.3958	1.7456	0.1615	10.8082	0.0000	0.0000	Up
BCL7A	DREADD-β2AR	IFNγ/IL1β vs. IFNγ/IL1β + CNO	758.3216	1.0001	0.0928	10.7824	0.0000	0.0000	Up
EMP1	DREADD-β2AR	IFNγ/IL1β vs. IFNγ/IL1β + CNO	621.8949	-1.2935	0.1253	-10.3191	0.0000	0.0000	Down
SMURF2	DREADD-β2AR	IFNγ/IL1β vs. IFNγ/IL1β + CNO	888.5571	-1.1518	0.1130	-10.1956	0.0000	0.0000	Down
GPRC5A	DREADD-β2AR	IFNγ/IL1β vs. IFNγ/IL1β + CNO	1020.0468	1.1022	0.1087	10.1410	0.0000	0.0000	Up
ETS1	DREADD-β2AR	IFNγ/IL1β vs. IFNγ/IL1β + CNO	2714.1997	-1.0606	0.1050	-10.1023	0.0000	0.0000	Down
F3	DREADD-β2AR	IFNγ/IL1β vs. IFNγ/IL1β + CNO	1457.0385	-1.6397	0.1660	-9.8771	0.0000	0.0000	Down
RGS2	DREADD-β2AR	IFNγ/IL1β vs. IFNγ/IL1β + CNO	1045.7971	1.8609	0.1910	9.7411	0.0000	0.0000	Up
FAM49A	DREADD-β2AR	IFNγ/IL1β vs. IFNγ/IL1β + CNO	88.1571	1.9557	0.2009	9.7339	0.0000	0.0000	Up
IDO1	DREADD-β2AR	IFNγ/IL1β vs. IFNγ/IL1β + CNO	464.5613	1.3077	0.1369	9.5540	0.0000	0.0000	Up
HMGA2	DREADD-β2AR	IFNγ/IL1β vs. IFNγ/IL1β + CNO	802.8837	-1.0549	0.1126	-9.3723	0.0000	0.0000	Down
CHMP1B	DREADD-β2AR	IFNγ/IL1β vs. IFNγ/IL1β + CNO	296.9243	1.2594	0.1347	9.3479	0.0000	0.0000	Up
GABARAPL1	DREADD-β2AR	IFNγ/IL1β vs. IFNγ/IL1β + CNO	209.8672	1.3333	0.1438	9.2698	0.0000	0.0000	Up
AVPI1	DREADD-β2AR	IFNγ/IL1β vs. IFNγ/IL1β + CNO	69.8208	2.0274	0.2200	9.2135	0.0000	0.0000	Up
PPAP2B	DREADD-β2AR	IFNγ/IL1β vs. IFNγ/IL1β + CNO	81.8155	2.0233	0.2307	8.7688	0.0000	0.0000	Up
EGR1	DREADD-β2AR	IFNγ/IL1β vs. IFNγ/IL1β + CNO	197.7618	-2.0347	0.2322	-8.7627	0.0000	0.0000	Down
ELK3	DREADD-β2AR	IFNγ/IL1β vs. IFNγ/IL1β + CNO	1109.4908	-1.0080	0.1161	-8.6842	0.0000	0.0000	Down
PMEPA1	DREADD-β2AR	IFNγ/IL1β vs. IFNγ/IL1β + CNO	160.3738	1.2949	0.1498	8.6433	0.0000	0.0000	Up
DNER	DREADD-β2AR	IFNγ/IL1β vs. IFNγ/IL1β + CNO	300.6379	1.2281	0.1429	8.5955	0.0000	0.0000	Up
NR4A3	DREADD-β2AR	IFNγ/IL1β vs. IFNγ/IL1β + CNO	28.2325	3.1166	0.3739	8.3360	0.0000	0.0000	Up
RNU6-36P	DREADD-β2AR	IFNγ/IL1β vs. IFNγ/IL1β + CNO	10.6933	22.1814	2.8185	7.8699	0.0000	0.0000	Up
PID1	DREADD-β2AR	IFNγ/IL1β vs. IFNγ/IL1β + CNO	95.9266	1.5121	0.1982	7.6284	0.0000	0.0000	Up
PDE7B	DREADD-β2AR	IFNγ/IL1β vs. IFNγ/IL1β + CNO	21.5652	3.7785	0.4961	7.6164	0.0000	0.0000	Up
DIO2	DREADD-β2AR	IFNγ/IL1β vs. IFNγ/IL1β + CNO	37.4922	2.7118	0.3581	7.5725	0.0000	0.0000	Up
SCHIP1	DREADD-β2AR	IFNγ/IL1β vs. IFNγ/IL1β + CNO	447.4692	-1.0175	0.1354	-7.5174	0.0000	0.0000	Down
CRISPLD2	DREADD-β2AR	IFNγ/IL1β vs. IFNγ/IL1β + CNO	92.2008	1.6371	0.2190	7.4761	0.0000	0.0000	Up
GPRC5C	DREADD-β2AR	IFNγ/IL1β vs. IFNγ/IL1β + CNO	44.3908	1.9927	0.2708	7.3586	0.0000	0.0000	Up
WDR66	DREADD-β2AR	IFNγ/IL1β vs. IFNγ/IL1β + CNO	134.5781	1.4454	0.1968	7.3447	0.0000	0.0000	Up
STC1	DREADD-β2AR	IFNγ/IL1β vs. IFNγ/IL1β + CNO	97.7202	1.5764	0.2201	7.1610	0.0000	0.0000	Up
ADARB1	DREADD-β2AR	IFNγ/IL1β vs. IFNγ/IL1β + CNO	131.8997	1.1724	0.1642	7.1403	0.0000	0.0000	Up
NHS	DREADD-β2AR	IFNγ/IL1β vs. IFNγ/IL1β + CNO	43.7281	2.3946	0.3355	7.1386	0.0000	0.0000	Up
LINC00473	DREADD-β2AR	IFNγ/IL1β vs. IFNγ/IL1β + CNO	18.7203	4.0958	0.5854	6.9966	0.0000	0.0000	Up
SERPINE1	DREADD-β2AR	IFNγ/IL1β vs. IFNγ/IL1β + CNO	9650.8148	-1.3840	0.1981	-6.9869	0.0000	0.0000	Down
MAP2K6	DREADD-β2AR	IFNγ/IL1β vs. IFNγ/IL1β + CNO	52.5561	1.8519	0.2660	6.9616	0.0000	0.0000	Up
LRRC37A	DREADD-β2AR	IFNγ/IL1β vs. IFNγ/IL1β + CNO	26.0020	24.1316	3.5256	6.8448	0.0000	0.0000	Up
XIRP1	DREADD-β2AR	IFNγ/IL1β vs. IFNγ/IL1β + CNO	34.9002	-2.9127	0.4259	-6.8383	0.0000	0.0000	Down
SNORD3C	DREADD-β2AR	IFNγ/IL1β vs. IFNγ/IL1β + CNO	145.6224	25.5220	3.7450	6.8149	0.0000	0.0000	Up
LINC00673	DREADD-β2AR	IFNγ/IL1β vs. IFNγ/IL1β + CNO	34.8490	2.2035	0.3236	6.8102	0.0000	0.0000	Up
CCL20	DREADD-β2AR	IFNγ/IL1β vs. IFNγ/IL1β + CNO	264.1183	1.6794	0.2518	6.6694	0.0000	0.0000	Up
HES1	DREADD-β2AR	IFNγ/IL1β vs. IFNγ/IL1β + CNO	123.2873	1.0764	0.1630	6.6042	0.0000	0.0000	Up
PDE3A	DREADD-β2AR	IFNγ/IL1β vs. IFNγ/IL1β + CNO	22.5278	3.0699	0.4810	6.3820	0.0000	0.0000	Up
HHIP	DREADD-β2AR	IFNγ/IL1β vs. IFNγ/IL1β + CNO	274.2449	-1.1001	0.1725	-6.3761	0.0000	0.0000	Down
FAM167A	DREADD-β2AR	IFNγ/IL1β vs. IFNγ/IL1β + CNO	73.9400	1.5066	0.2370	6.3557	0.0000	0.0000	Up
NCKAP5	DREADD-β2AR	IFNγ/IL1β vs. IFNγ/IL1β + CNO	52.2899	1.6485	0.2599	6.3435	0.0000	0.0000	Up
PTGES	DREADD-β2AR	IFNγ/IL1β vs. IFNγ/IL1β + CNO	23.0019	2.8628	0.4555	6.2850	0.0000	0.0000	Up
HAS2	DREADD-β2AR	IFNγ/IL1β vs. IFNγ/IL1β + CNO	140.5934	-1.3348	0.2231	-5.9836	0.0000	0.0000	Down
IGFN1	DREADD-β2AR	IFNγ/IL1β vs. IFNγ/IL1β + CNO	68.1654	1.2896	0.2229	5.7846	0.0000	0.0000	Up
LOXL1-AS1	DREADD-β2AR	IFNγ/IL1β vs. IFNγ/IL1β + CNO	172.7435	-1.0827	0.1896	-5.7103	0.0000	0.0000	Down
SPOCD1	DREADD-β2AR	IFNγ/IL1β vs. IFNγ/IL1β + CNO	71.6835	-1.4041	0.2487	-5.6467	0.0000	0.0000	Down
SMAD6	DREADD-β2AR	IFNγ/IL1β vs. IFNγ/IL1β + CNO	65.5400	1.2147	0.2186	5.5567	0.0000	0.0000	Up
PRKCE	DREADD-β2AR	IFNγ/IL1β vs. IFNγ/IL1β + CNO	83.1157	1.1036	0.2019	5.4667	0.0000	0.0000	Up
CREM	DREADD-β2AR	IFNγ/IL1β vs. IFNγ/IL1β + CNO	79.4316	1.3483	0.2484	5.4283	0.0000	0.0000	Up
EVA1A	DREADD-β2AR	IFNγ/IL1β vs. IFNγ/IL1β + CNO	102.5324	-1.1347	0.2101	-5.4000	0.0000	0.0000	Down
LYPD1	DREADD-β2AR	IFNγ/IL1β vs. IFNγ/IL1β + CNO	38.2942	1.8405	0.3421	5.3805	0.0000	0.0000	Up
DPF3	DREADD-β2AR	IFNγ/IL1β vs. IFNγ/IL1β + CNO	141.8754	-1.0103	0.1927	-5.2441	0.0000	0.0000	Down
GBP2	DREADD-β2AR	IFNγ/IL1β vs. IFNγ/IL1β + CNO	60.4148	1.1874	0.2296	5.1718	0.0000	0.0000	Up
C8orf31	DREADD-β2AR	IFNγ/IL1β vs. IFNγ/IL1β + CNO	13.4365	2.7482	0.5327	5.1593	0.0000	0.0000	Up
LOC100129940	DREADD-β2AR	IFNγ/IL1β vs. IFNγ/IL1β + CNO	82.3119	-1.2234	0.2373	-5.1562	0.0000	0.0000	Down
SYNPO	DREADD-β2AR	IFNγ/IL1β vs. IFNγ/IL1β + CNO	37.0617	1.6128	0.3129	5.1543	0.0000	0.0000	Up
SPTLC3	DREADD-β2AR	IFNγ/IL1β vs. IFNγ/IL1β + CNO	45.2938	1.4835	0.2911	5.0960	0.0000	0.0000	Up
DYX1C1-CCPG1	DREADD-β2AR	IFNγ/IL1β vs. IFNγ/IL1β + CNO	23.9949	21.0613	4.1640	5.0579	0.0000	0.0000	Up
NIPAL4	DREADD-β2AR	IFNγ/IL1β vs. IFNγ/IL1β + CNO	42.5678	-1.3852	0.2822	-4.9085	0.0000	0.0000	Down
KIAA1217	DREADD-β2AR	IFNγ/IL1β vs. IFNγ/IL1β + CNO	68.3466	1.0728	0.2197	4.8829	0.0000	0.0001	Up
ADAM12	DREADD-β2AR	IFNγ/IL1β vs. IFNγ/IL1β + CNO	38.8462	1.3473	0.2945	4.5741	0.0000	0.0002	Up
KIAA1644	DREADD-β2AR	IFNγ/IL1β vs. IFNγ/IL1β + CNO	42.7071	1.1778	0.2595	4.5391	0.0000	0.0002	Up
EBF1	DREADD-β2AR	IFNγ/IL1β vs. IFNγ/IL1β + CNO	39.9057	1.2817	0.2863	4.4769	0.0000	0.0003	Up
DDIT4	DREADD-β2AR	IFNγ/IL1β vs. IFNγ/IL1β + CNO	131.1081	1.0903	0.2438	4.4720	0.0000	0.0003	Up
ATOH8	DREADD-β2AR	IFNγ/IL1β vs. IFNγ/IL1β + CNO	22.2405	1.6869	0.3795	4.4449	0.0000	0.0003	Up
GNG4	DREADD-β2AR	IFNγ/IL1β vs. IFNγ/IL1β + CNO	26.9602	1.5999	0.3619	4.4206	0.0000	0.0004	Up
EPHA5	DREADD-β2AR	IFNγ/IL1β vs. IFNγ/IL1β + CNO	37.8641	1.2738	0.2899	4.3933	0.0000	0.0004	Up
PADI1	DREADD-β2AR	IFNγ/IL1β vs. IFNγ/IL1β + CNO	64.2771	-1.1075	0.2566	-4.3167	0.0000	0.0006	Down
MTSS1	DREADD-β2AR	IFNγ/IL1β vs. IFNγ/IL1β + CNO	60.8439	-1.2309	0.2864	-4.2975	0.0000	0.0006	Down
EDN2	DREADD-β2AR	IFNγ/IL1β vs. IFNγ/IL1β + CNO	14.1064	1.9294	0.4551	4.2393	0.0000	0.0008	Up
NR4A2	DREADD-β2AR	IFNγ/IL1β vs. IFNγ/IL1β + CNO	12.2332	2.4599	0.5873	4.1884	0.0000	0.0009	Up
APOL3	DREADD-β2AR	IFNγ/IL1β vs. IFNγ/IL1β + CNO	14.4057	2.0088	0.4808	4.1783	0.0000	0.0010	Up
HLA-DRA	DREADD-β2AR	IFNγ/IL1β vs. IFNγ/IL1β + CNO	12.7895	2.1054	0.5099	4.1290	0.0000	0.0012	Up
NR4A1	DREADD-β2AR	IFNγ/IL1β vs. IFNγ/IL1β + CNO	24.5922	1.3845	0.3407	4.0633	0.0000	0.0015	Up
EPHA2	DREADD-β2AR	IFNγ/IL1β vs. IFNγ/IL1β + CNO	444.5104	-1.0425	0.2571	-4.0558	0.0000	0.0015	Down
FAS	DREADD-β2AR	IFNγ/IL1β vs. IFNγ/IL1β + CNO	38.3345	1.1743	0.2918	4.0244	0.0001	0.0017	Up
LTB	DREADD-β2AR	IFNγ/IL1β vs. IFNγ/IL1β + CNO	44.9479	-1.2041	0.3003	-4.0091	0.0001	0.0018	Down
C11orf96	DREADD-β2AR	IFNγ/IL1β vs. IFNγ/IL1β + CNO	13.1747	2.0569	0.5169	3.9794	0.0001	0.0020	Up
MYEOV	DREADD-β2AR	IFNγ/IL1β vs. IFNγ/IL1β + CNO	11.3888	-3.4552	0.8715	-3.9647	0.0001	0.0021	Down
ANXA10	DREADD-β2AR	IFNγ/IL1β vs. IFNγ/IL1β + CNO	10.5552	2.1846	0.5577	3.9175	0.0001	0.0025	Up
FAT4	DREADD-β2AR	IFNγ/IL1β vs. IFNγ/IL1β + CNO	31.2486	1.3253	0.3392	3.9073	0.0001	0.0026	Up
MYPN	DREADD-β2AR	IFNγ/IL1β vs. IFNγ/IL1β + CNO	19.8065	2.0072	0.5164	3.8867	0.0001	0.0028	Up
ID4	DREADD-β2AR	IFNγ/IL1β vs. IFNγ/IL1β + CNO	20.7689	1.5632	0.4086	3.8256	0.0001	0.0034	Up
CYP24A1	DREADD-β2AR	IFNγ/IL1β vs. IFNγ/IL1β + CNO	25.9325	-1.6107	0.4241	-3.7981	0.0001	0.0038	Down
SAA2	DREADD-β2AR	IFNγ/IL1β vs. IFNγ/IL1β + CNO	27.6438	1.4030	0.3733	3.7587	0.0002	0.0043	Up
ELAVL2	DREADD-β2AR	IFNγ/IL1β vs. IFNγ/IL1β + CNO	41.3515	1.1188	0.2993	3.7381	0.0002	0.0046	Up
KANK1	DREADD-β2AR	IFNγ/IL1β vs. IFNγ/IL1β + CNO	50.6629	-1.1388	0.3050	-3.7335	0.0002	0.0047	Down
IFI27	DREADD-β2AR	IFNγ/IL1β vs. IFNγ/IL1β + CNO	29.4840	1.2602	0.3380	3.7283	0.0002	0.0048	Up

Gene	Cell line	Comparison	baseMean	log2FoldChange	lfcSE	Statistic	p-value	padj	Direction
NFATC2	DREADD-β2AR	IFNγ/IL1β vs. IFNγ/IL1β + CNO	17.1329	1.7264	0.4702	3.6713	0.0002	0.0057	Up
PDGFB	DREADD-β2AR	IFNγ/IL1β vs. IFNγ/IL1β + CNO	31.0992	-1.1876	0.3266	-3.6358	0.0003	0.0064	Down
SLC7A8	DREADD-β2AR	IFNγ/IL1β vs. IFNγ/IL1β + CNO	8.2984	2.8684	0.7970	3.5991	0.0003	0.0071	Up
LIF	DREADD-β2AR	IFNγ/IL1β vs. IFNγ/IL1β + CNO	63.0252	-1.2606	0.3506	-3.5951	0.0003	0.0072	Down
SCG2	DREADD-β2AR	IFNγ/IL1β vs. IFNγ/IL1β + CNO	27.5271	1.2011	0.3355	3.5796	0.0003	0.0075	Up
CSF2RB	DREADD-β2AR	IFNγ/IL1β vs. IFNγ/IL1β + CNO	28.4890	1.2684	0.3639	3.4857	0.0005	0.0101	Up
CERS6-AS1	DREADD-β2AR	IFNγ/IL1β vs. IFNγ/IL1β + CNO	9.3608	-21.7648	6.2983	-3.4557	0.0005	0.0110	Down
FLT1	DREADD-β2AR	IFNγ/IL1β vs. IFNγ/IL1β + CNO	21.9174	-1.4110	0.4087	-3.4521	0.0006	0.0110	Down
SCARF2	DREADD-β2AR	IFNγ/IL1β vs. IFNγ/IL1β + CNO	54.7851	-1.1050	0.3252	-3.3981	0.0007	0.0131	Down
SLC28A3	DREADD-β2AR	IFNγ/IL1β vs. IFNγ/IL1β + CNO	45.4368	-1.0045	0.2998	-3.3501	0.0008	0.0150	Down
RUNX3	DREADD-β2AR	IFNγ/IL1β vs. IFNγ/IL1β + CNO	19.2637	1.3789	0.4167	3.3088	0.0009	0.0168	Up
CITED4	DREADD-β2AR	IFNγ/IL1β vs. IFNγ/IL1β + CNO	17.7002	1.2912	0.3995	3.2321	0.0012	0.0207	Up
ZNF747	DREADD-β2AR	IFNγ/IL1β vs. IFNγ/IL1β + CNO	30.3884	1.1054	0.3484	3.1730	0.0015	0.0243	Up
ACSS1	DREADD-β2AR	IFNγ/IL1β vs. IFNγ/IL1β + CNO	8.5809	1.9339	0.6116	3.1623	0.0016	0.0250	Up
SH3RF2	DREADD-β2AR	IFNγ/IL1β vs. IFNγ/IL1β + CNO	26.8572	-1.2840	0.4076	-3.1501	0.0016	0.0258	Down
VCAM1	DREADD-β2AR	IFNγ/IL1β vs. IFNγ/IL1β + CNO	14.4034	-1.7231	0.5480	-3.1445	0.0017	0.0261	Down
C17orf100	DREADD-β2AR	IFNγ/IL1β vs. IFNγ/IL1β + CNO	25.7678	1.2652	0.4047	3.1260	0.0018	0.0273	Up
TLR3	DREADD-β2AR	IFNγ/IL1β vs. IFNγ/IL1β + CNO	18.5547	1.2345	0.3965	3.1137	0.0018	0.0281	Up
CCDC85A	DREADD-β2AR	IFNγ/IL1β vs. IFNγ/IL1β + CNO	17.9193	1.2756	0.4105	3.1071	0.0019	0.0286	Up
WNT10B	DREADD-β2AR	IFNγ/IL1β vs. IFNγ/IL1β + CNO	12.4779	1.6321	0.5288	3.0862	0.0020	0.0301	Up
TNFSF10	DREADD-β2AR	IFNγ/IL1β vs. IFNγ/IL1β + CNO	14.3998	1.4230	0.4623	3.0783	0.0021	0.0306	Up
CD74	DREADD-β2AR	IFNγ/IL1β vs. IFNγ/IL1β + CNO	19.0303	1.3538	0.4411	3.0695	0.0021	0.0313	Up
LOC653513	DREADD-β2AR	IFNγ/IL1β vs. IFNγ/IL1β + CNO	24.0274	1.3471	0.4400	3.0617	0.0022	0.0320	Up
ELF3	DREADD-β2AR	IFNγ/IL1β vs. IFNγ/IL1β + CNO	38.8246	1.0452	0.3432	3.0454	0.0023	0.0334	Up
XKR9	DREADD-β2AR	IFNγ/IL1β vs. IFNγ/IL1β + CNO	22.1323	-1.2180	0.4053	-3.0048	0.0027	0.0371	Down
REP15	DREADD-β2AR	IFNγ/IL1β vs. IFNγ/IL1β + CNO	19.3506	1.4390	0.4791	3.0039	0.0027	0.0371	Up
TGIF2-C20orf24	DREADD-β2AR	IFNγ/IL1β vs. IFNγ/IL1β + CNO	53.7498	-2.3789	0.7946	-2.9937	0.0028	0.0383	Down
CPNE5	DREADD-β2AR	IFNγ/IL1β vs. IFNγ/IL1β + CNO	9.1323	-1.9581	0.6566	-2.9820	0.0029	0.0395	Down
KRTAP4-9	DREADD-β2AR	IFNγ/IL1β vs. IFNγ/IL1β + CNO	8.2655	-2.1852	0.7329	-2.9814	0.0029	0.0395	Down
ONECUT2	DREADD-β2AR	IFNγ/IL1β vs. IFNγ/IL1β + CNO	20.2406	1.2525	0.4233	2.9589	0.0031	0.0419	Up
CFB	DREADD-β2AR	IFNγ/IL1β vs. IFNγ/IL1β + CNO	7.6237	1.9274	0.6529	2.9519	0.0032	0.0427	Up
HKDC1	DREADD-β2AR	IFNγ/IL1β vs. IFNγ/IL1β + CNO	20.2130	1.3891	0.4823	2.8803	0.0040	0.0500	Up
SUCLG2-AS1	DREADD-β2AR	IFNγ/IL1β vs. IFNγ/IL1β + CNO	22.7069	1.0520	0.3701	2.8425	0.0045	0.0546	Up
TVP23A	DREADD-β2AR	IFNγ/IL1β vs. IFNγ/IL1β + CNO	10.6436	1.5781	0.5572	2.8320	0.0046	0.0561	Up
ACTRT3	DREADD-β2AR	IFNγ/IL1β vs. IFNγ/IL1β + CNO	22.5181	1.0963	0.3878	2.8268	0.0047	0.0567	Up
PAG1	DREADD-β2AR	IFNγ/IL1β vs. IFNγ/IL1β + CNO	27.2321	1.0072	0.3598	2.7995	0.0051	0.0599	Up
LINC00969	DREADD-β2AR	IFNγ/IL1β vs. IFNγ/IL1β + CNO	18.1739	1.3371	0.4814	2.7775	0.0055	0.0625	Up
RN7SL2	DREADD-β2AR	IFNγ/IL1β vs. IFNγ/IL1β + CNO	30.9280	-1.3554	0.4910	-2.7607	0.0058	0.0647	Down
FBXO10	DREADD-β2AR	IFNγ/IL1β vs. IFNγ/IL1β + CNO	18.7450	1.1554	0.4186	2.7598	0.0058	0.0648	Up
LINC01003	DREADD-β2AR	IFNγ/IL1β vs. IFNγ/IL1β + CNO	17.0051	-1.3011	0.4727	-2.7526	0.0059	0.0657	Down
SLC41A2	DREADD-β2AR	IFNγ/IL1β vs. IFNγ/IL1β + CNO	18.8168	-1.1699	0.4266	-2.7423	0.0061	0.0674	Down
KBTBD8	DREADD-β2AR	IFNγ/IL1β vs. IFNγ/IL1β + CNO	12.8818	-1.6639	0.6110	-2.7231	0.0065	0.0703	Down
DAW1	DREADD-β2AR	IFNγ/IL1β vs. IFNγ/IL1β + CNO	20.2002	1.1029	0.4078	2.7049	0.0068	0.0730	Up
TFAP2A-AS1	DREADD-β2AR	IFNγ/IL1β vs. IFNγ/IL1β + CNO	9.4321	1.7916	0.6641	2.6979	0.0070	0.0742	Up
RAB42	DREADD-β2AR	IFNγ/IL1β vs. IFNγ/IL1β + CNO	16.0978	1.1120	0.4140	2.6862	0.0072	0.0764	Up
TNF	DREADD-β2AR	IFNγ/IL1β vs. IFNγ/IL1β + CNO	10.5056	-1.6435	0.6121	-2.6850	0.0073	0.0764	Down
NR2F1-AS1	DREADD-β2AR	IFNγ/IL1β vs. IFNγ/IL1β + CNO	28.3306	-1.0036	0.3742	-2.6824	0.0073	0.0767	Down
JHDM1D-AS1	DREADD-β2AR	IFNγ/IL1β vs. IFNγ/IL1β + CNO	14.6665	1.2986	0.4863	2.6705	0.0076	0.0784	Up
ADAMTS12	DREADD-β2AR	IFNγ/IL1β vs. IFNγ/IL1β + CNO	22.8266	-1.0707	0.4023	-2.6618	0.0078	0.0795	Down
LOC102724434	DREADD-β2AR	IFNγ/IL1β vs. IFNγ/IL1β + CNO	19.5175	-1.3035	0.4897	-2.6618	0.0078	0.0795	Down
SPRY4	DREADD-β2AR	IFNγ/IL1β vs. IFNγ/IL1β + CNO	20.8426	-1.1792	0.4448	-2.6514	0.0080	0.0808	Down
WFDC21P	DREADD-β2AR	IFNγ/IL1β vs. IFNγ/IL1β + CNO	23.2610	1.0711	0.4050	2.6445	0.0082	0.0819	Up
ZDHHC14	DREADD-β2AR	IFNγ/IL1β vs. IFNγ/IL1β + CNO	17.4349	1.0762	0.4093	2.6295	0.0086	0.0846	Up
MIR503HG	DREADD-β2AR	IFNγ/IL1β vs. IFNγ/IL1β + CNO	10.8700	-1.6281	0.6311	-2.5798	0.0099	0.0936	Down
CTIF	DREADD-β2AR	IFNγ/IL1β vs. IFNγ/IL1β + CNO	17.2532	1.0156	0.3976	2.5545	0.0106	0.0983	Up
ANGPTL4	DREADD-β2AR	IFNγ/IL1β vs. IFNγ/IL1β + CNO	10.4616	-1.6364	0.6416	-2.5507	0.0107	0.0990	Down
OAF	DREADD-β2AR	IFNγ/IL1β vs. IFNγ/IL1β + CNO	19.3933	1.1946	0.4687	2.5487	0.0108	0.0993	Up

Figure 29c

TM4SF1	DREADD-GPR65	IFNγ/IL1β vs. IFNγ/IL1β + CNO	1253.7217	2.4176	0.1201	20.1377	0.0000	0.0000	Up
CDKN1C	DREADD-GPR65	IFNγ/IL1β vs. IFNγ/IL1β + CNO	1154.7312	3.2417	0.1631	19.8751	0.0000	0.0000	Up
FGF5	DREADD-GPR65	IFNγ/IL1β vs. IFNγ/IL1β + CNO	1727.1772	-1.6658	0.0876	-19.0210	0.0000	0.0000	Down
NPTX1	DREADD-GPR65	IFNγ/IL1β vs. IFNγ/IL1β + CNO	1334.7631	2.9165	0.1589	18.3543	0.0000	0.0000	Up
IL11	DREADD-GPR65	IFNγ/IL1β vs. IFNγ/IL1β + CNO	1307.1058	1.3466	0.0743	18.1261	0.0000	0.0000	Up
TFPI2	DREADD-GPR65	IFNγ/IL1β vs. IFNγ/IL1β + CNO	1461.2215	1.5646	0.1006	15.5473	0.0000	0.0000	Up
CSGALNACT1	DREADD-GPR65	IFNγ/IL1β vs. IFNγ/IL1β + CNO	88.8010	3.3615	0.2615	12.8529	0.0000	0.0000	Up
AKAP12	DREADD-GPR65	IFNγ/IL1β vs. IFNγ/IL1β + CNO	3243.4861	1.1545	0.0920	12.5469	0.0000	0.0000	Up
IGFBP4	DREADD-GPR65	IFNγ/IL1β vs. IFNγ/IL1β + CNO	245.4927	1.6366	0.1373	11.9185	0.0000	0.0000	Up
ANKRD1	DREADD-GPR65	IFNγ/IL1β vs. IFNγ/IL1β + CNO	1877.2006	-1.9947	0.1693	-11.7807	0.0000	0.0000	Down
KRTAP2-3	DREADD-GPR65	IFNγ/IL1β vs. IFNγ/IL1β + CNO	225.3629	-2.0772	0.1906	-10.8986	0.0000	0.0000	Down
CHMP1B	DREADD-GPR65	IFNγ/IL1β vs. IFNγ/IL1β + CNO	296.9243	1.4544	0.1365	10.6545	0.0000	0.0000	Up
PDE4D	DREADD-GPR65	IFNγ/IL1β vs. IFNγ/IL1β + CNO	195.3763	1.8322	0.1723	10.6329	0.0000	0.0000	Up
CD24	DREADD-GPR65	IFNγ/IL1β vs. IFNγ/IL1β + CNO	155.3958	1.5017	0.1529	9.8207	0.0000	0.0000	Up
RGS2	DREADD-GPR65	IFNγ/IL1β vs. IFNγ/IL1β + CNO	1045.7971	1.8324	0.1919	9.5483	0.0000	0.0000	Up
EMP1	DREADD-GPR65	IFNγ/IL1β vs. IFNγ/IL1β + CNO	621.8949	-1.1238	0.1221	-9.2064	0.0000	0.0000	Down
IL15	DREADD-GPR65	IFNγ/IL1β vs. IFNγ/IL1β + CNO	249.8648	1.0850	0.1186	9.1468	0.0000	0.0000	Up
SMOC1	DREADD-GPR65	IFNγ/IL1β vs. IFNγ/IL1β + CNO	86.2921	2.6004	0.2844	9.1423	0.0000	0.0000	Up
CCL20	DREADD-GPR65	IFNγ/IL1β vs. IFNγ/IL1β + CNO	264.1183	2.0474	0.2505	8.1743	0.0000	0.0000	Up
CRISPLD2	DREADD-GPR65	IFNγ/IL1β vs. IFNγ/IL1β + CNO	92.2008	1.7956	0.2264	7.9295	0.0000	0.0000	Up
DIO2	DREADD-GPR65	IFNγ/IL1β vs. IFNγ/IL1β + CNO	37.4922	2.7066	0.3510	7.7111	0.0000	0.0000	Up
PID1	DREADD-GPR65	IFNγ/IL1β vs. IFNγ/IL1β + CNO	95.9266	1.5147	0.1974	7.6746	0.0000	0.0000	Up
NAV3	DREADD-GPR65	IFNγ/IL1β vs. IFNγ/IL1β + CNO	291.1661	-1.0032	0.1321	-7.5971	0.0000	0.0000	Down
NHS	DREADD-GPR65	IFNγ/IL1β vs. IFNγ/IL1β + CNO	43.7281	2.4325	0.3280	7.4154	0.0000	0.0000	Up
F3	DREADD-GPR65	IFNγ/IL1β vs. IFNγ/IL1β + CNO	1457.0385	-1.2203	0.1653	-7.3815	0.0000	0.0000	Down
FAM49A	DREADD-GPR65	IFNγ/IL1β vs. IFNγ/IL1β + CNO	88.1571	1.4631	0.2000	7.3161	0.0000	0.0000	Up
GPRC5C	DREADD-GPR65	IFNγ/IL1β vs. IFNγ/IL1β + CNO	44.3908	1.9932	0.2727	7.3081	0.0000	0.0000	Up
LINC00473	DREADD-GPR65	IFNγ/IL1β vs. IFNγ/IL1β + CNO	18.7203	4.1175	0.5776	7.1284	0.0000	0.0000	Up
AVPI1	DREADD-GPR65	IFNγ/IL1β vs. IFNγ/IL1β + CNO	69.8208	1.5109	0.2155	7.0100	0.0000	0.0000	Up
PDE3A	DREADD-GPR65	IFNγ/IL1β vs. IFNγ/IL1β + CNO	22.5278	3.0291	0.4348	6.9673	0.0000	0.0000	Up
PDE7B	DREADD-GPR65	IFNγ/IL1β vs. IFNγ/IL1β + CNO	21.5652	3.8502	0.5536	6.9546	0.0000	0.0000	Up
NR4A3	DREADD-GPR65	IFNγ/IL1β vs. IFNγ/IL1β + CNO	28.2325	2.5893	0.3770	6.8692	0.0000	0.0000	Up
PPAP2B	DREADD-GPR65	IFNγ/IL1β vs. IFNγ/IL1β + CNO	81.8155	1.4844	0.2163	6.8619	0.0000	0.0000	Up
C15orf48	DREADD-GPR65	IFNγ/IL1β vs. IFNγ/IL1β + CNO	192.3965	1.2661	0.1916	6.6064	0.0000	0.0000	Up
XIRP1	DREADD-GPR65	IFNγ/IL1β vs. IFNγ/IL1β + CNO	34.9002	-2.7074	0.4133	-6.5506	0.0000	0.0000	Down
FAM167A	DREADD-GPR65	IFNγ/IL1β vs. IFNγ/IL1β + CNO	73.9400	1.4518	0.2256	6.4353	0.0000	0.0000	Up
ARRDC3	DREADD-GPR65	IFNγ/IL1β vs. IFNγ/IL1β + CNO	190.3492	1.1010	0.1737	6.3394	0.0000	0.0000	Up
EGR1	DREADD-GPR65	IFNγ/IL1β vs. IFNγ/IL1β + CNO	197.7618	-1.4048	0.2290	-6.1355	0.0000	0.0000	Down
HAS2	DREADD-GPR65	IFNγ/IL1β vs. IFNγ/IL1β + CNO	140.5934	-1.3375	0.2216	-6.0346	0.0000	0.0000	Down
WNK4	DREADD-GPR65	IFNγ/IL1β vs. IFNγ/IL1β + CNO	126.8386	-1.1407	0.1931	-5.9074	0.0000	0.0000	Down
WDR66	DREADD-GPR65	IFNγ/IL1β vs. IFNγ/IL1β + CNO	134.5781	1.0767	0.1987	5.4190	0.0000	0.0000	Up
SERPINE1	DREADD-GPR65	IFNγ/IL1β vs. IFNγ/IL1β + CNO	9650.8148	-1.0743	0.1990	-5.3980	0.0000	0.0000	Down
IGFN1	DREADD-GPR65	IFNγ/IL1β vs. IFNγ/IL1β + CNO	68.1654	1.0588	0.2039	5.1918	0.0000	0.0000	Up
MAP2K6	DREADD-GPR65	IFNγ/IL1β vs. IFNγ/IL1β + CNO	52.5561	1.3680	0.2657	5.1493	0.0000	0.0000	Up
LRIG1	DREADD-GPR65	IFNγ/IL1β vs. IFNγ/IL1β + CNO	48.5240	1.3191	0.2570	5.1334	0.0000	0.0000	Up

Gene	Cell line	Comparison	baseMean	log2FoldChange	lfcSE	Statistic	p-value	padj	Direction
SCG2	DREADD-GPR65	IFNγ/IL1β vs. IFNγ/IL1β + CNO	27.5271	1.7737	0.3470	5.1122	0.0000	0.0000	Up
SMAD6	DREADD-GPR65	IFNγ/IL1β vs. IFNγ/IL1β + CNO	65.5400	1.1119	0.2247	4.9485	0.0000	0.0000	Up
SPTLC3	DREADD-GPR65	IFNγ/IL1β vs. IFNγ/IL1β + CNO	45.2938	1.4300	0.2897	4.9360	0.0000	0.0000	Up
C8orf31	DREADD-GPR65	IFNγ/IL1β vs. IFNγ/IL1β + CNO	13.4365	2.7062	0.5613	4.8213	0.0000	0.0001	Up
KIAA1644	DREADD-GPR65	IFNγ/IL1β vs. IFNγ/IL1β + CNO	42.7071	1.2101	0.2593	4.6659	0.0000	0.0002	Up
SPOCD1	DREADD-GPR65	IFNγ/IL1β vs. IFNγ/IL1β + CNO	71.6835	-1.0858	0.2361	-4.5985	0.0000	0.0002	Down
NCKAP5	DREADD-GPR65	IFNγ/IL1β vs. IFNγ/IL1β + CNO	52.2899	1.1414	0.2499	4.5680	0.0000	0.0002	Up
MTSS1	DREADD-GPR65	IFNγ/IL1β vs. IFNγ/IL1β + CNO	60.8439	-1.2392	0.2731	-4.5379	0.0000	0.0003	Down
SNAI1	DREADD-GPR65	IFNγ/IL1β vs. IFNγ/IL1β + CNO	50.5674	1.1630	0.2570	4.5259	0.0000	0.0003	Up
HIVEP3	DREADD-GPR65	IFNγ/IL1β vs. IFNγ/IL1β + CNO	37.7180	1.3248	0.2931	4.5195	0.0000	0.0003	Up
TBC1D2	DREADD-GPR65	IFNγ/IL1β vs. IFNγ/IL1β + CNO	101.9271	-1.0419	0.2305	-4.5196	0.0000	0.0003	Down
PADI1	DREADD-GPR65	IFNγ/IL1β vs. IFNγ/IL1β + CNO	64.2771	-1.1547	0.2575	-4.4835	0.0000	0.0003	Down
SLC28A3	DREADD-GPR65	IFNγ/IL1β vs. IFNγ/IL1β + CNO	45.4368	-1.2203	0.2791	-4.3724	0.0000	0.0005	Down
LINC00673	DREADD-GPR65	IFNγ/IL1β vs. IFNγ/IL1β + CNO	34.8490	1.3511	0.3144	4.2977	0.0000	0.0007	Up
NIPAL4	DREADD-GPR65	IFNγ/IL1β vs. IFNγ/IL1β + CNO	42.5678	-1.2112	0.2818	-4.2988	0.0000	0.0007	Down
PTGES	DREADD-GPR65	IFNγ/IL1β vs. IFNγ/IL1β + CNO	23.0019	1.8569	0.4377	4.2421	0.0000	0.0009	Up
NFATC1	DREADD-GPR65	IFNγ/IL1β vs. IFNγ/IL1β + CNO	40.5734	1.2977	0.3068	4.2300	0.0000	0.0009	Up
TNFRSF11B	DREADD-GPR65	IFNγ/IL1β vs. IFNγ/IL1β + CNO	34.0888	1.3032	0.3084	4.2262	0.0000	0.0009	Up
KITLG	DREADD-GPR65	IFNγ/IL1β vs. IFNγ/IL1β + CNO	35.6335	1.2318	0.2946	4.1820	0.0000	0.0011	Up
LYPD1	DREADD-GPR65	IFNγ/IL1β vs. IFNγ/IL1β + CNO	38.2942	1.3460	0.3273	4.1127	0.0000	0.0014	Up
HDAC9	DREADD-GPR65	IFNγ/IL1β vs. IFNγ/IL1β + CNO	59.4177	-1.1374	0.2787	-4.0805	0.0000	0.0016	Down
EPHA5	DREADD-GPR65	IFNγ/IL1β vs. IFNγ/IL1β + CNO	37.8641	1.1924	0.2975	4.0084	0.0001	0.0021	Up
RUNX3	DREADD-GPR65	IFNγ/IL1β vs. IFNγ/IL1β + CNO	19.2637	1.6028	0.4079	3.9291	0.0001	0.0028	Up
RGS7	DREADD-GPR65	IFNγ/IL1β vs. IFNγ/IL1β + CNO	49.8217	-1.1070	0.2973	-3.7238	0.0002	0.0056	Down
ID4	DREADD-GPR65	IFNγ/IL1β vs. IFNγ/IL1β + CNO	20.7689	1.4242	0.3948	3.6075	0.0003	0.0079	Up
SIK1	DREADD-GPR65	IFNγ/IL1β vs. IFNγ/IL1β + CNO	31.4746	1.0448	0.2905	3.5964	0.0003	0.0082	Up
NR4A1	DREADD-GPR65	IFNγ/IL1β vs. IFNγ/IL1β + CNO	24.5922	1.1755	0.3315	3.5462	0.0004	0.0096	Up
FLRT2	DREADD-GPR65	IFNγ/IL1β vs. IFNγ/IL1β + CNO	21.1234	1.4099	0.3987	3.5366	0.0004	0.0098	Up
AQP3	DREADD-GPR65	IFNγ/IL1β vs. IFNγ/IL1β + CNO	21.9766	1.5210	0.4342	3.5030	0.0005	0.0107	Up
IL6	DREADD-GPR65	IFNγ/IL1β vs. IFNγ/IL1β + CNO	210.3710	2.1272	0.6085	3.4956	0.0005	0.0109	Up
KCTD18	DREADD-GPR65	IFNγ/IL1β vs. IFNγ/IL1β + CNO	30.9651	1.1438	0.3294	3.4728	0.0005	0.0116	Up
NFATC2	DREADD-GPR65	IFNγ/IL1β vs. IFNγ/IL1β + CNO	17.1329	1.7982	0.5212	3.4500	0.0006	0.0125	Up
EDN2	DREADD-GPR65	IFNγ/IL1β vs. IFNγ/IL1β + CNO	14.1064	1.5606	0.4559	3.4230	0.0006	0.0136	Up
SGCD	DREADD-GPR65	IFNγ/IL1β vs. IFNγ/IL1β + CNO	16.4287	-1.8066	0.5344	-3.3806	0.0007	0.0154	Down
CCL11	DREADD-GPR65	IFNγ/IL1β vs. IFNγ/IL1β + CNO	187.2876	-1.0880	0.3243	-3.3548	0.0008	0.0167	Down
TRIM55	DREADD-GPR65	IFNγ/IL1β vs. IFNγ/IL1β + CNO	18.6986	-1.7178	0.5209	-3.2975	0.0010	0.0197	Down
MIR1244-1	DREADD-GPR65	IFNγ/IL1β vs. IFNγ/IL1β + CNO	16.3089	1.8602	0.5808	3.2029	0.0014	0.0259	Up
ELOVL7	DREADD-GPR65	IFNγ/IL1β vs. IFNγ/IL1β + CNO	17.8255	1.4268	0.4484	3.1822	0.0015	0.0274	Up
CCDC85A	DREADD-GPR65	IFNγ/IL1β vs. IFNγ/IL1β + CNO	17.9193	1.2374	0.4000	3.0939	0.0020	0.0345	Up
DAW1	DREADD-GPR65	IFNγ/IL1β vs. IFNγ/IL1β + CNO	20.2002	1.3209	0.4321	3.0569	0.0022	0.0377	Up
LOC728554	DREADD-GPR65	IFNγ/IL1β vs. IFNγ/IL1β + CNO	33.6551	1.3913	0.4670	2.9795	0.0029	0.0458	Up
MYPN	DREADD-GPR65	IFNγ/IL1β vs. IFNγ/IL1β + CNO	19.8065	1.4516	0.4874	2.9781	0.0029	0.0459	Up
CCDC81	DREADD-GPR65	IFNγ/IL1β vs. IFNγ/IL1β + CNO	14.8010	-1.4126	0.4748	-2.9748	0.0029	0.0462	Down
RGS4	DREADD-GPR65	IFNγ/IL1β vs. IFNγ/IL1β + CNO	44.7108	-1.1947	0.4028	-2.9657	0.0030	0.0471	Down
CD200	DREADD-GPR65	IFNγ/IL1β vs. IFNγ/IL1β + CNO	21.3772	1.1256	0.3877	2.9031	0.0037	0.0546	Up
ZNF436	DREADD-GPR65	IFNγ/IL1β vs. IFNγ/IL1β + CNO	20.9167	1.1888	0.4123	2.8832	0.0039	0.0575	Up
CBWD3	DREADD-GPR65	IFNγ/IL1β vs. IFNγ/IL1β + CNO	43.1686	-1.1934	0.4211	-2.8337	0.0046	0.0642	Down
CSF2RB	DREADD-GPR65	IFNγ/IL1β vs. IFNγ/IL1β + CNO	28.4890	1.0156	0.3598	2.8228	0.0048	0.0661	Up
TNFSF10	DREADD-GPR65	IFNγ/IL1β vs. IFNγ/IL1β + CNO	14.3998	1.2114	0.4402	2.7520	0.0059	0.0771	Up
HOPX	DREADD-GPR65	IFNγ/IL1β vs. IFNγ/IL1β + CNO	15.3960	-1.3927	0.5064	-2.7503	0.0060	0.0774	Down
H3F3A	DREADD-GPR65	IFNγ/IL1β vs. IFNγ/IL1β + CNO	54.7311	3.5560	1.3138	2.7066	0.0068	0.0847	Up
FIBCD1	DREADD-GPR65	IFNγ/IL1β vs. IFNγ/IL1β + CNO	19.8047	1.0010	0.3794	2.6388	0.0083	0.0974	Up
MLPH	DREADD-GPR65	IFNγ/IL1β vs. IFNγ/IL1β + CNO	16.2311	1.1083	0.4199	2.6396	0.0083	0.0974	Up
CITED4	DREADD-GPR65	IFNγ/IL1β vs. IFNγ/IL1β + CNO	17.7002	1.0748	0.4093	2.6262	0.0086	0.0997	Up
Figure 29e									
NUGGC	Non-transduced	IFNγ/IL1β vs. IFNγ/IL1β + CNO	0.4499	16.0000	3.4017	4.7035	0.0000	0.0489	Up
RAPGEF3	Non-transduced	IFNγ/IL1β vs. IFNγ/IL1β + CNO	0.7363	-20.6541	4.6340	-4.4571	0.0000	0.0794	Down

Supplementary Table S3: Gene clusters revealed by hierarchical clustering of all conditions.
Gene clusters as they appear in **Figure 29g** from top to bottom. *Cluster 1:* intermediately upregulated with GPCR stimulation compared to IFNγ/IL1β alone. *Cluster 2:* downregulated compared to IFNγ/IL1β alone. *Cluster 3:* strongly upregulated compared to IFNγ/IL1β alone.

Gene	Gene cluster
VCAM1	2
SCARF1	2
PCDHGA10	2
F2RL1	2
PLXNA2	2
SERPINB7	2
EPHA2	2
LIF	2
SLC28A3	2
EMP1	2
HHIP	2
PDGFB	2
NIPAL4	2
SERPINE1	2
KANK1	2
LOXL1-AS1	2
PDZD2	2
LINC01003	2
SLC41A2	2
FBXL2	2
LTBP2	2
CCL11	2
MTSS1	2
LTB	2
NR2F1-AS1	2
ANGPTL4	2
CCDC81	2
RGS7	2
TBC1D2	2
PADI1	2
HDAC9	2
NAV3	2
ELK3	2
SMURF2	2
DPF3	2
HMGA2	2
WNK4	2
LOC100129940	2
SPOCD1	2
RGS4	2
TRIM55	2
SPRY4	2
LOC102724434	2
HAS2	2
F3	2
FGF5	2
HOPX	2
SGCD	2
KBTBD8	2
SCARF2	2
FLT1	2
SH3RF2	2
SCHIP1	2
ETS1	2
EVA1A	2
CYP24A1	2
ADAMTS12	2
XKR9	2
RN7SL2	2
TNF	2
MIR503HG	2
CPNE5	2
EGR1	2
KRTAP4-9	2
MYEOV	2
XIRP1	2
ANKRD1	2
KRTAP2-3	2
H3F3A	1
TGIF2-C20orf24	1
KCTD18	1
MIR1244-1	1
SIK1	1
LOC728554	1
IL6	1
OAF	1
JHDM1D-AS1	1
LINC00969	1
ACSS1	1
APOL3	1
CFB	1
CCDC85A	1
TNFSF10	1
ONECUT2	1

Gene	Gene cluster
ZNF747	1
REP15	1
ADAM12	1
TLR3	1
KITLG	1
CD200	1
ZNF436	1
LRIG1	1
TNFRSF11B	1
AQP3	1
SNAI1	1
ID4	1
ACTRT3	1
MLPH	1
FAS	1
ARRDC3	1
BCL7A	1
IL15	1
HKDC1	1
CD74	1
WFDC21P	1
CBWD3	1
C17orf100	1
PAG1	1
TRPC4	1
SNAP25	1
FIBCD1	1
ISG20	1
ZDHHC14	1
BTN3A3	1
SLIT2	1
EPHA5	1
IDO1	1
FBXO10	1
IFI27	1
MYPN	1
TFAP2A-AS1	1
HLA-DRA	1
FLRT2	1
LOC653513	1
TVP23A	1
LYPD1	1
NCKAP5	1
RUNX3	1
RAB42	1
CSF2RB	1
ELAVL2	1
HES1	1
KIAA1217	1
C15orf48	1
PRKCE	1
EPAS1	1
SLC7A5	1
HIVEP3	1
NR4A1	1
CTIF	1
SYNPO	1
EBF1	1
SUCLG2-AS1	1
FAT4	1
PMEPA1	1
SMAD6	1
CREM	1
IGFN1	1
METRNL	1
STAMBPL1	1
DNER	1
GBP2	1
ATOH8	1
CD24	1
TFPI2	1
IL11	1
PPAP2B	1
DDIT4	1
KIAA1644	1
ELF3	1
GPRC5A	1
ADARB1	1
GABARAPL1	1
AKAP12	1
WDR66	1
DAW1	1
GNG4	1
RGS2	1

Gene	Gene cluster
SCG2	1
MAP2K6	1
SAA2	1
LRRC4C	1
ELOVL7	1
NFATC1	1
CHMP1B	1
GREM1	1
WNT10B	1
NFATC2	1
CCL20	1
CRISPLD2	1
FAM167A	1
PID1	1
STC1	1
EDN2	1
LINC00673	1
GPRC5C	1
FAM49A	1
IGFBP4	1
AVPI1	1
PDE4D	1
ANXA10	1
C11orf96	1
SPTLC3	1
CITED4	1
ARHGAP6	1
CSGALNACT1	3
SMOC1	3
CDKN1C	3
NPTX1	3
SLC7A8	3
PDE7B	3
LINC00473	3
NR4A2	3
NHS	3
TM4SF1	3
NR4A3	3
DIO2	3
PDE3A	3
PTGES	3
C8orf31	3

Supplementary Table S4: Gene clusters from hierarchical clustering of DREADD-β2AR and DREADD-GPR65.
Gene clusters in **Figure 31a** from top to bottom. *Cluster A:* upregulated upon CNO stiumulation of DREADD-β2AR but not DREADD-GPR65. *Cluster B:* upregulated upon CNO stiumulation of DREADD-β2AR and DREADD-GPR65. *Cluster C:* downregulated upon CNO stiumulation of DREADD-β2AR but not DREADD-GPR65. *Cluster D:* Downregulated upon CNO stiumulation of DREADD-β2AR and DREADD-GPR65. *Cluster E:* Strongly upregulated upon CNO stiumulation of DREADD-β2AR and DREADD-GPR65.

Gene	Gene cluster
CCL11	D
LOC102724434	D
NR2F1-AS1	D
SPRY4	D
HOPX	D
RGS4	D
TRIM55	D
HAS2	D
EMP1	D
SLC28A3	D
SERPINE1	D
SPOCD1	D
F3	D
NIPAL4	D
CCDC81	D
PADI1	D
RGS7	D
SGCD	D
LTB	D
MTSS1	D
TBC1D2	D
WNK4	D
DPF3	D
PDGFB	D
KANK1	D
PDZD2	D
HMGA2	D
LOC100129940	D
HDAC9	D
HHIP	D
SMURF2	D
ELK3	D
NAV3	D
MIR503HG	D
CPNE5	D
EGR1	D
VCAM1	D
KRTAP4-9	D
XIRP1	D
KRTAP2-3	D
MYEOV	D
ANGPTL4	D
ANKRD1	D
FGF5	D
H3F3A	C
SCARF1	C
TGIF2-C20orf24	C
PCDHGA10	C
RN7SL2	C
FBXL2	C
TRPC4	C
F2RL1	C
SERPINB7	C
TNF	C
CYP24A1	C
KBTBD8	C
LINC01003	C
SCARF2	C
SLC41A2	C
FLT1	C
SH3RF2	C
ADAMTS12	C
XKR9	C
EPHA2	C
LIF	C
PLXNA2	C
LTBP2	C
LOXL1-AS1	C
SCHIP1	C
ETS1	C
EVA1A	C
LINC00969	A
CBWD3	A
PAG1	A
FBXO10	A
SLIT2	A
CFB	A
C17orf100	A
LOC653513	A
TFAP2A-AS1	A
REP15	A
GBP2	A
IFI27	A
JHDM1D-AS1	A

Gene	Gene cluster
OAF	A
ACSS1	A
APOL3	A
IL11	B
PPAP2B	B
AVPI1	B
CD24	B
TFPI2	B
C11orf96	B
LYPD1	B
MYPN	B
ANXA10	B
NCKAP5	B
HKDC1	B
CD74	B
IDO1	B
CCDC85A	B
EPHA5	B
ACTRT3	B
STAMBPL1	B
SUCLG2-AS1	B
ADAM12	B
TLR3	B
TVP23A	B
ONECUT2	B
ZNF747	B
DDIT4	B
PMEPA1	B
FAS	B
ADARB1	B
GABARAPL1	B
SYNPO	B
EBF1	B
CREM	B
FAT4	B
TNFSF10	B
DNER	B
IGFN1	B
ATOH8	B
GNG4	B
PDE4D	B
GPRC5C	B
IGFBP4	B
HLA-DRA	B
PTGES	B
CCL20	B
CRISPLD2	B
NFATC2	B
RGS2	B
SCG2	B
SPTLC3	B
RUNX3	B
AKAP12	B
KIAA1644	B
NR4A1	B
ID4	B
MAP2K6	B
LINC00673	B
EDN2	B
FAM49A	B
WNT10B	B
CHMP1B	B
FAM167A	B
PID1	B
STC1	B
SAA2	B
WFDC21P	B
GPRC5A	B
ZDHHC14	B
BTN3A3	B
FLRT2	B
ISG20	B
SNAP25	B
AQP3	B
ELOVL7	B
KITLG	B
LRRC4C	B
SIK1	B
ARHGAP6	B
CD200	B
ARRDC3	B
IL15	B
BCL7A	B
EPAS1	B

Gene	Gene cluster
KIAA1217	B
SLC7A5	B
WDR66	B
SNAI1	B
METRNL	B
SMAD6	B
HIVEP3	B
C15orf48	B
LRIG1	B
CITED4	B
DAW1	B
ELF3	B
CTIF	B
RAB42	B
GREM1	B
NFATC1	B
CSF2RB	B
PRKCE	B
ELAVL2	B
HES1	B
MLPH	B
LOC728554	B
ZNF436	B
FIBCD1	B
TNFRSF11B	B
IL6	B
KCTD18	B
MIR1244-1	B
NR4A2	E
DIO2	E
NHS	E
TM4SF1	E
SLC7A8	E
NR4A3	E
PDE3A	E
SMOC1	E
NPTX1	E
C8orf31	E
LINC00473	E
CSGALNACT1	E
PDE7B	E
CDKN1C	E

Supplementary Table S5: Results of statistical analysis.

Figure 8c-e

Model	Chisq	Df	Pr>Chisq	
(Intercept)	421.5095	1.0000	0.0000	***
Time	126.8046	1.0000	0.0000	***
Experimental condition	1317.4295	21.0000	0.0000	***
Time:Experimental condition	312.4654	21.0000	0.0000	***

Posthoc comparisons	Estimate	Std.Error	z.value	Pr>z	
Baseline:Empty vector_CNO_10µM - Ligand:Empty vector_CNO_10µM	-0.5589	0.2798	-1.9971	0.4030	n.s.
Baseline:Empty vector_Levalbuterol_10µM - Ligand:Empty vector_Levalbuterol_10µM	-3.1122	0.3702	-8.4068	0.0000	***
Baseline:rM3Ds_CNO_10µM - Ligand:rM3Ds_CNO_10µM	-2.1796	0.4275	-5.0989	0.0000	***
Baseline:hM4Di_CNO_10µM - Ligand:hM4Di_CNO_10µM	-1.4679	0.3239	-4.5320	0.0001	***
Baseline:hM3Dq_CNO_10µM - Ligand:hM3Dq_CNO_10µM	-1.3507	0.3702	-3.6486	0.0029	**
Baseline:DREADD-β2AR_CNO_10µM - Ligand:DREADD-β2AR_CNO_10µM	-5.5240	0.3702	-14.9217	0.0000	***
Baseline:DREADD-β2AR_CNO_1µM - Ligand:DREADD-β2AR_CNO_1µM	-5.1272	0.3702	-13.8497	0.0000	***
Baseline:DREADD-β2AR_CNO_0.1µM - Ligand:DREADD-β2AR_CNO_0.1µM	-4.4378	0.3702	-11.9874	0.0000	***

Figure 10b

Groups	Estimate	Statistic	p.value	Parameter	Conf.low	Conf.high	Method	Alternative	
hM3Dq_CNO	2.3661	15.7987	0.0040	2.0000	1.9941	2.7381	One Sample t-test	two.sided	**
rM3Ds_CNO	0.5816	-5.5035	0.0315	2.0000	0.2544	0.9087	One Sample t-test	two.sided	*
hM4Di_CNO	0.4994	-27.4606	0.0013	2.0000	0.4210	0.5779	One Sample t-test	two.sided	**
DREADD-β2AR_CNO	0.1987	-57.9626	0.0003	2.0000	0.1392	0.2582	One Sample t-test	two.sided	***
β2AR_Levalbuterol	0.2387	-33.0845	0.0009	2.0000	0.1396	0.3377	One Sample t-test	two.sided	***
Empty vector_CNO	0.9445	-3.0876	0.0908	2.0000	0.8673	1.0218	One Sample t-test	two.sided	n.s.
Empty vector_Levalbuterol	0.6386	-13.6055	0.0054	2.0000	0.5243	0.7529	One Sample t-test	two.sided	**

Figure 11c

Groups	Estimate	Statistic	p.value	Parameter	Conf.low	Conf.high	Method	Alternative	
hM3Dq	0.9816	-0.2676	0.8064	3.0000	0.7621	1.2010	One Sample t-test	two.sided	n.s.
rM3Ds	12.3305	6.1650	0.0086	3.0000	6.4816	18.1794	One Sample t-test	two.sided	**
hM4Di	1.0469	0.8137	0.4754	3.0000	0.8635	1.2303	One Sample t-test	two.sided	n.s.
DREADD-β2AR	3.0898	5.5189	0.0117	3.0000	1.8847	4.2948	One Sample t-test	two.sided	*
β2AR	7.9563	5.8583	0.0099	3.0000	4.1774	11.7352	One Sample t-test	two.sided	**

Figure 11e

Groups	Estimate	Statistic	p.value	Parameter	Conf.low	Conf.high	Method	Alternative	
hM3Dq	0.7301	-5.9780	0.0010	6.0000	0.6196	0.8405	One Sample t-test	two.sided	***
rM3Ds	0.0676	-47.8805	0.0000	3.0000	0.0056	0.1296	One Sample t-test	two.sided	***
hM4Di	1.2098	1.2561	0.2980	3.0000	0.6783	1.7412	One Sample t-test	two.sided	n.s.
DREADD-β2AR	0.3077	-17.4916	0.0000	6.0000	0.2109	0.4046	One Sample t-test	two.sided	***
β2AR	0.1679	-62.7726	0.0000	8.0000	0.1374	0.1985	One Sample t-test	two.sided	***

Figure 12b

Model	Chisq	Df	Pr>Chisq	
(Intercept)	228.6208	1.0000	0.0000	***
Time_min	1.9352	1.0000	0.1642	n.s.
Current_treatment_Receptor	417.1650	7.0000	0.0000	***
Time_min:Current_treatment_Receptor	14.1726	7.0000	0.0482	*

Posthoc comparisons	Estimate	Std. Error	z.value	Pr>z	
Baseline:β2AR-SmBiT - Ligand:β2AR-SmBiT	-0.9549	0.1405	-6.7947	0.0000	***
Baseline:DREADD-β2AR-SmBiT - Ligand:DREADD-β2AR-SmBiT	-0.3708	0.1257	-2.9496	0.0127	*

Figure 13a

DREADD-β2AR treated with CNO

Model	Chisq	Df	Pr>Chisq	
(Intercept)	99.5762	1.0000	0.0000	***
Experimental condition	9.8080	3.0000	0.0203	*

Posthoc comparisons	Estimate	Std.Error	z.value	Pr>z	
untreated - 2min	-0.4316	0.1420	-3.0393	0.0065	**
untreated - 5min	-0.2188	0.1420	-1.5410	0.2849	n.s.
untreated - 15min	-0.1293	0.1420	-0.9101	0.6874	n.s.

β2AR treated with Levalbuterol

Model	Chisq	Df	Pr>Chisq	
(Intercept)	109.5771	1.0000	0.0000	***
Experimental condition	264.7820	3.0000	0.0000	***

Posthoc comparisons	Estimate	Std.Error	z.value	Pr>z	
untreated - 2min	-0.8846	0.0563	-15.7143	0.0000	***
untreated - 5min	-0.4498	0.0563	-7.9900	0.0000	***
untreated - 15min	-0.2508	0.0563	-4.4546	0.0000	***

Figure 13a

Empty vector treated with CNO

Model	Chisq	Df	Pr>Chisq	
(Intercept)	7.8311	1.0000	0.0051	**
Experimental condition	2.2282	3.0000	0.5264	n.s.

Posthoc comparisons	Estimate	Std.Error	z.value	Pr>z	
untreated - 2min	0.0037	0.0249	0.1497	0.9976	n.s.
untreated - 5min	0.0262	0.0249	1.0533	0.5868	n.s.
untreated - 15min	-0.0096	0.0249	-0.3862	0.9629	n.s.

Empty vector treated with Levalbuterol

Model	Chisq	Df	Pr>Chisq	
(Intercept)	4.3722	1.0000	0.0365	*
Experimental condition	20.7822	3.0000	0.0001	***

Posthoc comparisons	Estimate	Std.Error	z.value	Pr>z	
untreated - 2min	-0.1431	0.0326	-4.3944	0.0000	***
untreated - 5min	-0.0951	0.0326	-2.9203	0.0098	**
untreated - 15min	-0.0560	0.0326	-1.7199	0.2052	n.s.

Figure 13b

Comparison	Estimate	Estimate1	Estimate2	Statistic	p.value	Parameter	Conf.low	Conf.high	Method	Alternative	
Empty vector - β2AR	-0.1604	0.0363	0.1967	-7.3062	0.0019	4.0000	-0.2214	-0.0995	Two Sample t-test	two.sided	**
Empty vector - DREADD-β2AR	-0.3948	0.0659	0.4607	-3.2610	0.0311	4.0000	-0.7310	-0.0587	Two Sample t-test	two.sided	*

Figure 14e

Model	Sum.Sq	Df	F.value	Pr>F	
(Intercept)	3781.5080	1	131.0128	0.0000	***
Experimental condition	839.1230	6	4.8453	0.0003	***
Residuals	2568.8647	89			

Posthoc comparisons	Estimate	Std.Error	t.value	Pr>t	
CNO 15min - Vehicle 15min	0.6807	2.0693	0.3290	0.9827	n.s.
CNO 30min - Vehicle 30min	3.0933	2.2908	1.3503	0.4467	n.s.
CNO 60min - Vehicle 60min	6.7342	1.8459	3.6481	0.0014	**

Figure 16e

Model	Chisq	Df	Pr>Chisq	
(Intercept)	233.1706	1.0000	0.0000	***
Time	37.5278	1.0000	0.0000	***
Experimental_Condition	54.2834	7.0000	0.0000	***
Time:Experimental_Condition	47.0833	7.0000	0.0000	***

Posthoc comparisons	Estimate	Std. Error	z.value	Pr>z	
Baseline:Non-transduced_Levalbuterol - Ligand:Non-transduced_Levalbuterol	-196.8208	39.1935	-5.0218	0.0000	***
Baseline:Non-transduced_Vehicle - Ligand:Non-transduced_Vehicle	-39.1687	30.3591	-1.2902	0.5842	n.s.
Baseline:DREADD-β2AR_CNO - Ligand:DREADD-β2AR_CNO	-126.1303	37.9489	-3.3237	0.0035	**
Baseline:Non-transduced_CNO - Ligand:Non-transduced_CNO	-35.5406	39.1935	-0.9068	0.8369	n.s.

Figure 17

Model	Sum.Sq	Df	F.value	Pr>F	
(Intercept)	929.9056	1.0000	174597.0953	0.0000	***
Group_Time	6.8205	23.0000	55.6782	0.0000	***
Residuals	4.4099	828.0000			

Posthoc comparisons

1 minute time point	Estimate	Std. Error	t.value	Pr>t	
1min:Non-transduced_Vehicle - 1min:Non-transduced_CNO	-0.0059	0.0169	-0.3487	1.0000	n.s.
1min:Non-transduced_Vehicle - 1min:DREADD-β2AR_CNO	-0.0009	0.0165	-0.0558	1.0000	n.s.
1min:Non-transduced_Vehicle - 1min:Non-transduced_Levalbuterol	0.0141	0.0169	0.8387	1.0000	n.s.
1min:Non-transduced_CNO - 1min:DREADD-β2AR_CNO	0.0050	0.0185	0.2672	1.0000	n.s.
1min:Non-transduced_CNO - 1min:Non-transduced_Levalbuterol	0.0200	0.0188	1.0620	0.9994	n.s.
1min:DREADD-β2AR_CNO - 1min:Non-transduced_Levalbuterol	0.0151	0.0185	0.8118	1.0000	n.s.

5 minutes time point	Estimate	Std. Error	t.value	Pr>t	
5min:Non-transduced_Vehicle - 5min:Non-transduced_CNO	0.0051	0.0169	0.3002	1.0000	n.s.
5min:Non-transduced_Vehicle - 5min:DREADD-β2AR_CNO	0.0033	0.0165	0.2003	1.0000	n.s.
5min:Non-transduced_Vehicle - 5min:Non-transduced_Levalbuterol	0.0000	0.0169	-0.0008	1.0000	n.s.
5min:Non-transduced_CNO - 5min:DREADD-β2AR_CNO	-0.0018	0.0185	-0.0944	1.0000	n.s.
5min:Non-transduced_CNO - 5min:Non-transduced_Levalbuterol	-0.0051	0.0188	-0.2692	1.0000	n.s.
5min:DREADD-β2AR_CNO - 5min:Non-transduced_Levalbuterol	-0.0033	0.0185	-0.1792	1.0000	n.s.

Figure 17

10 minutes time point	Estimate	Std. Error	t.value	Pr>t	
10min:Non-transduced_Vehicle - 10min:Non-transduced_CNO	-0.0030	0.0169	-0.1786	1.0000	n.s.
10min:Non-transduced_Vehicle - 10min:DREADD-β2AR_CNO	-0.0066	0.0165	-0.3976	1.0000	n.s.
10min:Non-transduced_Vehicle - 10min:Non-transduced_Levalbuterol	-0.0195	0.0169	-1.1545	0.9982	n.s.
10min:Non-transduced_CNO - 10min:DREADD-β2AR_CNO	-0.0036	0.0185	-0.1919	1.0000	n.s.
10min:Non-transduced_CNO - 10min:Non-transduced_Levalbuterol	-0.0164	0.0188	-0.8729	1.0000	n.s.
10min:DREADD-β2AR_CNO - 10min:Non-transduced_Levalbuterol	-0.0129	0.0185	-0.6950	1.0000	n.s.

25 minutes time point	Estimate	Std. Error	t.value	Pr>t	
25min:Non-transduced_Vehicle - 25min:Non-transduced_CNO	-0.0056	0.0169	-0.3349	1.0000	n.s.
25min:Non-transduced_Vehicle - 25min:DREADD-β2AR_CNO	-0.0722	0.0165	-4.3717	0.0005	***
25min:Non-transduced_Vehicle - 25min:Non-transduced_Levalbuterol	-0.1344	0.0169	-7.9742	0.0000	***
25min:Non-transduced_CNO - 25min:DREADD-β2AR_CNO	-0.0666	0.0185	-3.5900	0.0119	*
25min:Non-transduced_CNO - 25min:Non-transduced_Levalbuterol	-0.1288	0.0188	-6.8328	0.0000	***
25min:DREADD-β2AR_CNO - 25min:Non-transduced_Levalbuterol	-0.0622	0.0185	-3.3522	0.0274	*

40 minutes time point	Estimate	Std. Error	t.value	Pr>t	
40min:Non-transduced_Vehicle - 40min:Non-transduced_CNO	0.0096	0.0169	0.5689	1.0000	n.s.
40min:Non-transduced_Vehicle - 40min:DREADD-β2AR_CNO	-0.1099	0.0165	-6.6490	0.0000	***
40min:Non-transduced_Vehicle - 40min:Non-transduced_Levalbuterol	-0.2045	0.0169	-12.1322	0.0000	***
40min:Non-transduced_CNO - 40min:DREADD-β2AR_CNO	-0.1194	0.0185	-6.4399	0.0000	***
40min:Non-transduced_CNO - 40min:Non-transduced_Levalbuterol	-0.2141	0.0188	-11.3602	0.0000	***
40min:DREADD-β2AR_CNO - 40min:Non-transduced_Levalbuterol	-0.0946	0.0185	-5.1020	0.0000	***

55 minutes time point	Estimate	Std. Error	t.value	Pr>t	
55min:Non-transduced_Vehicle - 55min:Non-transduced_CNO	0.0194	0.0169	1.1483	0.9983	n.s.
55min:Non-transduced_Vehicle - 55min:DREADD-β2AR_CNO	-0.1043	0.0165	-6.3103	0.0000	***
55min:Non-transduced_Vehicle - 55min:Non-transduced_Levalbuterol	-0.2298	0.0169	-13.6352	0.0000	***
55min:Non-transduced_CNO - 55min:DREADD-β2AR_CNO	-0.1236	0.0185	-6.6648	0.0000	***
55min:Non-transduced_CNO - 55min:Non-transduced_Levalbuterol	-0.2492	0.0188	-13.2228	0.0000	***
55min:DREADD-β2AR_CNO - 55min:Non-transduced_Levalbuterol	-0.1256	0.0185	-6.7695	0.0000	***

Figure 18c

Model	Chisq	Df	Pr>Chisq	
(Intercept)	421.5095	1.0000	0.0000	***
Time	126.8046	1.0000	0.0000	***
Experimental condition	1317.4295	21.0000	0.0000	***
Time:Experimental condition	312.4654	21.0000	0.0000	***

Posthoc comparisons	Estimate	Std.Error	z.value	Pr>z	
Baseline:Empty vector_CNO_10µM - Ligand:Empty vector_CNO_10µM	-0.5589	0.2798	-1.9971	0.4030	n.s.
Baseline:DREADD-GPR65_CNO_10µM - Ligand:DREADD-GPR65_CNO_10µM	-4.2552	0.3702	-11.4942	0.0000	***

Figure 18d

Groups	Estimate	Statistic	p.value	Parameter	Conf.low	Conf.high	Method	Alternative	
DREADD-GPR65_CNO	0.6742	-5.9997	0.0093	3.0000	0.5014	0.8470	One Sample t-test	two.sided	**
Empty vector_CNO	0.9445	-3.0876	0.0908	2.0000	0.8673	1.0218	One Sample t-test	two.sided	n.s.

Figure 18e

Model	Chisq	Df	Pr>Chisq	
(Intercept)	9.5047	1.0000	0.0020	**
Experimental condition	146.3962	5.0000	0.0000	***

Posthoc comparisons	Estimate	Std.Error	z.value	Pr>z	
Baseline:Empty vector - Ligand:Empty vector	-0.0116	0.0244	-0.4779	0.9859	n.s.
Baseline:Empty vector - Forskolin:Empty vector	0.0165	0.0244	0.6763	0.9499	n.s.
Ligand:Empty vector - Forskolin:Empty vector	0.0281	0.0201	1.3954	0.5663	n.s.
Baseline:DREADD-GPR109A - Ligand:DREADD-GPR109A	0.1154	0.0244	4.7401	0.0000	***
Baseline:DREADD-GPR109A - Forskolin:DREADD-GPR109A	0.1169	0.0244	4.7986	0.0000	***
Ligand:DREADD-GPR109A - Forskolin:DREADD-GPR109A	0.0014	0.0201	0.0707	1.0000	n.s.

Figure 19c

Groups	Estimate	Statistic	p.value	Parameter	Conf.low	Conf.high	Method	Alternative	
DREADD-GPR109A_CNO + NECA	0.7495	-4.0753	0.0267	3.0000	0.5539	0.9451	One Sample t-test	two.sided	*
Empty vector_CNO + NECA	1.1344	1.2348	0.3423	2.0000	0.6661	1.6028	One Sample t-test	two.sided	n.s.

Figure 19d

Groups	Estimate	Statistic	p.value	Parameter	Conf.low	Conf.high	Method	Alternative	
DREADD-GPR109A_CNO	0.9429	-0.6999	0.5564	2.0000	0.5922	1.2937	One Sample t-test	two.sided	n.s.
Empty vector_CNO	0.9433	-0.7825	0.4910	3.0000	0.7127	1.1739	One Sample t-test	two.sided	n.s.

Figure 19e

Groups	Estimate	Statistic	p.value	Parameter	Conf.low	Conf.high	Method	Alternative	
DREADD-GPR109A_CNO	1.1563	1.3514	0.2695	3.0000	0.7882	1.5244	One Sample t-test	two.sided	n.s.
Empty vector_CNO	0.9445	-3.0876	0.0908	2.0000	0.8673	1.0218	One Sample t-test	two.sided	n.s.

Figure 20b

Model	Chisq	Df	Pr>Chisq	
(Intercept)	228.6208	1.0000	0.0000	***
Time_min	1.9352	1.0000	0.1642	n.s.
Current_treatment_Receptor	417.1650	7.0000	0.0000	***
Time_min:Current_treatment_Receptor	14.1726	7.0000	0.0482	*

Posthoc comparisons	Estimate	Std. Error	z.value	Pr>z	
Baseline:DREADD-GPR65-SmBiT - Ligand:DREADD-GPR65-SmBiT	-0.6725	0.1623	-4.1443	0.0001	***
Baseline:DREADD-GPR109A-SmBiT - Ligand:DREADD-GPR109A-SmBiT	-2.4104	0.1623	-14.8542	0.0000	***

Figure 21c

Groups	Estimate	Statistic	p.value	Parameter	Conf.low	Conf.high	Method	Alternative	
hM3Dq	0.9816	-0.2676	0.8064	3.0000	0.7621	1.2010	One Sample t-test	two.sided	n.s.
rM3Ds	12.3305	6.1650	0.0086	3.0000	6.4816	18.1794	One Sample t-test	two.sided	**
hM4Di	1.0469	0.8137	0.4754	3.0000	0.8635	1.2303	One Sample t-test	two.sided	n.s.
DREADD-β2AR	3.0898	5.5189	0.0117	3.0000	1.8847	4.2948	One Sample t-test	two.sided	*
β2AR	7.9563	5.8583	0.0099	3.0000	4.1774	11.7352	One Sample t-test	two.sided	**
DREADD-mGPR65	11.8259	4.4136	0.0216	3.0000	4.0199	19.6319	One Sample t-test	two.sided	*
DREADD-mGPR109A	1.1242	1.6195	0.2038	3.0000	0.8801	1.3683	One Sample t-test	two.sided	n.s.

Figure 21e

Groups	Estimate	Statistic	p.value	Parameter	Conf.low	Conf.high	Method	Alternative	
hM3Dq	0.7301	-5.9780	0.0010	6.0000	0.6196	0.8405	One Sample t-test	two.sided	***
rM3Ds	0.0676	-47.8805	0.0000	3.0000	0.0056	0.1296	One Sample t-test	two.sided	***
hM4Di	1.2098	1.2561	0.2980	3.0000	0.6783	1.7412	One Sample t-test	two.sided	n.s.
DREADD-β2AR	0.3077	-17.4916	0.0000	6.0000	0.2109	0.4046	One Sample t-test	two.sided	***
β2AR	0.1679	-62.7726	0.0000	8.0000	0.1374	0.1985	One Sample t-test	two.sided	***
DREADD-mGPR65	0.3363	-11.5054	0.0075	2.0000	0.0880	0.5845	One Sample t-test	two.sided	**
DREADD-mGPR109A	1.1800	0.7839	0.5152	2.0000	0.1922	2.1678	One Sample t-test	two.sided	n.s.

Figure 25

Groups	Estimate	Statistic	p.value	Parameter	Conf.low	Conf.high	Method	Alternative	
IL6	8.4459	13.8481	0.0000	7.0000	7.1745	9.7173	One Sample t-test	two.sided	***
TNF	12.2683	4.3548	0.0033	7.0000	6.1497	18.3868	One Sample t-test	two.sided	**
IL1β	2.2579	2.9269	0.0221	7.0000	1.2416	3.2741	One Sample t-test	two.sided	*

Figure 26a

Non-transduced cells: IL6

Model	Chisq	Df	Pr>Chisq	
(Intercept)	398.1280	1.0000	0.0000	***
Experimental condition	2946.2105	2.0000	0.0000	***

Posthoc comparisons	Estimate	Std.Error	z.value	Pr>z	
IFNγ/IL1β - LB	2.5213	0.0705	35.7566	0.0000	***
IFNγ/IL1β+LB - LB	3.7544	0.0705	53.2443	0.0000	***
IFNγ/IL1β+LB - IFNγ/IL1β	1.2331	0.0705	17.4877	0.0000	***

Non-transduced cells: TNF

Model	Chisq	Df	Pr>Chisq	
(Intercept)	9.9774	1.0000	0.0016	**
Experimental condition	1384.6875	2.0000	0.0000	***

Posthoc comparisons	Estimate	Std.Error	z.value	Pr>z	
IFNγ/IL1β - LB	4.3858	0.1261	34.7933	0.0000	***
IFNγ/IL1β+LB - LB	3.6333	0.1261	28.8240	0.0000	***
IFNγ/IL1β+LB - IFNγ/IL1β	-0.7524	0.1261	-5.9693	0.0000	***

Non-transduced cells: IL1β

Model	Chisq	Df	Pr>Chisq	
(Intercept)	8.6739	1.0000	0.0032	**
Experimental condition	14.8634	2.0000	0.0006	***

Posthoc comparisons	Estimate	Std.Error	z.value	Pr>z	
IFNγ/IL1β - LB	1.0635	0.3065	3.4699	0.0015	**
IFNγ/IL1β+LB - LB	0.9778	0.3065	3.1901	0.0043	**
IFNγ/IL1β+LB - IFNγ/IL1β	-0.0858	0.3065	-0.2798	0.9578	n.s.

Figure 26b

DREADD-β2AR: IL6

Model	Chisq	Df	Pr>Chisq	
(Intercept)	90.4207	1.0000	0.0000	***
Experimental condition	665.2528	2.0000	0.0000	***

Posthoc comparisons	Estimate	Std.Error	z.value	Pr>z	
IFNγ/IL1β - CNO	2.4466	0.1561	15.6736	0.0000	***
IFNγ/IL1β+CNO - CNO	3.9923	0.1561	25.5764	0.0000	***
IFNγ/IL1β+CNO - IFNγ/IL1β	1.5458	0.1561	9.9029	0.0000	***

DREADD-β2AR: TNF

Model	Chisq	Df	Pr>Chisq	
(Intercept)	17.7278	1.0000	0.0000	***
Experimental condition	781.6119	2.0000	0.0000	***

Posthoc comparisons	Estimate	Std.Error	z.value	Pr>z	
IFNγ/IL1β - CNO	4.0799	0.1515	26.9290	0.0000	***
IFNγ/IL1β+CNO - CNO	3.0257	0.1515	19.9707	0.0000	***
IFNγ/IL1β+CNO - IFNγ/IL1β	-1.0542	0.1515	-6.9583	0.0000	***

DREADD-β2AR: IL1β

Model	Chisq	Df	Pr>Chisq	
(Intercept)	4.9873	1.0000	0.0255	*
Experimental condition	56.2445	2.0000	0.0000	***

Posthoc comparisons	Estimate	Std.Error	z.value	Pr>z	
IFNγ/IL1β - CNO	2.1010	0.3040	6.9117	0.0000	***
IFNγ/IL1β+CNO - CNO	1.8168	0.3040	5.9767	0.0000	***
IFNγ/IL1β+CNO - IFNγ/IL1β	-0.2842	0.3040	-0.9350	0.6181	n.s.

Figure 26c

Non-transduced cells: IL6

Model	Chisq	Df	Pr>Chisq	
(Intercept)	501.0771	1.0000	0.0000	***
Experimental condition	419.9402	2.0000	0.0000	***

Posthoc comparisons	Estimate	Std.Error	z.value	Pr>z	
IFNγ/IL1β - CNO	3.2941	0.1838	17.9183	0.0000	***
IFNγ/IL1β+CNO - CNO	3.2301	0.1838	17.5706	0.0000	***
IFNγ/IL1β+CNO - IFNγ/IL1β	-0.0639	0.1838	-0.3477	0.9355	n.s.

Non-transduced cells: TNF

Model	Chisq	Df	Pr>Chisq	
(Intercept)	63.4820	1.0000	0.0000	***
Experimental condition	1284.8449	2.0000	0.0000	***

Posthoc comparisons	Estimate	Std.Error	z.value	Pr>z	
IFNγ/IL1β - CNO	3.7620	0.1225	30.7063	0.0000	***
IFNγ/IL1β+CNO - CNO	3.8431	0.1225	31.3680	0.0000	***
IFNγ/IL1β+CNO - IFNγ/IL1β	0.0811	0.1225	0.6617	0.7857	n.s.

Non-transduced cells: IL1β

Model	Chisq	Df	Pr>Chisq	
(Intercept)	11.0622	1.0000	0.0009	***
Experimental condition	47.1863	2.0000	0.0000	***

Posthoc comparisons	Estimate	Std.Error	z.value	Pr>z	
IFNγ/IL1β - CNO	1.6799	0.2637	6.3705	0.0000	***
IFNγ/IL1β+CNO - CNO	1.4268	0.2637	5.4107	0.0000	***
IFNγ/IL1β+CNO - IFNγ/IL1β	-0.2531	0.2637	-0.9598	0.6024	n.s.

Figure 26d

DREADD-GPR65: IL6

Model	Chisq	Df	Pr>Chisq	
(Intercept)	123.0422	1.0000	0.0000	***
Experimental condition	595.8438	2.0000	0.0000	***

Posthoc comparisons	Estimate	Std.Error	z.value	Pr>z	
IFNγ/IL1β - CNO	2.3949	0.1647	14.5387	0.0000	***
IFNγ/IL1β+CNO - CNO	3.9947	0.1647	24.2503	0.0000	***
IFNγ/IL1β+CNO - IFNγ/IL1β	1.5998	0.1647	9.7116	0.0000	***

DREADD-GPR65: TNF

Model	Chisq	Df	Pr>Chisq	
(Intercept)	34.0849	1.0000	0.0000	***
Experimental condition	801.4208	2.0000	0.0000	***

Posthoc comparisons	Estimate	Std.Error	z.value	Pr>z	
IFNγ/IL1β - CNO	3.8366	0.1459	26.2932	0.0000	***
IFNγ/IL1β+CNO - CNO	3.2442	0.1459	22.2331	0.0000	***
IFNγ/IL1β+CNO - IFNγ/IL1β	-0.5924	0.1459	-4.0601	0.0002	***

DREADD-GPR65: IL1β

Model	Chisq	Df	Pr>Chisq	
(Intercept)	11.9318	1.0000	0.0006	***
Experimental condition	80.2268	2.0000	0.0000	***

Posthoc comparisons	Estimate	Std.Error	z.value	Pr>z	
IFNγ/IL1β - CNO	1.9961	0.2518	7.9278	0.0000	***
IFNγ/IL1β+CNO - CNO	1.9070	0.2518	7.5739	0.0000	***
IFNγ/IL1β+CNO - IFNγ/IL1β	-0.0891	0.2518	-0.3539	0.9333	n.s.

Figure 26e

DREADD-GPR109A: IL6

Model	Chisq	Df	Pr>Chisq	
(Intercept)	278.2546	1.0000	0.0000	***
Experimental condition	325.9092	2.0000	0.0000	***

Posthoc comparisons	Estimate	Std.Error	z.value	Pr>z	
IFNγ/IL1β - CNO	2.9557	0.2005	14.7435	0.0000	***
IFNγ/IL1β+CNO - CNO	3.2866	0.2005	16.3941	0.0000	***
IFNγ/IL1β+CNO - IFNγ/IL1β	0.3309	0.2005	1.6506	0.2245	n.s.

DREADD-GPR109A: TNF

Model	Chisq	Df	Pr>Chisq	
(Intercept)	58.9111	1.0000	0.0000	***
Experimental condition	246.5455	2.0000	0.0000	***

Posthoc comparisons	Estimate	Std.Error	z.value	Pr>z	
IFNγ/IL1β - CNO	3.1096	0.2369	13.1260	0.0000	***
IFNγ/IL1β+CNO - CNO	3.3228	0.2369	14.0256	0.0000	***
IFNγ/IL1β+CNO - IFNγ/IL1β	0.2131	0.2369	0.8996	0.6405	n.s.

DREADD-GPR109A: IL1β

Model	Chisq	Df	Pr>Chisq	
(Intercept)	38.6998	1.0000	0.0000	***
Experimental condition	42.0871	2.0000	0.0000	***

Posthoc comparisons	Estimate	Std.Error	z.value	Pr>z	
IFNγ/IL1β - CNO	1.2774	0.2823	4.5244	0.0000	***
IFNγ/IL1β+CNO - CNO	1.7755	0.2823	6.2887	0.0000	***
IFNγ/IL1β+CNO - IFNγ/IL1β	0.4981	0.2823	1.7643	0.1817	n.s.

Figure 26f

Non-transduced cells: IL6

Model	Chisq	Df	Pr>Chisq	
(Intercept)	1022.2289	1.0000	0.0000	***
Experimental condition	1032.8352	2.0000	0.0000	***

Posthoc comparisons	Estimate	Std.Error	z.value	Pr>z	
IFNγ/IL1β - FSK	1.7688	0.1187	14.9017	0.0000	***
IFNγ/IL1β+FSK - FSK	3.8113	0.1187	32.1101	0.0000	***
IFNγ/IL1β+FSK - IFNγ/IL1β	2.0425	0.1187	17.2084	0.0000	***

Non-transduced cells: TNF

Model	Chisq	Df	Pr>Chisq	
(Intercept)	9.1921	1.0000	0.0024	**
Experimental condition	329.0545	2.0000	0.0000	***

Posthoc comparisons	Estimate	Std.Error	z.value	Pr>z	
IFNγ/IL1β - FSK	4.9054	0.2714	18.0741	0.0000	***
IFNγ/IL1β+FSK - FSK	2.8155	0.2714	10.3736	0.0000	***
IFNγ/IL1β+FSK - IFNγ/IL1β	-2.0900	0.2714	-7.7005	0.0000	***

Non-transduced cells: IL1β

Model	Chisq	Df	Pr>Chisq	
(Intercept)	0.0878	1.0000	0.7670	n.s.
Experimental condition	95.6775	2.0000	0.0000	***

Posthoc comparisons	Estimate	Std.Error	z.value	Pr>z	
IFNγ/IL1β - FSK	1.1804	0.1276	9.2525	0.0000	***
IFNγ/IL1β+FSK - FSK	0.2396	0.1276	1.8784	0.1449	n.s.
IFNγ/IL1β+FSK - IFNγ/IL1β	-0.9408	0.1276	-7.3742	0.0000	***

Figure 33e

Crushed retina

Model	Sum.Sq	Df	F.value	Pr>F	
(Intercept)	13.8082	1.0000	53.8157	0.0000	
Experimental condition	3.1802	2.0000	6.1973	0.0203	
Residuals	2.3092	9.0000	#N/A	#N/A	
Posthoc comparisons	**Estimate**	**Std.Error**	**t.value**	**Pr>t**	
hM4Di:CNO - hM4Di:Saline	1.1130	0.3582	3.1075	0.0305	*
Wild type:CNO - hM4Di:Saline	0.0432	0.3582	0.1207	0.9920	n.s.
Wild type:CNO - hM4Di:CNO	-1.0698	0.3582	-2.9868	0.0368	*

Non-crushed retina

Model	Sum.Sq	Df	F.value	Pr>F
(Intercept)	1.4460	1.0000	70.4601	0.0000
Experimental condition	0.1598	2.0000	3.8930	0.0605
Residuals	0.1847	9.0000	#N/A	#N/A
Posthoc comparisons	**Estimate**	**Std.Error**	**t.value**	**Pr>t**
hM4Di:CNO - hM4Di:Saline	-0.2724	0.1013	-2.6888	0.0588
Wild type:CNO - hM4Di:Saline	-0.2016	0.1013	-1.9904	0.1701
Wild type:CNO - hM4Di:CNO	0.0708	0.1013	0.6984	0.7704

7 References

1. Stevens, R. C. *et al.* The GPCR Network: a large-scale collaboration to determine human GPCR structure and function. *Nature reviews. Drug discovery* 12, 25–34 (2013).
2. Fredriksson, R. The G-Protein-Coupled Receptors in the Human Genome Form Five Main Families. Phylogenetic Analysis, Paralogon Groups, and Fingerprints. *Molecular Pharmacology* 63, 1256–1272 (2003).
3. Sun, L. & Ye, R. D. Role of G protein-coupled receptors in inflammation. *Acta pharmacologica Sinica* 33, 342–50 (2012).
4. Wettschureck, N. & Offermanns, S. Mammalian G Proteins and Their Cell Type Specific Functions. *Physilological Review* 1159–1204 (2005). doi:10.1152/physrev.00003.2005.
5. Tang, X., Wang, Y., Li, D., Luo, J. & Liu, M. Orphan G protein-coupled receptors (GPCRs): biological functions and potential drug targets. *Acta Pharmacologica Sinica* 33, 363–371 (2012).
6. Sriram, K. & Insel, P. A. G protein-coupled receptors as targets for approved drugs: How many targets and how many drugs? in *Molecular Pharmacology* 93, 251–258 (American Society for Pharmacology and Experimental Therapy, 2018).
7. Alexander, S. P. H. *et al.* Class A Orphans (version 2020.5) in the IUPHAR/BPS Guide to Pharmacology Database. *IUPHAR/BPS Guide to Pharmacology CITE* 2020, (2020).
8. Bikle, D., Bräuner-Osborne, H., Brown, E. M., Conigrave, A. & Shoback, D. Class C Orphans (version 2019.4) in the IUPHAR/BPS Guide to Pharmacology Database. *IUPHAR/BPS Guide to Pharmacology CITE* 2019, (2019).
9. Wu, L. *et al.* Bidirectional role of β2-adrenergic receptor in autoimmune diseases. *Frontiers in Pharmacology* (2018). doi:10.3389/fphar.2018.01313
10. Johnson, M. Molecular mechanisms of β2-adrenergic receptor function, response, and regulation. *Journal of Allergy and Clinical Immunology* (2006). doi:10.1016/j.jaci.2005.11.012
11. Philipson, L. H. β-agonists and metabolism. in *Journal of Allergy and Clinical Immunology* (2002). doi:10.1067/mai.2002.129702
12. O'Donnell, J., Zeppenfeld, D., McConnell, E., Pena, S. & Nedergaard, M. Norepinephrine: A neuromodulator that boosts the function of multiple cell types to optimize CNS performance. *Neurochemical Research* (2012). doi:10.1007/s11064-012-0818-x
13. Karnik, S., Gogonea, C., Patil, S., Saad, Y. & Takezako, T. Activation of G-protein-coupled receptors: a common molecular mechanism. *Trends in Endocrinology and Metabolism* 14, 431–437 (2003).
14. Sandhu, M. *et al.* Conformational plasticity of the intracellular cavity of GPCR–G-protein complexes leads to G-protein promiscuity and selectivity. *Proceedings of the National Academy of Sciences of the United States of America* (2019). doi:10.1073/pnas.1820944116
15. Abreu, A. P. *et al.* Evidence of the importance of the first intracellular loop of prokineticin receptor 2 in receptor function. *Molecular Endocrinology* (2012). doi:10.1210/me.2012-1102
16. Wess, J. Molecular basis of receptor/G-protein-coupling selectivity. *Pharmacology and Therapeutics* (1998). doi:10.1016/S0163-7258(98)00030-8
17. Zhang, B., Yang, X. & Tiberi, M. Functional importance of two conserved residues in intracellular loop 1 and transmembrane region 2 of Family A GPCRs: Insights from ligand binding and signal transduction responses of D1 and D5 dopaminergic receptor mutants. *Cellular Signalling* (2015). doi:10.1016/j.cellsig.2015.07.006
18. Preininger, A. M. & Hamm, H. E. G protein signaling: insights from new structures. *Science Signaling* 2004, re3 (2004).
19. Krasel, C. *et al.* Dual role of the β2-adrenergic receptor C terminus for the binding of β-arrestin and receptor internalization. *Journal of Biological Chemistry* (2008). doi:10.1074/jbc.M806086200
20. Luttrell, L. M. & Gesty-Palmer, D. Beyond desensitization: Physiological relevance of arrestin-dependent signaling. *Pharmacological Reviews* (2010). doi:10.1124/pr.109.002436
21. Bruchas, M. R., Macey, T. A., Lowe, J. D. & Chavkin, C. Kappa opioid receptor activation of p38 MAPK is GRK3- and arrestin-dependent in neurons and astrocytes. *Journal of Biological Chemistry* (2006). doi:10.1074/jbc.M513640200
22. Wei, H. *et al.* Independent β-arrestin 2 and G protein-mediated pathways for angiotensin II activation of extracellular signal-regulated kinases 1 and 2. *Proceedings of the National Academy of Sciences of the United States of America* (2003). doi:10.1073/pnas.1834556100
23. Ren, X. R. *et al.* Different G protein-coupled receptor kinases govern G protein and β-arrestin-mediated signaling of V2 vasopressin receptor. *Proceedings of the National Academy of Sciences of the United States of America* (2005). doi:10.1073/pnas.0409534102
24. Ahn, S., Shenoy, S. K., Wei, H. & Lefkowitz, R. J. Differential kinetic and spatial patterns of β-arrestin and G protein-mediated ERK activation by the angiotensin II receptor. *Journal of Biological Chemistry* (2004). doi:10.1074/jbc.M405878200
25. Shenoy, S. K. *et al.* β-arrestin-dependent, G protein-independent ERK1/2 activation by the β2 adrenergic receptor. *Journal of Biological Chemistry* (2006). doi:10.1074/jbc.M506576200
26. Kim, J. M. *et al.* Light-driven activation of β2-adrenergic receptor signaling by a chimeric rhodopsin containing the β2-adrenergic receptor cytoplasmic loops. *Biochemistry* 44, 2284–2292 (2005).
27. Airan, R. D., Thompson, K. R., Fenno, L. E., Bernstein, H. & Deisseroth, K. Temporally precise in vivo control of intracellular signalling. *Nature* 458, 1025–1029 (2009).
28. van Wyk, M., Pielecka-Fortuna, J., Löwel, S. & Kleinlogel, S. Restoring the ON Switch in Blind Retinas: Opto-mGluR6, a Next-Generation, Cell-Tailored Optogenetic Tool. *PLoS Biology* 13, (2015).
29. Kleinlogel, S. Optogenetic user's guide to Opto-GPCRs. *Frontiers in Bioscience (Landmark Edition)* 21, 794–805 (2016).

30. Morri, M. *et al.* Optical functionalization of human Class A orphan G-protein-coupled receptors. *Nature Communications* (2018). doi:10.1038/s41467-018-04342-1

31. Tichy, A. M., Gerrard, E. J., Sexton, P. M. & Janovjak, H. Light-activated chimeric GPCRs: limitations and opportunities. *Current Opinion in Structural Biology* (2019). doi:10.1016/j.sbi.2019.05.006

32. Cheng, K. P., Kiernan, E. A., Eliceiri, K. W., Williams, J. C. & Watters, J. J. Blue Light Modulates Murine Microglial Gene Expression in the Absence of Optogenetic Protein Expression. *Scientific Reports* (2016). doi:10.1038/srep21172

33. Stockley, J. H. *et al.* Surpassing light-induced cell damage in vitro with novel cell culture media. *Scientific Reports* (2017). doi:10.1038/s41598-017-00829-x

34. Tyssowski, K. M. & Gray, J. M. Blue light increases neuronal activity-regulated gene expression in the absence of optogenetic proteins. *eNeuro* (2019). doi:10.1523/ENEURO.0085-19.2019

35. Duke, C. G., Savell, K. E., Tuscher, J. J., Phillips, R. A. & Day, J. J. Blue light-induced gene expression alterations in cultured neurons are the result of phototoxic interactions with neuronal culture media. *eNeuro* (2020). doi:10.1523/ENEURO.0386-19.2019

36. Delbeke, J., Hoffman, L., Mols, K., Braeken, D. & Prodanov, D. And then there was light: Perspectives of optogenetics for deep brain stimulation and neuromodulation. *Frontiers in Neuroscience* (2017). doi:10.3389/fnins.2017.00663

37. Tan, J. K., McKenzie, C., Mariño, E., Macia, L. & Mackay, C. R. Metabolite-sensing G protein-coupled receptors-facilitators of diet-related immune regulation. *Annual Review of Immunology* (2017). doi:10.1146/annurev-immunol-051116-052235

38. Wang, X., Iyer, A., Lyons, A. B., Körner, H. & Wei, W. Emerging roles for G-protein coupled receptors in development and activation of macrophages. *Frontiers in Immunology* (2019). doi:10.3389/fimmu.2019.02031

39. Armbruster, B. N., Li, X., Pausch, M. H., Herlitze, S. & Roth, B. L. Evolving the lock to fit the key to create a family of G protein-coupled receptors potently activated by an inert ligand. *Proceedings of the National Academy of Sciences of the United States of America* 104, 5163–8 (2007).

40. Farrell, M. S. & Roth, B. L. Pharmacosynthetics: Reimagining the pharmacogenetic approach. *Brain research* 1511, 6–20 (2013).

41. Urban, D. J. & Roth, B. L. DREADDs (Designer Receptors Exclusively Activated by Designer Drugs): Chemogenetic Tools with Therapeutic Utility. *Annual Review of Pharmacology and Toxicology* 55, 399–417 (2015).

42. Jendryka, M. *et al.* Pharmacokinetic and pharmacodynamic actions of clozapine-N-oxide, clozapine, and compound 21 in DREADD-based chemogenetics in mice. *Scientific Reports* (2019). doi:10.1038/s41598-019-41088-2

43. Guettier, J.-M. *et al.* A chemical-genetic approach to study G protein regulation of beta cell function in vivo. *Proceedings of the National Academy of Sciences of the United States of America* 106, 19197–202 (2009).

44. Qian, L. *et al.* β2 adrenergic receptor activation induces microglial NADPH oxidase activation and dopaminergic neurotoxicity through an ERK-dependent/protein kinase A-independent pathway. *GLIA* (2009). doi:10.1002/glia.20873

45. Bernier, L. P. *et al.* Nanoscale Surveillance of the Brain by Microglia via cAMP-Regulated Filopodia. *Cell Reports* (2019). doi:10.1016/j.celrep.2019.05.010

46. Siegert, S. *et al.* Transcriptional code and disease map for adult retinal cell types. *Nat Neurosci* 15, 487–95, S1-2 (2012).

47. Edgar, R. C. MUSCLE: Multiple sequence alignment with high accuracy and high throughput. *Nucleic Acids Res* 32, 1792–1797 (2004).

48. Krogh, A., Larsson, B., von Heijne, G. & Sonnhammer, E. L. . Predicting transmembrane protein topology with a hidden markov model: application to complete genomes11Edited by F. Cohen. *Journal of Molecular Biology* 305, 567–580 (2001).

49. Almagro Armenteros, J. J. *et al.* SignalP 5.0 improves signal peptide predictions using deep neural networks. *Nature Biotechnology* (2019). doi:10.1038/s41587-019-0036-z

50. Dupuis, N. *et al.* Activation of the orphan G protein-coupled receptor GPR27 by surrogate ligands promotes β-arrestin 2 recruitment. *Molecular Pharmacology* (2017). doi:10.1124/mol.116.107714

51. Guan, X. M., Tong Sun Kobilka & Kobilka, B. K. Enhancement of membrane insertion and function in a type IIIb membrane protein following introduction of a cleavable signal peptide. *Journal of Biological Chemistry* (1992).

52. Soldati, T. & Perriard, J. C. Intracompartmental sorting of essential myosin light chains: Molecular dissection and in vivo monitoring by epitope tagging. *Cell* 66, 277–289 (1991).

53. Pujar, S. *et al.* Consensus coding sequence (CCDS) database: A standardized set of human and mouse protein-coding regions supported by expert curation. *Nucleic Acids Research* (2018). doi:10.1093/nar/gkx1031

54. Akerblom, M. *et al.* Visualization and genetic modification of resident brain microglia using lentiviral vectors regulated by microRNA-9. *Nat Commun* 4, 1770 (2013).

55. Brawek, B. *et al.* A new approach for ratiometric in vivo calcium imaging of microglia. *Scientific Reports* 7, (2017).

56. Buccioni, M. *et al.* Innovative functional cAMP assay for studying G protein-coupled receptors: Application to the pharmacological characterization of GPR17. *Purinergic Signalling* 7, 463–468 (2011).

57. Gilissen, J. *et al.* Forskolin-free cAMP assay for Gi-coupled receptors. *Biochemical Pharmacology* (2015). doi:10.1016/j.bcp.2015.09.010

58. Cheng, Z. *et al.* Luciferase Reporter Assay System for Deciphering GPCR Pathways. *Current chemical genomics* 4, 84–91 (2010).

59. Bronstein, R., Torres, L., Nissen, J. C. & Tsirka, S. E. Culturing Microglia from the Neonatal and Adult Central Nervous System. *Journal of Visualized Experiments* (2013). doi:10.3791/50647

60. Bohlen, C. J. *et al.* Diverse Requirements for Microglial Survival, Specification, and Function Revealed by Defined-Medium Cultures. *Neuron* (2017). doi:10.1016/j.neuron.2017.04.043

61. Artimovich, E., Jackson, R. K., Kilander, M. B. C., Lin, Y. C. & Nestor, M. W. PeakCaller: an automated graphical interface for the quantification of intracellular calcium obtained by high-content screening. *BMC Neuroscience* 18, 72 (2017).

62. Patro, R., Duggal, G., Love, M. I., Irizarry, R. A. & Kingsford, C. Salmon: fast and bias-aware quantification of transcript expression using dual-phase inference. doi:10.1038/nmeth.4197

63. Love, M. I., Huber, W. & Anders, S. Moderated estimation of fold change and dispersion for RNA-seq data with DESeq2. *Genome Biology* 15, 1–21 (2014).

64. Alexa, A., Rahnenführer, J. & Lengauer, T. Improved scoring of functional groups from gene expression data by decorrelating GO graph structure. *Bioinformatics* 22, 1600–1607 (2006).

65. Ackermann, M. & Strimmer, K. A general modular framework for gene set enrichment analysis. *BMC Bioinformatics* 10, 1–20 (2009).

66. Parkhurst, C. N. *et al.* Microglia promote learning-dependent synapse formation through brain-derived neurotrophic factor. *Cell* 155, 1596–1609 (2013).

67. Bates, D., Mächler, M., Bolker, B. M. & Walker, S. C. Fitting linear mixed-effects models using lme4. *Journal of Statistical Software* 67, 1–48 (2015).

68. Hothorn, T., Bretz, F. & Westfall, P. Simultaneous inference in general parametric models. *Biometrical Journal* 50, 346–363 (2008).

69. Wolf, S. A., Boddeke, H. W. G. M. & Kettenmann, H. Microglia in Physiology and Disease. *Annual Review of Physiology* 79, 619–643 (2017).

70. Kettenmann, H., Hanisch, U.-K., Noda, M. & Verkhratsky, A. Physiology of microglia. *Physiological reviews* 91, 461–553 (2011).

71. Liu, Y. U. *et al.* Neuronal network activity controls microglial process surveillance in awake mice via norepinephrine signaling. *Nature Neuroscience* (2019). doi:10.1038/s41593-019-0511-3

72. Siuda, E. R. *et al.* Optodynamic simulation of β-adrenergic receptor signalling. *Nature Communications* (2015). doi:10.1038/ncomms9480

73. Billington, C. K., Penn, R. B. & Hall, I. P. β2 Agonists. in *Handbook of Experimental Pharmacology* (2016). doi:10.1007/164_2016_64

74. Boulton, D. W. & Fawcett, J. P. The Pharmacokinetics of Levosalbutamol. *Clinical Pharmacokinetics* (2001). doi:10.2165/00003088-200140010-00003

75. Atwood, B. K., Lopez, J., Wager-Miller, J., Mackie, K. & Straiker, A. Expression of G protein-coupled receptors and related proteins in HEK293, AtT20, BV2, and N18 cell lines as revealed by microarray analysis. *BMC Genomics* (2011). doi:10.1186/1471-2164-12-14

76. Seifert, R. & Wenzel-Seifert, K. Constitutive activity of G-protein-coupled receptors: cause of disease and common property of wild-type receptors. *Naunyn-Schmiedeberg's archives of pharmacology* 366, 381–416 (2002).

77. Dixon, A. S. *et al.* NanoLuc Complementation Reporter Optimized for Accurate Measurement of Protein Interactions in Cells. *ACS Chemical Biology* (2016). doi:10.1021/acschembio.5b00753

78. Storme, J., Cannaert, A., Van Craenenbroeck, K. & Stove, C. P. Molecular dissection of the human A3 adenosine receptor coupling with β-arrestin2. *Biochemical Pharmacology* (2018). doi:10.1016/j.bcp.2018.01.008

79. Shintani, Y. *et al.* β-Arrestin1 and 2 differentially regulate PACAP-induced PAC1 receptor signaling and trafficking. *PLoS ONE* (2018). doi:10.1371/journal.pone.0196946

80. Retamal, J. S., Ramírez-García, P. D., Shenoy, P. A., Poole, D. P. & Veldhuis, N. A. Internalized GPCRs as Potential Therapeutic Targets for the Management of Pain. *Frontiers in Molecular Neuroscience* (2019). doi:10.3389/fnmol.2019.00273

81. Calebiro, D. & Godbole, A. Internalization of G-protein-coupled receptors: Implication in receptor function, physiology and diseases. *Best Practice and Research: Clinical Endocrinology and Metabolism* (2018). doi:10.1016/j.beem.2018.01.004

82. Kim, J. H. *et al.* High cleavage efficiency of a 2A peptide derived from porcine teschovirus-1 in human cell lines, zebrafish and mice. *PLoS ONE* 6, (2011).

83. Maes, M. E., Colombo, G., Schulz, R. & Siegert, S. Targeting microglia with lentivirus and AAV: Recent advances and remaining challenges. *Neuroscience Letters* (2019). doi:10.1016/j.neulet.2019.134310

84. Anthony P. Davenport, Stephen Alexander, Joanna L. Sharman, Adam J. Pawson, Helen E. Benson, Amy E. Monaghan, Wen Chiy Liew, Chido Mpamhanga, Jim Battey, Richard V. Benya, Robert T. Jensen, Sadashiva Karnik, Evi Kostenis, Eliot Spindel, Laura Storjohann, A. H. IUPHAR/BPS Guide to PHARMACOLOGY: GPR65. Available at: http://www.guidetopharmacology.org/GRAC/ObjectDisplayForward?objectId=113. (Accessed: 30th August 2017)

85. Stefan Offermanns, Steven L. Colletti, Adriaan P. IJzerman, Timothy W. Lovenberg, Graeme Semple, A. W. IUPHAR/BPS Guide to PHARMACOLOGY: GPR109A. Available at: http://www.guidetopharmacology.org/GRAC/ObjectDisplayForward?objectId=312. (Accessed: 30th August 2017)

86. Jin, Y. *et al.* Inhibition of interleukin-1β production by extracellular acidification through the TDAG8/cAMP pathway in mouse microglia. *Journal of Neurochemistry* (2014). doi:10.1111/jnc.12661

87. Parodi, B. *et al.* Fumarates modulate microglia activation through a novel HCAR2 signaling pathway and rescue synaptic dysregulation in inflamed CNS. *Acta Neuropathologica* 130, 279–295 (2015).

88. Kellum, J. A., Song, M. & Li, J. Science review: Extracellular acidosis and the immune response: Clinical and physiologic implications. *Critical Care* (2004). doi:10.1186/cc2900

89. Lardner, A. The effects of extracellular pH on immune function. *Journal of leukocyte biology* (2001). doi:10.1189/jlb.69.4.522

90. Huang, C. *et al.* The ketone body metabolite β-hydroxybutyrate induces an antidepression-associated ramification of microglia via HDACs inhibition-triggered Akt-small RhoGTPase activation. *GLIA* (2018). doi:10.1002/glia.23241

91. Shimazu, T. *et al.* Suppression of oxidative stress by β-hydroxybutyrate, an endogenous histone deacetylase inhibitor. *Science* (2013). doi:10.1126/science.1227166

92. Seamon, K. B. & Daly, J. W. Forskolin: A unique diterpene activator of cyclic AMP-generating systems. *Journal of Cyclic Nucleotide Research* (1981).

93. Seamon, K. B., Padgett, W. & Daly, J. W. Forskolin: Unique diterpene activator of adenylate cyclase in membranes and in intact cells. *Proceedings of the National Academy of Sciences of the United States of America* (1981). doi:10.1073/pnas.78.6.3363

94. Goulding, J., May, L. T. & Hill, S. J. Characterisation of endogenous A2A and A2B receptor-mediated cyclic AMP responses in HEK 293 cells using the GloSensor™ biosensor: Evidence for an allosteric mechanism of action for the A2B-selective antagonist PSB 603. *Biochemical Pharmacology* (2018). doi:10.1016/j.bcp.2017.10.013

95. Dello Russo, C. *et al.* The human microglial HMC3 cell line: Where do we stand? A systematic literature review. *Journal of Neuroinflammation* (2018). doi:10.1186/s12974-018-1288-0

96. Su, W. *et al.* Recombinant adeno-associated viral (rAAV) vectors mediate efficient gene transduction in cultured neonatal and adult microglia. *Journal of Neurochemistry* 136, 49–62 (2016).

97. Eichhoff, G., Brawek, B. & Garaschuk, O. Microglial calcium signal acts as a rapid sensor of single neuron damage in vivo. *Biochimica et Biophysica Acta (BBA) - Molecular Cell Research* 1813, 1014–1024 (2011).

98. Cappoli, N. *et al.* The mTOR kinase inhibitor rapamycin enhances the expression and release of pro-inflammatory cytokine interleukin 6 modulating the activation of human microglial cells. *EXCLI Journal* (2019). doi:10.17179/excli2019-1715

99. Jadhav, V. S., Krause, K. H. & Singh, S. K. HIV-1 Tat C modulates NOX2 and NOX4 expressions through miR-17 in a human microglial cell line. *Journal of Neurochemistry* (2014). doi:10.1111/jnc.12933

100. Roy, A. A. *et al.* RGS2 interacts with Gs and adenylyl cyclase in living cells. *Cellular signalling* 18, 336–348 (2006).

101. Liu, S. *et al.* Tracking retinal microgliosis in models of retinal ganglion cell damage. *Investigative Ophthalmology and Visual Science* (2012). doi:10.1167/iovs.12-9450

102. Bodea, L. G. *et al.* Neurodegeneration by activation of the microglial complement-phagosome pathway. *Journal of Neuroscience* (2014). doi:10.1523/JNEUROSCI.5002-13.2014

103. Hopperton, K. E., Mohammad, D., Trépanier, M. O., Giuliano, V. & Bazinet, R. P. Markers of microglia in post-mortem brain samples from patients with Alzheimer's disease: A systematic review. *Molecular Psychiatry* (2018). doi:10.1038/mp.2017.246

104. Pei, Y., Rogan, S. C., Yan, F. & Roth, B. L. Engineered GPCRs as tools to modulate signal transduction. *Physiology* (2008). doi:10.1152/physiol.00025.2008

105. Tan, K. S. *et al.* β2 adrenergic receptor activation stimulates pro-inflammatory cytokine production in macrophages via PKA- and NF-κB-independent mechanisms. *Cellular Signalling* (2007). doi:10.1016/j.cellsig.2006.06.007

106. Farmer, P. & Pugin, J. β-Adrenergic agonists exert their 'anti-inflammatory' effects in monocytic cells through the IκB/NF-κB pathway. *American Journal of Physiology - Lung Cellular and Molecular Physiology* (2000). doi:10.1152/ajplung.2000.279.4.l675

107. Saika, F. *et al.* Chemogenetic Regulation of CX3CR1-Expressing Microglia Using Gi-DREADD Exerts Sex-Dependent Anti-Allodynic Effects in Mouse Models of Neuropathic Pain. *Frontiers in Pharmacology* (2020). doi:10.3389/fphar.2020.00925

108. Butovsky, O. *et al.* Identification of a unique TGF-β-dependent molecular and functional signature in microglia. *Nature Neuroscience* (2014). doi:10.1038/nn.3599

109. Ryan, S. K. *et al.* Neuroinflammation and EIF2 Signaling Persist despite Antiretroviral Treatment in an hiPSC Tri-culture Model of HIV Infection. *Stem Cell Reports* 14, 703–716 (2020).

110. Guttikonda, S. R. *et al.* Fully defined human pluripotent stem cell-derived microglia and tri-culture system model C3 production in Alzheimer's disease. *Nature Neuroscience 2021 24:3* 24, 343–354 (2021).